# Identification of functional binding partners of *Listeria monocytogenes* DivIVA

Von der Fakultät für Lebenswissenschaften

der Technischen Universität Carolo-Wilhelmina zu Braunschweig

zur Erlangung des Grades

eines Doktors der Naturwissenschaften

(Dr. rer. nat.)

genehmigte

D i s s e r t a t i o n

von Karan Gautam Kaval
aus Mumbai, Indien

1. Referentin: Professorin. Dr. Antje Flieger
2. Referentin: Professorin. Dr. Susanne Engelmann
eingereicht am: 17.12.2014
mündliche Prüfung (Disputation) am: 06.03.2015

Druckjahr 2015

## Vorveröffentlichungen der Dissertation

Teilergebnisse aus dieser Arbeit wurden mit Genehmigung der Fakultät für Lebenswissenschaften, vertreten durch die Mentorin der Arbeit in folgenden Beiträgen vorab veröffentlicht:

### Publikationen

**Kaval, K. G., Rismondo, J. & Halbedel, S.** (2014). A function of DivIVA in *Listeria monocytogenes* division site selection. *Mol Microbiol,* 94**,** 637-54.

**van Baarle, S., Celik, I. N., Kaval, K. G., Bramkamp, M., Hamoen, L. W. & Halbedel, S.** (2013). Protein-protein interaction domains of *Bacillus subtilis* DivIVA. *J Bacteriol,* 195**,** 1012-21.

**Kaval, K. G. & Halbedel, S.** (2012). Architecturally the same, but playing a different game: the diverse species-specific roles of DivIVA proteins. *Virulence,* 3**,** 406-7.

### Tagungsbeiträge

**Kaval, K. G. & Halbedel, S.** „A role for *L. monocytogenes* DivIVA in division-site selection*"*. (Talk). *BACELL 2014*. Bratislava, Slovakia (2014).

### Posterbeiträge

**Kaval, K. G. & Halbedel, S.** „Identification of DivIVA interaction partners in *Listeria monocytogenes"*. (Poster) CEP020. Jahrestagung der Vereinigung für Allgemeine und Angewandte Mikrobiologie (VAAM). Tübingen (2012).

**Kaval, K. G. & Halbedel, S.** „Adressing the role of DivIVA in SecA2-dependent protein secretion and virulence of *Listeria monocytogenes"*. (Poster) MPP62. 64. Jahrestagung der Deutschen Gesellschaft für Hygiene und Mikrobiologie (DGHM). Hamburg (2012)

**Kaval, K. G. & Halbedel, S.** „Hopping and stumbling into a novel gene related to DivIVA function in *Listeria monocytogenes"*. (Poster) CBP011. Jahrestagung der Vereinigung für Allgemeine und Angewandte Mikrobiologie (VAAM). Bremen (2013).

**Kaval, K. G. & Halbedel, S.** „Transposition reveals the disposition of a novel gene related to DivIVA function in *Listeria monocytogenes"*. (Poster). 7th International Conference on Gram-Positive Microorganisms. Montecatini Terme, Tuscany, Italy (2013).

**Kaval, K. G. & Halbedel, S.** „A pre-divisional function for DivIVA in *Listeria monocytogenes"*. (Poster) CBP016. 4. Gemeinsamer Kongress der Deutschen Gesellschaft für Hygiene und Mikrobiologie (DGHM) e. V. und der Vereinigung für Allgemeine und Angewandte Mirkobiologie (VAAM) e. V. Dresden (2014).

# Index

# List of Figures

# List of Tables

## List of Abbreviations

**a.d:** add

**$A_*$:** absorbance

**ABC:** ATP-binding cassette

**ADEPs:** acyldepsipeptides

**ADP:** adenosine diphosphate

**APS:** ammonium persulphate

**ATP:** adenosine triphosphate

**BACTH:** bacterial adenylate cyclase-based two-hybrid

**BHI:** brain heart Infusion

**bp:** base pairs

**BSA:** bovine serum albumin

**ºC:** degree Celsius

**CDC:** cholesterol-dependent cytolysin

**CFU:** colony forming units

**cm:** centimetres

**CTD:** C-terminal coiled-coil domain

**CTP:** C-terminal peptide

**DAPI:** 4',6-diamidino-2-phenylindole

**$dH_2O$:** deionized water

**DMEM:** Dulbecco's modified Eagle's medium

**DMSO:** dimethyl sulfoxide

**DNA:** deoxyribonucleic acid

**dNTPs:** deoxynucleotide triphosphates

**EDTA:** ethylenediamine tetra-acetic acid

**EPS:** extracellular polymeric substances

**FCS:** fetal calf serum

**FITC:** fluorescein isothiocyanate

**Fts:** filamentation thermo sensitive

**fw:** forward

**g:** grams

**GAPDH:** glyceraldehyde 3-phosphate dehydrogenase

**GFP:** green fluorescent protein

**GTP:** guanosine triphosphate

**h:** hours

**His:** histidine

**HRP:** horse-radish peroxidase

**IPTG:** isopropyl β-D-1-thiogalactopyranoside

**IRA:** intramolecular regulator of ATPase

**ITR:** inverted terminal repeat

**kb:** kilobase pairs

**kDa:** kilodaltons

**kV:** kilovolts

**l:** litres

**LB:** Luria-Bertani

**LBD:** lipid binding domain

**LLO:** Listeriolysin O

**LPXTG:** Leu-Pro-any-Thr-Gly motif

**LRR:** leucine-rich repeat

**LTAs:** lipoteichoic acids

**GW:** glycine-tryptophane motif

**M:** molar

**mA:** milliamperes

**MALDI-TOF:** matrix assisted laser desorption ionization time-of-flight

**mb:** megabase pairs

**mg:** milligrams

**min:** minutes

**ml:** millilitres

**mM:** millimolar

**$M_m$:** molecular mass

**MQ:** Milli-Q

**NBD:** nucleotide binding domain

**NBS:** noc-binding DNA sequences

**NOC:** nucleoid occlusion

**nm:** nanometer

**$OD_{595}$:** optical density at 595 nm

**$OD_{600}$:** optical density at 600 nm

**ORF:** open reading frame

**PBP:** penicillin-binding protein

**PBS:** phosphate buffer saline

**PC:** phosphatidylcholine

**PCR:** polymerase chain reaction

**PDZ:** post synaptic density protein, drosophila disc large tumor suppressor, and zonula occludens-1 protein

**PG:** peptidoglycan

**pI:** isoelectric point

**PI:** phosphatidylinositol

**PLC:** phospholipases C

**PVDF:** polyvinylidene fluoride

**rev:** reverse

**ROS:** reactive oxygen species

**rpm:** revolutions per minute

**RT:** room temperature

**s or sec:** seconds

**sd$H_2O$:** single deionized water

**SDS:** sodium dodecyl sulphate

**SDS-PAGE:** sodium dodecyl sulphate polyacrylamide gel electrophoresis

**SGWB:** sucrose-glycerol wash buffer

**SNPs:** single nucleotide polymorphisms

**t:** time

**TAE:** tris-acetate-EDTA

**TD:** tetramerization domain

**TE:** tris-EDTA

**TES:** tris-EDTA-SDS

**TEMED:** tetramethylethylenediamine

**Tris:** tris(hydroxymethyl) aminomethane

**V:** volts

**v/v:** volume per volume

**w/v:** weight per volume

**x:** times

**X-Gal:** 5-bromo-4-chloro-3-indolyl-β-D-galactopyranoside

**x g:** relative centrifugal force

**Ω:** ohm (electrical resistance)

**µF:** microfarads

**µg:** micrograms

**µl:** microliters

**µm:** micrometers

**λ:** wavelength (nm)

## Summary

DivIVA is a widely conserved protein found in firmicutes and actinobacteria, and has the capability of binding membrane regions having negative curvature such as division sites and cell poles. The role played by DivIVA seems to vary depending on the organism, with the *divIVA* gene being essential for cell viability in some species, while being dispensable in others, where deletion of the *divIVA* gene does lead to severely perturbed phenotypes. The varied morphogenetic functions of DivIVA orthologs in different bacterial species are postulated to arise from its ability to bind to an assortment of species-specific interaction partners.

Previous studies have shown that in the pathogenic bacteria *L. monocytogenes*, DivIVA not only seems to influence the secretion of virulence-associated autolysins via the accessory ATPase SecA2, but also seems to play no conspicuous role in the Min system-based division-site selection process during cell division, which is in contrast to that observed in its close relative, *B. subtilis*. This PhD study was therfore aimed at characterizing the putative influence of DivIVA on SecA2-dependent autolysin secretion as well as on division-site selection in *L. monocytogenes*. Genetic studies, including bacterial two-hybrid assays and affinity pull down experiments that were performed to better ascertain the association/lack of association of listerial DivIVA with either of these two pathways of cell division, showed no detectable association of DivIVA with either SecA2 or its autolysin substrates; however, *L. monocytogenes* DivIVA did show a clear association with components of the Min system, though in a manner that is postulated to be bifurcated rather than the linear mode of interaction that is observed in *B. subtilis*. The visually indistinguishable Δ*divIVA* and Δ*secA2* deletion mutant phenotypes of *L. monocytogenes* were also shown to be distinct, with the Δ*divIVA* mutant phenotype being a combination of a Δ*secA2*-like cell separation defect and a cell elongation defect. DivIVA was therefore revealed to serve a dual function in *L. monocytogenes*, namely to control the secretion of SecA2-dependent autolysins as well as to modulate the process of division-site selection via the Min system. Domain-swap studies have indicated that these two functions of DivIVA are possibly separable, with the C-terminal domain of DivIVA being responsible for its interactions with MinD of the Min system, and the N-terminal lipid binding domain, the linker and a short span of the C-terminal domain mediating an interaction with components of the SecA2-dependent secretion pathway. In addition, a strategy has also been devised to

increase minicell formation frequencies of *L. monocytogenes*, so as to provide a basis for improving the economic viability of listerial minicells, for use as potential drug-delivery vectors in the field of novel therapeutics.

A genome-wide, transposon mutagenesis-based approach to decipher additional interaction partners of *L. monocytogenes* DivIVA, led to the identification of a previously unknown regulatory gene operon *lmo0719-720*. Preliminary phenotypic and proteomic analysis have indicated the corresponding gene products of *lmo0719* and *lmo0720* to be a putative PadR-like repressor protein and a putative inhibitor of the stress sigma factor $\sigma^B$, respectively. Lmo0719 is postulated to have a dual regulatory effect: 1) It possibly controls the expression of the *lmo0719-720* operon itself. 2) It may have an influence on the expression of a putative multi-drug resistance efflux pump encoded by the *lmo0979-980* operon. Lmo0720 on the other hand is thought to have an inhibitory effect on $\sigma^B$ and its associated stress response pathway. This PhD study therefore also provides a good starting point for future studies on the regulatory role of this novel operon.

## Zusammenfassung

DivIVA ist ein in den Firmicutes und Actinobacteria hochkonserviertes Protein. Es besitzt die Fähigkeit, an konkave Membranregion zu binden, die an den Zellpolen oder dem Septum auftreten, und andere Proteine dorthin zu rekrutieren. Abhängig vom Organismus besitzt DivIVA unterschiedliche Funktionen. In einigen Spezies ist *divIVA* essentiell, in anderen führen *divIVA*-Mutationen zu starken Veränderungen in der Zellmorphologie. Diese variierenden Funktionen von DivIVA werden auf ein breites Interaktionsspektrum mit unterschiedlichen, spezies-spezifischen Bindungspartnern zurückgeführt.

In dem human-pathogenen Bakterium *L. monocytogenes* beeinflusst DivIVA die SecA2-abhängige Sekretion der Autolysine p60 und MurA, und schien im Gegensatz zu *Bacillus subtilis* keine Rolle in der MinCD-kontrollierten Zellteilung zu besitzen. In Pull down- und Bacterial Two Hybrid-Experimenten konnte keine Interaktion von DivIVA mit SecA2 oder seinen Autolysin-Substraten nachgewiesen werden. Allerdings zeigten sich klare Interaktionen zwischen DivIVA und den Komponenten des Min-Systems. Im Gegensatz zur streng linearen Interaktionssequenz dieser Proteine aus *B. subtilis* (DivIVA→MinJ→MinD→MinC), interagierte *L. monocytogenes* DivIVA direkt mit MinJ und MinD. Zelllängenmessungen von Δ*divIVA* und Δ*secA2*-Mutanten wiesen erstmals einen bislang übersehenen Zellteilungsdefekt der Δ*divIVA*-Mutante nach. Lokalisationstudien von Komponenten des Min-Systems zeigten weiterhin, dass die septale Lokalisation von MinC und MinD DivIVA-abhängig ist. Somit konnte bewiesen werden, dass DivIVA zwei Funktionen in *L. monocytogenes* besitzt. Zum einen kontrolliert es die Sekretion von SecA2-abhängigen Autolysinen, zum anderen steuert es das Min-System, welches für korrekte Positionierung der Zellteilungsstelle verantwortlich ist. Mithilfe von domain-swap-Untersuchungen konnten beide Funktionen von DivIVA genetisch voneinander getrennt werden. Die C-terminale Domäne von DivIVA ist hierbei zuständig für die Interaktion mit dem Min-System. Die N-terminale Lipidbindedomäne, der Linker zwischen C- und N-terminalem Bereich als auch ein kurzer Abschnitt der C-terminalen Domäne sind verantwortlich für Interaktionen mit Komponenten des SecA2-abhängigen Sekretionssystems.

Mit Hilfe einer Transposonmutagenese wurden weitere Gene mit *divIVA*-ähnlichen Phänotypen gesucht. Dies führte zur Identifizierung eines Stamms mit einer Tn-Insertion im

regulatorischen *lmo0719-720*-Operon und einer Mutation in *secA2* (G484E). Komplementationsstudien zeigten, dass diese Punktmutation ursächlich für den *divIVA*-ähnlichen Phänotyp war. Weiterführende phänotypische und proteomische Analysen zeigten, dass Lmo0719 ein putatives PadR-ähnliches Repressorprotein und Lmo0720 ein putativer Inhibitor der $\sigma^B$-abhängigen Stressantwort ist. Für Lmo0719 ist eine zweifache regulatorische Funktion wahrscheinlich. Zum einen autoreguliert es möglicherweise die Expression des *lmo0719-720*-Operons, zum anderen reprimiert es die Expression einer MDR-Efflux-Pumpe (*lmo0979-980*). Lmo0720 besitzt einen inhibitorischen Effekt auf die $\sigma^B$-Antwort und steht somit im Zusammenhang mit der Adaptation an Umweltstress und der Expression von Virulenzfaktoren. Diese Ergebnisse stellen einen guten Ausgangspunkt für weitere Arbeiten zur physiologischen Funktion dieser beiden uncharakterisierten Gene dar.

# 1. Introduction

## 1.1 Bacterial pathogenesis

Bacteria are single-celled prokaryotes, omnipresent in nature, which interact extensively with the organisms around them. Majority of the bacteria associated with humans are either harmless or symbiotic, but due to their inherent capability of persisting as part of the natural flora in humans, they sometimes take advantage of hosts bearing a compromised immune system, where they behave as opportunistic pathogens. *Escherichia coli*, a Gram-negative bacterium is one such example of a commensal, inhabiting the gastrointestinal tracts of mammals, which occasionally breaches the barriers of the innate immune system to cause infections of the urinary, enteric, nervous and pulmonary systems (Diaz et al., 2001). The Gram-positive organism *Staphylococcus aureus*, which normally colonizes the skin as well as the nasal mucosa in humans, on certain occasions, causes systemic infections such as septicaemia, pneumonia and endocarditis (von Kockritz-Blickwede et al., 2008). Microbial pathogenicity is intricate and multifactorial, involving various biochemical processes for the establishment of a disease (Finlay and Falkow, 1989). Two general classes of determinants, also known as virulence factors, are required for these processes. The first being determinants which are encoded by genes involved in the survival of these organisms both in the environment as well as within the hosts, and are found in both the pathogenic as well as the non-pathogenic bacteria. The second class of determinants is pathogen-specific and encoded by virulence genes, present either in the chromosome or in extra-chromosomal DNA, conferring specific virulence-related phenotypes to these pathogens (Groisman and Ochman, 1996). The need to reduce the burden of diseases caused by such pathogens demanded more effective pharmaceutical interventions, the answer to which came in the form of antibiotics.

## 1.2 The era of antibiotics and the advent of antimicrobial resistance

Antibiotics are a class of antimicrobial agents responsible for either killing or inhibiting bacterial growth. They are classified and grouped on the basis of, firstly, their chemical structure, secondly, their mechanism or mode of action, and lastly, their spectrum of activity. Another mean of classifying antibiotics is to group them in two broad categories depending on whether they kill the bacteria or just inhibit their growth i.e. bactericidal and bacteriostatic

antibiotics respectively (Davey, 2000). Majority of the clinically relevant antibiotics target either the synthesis of the bacterial cell wall (penicillins & cephalosporins) or protein synthesis (aminoglycosides, macrolides and tetracyclines), whereas a few types target the cell membrane of the bacteria (polymixins) and also other enzymes (fluoroquinolones, sulphonamides and daptomycin) (Finberg et al., 2004). β-lactams are among the most predominantly used cell wall biosynthesis-targeting antibiotics. They competitively bind and inhibit DD-transpeptidase activity of penicillin binding proteins due to their structural analogy to D-alanyl-D-alanine, a component of the *N*-acetylmuramic acid-associated pentapeptide linker. As a result, the penicillin-binding proteins (PBPs) are unable to crosslink peptidoglycan chains, causing disruption of peptidoglycan biosynthesis that eventually leads to death of the cells (Waxman and Strominger, 1983, Goffin and Ghuysen, 1998). However, the inhibitory effect of these β-lactam antibiotics on PBPs was short-lived due to the rapid emergence of resistant variants within susceptible bacterial populations. Bacteria resistant to these drugs have evolved a number of mechanisms to counteract their effects. One of the resistance mechanisms involves the secretion of an enzyme called β-lactamase into their periplasmic space by Gram-negative bacteria such as *P. aeruginosa* and *E. coli* so as to degrade the β-lactam rings of these antibiotics (Macheboeuf et al., 2006). Gram-positive bacteria such as *S. aureus* and *E. faecium* that do not secrete β-lactamases have evolved an alternative strategy. *S. aureus* bypasses the action of the β-lactam antibiotics by acquiring the *mecA* gene via horizontal transfer, allowing it to express the highly β-lactam resistant class B PBP2a (Pinho et al., 2001, Wu et al., 2001). *E. faecium* possesses the PBP5fm, which confers a natural resistance to β-lactams due to its low affinity for penicillin that is further enhanced either by its overproduction (Zorzi et al., 1996) or acquirement of point mutations (Sauvage et al., 2002).

### 1.3 Cell division proteins as antibacterial drug targets

Over the years there has been a substantial increase in bacterial resistance towards various antibiotics, including the PBP targeting antibiotics. Therefore, alternative components of the cell division machinery are being looked at and screened as potential targets for new antimicrobial drugs. The tubulin-homolog, FtsZ, was identified as a potential target for antibacterial treatment due to its essentiality for cell division and its high degree of conservation. A variety of inhibitors of FtsZ have been identified including the 9-phenoxyalkyl derivatives of the benzylisoquinoline alkaloid known as Berberine (Sun et al.,

2014). A peptide inhibitor, Kil, isolated from bacteriophage λ has been shown to inhibit FtsZ in a ZipA-dependent manner (Haeusser et al., 2014). The sporulation-specific MciZ protein of *B. subtilis*, which is also a small peptide FtsZ inhibitor (40 amino acids), was found to prevent FtsZ polymerization by obstructing the binding of GTP at the nucleotide-binding pocket of FtsZ (Handler et al., 2008). High throughput assays used for the identification of FtsZ inhibitors have yielded compounds that were found to competitively inhibit the GTPase activity of FtsZ such as PC58538, a synthetic compound belonging to a drug library (Stokes et al., 2005) and Viridotoxin, a small molecule inhibitor isolated from fermentation broths of *Aspergillus sp.* (MF6890) (Wang et al., 2003). A similar approach of inhibitory peptide isolation from phages has been used to identify agents effective against the cell division protein FtsA (Paradis-Bleau et al., 2005). Competitive inhibitors targeting proteins involved in cell elongation have also been looked into. The synthetically synthesized compound A22 [S-(3,4-Dichlorobenzyl)isothiourea] was found to bind to the nucleotide binding pocket of MreB and prevent the simultaneous binding of ATP at the site, thereby inhibiting MreB polymerization and disrupting cell elongation (Bean et al., 2009). Bacterial cellular proteins belonging to pathways other than those responsible for cell division have also been targeted for therapeutic outcomes. One such example includes a group of acyldepsipeptides (ADEPs), which specifically bind to and overactivate the catalytic core of the tightly regulated ClpAP/XP protease complex, ClpP (Brötz-Oesterhelt et al., 2005). One of the substrates of the ClpXP protease complex is FtsZ, the interaction with which is mediated via the AAA+ ATPase ClpX subunit (Weart et al., 2005). Upregulation of ClpXP activity by ADEP possibly results in increased proteolytic degradation of FtsZ, cell division cessation and consequently cell death at least in *E. coli* (Camberg et al., 2014). In *B. subtilis,* the inhibition of FtsZ by ClpXP complex was thought to be ClpP-independent (Weart et al., 2005); however that does not seem to be the case as more recent studies have shown that FtsZ is rather predisposed to the degradation by the ADEP-complexed ClpP protein (Sass et al., 2011). Such studies provided the impetus for the ongoing search for other well conserved cell division proteins as targets for novel antimicrobial agents. However, if the process of drug discovery and their use is to be made more efficient, a better understanding of the yet-to-be functionally characterized cell division proteins is required in terms of their phylogenetic conservation and their roles in biochemical pathways.

### 1.4 Bacterial cell division

Cell division is a prerequisite process for every organism and involves the formation of two or more daughter cells from a single parent cell, so as to maintain growth and proliferation. Prokaryotes, especially rod shaped bacteria such as *Bacillus subtilis* and *E. coli*, employ a mode of cell division known as binary fission (Fig. 1). This is a form of asexual reproduction,

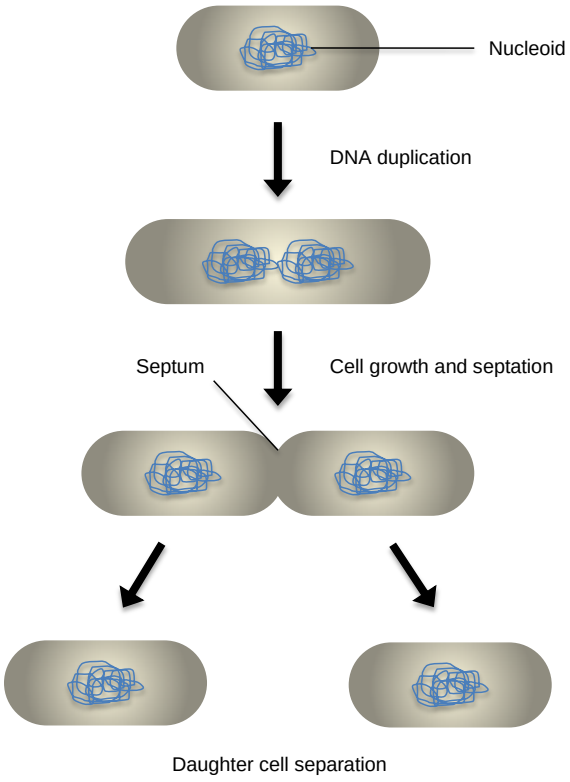


**Figure 1: Binary fission mode of bacterial cell division.** Illustration of binary fission in rod shaped bacteria. The nucleus (indicated in blue) is duplicated followed by cell length doubling, chromosome segregation, cell wall invagination, septation and separation of daughter cells. [Adaptation of figure from Madigan (2000)].

which ideally leads to the generation of genetically identical progeny. The process is initiated by chromosomal duplication and a gradual doubling of the cell length. Once the duplicated chromosomes are sufficiently separated from each other, the cell division machinery comes into play, normally at the mid-cell region, leading to the inward invagination of the bacterial cell wall to form the division septum.

The septum partitions the two sections of the parent cell, each containing a copy of the parental chromosome, into two daughter cells. These two daughter cells then separate from each other and repeat the process for a fresh round of cell division (Madigan, 2000). *S. aureus*, which is a true coccus also undergoes binary fission, however does not possess the traditional cell division geometry of rod shaped bacteria (Tzagoloff and Novick, 1977). It rather displays the characteristic "Bunch of Grapes" morphology that results from cell division in three alternating orthogonal planes (Turner et al., 2010).

### 1.5 The Divisome

During the process of cell division, prokaryotes employ a multiprotein complex comprising of several well-conserved **f**ilamentation **t**hermo **s**ensitive proteins (Fts) at the division site, which are collectively called the divisome. The protein constituents of the divisome do however vary between Gram positive and Gram negative bacteria (Fig. 2). The Fts terminology was used for these proteins as the conditional mutants for their respective genes were unable to undergo cell division under restrictive temperature conditions; however, it is now being used to designate most cell division genes irrespective of whether their mutated gene product is temperature sensitive or not (Bramhill, 1997). The Fts nomenclature of these proteins originated from work done in *E. coli* (Buddelmeijer and Beckwith, 2002) and is used for Gram-negative bacteria, whereas their homologs in Gram-positive bacteria such as *B. subtilis*, which have weak sequence similarity as well as behavioral differences as compared to those in *E. coli*, are named Div proteins instead (Errington et al., 2003). Eight of these conserved and essential cell division proteins have been identified in cell wall-bearing eubacteria, i.e., FtsZ, FtsK, FtsA, FtsQ (DivIB), FtsB (DivIC), FtsL, FtsI and FtsW. Both in *B. subtilis* and *E.coli*, these proteins have been shown to bear dependencies for their recruitment at the division site, although a few variations have been reported which were organism-dependent (Buddelmeijer and Beckwith, 2002, Errington et al., 2003). In *E.coli*, the assembly pathway of the late division proteins (division proteins downstream of FtsA) and their dependencies are linear as the localization of a particular protein depends only the protein lying immediately upstream to it in the pathway, with the proteins lying downstream bearing no consequence on its localization pattern (Buddelmeijer et al., 2002). However in *B. subtilis*, the equivalent proteins are entirely interdependent for their mid-cell assembly hence a deletion or mutation in any of the encoding genes of the pathway results in a failure in the assembly of all the other associated proteins (Daniel et al., 2006).

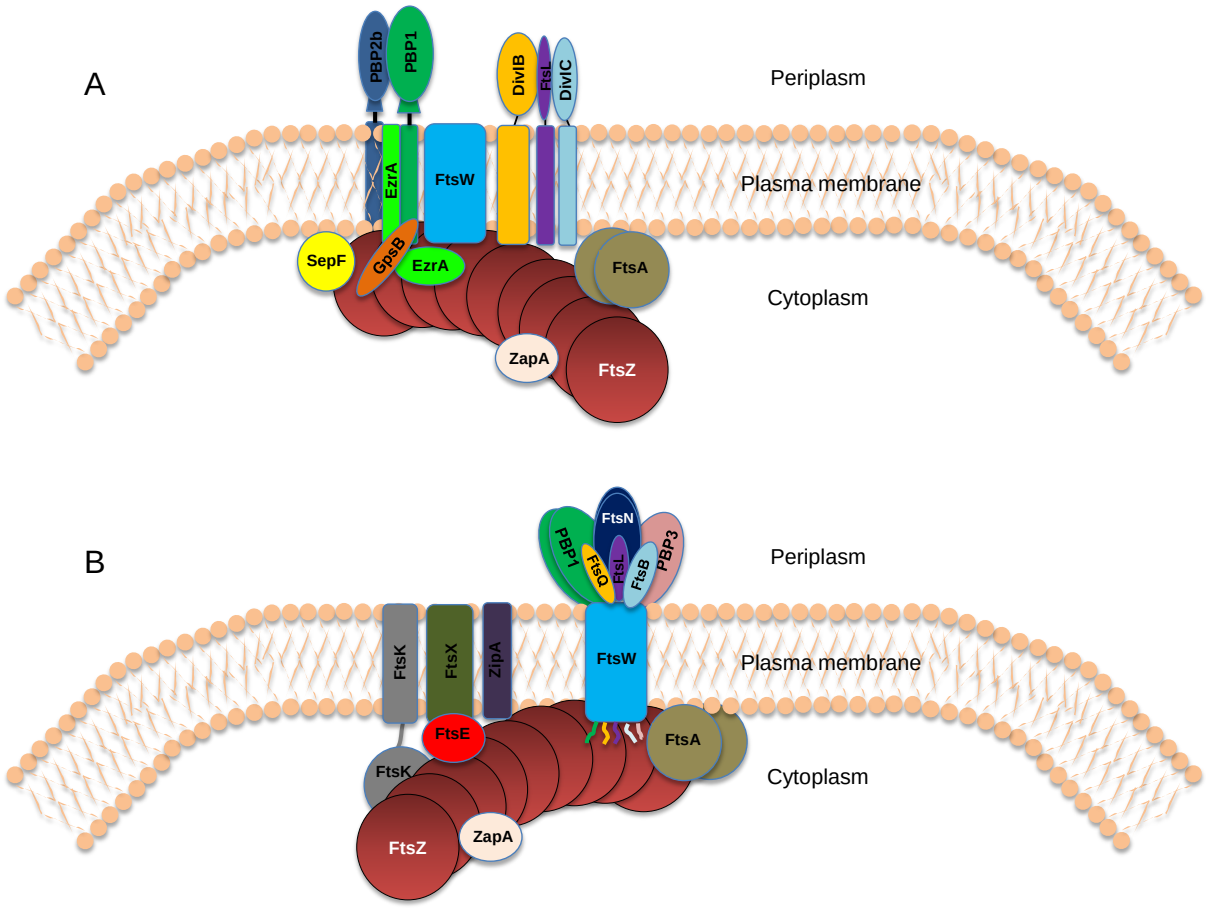


**Figure 2: Bacterial cell division machineries.** Illustration of the cell division machinery in (A) *B. subtilis* [adaptation of figure from Carballido-Lopez and Formstone (2007)] and (B) *E. coli* [adaptation of figure from den Blaauwen et al. (2008)]. Homologous proteins in the two divisomes are represented by the same colors.

### 1.5.1 FtsZ

FtsZ is the most highly conserved among all of the cell division proteins and is present in most, if not all, prokaryotes with only two exceptions, namely, the free-living species *Aeropyrum pernix* and *Ureaplasma urealyticum* (Margolin, 2000). The onset of cell division is demarcated by the formation of the Z-ring at the future site of septation, which is composed of the bacterial tubulin homologue FtsZ (Adams and Errington, 2009, Bi and Lutkenhaus, 1991). The polymerization of FtsZ monomers into protofilaments is achieved by means of its GTPase activity, which cleaves available GTP bound to its glycine-rich GTP binding domain (Lutkenhaus, 1993). These protofilaments then undergo lateral interactions to assemble into a structure that resembles a ring (Dajkovic et al., 2008, Erickson et al., 1996, Mukherjee and

Lutkenhaus, 1998). The Z-ring formation is facilitated by a number of other cell division proteins that promote FtsZ assembly, including ZapA, FtsA and SepF (Adams and Errington, 2009, Gueiros-Filho and Losick, 2002, Jensen et al., 2005, Singh et al., 2008). FtsZ is considered to be indispensable for bacterial survival due to its pole position in the hierarchy of cell division protein assembly (Errington et al., 2003); however the essentiality of FtsZ for cell division was challenged by the observation that cell wall-less mollicute bacteria tolerate deletion of FtsZ (Lluch-Senar et al., 2010). Another exception to the indispensability of FtsZ is the presence of bacterial L-forms, which are cell wall-lacking variants of commonly occurring bacteria that are capable of propagating without the need for the traditional FtsZ-dependent division machinery (Leaver et al., 2009).

### 1.5.2 FtsZ associated proteins

A functional divisome in *B. subtilis* is comprised of the FtsZ protein, which is either directly or indirectly associated with a series of other proteins that mediate a variety of functions necessary for cell division. The functions of the FtsZ-associated proteins include the establishment of the FtsZ ring, segregation of the replicated chromosomes, synthesis of the septal peptidoglycan cross-wall, and invagination of the membrane along the constricting septum. Like FtsZ, the absence of some of these proteins leads to a dysfunctional divisome, which is no longer capable of efficiently carrying out cell division. Despite their importance in the process of cell divison, they are not of prime relevance to this PhD study, therefore, a list of the known FtsZ-associated and late cell division proteins of the *B. subtilis* divisome, including their known function, are mentioned in the table below:

**Table 1: FtsZ associated proteins and their functions**

| Protein | Function | Reference |
|---|---|---|
| FtsA | Recruitment of FtsZ filaments to the membrane and negative regulation of FtsZ organization | (Loose and Mitchison, 2014) |
| SepF | Stabilization and bundling of FtsZ protofilaments Membrane anchor for Z | (Duman et al., 2013, Singh et al., 2008) |
| ZapA | Inhibition of GTPase activity of FtsZ and stabilization of FtsZ protofilaments | (Gueiros-Filho and Losick, 2002, Small et al., 2007) |
| EzrA | Destabilization of FtsZ ring and dynamic reorganization of FtsZ monomers | (Singh et al., 2007) |
| FtsW | Translocation of peptidoglycan precursors (Lipid II) from the cytoplasmic side to the outside of the plasma membrane | (Mohammadi et al., 2011) |
| DivIB-FtsL-DivIC | Scaffolding protein complex for recruitment of downstream, divisome-associated proteins | (Errington et al., 2003, Noirclerc-Savoye et al., 2005, Sievers and |

| Protein | Function | Reference |
|---|---|---|
| | | Errington, 2000) |
| GpsB | Control of peptidoglycan synthesis during cell division and cell elongation (shuttling of PBPA1) | (Claessen et al., 2008) |
| PBP1 | Transglycosylation and transpeptidation of peptidoglycan precursors at the division septum | (Murray et al., 1998, Pedersen et al., 1999, Scheffers and Errington, 2004) |
| PBP2B | Transpeptidation of peptidoglycan precursors at the division septum | (Daniel et al., 2000, Scheffers et al., 2004) |

### 1.6 Division-site selection

Precise localization of the divisome at the mid-cell region is crucial for efficient cell division and requires synchronization with other simultaneously occurring processes such as DNA replication and segregation, so as to preclude any loss of genetic information during its transfer to the progeny. This mid-cell placement of the cell division apparatus is facilitated by the coordinated effort of the NOC and the Min system, which are elaborated below.

#### 1.6.1 Nucleoid occlusion (NOC)

The nucleoid is the bearer of the majority of the genetic information in bacteria. During cell division there is the risk of the nucleoid being guillotined by the constricting FtsZ ring before completion of chromosome segregation; however, there is a localized inhibitory effect on assembly of the divisome over the unsegregated nucleoid (Wu and Errington, 2004). The phenomenon is brought about by the action of the DNA-bound inhibitor Noc, in the absence of which *B. subtilis* Δ*noc* mutants form division septa through the nucleoid (Wu and Errington, 2004). Noc activity is regulated by its ability to bind to Noc-binding DNA sequences (NBS) in the bacterial chromosome (Wu et al., 2009), however the manner in which it influences FtsZ polymerization and ring formation is still unknown (Wu and Errington, 2012).

#### 1.6.2 Min system

The Min system works in conjunction with the nucleoid occlusion (NOC) system to prevent Z ring formation at sites in the bacterial cell other than the mid-cell region. It contributes to division-site selection by inhibiting FtsZ ring formation at regions adjacent to sites of recent septation (Bramkamp and van Baarle, 2009, Gregory et al., 2008). There also is recent evidence showing that the Min system is not only involved in inhibition of formation of new

Z-rings at the sites adjacent to the pre-existing division complex, but is also involved in disassembly of the pre-existing division complex itself, so as to prevent it from reinitiating another round of cell division close to the original septation site (van Baarle and Bramkamp, 2010). The Min system is a multi-protein complex comprising of the MinC, MinD, MinJ and DivIVA proteins (Bramkamp et al., 2008, Edwards and Errington, 1997).

#### 1.6.2.1 MinCD

MinC is the cytoplasmic protein component of the Min system, which inhibits polymerization of FtsZ (Blasios et al., 2013). MinC interacts with the H9-H10 helix and the C-terminal peptide (CTP) of FtsZ, thereby preventing bundling of FtsZ filaments (Blasios et al., 2013). The localization of MinC to the cytoplasmic membrane is mediated via its interaction with the membrane-associated protein MinD, which facilities its interaction with FtsZ (Marston and Errington, 1999). MinD is a widely conserved ATPase belonging to the ParA superfamily, the members of which are believed to be involved in segregation of chromosomes or plasmids (Gerdes et al., 2000). Unlike that observed for other members of the ParA family of ATPases, the C-terminal section of MinD houses a motif that is highly conserved and forms an amphipathic helix, which mediates its interaction with the phospholipid membrane (Szeto et al., 2002). This interaction of MinD with the cytoplasmic membrane is crucial as MinC, when present at normal physiological concentrations, can serve as a cell division inhibitor only when recruited by MinD to the plasma membrane (Raskin and de Boer, 1999). Hence the deletion of either the *minC* or *minD* gene results in the formation of anucleate cells called minicells due to deregulated FtsZ polymerization and septation at the chromosome free spaces at the cell poles (Levin et al., 1998). The spatial orientation of the MinCD complex is crucial for its role in division site selection and is achieved by the action of the topological specificity factor DivIVA(Edwards and Errington, 1997).

#### 1.6.2.2 MinJ

In *B. subtilis*, the protein DivIVA (to be dealt with in further detail in the upcoming chapters) is responsible for targeting the MinCD complex to the regions adjacent to the constricting septum and the newly formed cell pole of the daughter cells (Edwards and Errington, 1997) due to its ability to sense negatively curved membranes (Lenarcic et al., 2009), such as those found at the septum-adjacent areas, and the daughter cell poles which form due to septum

constriction. The localization cue for this DivIVA-associated targeting is provided by the protein interaction partner, MinJ (Bramkamp et al., 2008, Patrick and Kearns, 2008). *B. subtilis* MinJ is a 44 kDa integral membrane protein and is predicted to possess six successive membrane-spanning segments at its N-terminus, while its C-terminus is believed to harbour a PDZ (post synaptic density protein, drosophila disc large tumor suppressor, and zonula occludens-1 protein) domain (Patrick and Kearns, 2008). Though the exact function of the PDZ domain in MinJ is not known, the structure itself is believed to mediate protein-protein interactions (Jemth and Gianni, 2007). Despite the far-reaching occurence of the PDZ domain, with these structures being found in all kingdoms, proteins with the MinJ-like architecture are found only in rod-shaped, Gram-positive firmicutes including *Listeria* (Bramkamp et al., 2008). MinJ is believed to be a bridging protein that links MinD to DivIVA, as it bears direct interactions with both DivIVA and MinD (Patrick and Kearns, 2008, Bramkamp et al., 2008). In addition to these direct interactions, MinJ is also known to interact with FtsA, FtsL, EzrA, and PBP2B, which is thought to facilitate the linkage of the integral membrane protein subset of the divisome with the division site selection system of *B. subtilis* (Bramkamp and van Baarle, 2009). In the past, the targeting of MinCD in *B. subtilis* was believed to be a static process, with the complex arriving at the division site during the later stages of cell division and being maintained at the subsequent newly formed poles of the cell by DivIVA (Marston et al., 1998, Marston and Errington, 1999). However, there is evidence indicating that *B. subtilis* MinC is in fact dynamic, with small populations of this protein moving along the cell membrane from the newly formed cell pole to the mid-cell region, and also rotating around the invaginating septum (Gregory et al., 2008). MinJ, when complexed with MinCD, facilitates the disassembly of the divisome after initiation of septum formation so that only one round of division occurs per cell cycle (van Baarle and Bramkamp, 2010). For the divisome disassembly process, MinJ is thought to relay information about the division status to the MinCD complex so that MinC is able to destabilize the Z-ring following septum formation (van Baarle and Bramkamp, 2010). MinJ has also been shown to indirectly affect swarming behaviour of *B. subtilis* as in a *minJ* mutant, swarming motility is impaired (Patrick and Kearns, 2008) Whether MinJ has an influence on the subcellular dynamics of MinCD, and if so, how this is achieved is still to be deciphered.

### 1.6.3 Min and NOC-independent systems

The essentiality of the Min system in division-site selection was brought into question when it was reported that the accurate mid-cell positioning of the FtsZ ring in *B. subtilis* does not require either MinC or MinD (Migocki et al., 2002). However, the simultaneous lack of both the Min and NOC systems in *B. subtilis* as well as *E. coli* leads to long, division-defective cells, which seldom form FtsZ rings probably due to an exhaustion of the limited cytoplasmic pool of FtsZ that results from FtsZ polymerization activities occurring along the entire length of the cells (Bernhardt and de Boer, 2005, Wu and Errington, 2004). Experiments performed with outgrown spores of *B. subtilis* have shown that despite the total absence of both the Min as well as the NOC systems, FtsZ rings are capable of forming at the midcell foci of this organism, which has led to a model that states that rather than functioning as "division signposts" to identify the correct site of division at the mid-cell, the Min and NOC systems ensure efficient utilization of the established mid-cell signpost so that FtsZ rings occur only there (Rodrigues and Harry, 2012). The absence of homologs for the Min proteins and/or SlmA/Noc in several bacteria further highlights the existence and importance of alternative Z-ring positioning mechanisms that are Min/NOC-independent (Harry et al., 2006, Margolin, 2005). These novel Z-ring placement mechanisms include both negative as well as positive regulators of FtsZ, which due to the lack of conservation suggest a difference among various bacterial species in the placement of the FtsZ-ring [reviewed in (Monahan et al., 2014)]. In *Caulobacter crescentus*, which is devoid of both the Noc and Min system proteins, MipZ serves the role of a negative regulator of FtsZ and is involved in the positioning in the Z-ring by the establishment of a bipolar gradient (Thanbichler and Shapiro, 2006). The SsgAB system of *Streptomyces coelicolor* was the first reported positive regulatory mechanism of FtsZ placement (Willemse et al., 2011). The membrane-associated protein SsgB, which requires SsgA for its localization, has been shown to promote the polymerization of FtsZ, thereby facilitating its assembly *in vitro* (Traag and van Wezel, 2008, Willemse et al., 2011).

## 1.7 DivIVA

### 1.7.1 Intracellular localization and domain architecture of DivIVA proteins

DivIVA is a protein found almost exclusively in Gram-positive bacteria, where it is well conserved and plays a role in a multitude of morphogenetic processes. DivIVA proteins are found to be associated with the cytoplasmic membrane and congregate at strongly bent membranous regions (Lenarcic et al., 2009). Due to their ability to sense concave/negative membrane curvature, they cluster at the invaginating septum as well as the cell poles (Oliva et al., 2010). The underlying mechanism of curvature sensing by DivIVA has yet to be elucidated, however, mathematical modeling using Monte-Carlo computation algorithms have predicted the tendency of oligomeric proteins with low membrane affinity to accumulate at negatively curved membranes (Lenarcic et al., 2009). Structural analysis of DivIVA from *B. subtilis* has revealed a two-domain architecture. It is shown to comprise of the N-terminal lipid binding domain (LBD) and the C-terminal coiled-coil domain (CTD), which is separated by a flexible linker (Oliva et al., 2010) (Fig. 3). The LBD is the one that is responsible for binding DivIVA to lipid membranes (Lenarcic et al., 2009) and possesses a coiled-coil section, which facilitates dimerization. Their N-termini cross each other and fold back onto the dimer in a complicated manner (Oliva et al., 2010). Due to this complex fold, the side chains of the hydrophobic phenylalanine residues at position 17 (F17) are exposed to the solvent. Membrane binding is achieved via insertion of these side chains into the hydrophobic core of the phospholipid bilayer. The adjacent, positively charged arginine residues (R18) are thought to stabilize this insertion by interacting with the negatively charged head groups of the phospholipids (Oliva et al., 2010). The CTD of DivIVA has extensive coiled-coils which stretch almost along its entire length, with the section from residue 130-154 being utilized for tetramerization (referred to as the tetramerization domain). The C-terminal tail though is described to be structurally disordered (Oliva et al., 2010, van Baarle et al., 2013) and is believed to contain certain sections to which other interaction partners bind for their recruitment to the cell poles and the division septum. In fact, it was shown that when the 11 non-conserved residues following the tetramerization domain of *B. subtilis* DivIVA were truncated, it severely affected its ability to interact with its interaction partner RacA (van Baarle et al., 2013).

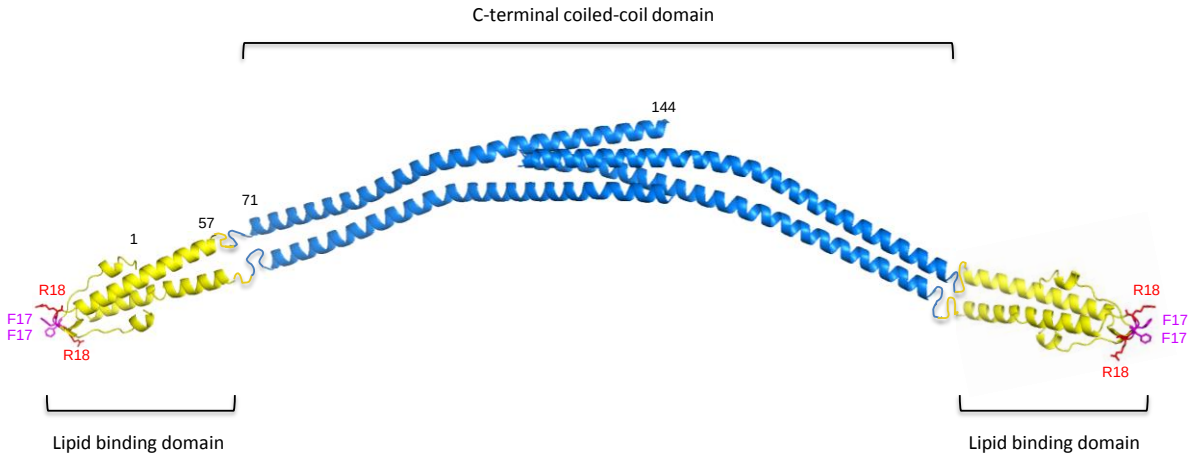


**Figure 3: DivIVA crystal structure.** Crystal structure of a *B. subtilis* DivIVA tetramer [adaptation of the crystal structure of DivIVA from Oliva et al. (2010)]. The N-terminal lipid binding domain (LBD, indicated in yellow) allows for dimerization, while the C-terminal coiled-coil domain (CTD, indicated in blue) mediates tetramerization of DivIVA dimers via interactions of their ends. F17 (magenta coloured) and R18 (red coloured) residues, found at the tip of the LBD are responsible for attachment of DivIVA to the membrane and stabilization of the insertion, respectively. Numbers 1, 57, 71 and 144 indicates amino acid residues demarcating the borders of the two domains. The C-terminal tail was not resolved by the crystallographic analysis and is therefore excluded here.

### 1.7.2 Multitude of morphogenetic functions of DivIVA in various bacterial species

Most of the current knowledge about DivIVA is based on studies performed in the Gram-positive model organism, *B. subtilis*, where it is known to play a role in division site selection by targeting the Min system to the regions adjacent to septation site and the new cell poles of the daughter cells (Bramkamp et al., 2008, Edwards and Errington, 1997, Patrick and Kearns, 2008)(Fig. 4A, left image) and in endospore formation (Edwards and Errington, 1997, Thomaides et al., 2001). During the process of sporulation, DivIVA directly interacts with the kinetochore binding protein RacA, and therefore tethers it along with the bound prespore chromosomal copy to the pole of the prespore compartment (Wu and Errington, 2003) (Fig. 4A, right image). Therefore, the deletion of *divIVA* in *B. subtilis* leads to division-defective, asporogenic phenotype due to defective chromosome segregation. In addition, DivIVA is also known to tether SpoIIE to the polar septum on the forespore side and therefore mediate both asymmetric division as well as prespore compartment-specific $\sigma^F$ transcription factor activation, thereby ensuring successful sporulation (Eswaramoorthy et al., 2014). In *B. subtilis*, the establishment of competence (ability to take up transforming DNA) is known to

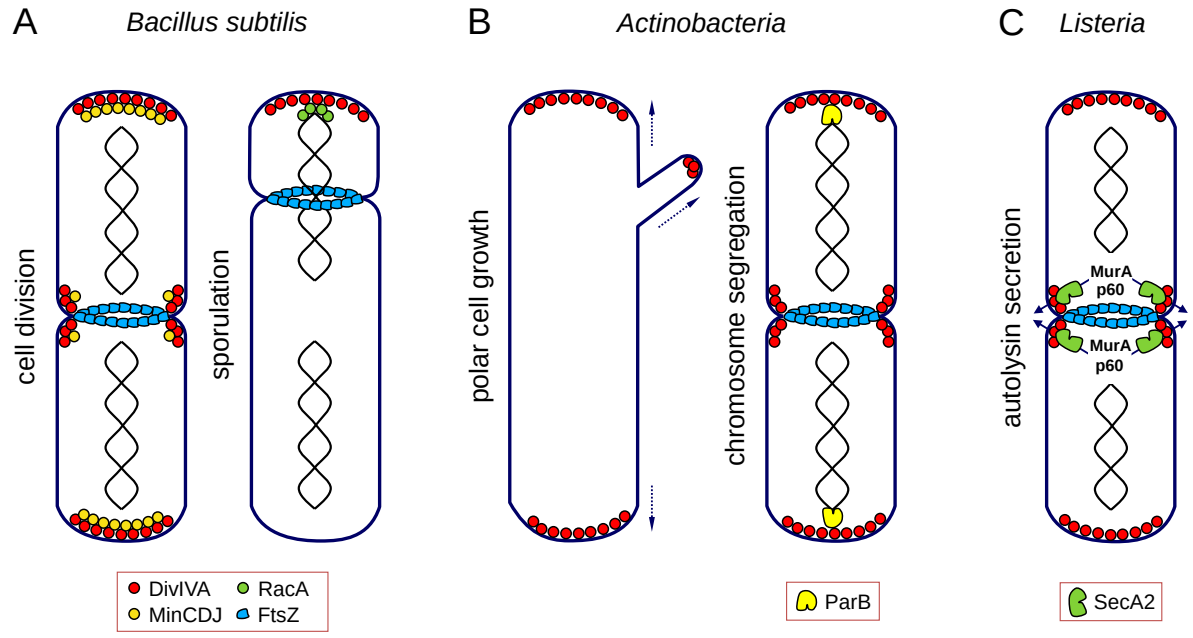


**Figure 4: Species-specific functions of DivIVA**. Illustrations depicting the diverse roles played by DivIVA in various Gram-positive bacteria [adapted from the illustration described by Kaval and Halbedel (2012)]. (A) During vegetative growth, *B. subtilis* DivIVA targets the MinCDJ division site-selection complex to the areas adjacent to the division septum and the newly formed cell poles in order to ensure FtsZ-ring formation in the chromosome-devoid region at mid-cell. During sporulation, DivIVA binds to the chromosome via the kinetochore-associated protein, RacA and therefore targets the prespore chromosome copy to the pole of the prespore compartment. (B) In actinobacteria, DivIVA serves the purpose of directing the cell wall synthesis machinery to the poles and the hyphal tips. Prior to cell division, DivIVA performs a role in chromosome segregation via an interaction with the origin binding protein ParB. This interaction helps DivIVA recruit the origin of replication of the daughter chromosomes to the cell poles. It is believed that this event is necessary for efficient chromosome segregation. (C) *L. monocytogenes* DivIVA mediates the secretion of the autolytic proteins MurA and p60 via the accessory secretion ATPase SecA2 by first recruiting these autolysins to the site of septation. However the septal localisation of SecA2 is not dependent on DivIVA.

be mediated via DivIVA. Competence for transformation is dependent on Maf, whose encoding gene is regulated by ComK, and works in association with ComGA to block cell division of *B. subtilis* cells when switching from competence to exponential growth state (Briley et al., 2011). Maf as well as the posttranscriptional regulator of late competence, ComN, bear direct interactions with DivIVA, which is believed to be responsible for the polar localization of these two competence-associated proteins (Briley et al., 2011, dos Santos et al., 2012). In contrast to firmicutes, actinomycetes grow by extension of polar hyphal filaments rather than undergoing lateral extension and binary fission. DivIVA in this bacterial family has been demonstrated to polarly recruit enzymes involved in cell wall precursor generation (Letek et al., 2008, Xu et al., 2008) (Fig. 4B, left image). The resultant cell wall precursors

are then incorporated by the terminal cell wall synthetic systems to the nascent cell wall at the subpolar region in an annular fashion (Meniche et al., 2014). Attempts made to delete *divIVA* in *Streptomyces coelicolor* A3(2) were unsuccessful, thus hinting to the essentiality of DivIVA for cell viability (Flärdh, 2003). The polarly localised DivIVA interacts directly with the centromere-binding protein ParB and therefore tethers the chromosomes to the cell poles, facilitating chromosome segregation in *C. glutamicum* (Donovan et al., 2012) (Fig. 4B, right image). The importance of DivIVA for cell division is not only restricted to rod-shaped Gram-positive bacteria. *Streptococcus pneumoniae*, a coccoid bacterium, also requires DivIVA for septum formation and separation of its daughter cells despite the absence of the Min system; however, the exact molecular mechanisms associated with the phenomenon are unknown (Fadda et al., 2007, Fadda et al., 2003). Just recently it was proposed that in *S. pneumoniae*, the serine/threonine kinase StkP, DivIVA and GpsB form a triad to modulate the ellipsoidal cell shape of the bacteria by finely tuning both septal and peripheral peptidoglycan synthesis (Fleurie et al., 2014). The abundance of information proving the involvement of DivIVA in various morphogenetic processes has led to the assumption that DivIVA binds to an assortment of different species-specific interaction partners [discussed in Kaval and Halbedel (2012)].

### 1.7.3 Contribution of DivIVA to cell division and virulence of *Listeria monocytogenes*

Two independent proteomic studies have suggested that *L. monocytogenes* DivIVA putatively plays a role in biofilm formation (Helloin et al., 2003, Tremoulet et al., 2002). Recent evidence has suggested that DivIVA influences the secretion and localization of the autolysins p60 and MurA via the accessory ATPase SecA2 (Fig. 5C). As a result of this, DivIVA has also been shown to have an effect on swarming motility and biofilm formation of *L. monocytogenes*. Furthermore, a deletion of the *divIVA* gene (*lmo2020)* leads to an attenuation of the capacity of *L. monocytcogenes* to invade and effectively replicate intracellularly within HeLa cells as well as to spread efficiently from one cell to another in a monolayer of 3T3 mouse fibroblast cells (Halbedel et al., 2012). In terms of cell division, it is assumed that the Min system of division site selection works independently of DivIVA in *L. monocytogenes* as the *divIVA* mutant displays cell chaining and lacks any observable minicells (Halbedel et al., 2012), which is in contrast to the corresponding gene deletion mutant in *B. subtilis* that is characterized by cell filamentation and minicell formation (Edwards and Errington, 1997). The cell chaining defect seen in a *L. monocytogenes divIVA* mutant is due to a disruption in

the secretion of SecA2-dependent autolysins resulting in the formation of chains of divided cells, incapable of post-divisional separation (Halbedel et al., 2012).

### 1.7.4 Potential of DivIVA-like proteins to serve as targets of antimicrobial drugs

GpsB is a small (98 amino acids), DivIVA-like protein, which was first discovered in *B. subtilis* and has a coiled-coil section in its N-terminal domain that is homologous to that found in the N-terminal LBD of DivIVA (Claessen et al., 2008, Lenarcic et al., 2009). These membrane-binding structures and their ability to sense negative membrane curvature are unique to such DivIVA-like proteins, and so far their presence in other proteins has not been described. The functionality of DivIVA is highly dependent on the LBD as even minor modifications to this structure results in inactivation of this protein (Oliva et al., 2010). Also, associations of DivIVA-like proteins to transmembrane proteins are suggested to be mediated via this LBD (van Baarle et al., 2013). In addition to its interaction with EzrA, GpsB is also known to show strong interactions with the transmembrane penicillin-binding protein PBP A1 in *B. subtilis* (Claessen et al., 2008), which is known to be responsible for transpeptidation and transglcosylation of peptidoglycan (PG) precursors (Murray et al., 1998, Pedersen et al., 1999). GpsB has been described to work in sync with EzrA to control the shuttling of PBP A1 from the lateral cell wall to the division site and vice versa so as to control PG synthesis during cell division and cell elongation (Claessen et al., 2008).

In *L. monocytogenes*, GpsB was not only observed to interact with PBP A1, but also with the other HMW PBPs such as PBP B1, PBP B2 and PBP B3 (Rismondo and Halbedel, unpublished data). In a *L. monocytogenes* Δ*gpsB* mutant, PBP A1 seems to be deregulated leading to an attenuation of this strain that is characterized by reduced intracellular replication rates and diminished cell-to-cell spreading in *in vitro* infection models (Rismondo and Halbedel, unpublished data). As mentioned earlier (Chapter 1.8.2) deletion of *divIVA* in *L. monocytogenes* also leads to an attenuated behaviour of the bacteria *in vitro* (Halbedel et al., 2012). DivIVA has been reported to be essential for the survival of several Gram positive pathogens such as *Streptococcus pneumoniae, Enterococcus faecalis* and *Mycobacterium tuberculosis*, where the deletion of the *divIVA* gene is either not possible or has deleterious morphological consequences (Fadda et al., 2007, Ramirez-Arcos et al., 2005, Kang et al., 2008). Since both DivIVA and GpsB appear to harbor a structurally unique LBD and are

indispensable for the virulence of *L. monocytogenes*, they putatively might serve as useful targets for the development of novel antibacterial compounds.

### 1.8 *Listeria monocytogenes*

*Listeria monocytogenes* is a member of the *Listeria* genus, which comprises of gram-positive bacteria having a low G+C content and bearing close relatedness to *Bacillus, Staphylococcus, Enterococcus, Clostridium* and *Streptococcus.* Members of the *Listeria spp.,* including *L. monocytogenes*, are facultatively anaerobic, non-spore forming, rods that are incapable of forming capsules and are motile at temperatures ranging from 10 - 30°C (Collins et al., 1991, Sallen et al., 1996). Their natural environmental habitat includes soil, water bodies, a variety of foods, sewage as well as animal and human faeces; however they are predominantly found in decomposing plant matter, which they use as a source of nutrition and lead a saprophytic lifestyle. Often, they do find their way into a variety of vertebrates, including humans as well as wild and domesticated animals and birds, where they cause debilitating localized and generalized infections (Freitag, 2006). Such infections are commonly termed as listeriosis; however the severity of the clinical manifestations of this disease depends on the underlying health status of the patients, with the disease being restricted to non-invasive and self-limiting gastroenteritis in individuals with an intact immune system (Drevets and Bronze, 2008). In individuals exhibiting compromised immune responses, such as the elderly and pregnant women, the disease is capable of breaching a variety of immune system barriers and therefore becomes invasive and causes systemic infections. Depending on the type of immune barrier breached, it can cause septicaemia (intestinal barrier), meningitis, encephalitis (blood-brain barrier), and in the case of pregnant women it can lead to either prenatal or neonatal (placental barrier) infections, resulting in abortions and still-births, respectively (Drevets and Bronze, 2008). Despite the fact that <1% of all reported cases of diseases caused by enteric pathogens (viral and bacterial) are *L. monocytogenes*-related, listeriosis accounts for the highest number of case-related premature deaths when compared to those caused by other bacterial enteric pathogens such as *Salmonella spp., Campylobacter spp.* and STEC (Shiga toxin-producing *E. coli* ) (Werber et al., 2013). This makes *L. monocytogenes* one of the most lethal bacterial enteric pathogens.

### 1.8.1 Infection cycle of *Listeria*

Being a facultative intracellular pathogen, L. monocytogenes is capable of invading, surviving and multiplying inside a multitude of cell types of the hosts including macrophages, epithelial and dendritic cells (Fig. 5) (Lecuit, 2007, Kolb-Maurer et al., 2000). Upon attachment to the

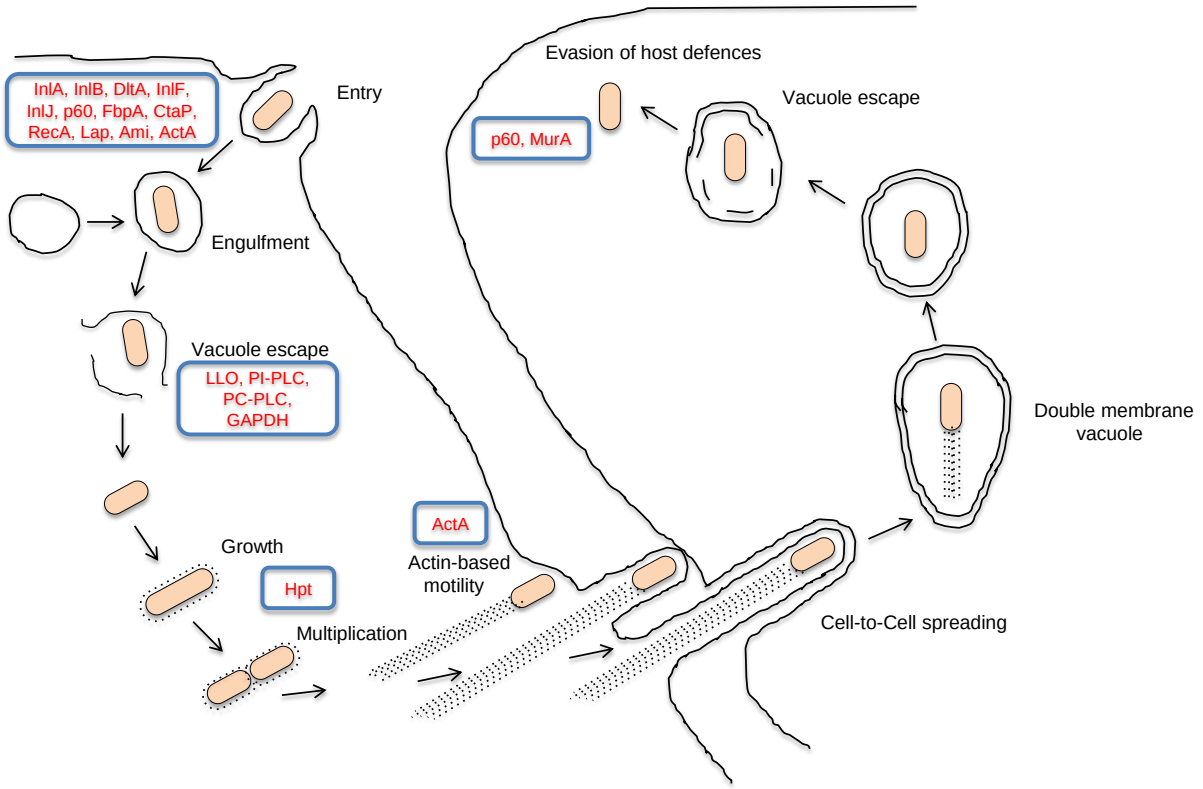


**Figure 5: *L. monocytogenes* infection cycle.** Diagrammatic representation of the infection cycle of *L. monocytogenes*. The various stages of the intracellular life cycle of Listeria, all the way from its entry into the host cell to the infection of adjacent cells via cell-to-cell spread, have been shown [adaptation of figure from Tilney and Portnoy (1989)]. Blue boxes with red text indicate some of the major virulence factors associated with each step of the infection cycle.

host cell, invasion is mediated via its engulfment into an internalization vacuole, which it quickly disrupts and escapes into the host cytoplasm. It is here that the bacterium freely replicates and moves around using an actin-based motility process that it uses for propulsion. In order to spread to neighbouring cells, it thrusts itself against the plasma membrane of the occupied host cell in the direction of the neighbouring cell (Kocks et al., 1995). As a result a double membrane protrusion is formed as it enters into the adjacent cell, which pinches off

into a secondary vacuole. This vacuole is lysed as well, allowing it to begin a fresh round of its infection cycle in adjoining cells (Camejo et al., 2011) .

### 1.8.2 Virulence factors of *L. monocytogenes*

Bacterial entry into mammalian cells is mediated via adhesion factors, which interact with host cell receptors thereby triggering specific host cell signalling pathways (Suarez et al., 2001). Lap, the surface-bound alcohol acetaldehyde dehydrogenase is known to interact with its corresponding host cell receptor, Hsp60, therefore stimulating the attachment of the bacterium to the intestinal epithelial cells (Burkholder and Bhunia, 2010, Pandiripally et al., 1999). The expression of the *lap* gene is stimulated by growth under anaerobic conditions followed by secretion of the protein via the accessory ATPase SecA2 (Burkholder et al., 2009). Another surface adhesion-associated protein is Ami, which exhibits N-acetylmuramoyl-L-alanine amidase activity (McLaughlan and Foster, 1998), and has been shown to facilitate adherence of the bacterium to human epithelial cells via its C-terminal cell wall-anchoring domain (CWA) (Burkholder et al., 2009, Milohanic et al., 2001, Milohanic et al., 2004). Other important adhesion factors include the fibronectin binding protein, FbpA (Dramsi et al., 2004), the D-alanine-polyphosphoribitol ligase, DltA (Abachin et al., 2002), as well as CtaP (cysteine transport-associated protein), LapB (Reis et al., 2010), ActA (Alvarez-Dominguez et al., 1997), RecA (van der Veen and Abee, 2011), and the members of the internalin family, InlF and InlJ (Sabet et al., 2008, Kirchner and Higgins, 2008).

Invasion of *L. monocytogenes* into macrophage cells is carried out by the macrophages itself due to its capacity to phagocytize microorganisms. However, for entry into non-phagocytotic cells, *Listeria* employs several specific invasion-associated factors. The expression of the genes encoding these invasion factors as well as other factors responsible for bacterial entry into the cytosol, intracellular growth, actin-based motility and cell-to-cell spread, are regulated by the virulence regulatory protein PrfA [reviewed in Freitag et al. (2009)]. The earliest identified and among the most important *L. monocytogenes* invasion proteins were internalins A (InlA) and B (InlB) (Dramsi et al., 1995, Gaillard et al., 1991). The internalin family, of which both these proteins are a part of, have 25 genes in *L. monocytogenes* EGD-e coding for them (Cabanes et al., 2002). Members of this family have characteristic protein architecture and are comprised of an N-terminal signal peptide sequence, which is followed by a leucine-rich repeat (LRR) region, a conserved IR (inter-repeat) domain, various other

repeats and variable motifs at its C-termini (Cabanes et al., 2002). It is the LRR region that mediates protein-protein interactions between the internalins and the host cell receptor proteins (Cabanes et al., 2002). InlA and 18 other internalins out of the 25 found in *L. monocytogenes* are covalently bound to the cell wall due the presence of the LPXTG motif (Cabanes et al., 2002). However, the interaction of InlB with the cell wall is achieved via non-covalent forces between the LTAs (lipoteichoic acids) of the cell wall and glycine-tryptophan repeats (GW repeats) present in its C-terminal domain (Jonquieres et al., 1999). InlA is recognized by the host cell receptor, E-cadherin, which is a transmembrane glycoprotein responsible for cell-cell adhesion (Mengaud et al., 1996, Smutny and Yap, 2010). On the other hand, InlB has a greatly elongated structure, due to which the cooperation of multiple receptors (gC1qR, glycosaminoglycans and c-Met) is required to mediate interaction of the host cell surface with InlB of *L. monocytogenes* for bacterial uptake (Marino et al., 2002, Marino et al., 1999, Schubert et al., 2001). Interaction of InlA with E-cadherin initiates host Src kinase activation, which ultimately results in E-cadherin endocytosis due to clathrin recruitment and polymerization of actin filaments (Sousa et al., 2007, Bonazzi et al., 2008). A similar clathrin-mediated endocytic mechanism for bacterial internalization is initiated by InlB-induced Met ubiquitination (Veiga and Cossart, 2005).

Upon engulfment, *Listeria* is enclosed in a phagocytic vacuole. In order to escape the vacuole, *L. monocytogenes* secretes a bacterial GAPDH which inactivates the host small GTPase, Rab5a, thereby delaying vacuole maturation (Alvarez-Dominguez et al., 2008). *L. monocytogenes* then utilizes Listeriolysin O (LLO), a secreted protein of the CDC (cholesterol-dependent cytolysin) family of toxins, to perforate vacuole membranes (Gedde et al., 2000, Gilbert, 2010, Portnoy et al., 1988). Disruption of the phagosomal membrane is also boosted by the expression of two types of phospholipases C (PLC), namely, phosphatidylcholine and phosphatidylinositol phospholipases C (PC-PLC and PI-PLC, respectively) (Geoffroy et al., 1991).

Once *L. monocytogenes* enters into the cytoplasm of the host cell, it expresses a variety of transporters and enzymes that enable it to replicate intracellularly with efficiency similar to that of its growth in pure culture (Cossart et al., 2003). One of the many proteins expressed is Hpt, which serves as a hexose phosphate transporter and allows the bacteria to take up glucose-1-phosphate from the host cell cytosol for its energy needs (Chico-Calero et al., 2002).

Movement within the host cytoplasm of *L. monocytogenes* is achieved by one of its main virulence factors, ActA. It is bound to the bacterial cytoplasmic membrane via a transmembrane hydrophobic tail at its C-terminal domain (Domann et al., 1992, Kocks et al., 1992). This protein leads to the formation of a structure that resembles the tail of a comet due to actin filament polymerization at one of the poles of the listerial cells that is mediated by its N-terminal region, allowing for movement within the cytosol of the host cell. This also allows the bacteria to invade adjoining cells by cell-to-cell spreading (Kocks et al., 1995).

### 1.8.3 Accessory virulence-mediating proteins

#### 1.8.3.1 SecA2

SecA2 was first identified in *L. monocytogenes* during studies aimed at characterizing the genes whose disruption or deletion leads to a smooth-rough colony morphology transition (Lenz and Portnoy, 2002). The ORF (Open Reading Frame) sequence of this SecA paralogue bears only 44% identity and 62% similarity to *L. monocytogenes* SecA; however, the translated sequence of SecA2 is homologous to SecA proteins of both *B. subtilis* and *E. coli* and retains important functional motifs such as the Walker-type ATP-binding domains A and B (Lenz and Portnoy, 2002). In *L.* monocytogenes, the domain organization of SecA2 is also nearly identical to that of SecA, with the only difference being that SecA2 lacks the C-terminal domain [reviewed by Bensing et al. (2014)]. *Streptococcus, Staphylococcus* and *Mycobacterium sp.* were also found to contain multiple *secA* paralogues (Lenz and Portnoy, 2002). A total of 17 proteins were identified to be SecA2-dependent in the culture supernatants of *L. monocytogenes*, of which the autolysins MurA (formerly known as NamA) and p60 (also known as CwhA) were found to be most abundant (Lenz et al., 2003). Both these protein substrates of SecA2 possess a canonical signal peptide (Lenz et al., 2003); however, one of the other identified substrates, namely the Mn-containing superoxide dismutase was shown to lack such an N-terminal signal peptide (Archambaud et al., 2006). *In vitro* cell culture infection experiments, aimed to quantify the role of SecA2 in the intracellular growth of bacteria in the cytosol of mammalian cells and bacterial cell-to-cell migration, showed that SecA2 is dispensable for intracellular replication but promotes cell-to-cell spreading of *L. monocytogenes* (Lenz et al., 2003). *In vivo* infection models using BALB/c mice, co-infected with *L. monocytogenes* wild type as well as the Δ*secA2* mutant, have demonstrated that SecA2 plays an important role in the later stages of infection

including cell-to-cell spreading, while it is expendable for bacterial entry by phagocytosis and the initial stages of intracellular replication (Lenz et al., 2003). Recent studies have shown that the cell division protein DivIVA influences the localization and subsequent secretion of p60 and MurA by SecA2 in the vicinity of the division septum, which facilitates cell separation upon completion of cell division (Halbedel et al., 2012).

#### 1.8.3.2 p60/CwhA

p60 is a surface-bound protein of *L. monocytogenes* having peptidoglycan hydrolase activity, and derives its name from the fact that it has a molecular weight of 60 kDa (kilodaltons) (Kuhn and Goebel, 1989). The protein possesses a distinct domain architecture and bears two highly conserved sections in the N and C-terminal regions (Bubert et al., 1992). The N-terminal of the protein contains a signal sequence, which is cleaved prior to secretion (Kohler et al., 1991), and the middle section of the protein contains a series of threonine-asparagine repeats and is highly variable (Bubert et al., 1992). The C-terminal region of p60 is believed to impart the hydrolytic activity due to its homology with other hydrolytic enzymes and the bacteriolysis caused when *iap* is overexpressed either in *B. subtilis* or *L. monocytogenes* (Wuenscher et al., 1993). It is encoded by the *iap* gene that lies directly upstream of the *secA2* gene (Lenz and Portnoy, 2002), and in its absence bacterial cells undergo chaining resulting in short filaments during the logarithmic growth phase (Pilgrim et al., 2003). The necessity of p60 for invasion was demonstrated using a Δ*iap* mutant, which displayed a decreased ability to invade epithelial cells and fibroblasts as compared to the *L. monocytogenes* wild type (Pilgrim et al., 2003, Kuhn and Goebel, 1989).

#### 1.8.3.3 MurA/NamA

MurA, encoded by the *murA* gene, is a 66 kDa cell surface protein having a characteristic N-terminal domain, which is homologous to gram-positive-specific muramidases, and a C-terminal domain that contains 4 copies of the LysM motif, with which MurA anchors itself to the cell wall (Carroll et al., 2003). The peptidoglycan hydrolase activity of MurA was demonstrated by utilizing the purified protein (generated *in E.* coli) to hydrolyse preparations of *Micrococcus lysodeikticus* cell wall (Carroll et al., 2003). Deletion of the *murA* gene in *L. monocytogenes* leads to formation of bacterial cell chains during logarithmic growth, but not during the lag phase, which is due to an inability of the individual Δ*murA* daughter cells to

separate after cell division (Carroll et al., 2003, Halbedel et al., 2012, Machata et al., 2005). Studies have shown that a simultaneous deletion of both MurA and p60 in *L. monocytogenes* results in cell chaining similar to that observed for the *secA2* deletion mutant (Halbedel et al., 2012, Machata et al., 2005). *In vitro* mammalian cell infection experiments show that the deletion mutant of *murA* displays slight attenuation in terms of bacterial invasion and cell-to-cell migration when compared to the *L. monocytogenes* wild type strain (Halbedel et al., 2012).

## 1.9 Aims of the project

This study aims to identify and characterize the putative interaction partners of *L. monocytogenes* DivIVA so as to answer two primary questions regarding DivIVA's function:

1) How does DivIVA effect the secretion of the autolysins p60 and MurA via the accessory ATPase SecA2?
2) Does DivIVA affect division site selection in *L. monocytogenes* via the Min system?

For this purpose, a variety of genetic techniques are to be employed that would help ascertain the involvement of DivIVA in the processes responsible for cell division of *L. monocytogenes*.

This work provides a variety of exciting possibilities including the opportunity of identifying factors having possibly vital functions in the cell division and infection cycles of *Listeria*. Not only would this give us a better insight into molecular mechanisms employed by DivIVA proteins to carry its myriad of physiological functions, but would also provide us with new targets for the screening of novel antimicrobial drugs.

# 2. Materials and Methods

## 2.1 Microbiological techniques

### 2.1.1 Bacterial strains and plasmids

The list of all the bacterial strains and plasmids used in this study can be found in the tables 2, 3 and 4, shown below:

**Table 2: Oligonucleotides used in this study.**

| Name | Sequence (5´→3´) | Description** |
|---|---|---|
| KK3 | CACCATCACCACCATCACCATTA AGTCGACCTCGAGGGGGG | removal of *gfp* and addition of *his10* into pIMK2 (fw) |
| KK4 | GTGGTGATGGTGATGGTGATGTT CGTTATCGTCCAGCTTATTTC | *gpsB* (*lmo1888*)-*his10* into pIMK2 (rev) |
| KK5 | GTGGTGATGGTGATGGTGATGG CCTTGGATTAAGCCGTCTGG | *secA2* (*lmo0583*)-*his10* into pIMK2 (rev) |
| KK6 | GCTCTAGAGAAAAAAGCAACTA TCGCGGC | *iap* (*lmo0582*)into BACTH plasmids (fw), XbaI |
| KK7 | CGGGGTACCACGCGACCGAAGC CAACTAG | *iap* into BACTH plasmids (rev), KpnI |
| KK8 | AACTGCAGAGCAAAAAACGAGA AAAGAACGA | *murA* (*lmo2691*) into BACTH plasmids (fw), PstI |
| KK9 | CGCGGATCCTTAATTGTTAATTT CTGACCAACATG | *murA* into BACTH plasmids (rev), BamHI |
| KK21 | GATCGTCGACTCTAGAGGATCCC CGCGCTCGAGTTATTCCTTTTCC TCAAATACAGC | replacement of $divIVA^{Lm}$ (*lmo2020*) with $divIVA^{Bs}$ in pIMK3 (rev) |
| KK36 | GCTCTAGAGATGGATGTTTTTGT TGAAATACTAAATGGA | *minJ* (*lmo2502*) into BACTH plasmids (fw), XbaI |
| KK37 | CGGGGTACCCGTCTTGGTTCTAT TAATAACAAACCAAG | *minJ* into BACTH plasmids (rev), KpnI |
| KK40 | GCTCTAGAGTTTAATTGGTACAA AAAATACCGCGAA | *lmo0720* into BACTH plasmids (fw), XbaI |
| KK41 | CGGGGTACCCGTTTAATCGAATC TCGCAATTTCTGACG | *lmo0720* into BACTH plasmids (rev), KpnI |
| KK42 | ATATGTCGACGCAAGCCAACTTC AAAACATAG | Upstream region of *lmo0720* into pMAD (fw), SalI |
| KK43 | GCATGCCATGGAAGGCAAGGTG GTGATCAAAG | Downstream region of *lmo0720* into pMAD (rev), NcoI |
| KK44 | GTAATGGGATCCTAAAAAAACA GAAAGCCTCTCAAAA | removal of *lmo720* and addition of BamHI site in pMAD (fw), BamHI |
| KK45 | TTTAGGATCCCATTACGCTTGCC CTCCTTTAAC | removal of *lmo720* and addition of BamHI site in pMAD (rev), BamHI |
| KK46 | GAAACCCATGGTTAATTGGTACA | *lmo0720* into pIMK3 (fw), NcoI |

| Name | Sequence (5´→3´) | Description** |
|---|---|---|
| | AAAAATACCGCG | |
| KK47 | ATATGTCGACTTATTTAATCGAA TCTCGCAATTTC | *lmo0720* into pIMK3 (rev), SalI |
| KK50 | GACGGCTTAATCCAAGGCTAAG TCGACCTCGAGGGGGGG | removal of *gfp* from pIMK2-*secA2-gfp* (fw) |
| KK51 | CCCCTCGAGGTCGACTTAGCCTT GGATTAAGCCGTCTGG | removal of *gfp* from pIMK2-*secA2-gfp* (rev) |
| KK54 | GGAACAAAACAACTGGCTAGTT AC | verification of *lmo0720* deletion (fw) |
| KK55 | CTCCTCCCATGGATGTTTTCTCT AATG | verification of *lmo0720* deletion (rev) |
| KK56 | TTTTAGGATCCTTAGTAGCCGTA TGTTTCTCCTC | removal of *lmo0719* from pMAD-Δ*lmo0720* (rev) |
| KK57 | TACTAAGGATCCTAAAAAAACA GAAAGCC | removal of *lmo0719* from pMAD-Δ*lmo0720* (fw) |
| KK58 | TCCCCCCGGGATGACTAGTATGA AGAAGAATGTTC | *minC-gfpA206K* into pIMK3 (fw), XmaI |
| KK59 | TTCTGCAGTTATTTGTATAGTTC ATCCATGCC | *minC-gfpA206K* into pIMK3 (rev), PstI |
| KK60 | CGCGGATCCATGGAAAAGGATC CCAGTAAAGGAG | *gfpA206K-minD* into pIMK3 (fw), BamHI |
| KK61 | ACGCGTCGACTTATTTTCCACTA AAAAGTTGCTTTAAG | *gfpA206K-minD* into pIMK3 (rev), SalI |
| KK66 | CATGCCATGGATGAAAGGACTT ACCGAGTTACTC | *lmo0719* into pIMK3 (fw), NcoI |
| KK67 | ATATGTCGACTTACGCTTGCCCT CCTTTAACTTG | *lmo0719* into pIMK3 (rev), SalI |
| KK68 | GCTCTAGAGAAGAAGAATGTTC AAATTAAAGGCAC | *minC* into BACTH plasmids (fw), XbaI |
| KK69 | CGGGGTACCACGCCCTCCTTGAA AATTAGAAAT | *minC* into BACTH plasmids (rev), KpnI |
| KK70 | GCTCTAGAGGGAGAAGCTATAG TCATTACTT | *minD* into BACTH plasmids (fw), XbaI |
| KK71 | CGGGGTACCTTTTCCACTAAAAA GTTGCTTTAAGCG | *minD* into BACTH plasmids (rev), KpnI |
| KK72 | CTAGCTAGCATGTTAGAATTTGA CACTAGTTCAGAAAG | *ftsZ* (*lmo2032*) into pIMK2 (fw), NheI |
| KK73 | CCCATCGATTCCGCGACGGTTAC GGTTACGG | *ftsZ* into pIMK2 (rev), ClaI |
| KK75 | CCTCCGCTAGCCATTTGAATTCA CTCCTCTACTAG | removal of *lmo0719* from pUC19-*lmo0718-721* (rev) |
| KK76 | AAATGGCTAGCGGAGGGCAAGC GTAATGTTTAATTG | removal of *lmo0719* from pUC19-*lmo0718-721* (fw) |
| KK77 | CGCGGATCCATGTTAGAATTTGA CACTAGTTCAGAAAG | *ftsZ-gfp* into pIMK3 (fw), BamHI |
| KK78 | ACGCGTCGACTTATTTGTATAGT TCATCCATGCC | *ftsZ-gfp* into pIMK3 (rev), SalI |
| KK79 | CATGCCATGGATGAAGAAGAAT GTTCAAATTAAAGGC | *minCD* (*lmo1545-1544*) into pIMK3 (fw), NcoI |
| KK80 | ACGCGTCGACTTATTTTCCACTA AAAAGTTGCTTTAAG | *minCD* into pIMK3 (rev), SalI |

| Name | Sequence (5´→3´) | Description** |
|---|---|---|
| KK81 | CATGCCATGGATGGATGTTTTTG TTGAAATACTA | *minJ* into pIMK3 (fw), NcoI |
| KK82 | ACGCGTCGACTTATCTTGGTTCT ATTAATAACAAACCAAG | *minJ* into pIMK3 (rev), SalI |
| KK83 | CCGTAACCGTAACCGTCGCGGAT AAGTCGACGATCCC | removal of *gfp* from pIMK3-*ftsZ-gfp* (fw) |
| KK84 | CAAAGCATAATGGGATCGTCGA CTTATCCGCGACGGTT | removal of *gfp* from pIMK3-*ftsZ-gfp* (rev) |
| KK111 | AAAACTGCAGATGGATGTTTTTG TTGAAATACTA | *minJ- gfp* into pIMK2 (fw), PstI |
| KK112 | CTAGACTAGTTCTTGGTTCTATT AATAACAAACCAAG | *minJ- gfp* into pIMK2 (rev), SpeI |
| SHW52 | ATATGTCGACACGAATTCGAGCT CGGTACCC | *divIVA-his10* into pIMK2 (rev), SalI |
| SHW134 | GCATGCCATGGAAGCTAGTAAC TATGGTAGAATG | $divIVA^{Bs\text{-}57\text{-}Lm}$ into pIMK3 (fw), NcoI |
| SHW208 | TAGAGTAATTCTGTAAAGGTCC | $divIVA^{Lm\text{-}57\text{-}Bs}$ into pIMK3 (fw) |
| SHW235 | CAGTTGTAAAAGGGGACTCAC | sequencing of *murA* (fw) |
| SHW266 | GCAGAAAAAAATGCTGACCGAA TTATCAACGAATCGTTATCAAAA TC | $divIVA^{Lm\text{-}140\text{-}Bs}$ into pIMK3 (fw) |
| SHW311 | AAAACTGCAGAGACAGAATTAT GATGATCG | *secA2* for cloning into pIMK2 (fw), PstI |
| SHW353 | CTTTAAATAATAGTGAAGAACGT ATCGGACACTTTGCCAATATTG | $divIVA^{Lm\text{-}57\text{-}Bs}$ into pIMK3 (rev) |
| SHW425 | CACAATCTAAACTTTCCAAAGAT CCCAACG | A206K mutation into *gfp* (fw) |
| SHW426 | GGAAAGTTTAGATTGTGTGGAC AGGTAATG | A206K mutation into *gfp* (rev) |
| SHW427 | GTGAAATACCGCACAGATGC | inverse PCR for pMC38 (fw) |
| SHW428 | GGCATCCGCTTACAGACAAG | inverse PCR for pMC38 (rev) |
| SHW437 | CTGGTCGGGAAACGGATATCAA ACTGG | G484E mutation into *secA2* (fw) |
| SHW438 | GATATCCGTTTCCCGACCAGCCA TGTTCG | G484E mutation into *secA2* (rev) |
| SV30 | GTATGTTGCATCACCTTCACCC | $divIVA^{Bs\text{-}57\text{-}Lm}$ into pIMK3 (rev) |

** The forward and reverse primers are denoted by (fw) and (rev) respectively, followed by the restriction site that they introduce into the amplified product.

**Table 3: Plasmids and used in this study**

| Name | relevant characteristics | source*/ reference |
|---|---|---|
| pAUL-A | *lacZα erm* | (Chakraborty et al., 1992) |
| pIMK2 | $P_{help}$ *neo* | (Monk et al., 2008) |
| pIMK3 | $P_{help}$-*lacO lacI neo* | (Monk et al., 2008) |
| pMAD | *bla erm bgaB* | (Arnaud et al., 2004) |
| pMC38 | Transposon delivery vector | (Cao et al., 2007) |
| pUT18 | *bla* $P_{lac}$-*cya(T18)* | (Karimova et al., 1998) |
| pUT18C | *bla* $P_{lac}$-*cya(T18)* | (Karimova et al., 1998) |

| Name | relevant characteristics | source*/ reference |
|---|---|---|
| pKT25 | *kan* $P_{lac}$-*cya(T25)* | (Karimova et al., 1998) |
| p25-N | *kan* $P_{lac}$-*cya(T25)* | (Karimova et al., 1998) |
| pKK1 | $P_{help}$-*gpsB-his10 neo* | *lmo1888-his10*, (KK3/KK4), pIMK2 |
| pKK3 | $P_{help}$-*secA2-his10 neo* | *lmo0583-his10*, (KK3/KK5), pIMK2 |
| pKK4 | $P_{help}$-*divIVA-his10 neo* | *lmo2020-his10*, (SHW134/SHW52), pIMK2 |
| pKK5 | *kan* $P_{lac}$-*iap-cya(T25)* | *lmo0582*, (KK6/KK7), pKNT25 |
| pKK6 | *kan* $P_{lac}$-*cya(T25)-murA* | *lmo2691*, (KK8/KK9), pKT25 |
| pKK7 | *bla* $P_{lac}$-*iap-cya(T18)* | *lmo0582*, (KK6/KK7), pUT18 |
| pKK8 | *bla* $P_{lac}$-*cya(T18)-iap* | *lmo0582*, (KK6/KK7), pUT18C |
| pKK9 | *bla* $P_{lac}$-*murA-cya(T18)* | *lmo2691*, (KK8/KK9), pUT18 |
| pKK10 | *kan* $P_{lac}$-*cya(T25)-iap* | *lmo0582*, (KK6/KK7), pKT25 |
| pKK11 | *kan* $P_{lac}$-*murA-cya(T25)* | *lmo2691*, (KK8/KK9), pKNT25 |
| pKK16 | $P_{help}$-*lacO-* $P_{divIVA}^{Lm}$- $divIVA^{Bs}$ *lacI neo* | $P_{lmo2020}$- $divIVA^{Bs}$, (megaprimer KK20, KK21), pIMK3 |
| pKK17 | $P_{help}$-*lacO-* $P_{divIVA}^{Lm}$- $divIVA^{Lm\text{-}104\text{-}Bs}$ *lacI neo* | $P_{lmo2020}$- *lmo2020* 104 a.a- $divIVA^{Bs}$, (megaprimer SHW266, KK21), pIMK3 |
| pKK18 | $P_{help}$-*lacO-* $P_{divIVA}^{Lm}$- $divIVA^{Lm\text{-}57\text{-}Bs}$ *lacI neo* | $P_{lmo2020}$- *lmo2020* 57 a.a- $divIVA^{Bs}$, (megaprimer SHW353, SHW208), pIMK3 |
| pKK21 | $P_{help}$-*lacO-* $P_{divIVA}^{Lm}$- $divIVA^{Bs\text{-}57\text{-}Lm}$ *lacI neo* | $P_{lmo2020}$- $divIVA^{Bs}$ 57 a.a- *lmo2020*, (SHW134/SV30), pIMK3 |
| pKK25 | *kan* $P_{lac}$-*cya(T25)-minJ* | *lmo2502*, (KK36/KK37), pKT25 |
| pKK26 | *bla* $P_{lac}$-*minJ-cya(T18)* | *lmo2502*, (KK36/KK37), pUT18 |
| pKK32 | *kan* $P_{lac}$-*minJ-cya(T25)* | *lmo2502*, (KK36/KK37), pKNT25 |
| pKK33 | *bla* $P_{lac}$-*cya(T18)-minJ* | *lmo2502*, (KK36/KK37), pUT18C |
| pKK35 | *bla* $P_{lac}$-*secY-cya(T18)* | *lmo2612*, (KK38/KK39), pUT18 |
| pKK36 | $P_{help}$-*secA2 neo* | *lmo0583*, (SHW311/KK53), pIMK2 |
| pKK37 | *bla* Δ*lmo0720* | Δ*lmo0720*, (ligation product of KK42/KK45-KK43/KK44), (KK42/KK43), pUC19 |
| pKK38 | $P_{help}$-*secA2G484E neo* | *lmo0583G484E*, (SHW437/SHW438), $pKK36^{QC**}$ |
| pKK39 | *bla erm bgaB* Δ*lmo0720* | Δ*lmo0720*, from pKK37 into pMAD |
| pKK40 | *bla erm bgaB* Δ*lmo0719-720* | Δ*lmo0719-720*, (KK56/KK57), $pKK39^{QC**}$ |
| pKK41 | $P_{help}$-*lacO-minC-gfpA206K lacI neo* | *lmo1545-gfpA206K*, (KK58/KK59), pIMK3 |
| pKK42 | $P_{help}$-*lacO-gfpA206K-minD lacI neo* | *gfpA206K-lmo1544*, (KK60/KK61), pIMK3 |
| pKK43 | $P_{help}$-*lacO-lmo0719 lacI neo* | *lmo0719*, (KK66/KK67), pIMK3 |
| pKK44 | *bla* $P_{lac}$-*cya(T18)-minC* | *lmo1545*, (KK68/KK69), pUT18C |
| pKK45 | *bla* $P_{lac}$-*minD-cya(T18)* | *lmo1544*, (KK70/KK71), pUT18 |
| pKK46 | *bla* $P_{lac}$-*cya(T18)-minD* | *lmo1544*, (KK70/KK71), pUT18C |
| pKK47 | *kan* $P_{lac}$-*minC-cya(T25)* | *lmo1545*, (KK68/KK69), pKNT25 |
| pKK48 | *kan* $P_{lac}$-*cya(T25)-minD* | *lmo1544*, (KK70/KK71), pKT25 |
| pKK49 | *kan* $P_{lac}$-*minD-cya(T25)* | *lmo1544*, (KK70/KK71), pKNT25 |
| pKK50 | *kan* $P_{lac}$-*cya(T25)-minC* | *lmo1545*, (KK68/KK69), pKT25 |
| pKK51 | $P_{help}$-*ftsZ-gfp neo* | *lmo2032-gfp*, (KK72/KK73), pIMK2 |
| pKK52 | *bla* $P_{lac}$-*minC-cya(T18)* | *lmo1545*, (KK68/KK69), pUT18 |
| pKK53 | *bla lmo0718-721* | *lmo0718-721*, (KK42/KK43), pUC19 |
| pKK54 | *bla* Δ*lmo0719* | Δ*lmo0719*, (KK75/KK76), $pKK53^{QC**}$ |
| pKK55 | $P_{help}$-*lacO-ftsZ-gfp lacI neo* | *lmo2032-gfp*, (KK77/KK78), pIMK3 |
| pKK56 | *bla erm bgaB* Δ*lmo0719* | Δ*lmo0719*, from pKK54 into pMAD |
| pKK57 | $P_{help}$-*lacO-minCD lacI neo* | *lmo1545-1544*, (KK79/KK80), pIMK3 |
| pKK58 | $P_{help}$-*lacO-minJ lacI neo* | *lmo2502*, (KK81/KK82), pIMK3 |
| pKK59 | $P_{help}$-*lacO-ftsZ lacI neo* | *lmo2032*, (KK77/KK84), pIMK3 |
| pKK64 | *bla erm bgaB lmo0720::Tn* | *lmo0720::Tn* from LMKK18, (KK42/43), pMAD |

| Name | relevant characteristics | source*/ reference |
|---|---|---|
| pKK77 | $P_{help}$-*minJ-gfp* | *lmo2502-gfp*, (KK111/KK112), pIMK2 |
| pSH186 | *bla erm bgaB* Δ*divIVA* | (Halbedel et al., 2012) |
| pSH195 | $P_{help}$-*gfp neo* | (Halbedel et al., 2012) |
| pSH222 | *bla* $P_{lac}$-*divIVA-cya(T18)* | Sven Halbedel, |
| pSH223 | *bla* $P_{lac}$-*cya(T18)-divIVA* | Sven Halbedel |
| pSH224 | *kan* $P_{lac}$-*cya(T25)-divIVA* | Sven Halbedel |
| pSH225 | *kan* $P_{lac}$-*divIVA-cya(T25)* | Sven Halbedel |
| pSH295 | *bla* $P_{lac}$-*secA2-cya(T18)* | Sven Halbedel |
| pSH296 | *bla* $P_{lac}$-*cya(T18)-secA2* | Sven Halbedel |
| pSH297 | *kan* $P_{lac}$-*cya(T25)-secA2* | Sven Halbedel |
| pSH298 | *kan* $P_{lac}$-*secA2-cya(T25)* | Sven Halbedel |
| pSH303 | $P_{help}$-*secA2-gfp neo* | (Halbedel et al., 2012) |
| pSH314 | *bla erm bgaB* Δ*secA2* | (Halbedel et al., 2012) |
| pSH363 | $P_{help}$-*lacO-lmo0720 lacI neo* | Sven Halbedel |
| pSH378 | *bla erm bgaB* Δ*minCD* | Sven Halbedel |
| pSH379 | *bla erm bgaB* Δ*minJ* | Sven Halbedel |

*Escherichia coli* TOP 10 was used as the standard plasmid host for all cloning procedures (Sambrook, 1989).

* Description for the newly constructed plasmids includes the gene/gene fragment that was cloned, the primers used, and the recipient plasmid.

** Quick change modifications are denoted by the "QC" superscript on recipient plasmids.

**Table 4: Strains used in this study**

| Name | relevant characteristics | source*/ reference |
|---|---|---|
| EGD-e | wild-type, serovar 1/2a strain | (Glaser et al., 2001) |
| LMKK1 | *attB*::$P_{help}$-*gpsB-his10 neo* | pKK1 → EGD-e |
| LMKK3 | *attB*::$P_{help}$-*secA2-his10 neo* | pKK3 → EGD-e |
| LMKK4 | *attB*::$P_{help}$-*divIVA*$^{Lm}$-*his10 neo* | pKK4 → EGD-e |
| LMKK7 | *attB*::$P_{help}$-*lacO*-$P_{divIVA}$-*divIVA*$^{Bs}$ *lacI neo* | pKK16 → EGD-e |
| LMKK8 | Δ*divIVA*$^{Lm}$ *attB*::$P_{help}$-*lacO*-$P_{divIVA}$-*divIVA*$^{Bs}$ *lacI neo* | pSH186 ↔ LMKK7 |
| LMKK9 | *attB*::$P_{help}$-*lacO*-$P_{divIVA}$-*divIVA*$^{Lm\text{-}57\text{-}Bs}$ *lacI neo* | pKK18 → EGD-e |
| LMKK10 | *attB*::$P_{help}$-*lacO*-$P_{divIVA}$-*divIVA*$^{Lm\text{-}104\text{-}Bs}$ *lacI neo* | pKK17 → EGD-e |
| LMKK11 | *attB*::$P_{help}$-*lacO*-$P_{divIVA}$-*divIVA*$^{Bs\text{-}57\text{-}Lm}$ *lacI neo* | pKK21 → EGD-e |
| LMKK12 | Δ*divIVA*$^{Lm}$ *attB*::$P_{help}$-*lacO*- $P_{divIVA}$- *divIVA*$^{Lm\text{-}57\text{-}Bs}$ *lacI neo* | pSH186 ↔ LMKK9 |
| LMKK13 | Δ*divIVA*$^{Lm}$ *attB*::$P_{help}$-*lacO*-$P_{divIVA}$-*divIVA*$^{Lm\text{-}104\text{-}Bs}$ *lacI neo* | pSH186 ↔ LMKK10 |
| LMKK14 | Δ*divIVA*$^{Lm}$ *attB*::$P_{help}$-*lacO*-$P_{divIVA}$-*divIVA*$^{Bs\text{-}57\text{-}Lm}$ *lacI neo* | pSH186 ↔ LMKK11 |
| LMKK15 | *attB*::$P_{help}$-*minC-gfpA206K neo* | pKK29 → EGD-e |
| LMKK16 | *attB*::$P_{help}$-*gfpA206K-minD neo* | pKK30 → EGD-e |
| LMKK18 | *lmo0720::Tn secA2G484E* | pMC38 ↔ EGD-e |
| LMKK19 | *attB*::$P_{help}$-*lacO-lmo0720 lacI neo* | pSH363 → EGD-e |
| LMKK20 | *lmo0720::Tn secA2G484E attB*::$P_{help}$-*secA2-gfp neo* | pSH303 → LMKK18 |
| LMKK20R | *lmo0720::Tn secA2G484E attB*::$P_{help}$-*secA2-gfp G484E neo* (rough colony isolate of LMKK20) | |
| LMKK21 | Δ*secA2 attB*::$P_{help}$-*secA2-gfp neo* | pSH303 → LMS81 |
| LMKK21R | Δ*secA2 attB*::$P_{help}$-*secA2-gfp neo* | |

| Name | relevant characteristics | source*/ reference |
|---|---|---|
| | (rough colony isolate of LMKK21) | |
| LMKK24 | *attB::*$P_{help}$*-secA2 neo* | pKK36 → EGD-e |
| LMKK25 | *attB::*$P_{help}$*-secA2G484E neo* | pKK38 → EGD-e |
| LMKK26 | Δ*lmo0720* | pKK39 ↔ EGD-e |
| LMKK27 | Δ*secA2 attB::*$P_{help}$*-secA2 neo* | pSH314 ↔ LMKK24 |
| LMKK28 | Δ*secA2 attB::*$P_{help}$*-secA2G484E neo* | pSH314 ↔ LMKK25 |
| LMKK29 | *attB::*$P_{help}$*-lacO-minC-gfpA206K lacI neo* | pKK41 → EGD-e |
| LMKK30 | *attB::*$P_{help}$*-lacO-gfpA206K-minD lacI neo* | pKK42 → EGD-e |
| LMKK31 | Δ*lmo0719-720* | pKK40 ↔ EGD-e |
| LMKK32 | Δ*divIVA attB::*$P_{help}$*-lacO-minC-gfpA206K lacI neo* | pSH186 ↔ LMKK29 |
| LMKK33 | Δ*divIVA attB::*$P_{help}$*-lacO-gfpA206K-minD lacI neo* | pSH186 ↔ LMKK30 |
| LMKK34 | *attB::*$P_{help}$*-lacO-lmo0719 lacI neo* | pKK43 → EGD-e |
| LMKK35 | Δ*minCD (lmo1545-1544)* | pSH378 ↔ EGD-e |
| LMKK36 | Δ*minCD attB::*$P_{help}$*-gfp neo* | pSH195 → LMKK35 |
| LMKK37 | Δ*minJ attB::*$P_{help}$*-gfp neo* | pSH195 → LMS120 |
| LMKK38 | *attB::*$P_{help}$*-lacO-ftsZ-gfp lacI neo* | pKK55 → EGD-e |
| LMKK39 | Δ*divIVA attB::*$P_{help}$*-lacO-ftsZ-gfp lacI neo* | pKK55 → LMS2 |
| LMKK40 | Δ*minCD attB::*$P_{help}$*-lacO-ftsZ-gfp lacI neo* | pKK55 → LMKK35 |
| LMKK41 | Δ*minJ attB::*$P_{help}$*-lacO-ftsZ-gfp lacI neo* | pKK55 → LMS120 |
| LMKK42 | Δ*lmo0719* | pKK56 ↔ EGD-e |
| LMKK43 | Δ*minCD attB::*$P_{help}$*-lacO-minCD lacI neo* | pKK57 → LMKK35 |
| LMKK44 | Δ*minJ attB::*$P_{help}$*-lacO-minJ lacI neo* | pKK58 → LMS120 |
| LMKK45 | *attB::*$P_{help}$*-lacO-ftsZ lacI neo* | pKK59 → EGD-e |
| LMKK46 | Δ*minCD attB::*$P_{help}$*-lacO-ftsZ lacI neo* | pKK59 → LMKK35 |
| LMKK47 | Δ*minJ attB::*$P_{help}$*-lacO-ftsZ lacI neo* | pKK59 → LMS120 |
| LMKK54 | Δ*minCDJ* | pSH379 ↔ LMKK35 |
| LMKK55 | Δ*minJ attB::*$P_{help}$*-lacO-minC-gfpA206K lacI neo* | pKK41 → LMS120 |
| LMKK56 | Δ*minJ attB::*$P_{help}$*-lacO-gfpA206K-minD lacI neo* | pKK42 → LMS120 |
| LMKK62 | Δ*lmo0719 attB::*$P_{help}$*-lmo0719* | pKK43 → LMKK42 |
| LMKK64 | *lmo0720::Tn* | pKK64 ↔ EGD-e |
| LMKK71 | *attB::*$P_{help}$*-minJ-gfp* | pKK77 → EGD-e |
| LMKK72 | Δ*divIVA attB::*$P_{help}$*-minJ-gfp* | pKK77 → LMS2 |
| LMS2 | Δ*divIVA* | (Halbedel et al., 2012) |
| LMS10 | *attB::*$P_{help}$*-gfp neo* | (Halbedel et al., 2012) |
| LMS30 | *ΔdivIVA attB::*$P_{help}$*-lacO-PdivIVA-divIVA lacI neo* | (Halbedel et al., 2012) |
| LMS54 | Δ*divIVA attB::*$P_{help}$*-gfp neo* | (Halbedel et al., 2012) |
| LMS81 | Δ*secA2* | (Halbedel et al., 2012) |
| LMS120 | Δ*minJ* | Sven Halbedel |
| LMS124 | Δ*divIVA* Δ*minJ* | Sven Halbedel |
| LMS125 | Δ*divIVA* Δ*minCD* | Sven Halbedel |
| LMS127 | Δ*divIVA* Δ*secA2* | Sven Halbedel |

* The arrow (→) stands for a transformation event and the double arrow (↔) indicates gene deletions obtained by chromosomal insertion and subsequent excision of pMAD plasmid derivatives (see experimental procedures for details).

### 2.1.2 Growth media

All solutions, buffers and media were prepared using deionized water followed by autoclaving at 121°C, 2 bar for 20 min. Solvents, other than water, for making solutions have been indicated if used. Filter sterilization was employed for thermolabile substances after dissolution in their respective solvents. Growth media were also supplemented with antibiotics, when and where required, depending on the selection criteria.

#### 2.1.2.1 Media used for *Escherichia coli*

| | | |
|---|---|---|
| **Luria Bertani Medium** | Trypton | 10 g |
| | Yest extract | 5 g |
| | Sodium chloride | 10 g |
| | $dH_2O$ | ad. 1 l |
| **LB Agar** | add 10 g agar per litre | |

#### 2.1.2.2 Media used for *Listeria monocytogenes*

The Brain Heart Infusion (BHI) broth was available in the form of a desiccated powder provided by Oxoid Ltd. (Cat-No: CM1135) and was prepared and used as per their directions. For solidification, agar was added to a final concentration of 1% (w/v) to liquid BHI medium.

#### 2.1.2.3 Antibiotics and other additives

All antibiotics and selection additives used in this study (Table. 5) were prepared by dissolving the required amount in 10 ml of their respective solvents, after which they were filter sterilized and stored at -20°C as 1 ml aliquots. The aliquots were always thawed on ice and added fresh to autoclaved media which were cooled to approximately 50°C prior to use. The table below indicates the final concentration of antibiotics and additives used depending on the organism in question.

**Table 5: Antibiotics and other additives**

| **Antibiotic** | **Stock solution** | **Selection concentration** | |
|---|---|---|---|
| | | *E. coli* | *Listeria* |
| Ampicillin | 100 mg/ml | 100 µg/ml | - |
| Kanamycin | 50 mg/ml | 50 µg/ml | 50 µg/ml |
| Erythromycin | 5 mg/ml (Ethanol) | - | 5 µg/ml |
| | 100 mg/ml (Ethanol) | 300 µg/ml | - |
| **Additive** | **Stock solution** | **Selection concentration** | |
| | | *E. coli* | *Listeria* |
| X-Gal | 50 mg/ml (DMSO) | 100 µg/ml | 100 µg/ml |
| IPTG | 1 M | 1 mM | 1 mM |

### 2.1.3 Bacterial cultivation techniques

#### 2.1.3.1 Cultivation of *E. coli* and its storage

*E. coli* was propagated overnight at 37°C with 250 rpm shaking in 10 ml capped glass test tubes containing 3 ml LB broth with/without antibiotics or additives. These cultures were initially seeded using single colonies from fresh agar plates that were incubated overnight.

Temporary storage of these cultures was done on LB agar plates for up to 1 week at 4°C. Long-term storage demanded these cultures to be mixed with a 50% glycerol solution to give a final concentration of 25%, followed by freezing and storage at -80°C.

#### 2.1.3.2 Cultivation of *L. monocytogenes* and its storage

*L. monocytogenes* was grown, unless otherwise stated, at 37°C overnight in 3 ml BHI broth in capped 10 ml glass test tubes with 250 rpm shaking with/without antibiotics or additives. Inoculation of these cultures was done with single colonies from BHI agar plates.

Due to the ability of *L. monocytogenes* to grow even at 4°C, cultures were stored on BHI agar plates at 4°C on a temporary basis for not more than one week. Storage of these cultures as 25% glycerol stocks at -80°C was performed for long-term storage.

## 2.2 Molecular biological and biochemical techniques

### 2.2.1 Genetic manipulation of *E. coli* and *L. monocytogenes*

#### 2.2.1.1 Preparation of chemically competent *E. coli*

Firstly, an overnight culture of *E. coli* TOP 10 was established at 37°C in 3 ml LB broth in a capped 10 ml glass test tube with shaking at 250 rpm. This was then used as a pre-culture to inoculate 25 ml of fresh LB broth in a ratio of 1:100 in a 50 ml Falcon tube. The same culturing conditions were employed as stated above for 2 h till an $OD_{600}$ value of approx. 0.3 – 0.4 was reached. The cells were collected by means of a pre-cooled centrifuge (5 min, 4629 x g, 4°C). The supernatant was discarded; the cell pellet was re-suspended in 12.5 ml of ice-cold 0.1 M $CaCl_2$, followed by incubation on ice for at least 30 min. Cells were collected in the same manner as above and then the pellet was re-suspended in 1 ml of the ice-cold 0.1 M $CaCl_2$ solution. The chemically competent *E. coli* was stored on ice till it was used up the very same day and was always freshly prepared.

#### 2.2.1.2 Transformation of chemically competent *E. coli*

Unless otherwise mentioned, the transformation mixture was prepared by gently mixing 100 – 200 µl of the freshly prepared chemically competent *E. coli* with the genetic material to be transformed (1 µl whole plasmids/ 20 µl ligations) and incubated on ice for 30 min. This mixture was heat-shocked at 42°C for 1 min in a water-bath and then re-incubated on ice for 3 min. 900 µl of fresh, sterile LB broth was added to this transformation mixture and incubated for 1 h at 37°C with shaking at 250 rpm. 100 µl of this transformation mixture as well as the remaining 900 µl (spun down and suspended in 100 µl) were plated on separate selective LB agar plates and incubated overnight at 37°C.

#### 2.2.1.3 Preparation of electrocompetent *L. monocytogenes*

An overnight pre-culture of *L. monocytogenes* was prepared in 3 ml LB broth in a 10 ml capped glass test tube at 37°C with shaking at 250 rpm. After measuring its $OD_{600}$ value, it was used to seed 50 ml of fresh, sterile BHI broth in a 200 ml Erlenmeyer flask to give a start $OD_{600}$ value of approx. 0.01 – 0.02. This culture was grown at 37°C with 250 rpm shaking till $OD_{600}$ = 0.2 – 0.25, after which ampicillin was added to a final concentration of 10 µg/ml and

then returned to the same shaker for an additional 2 h. The cell culture was cooled down on ice for 10 min. The cells were centrifuged (10 min, 12857 x g, 4°C) and then re-suspended in 50 ml of ice-cold SGWB with gentle swirling on ice. This cell collection and re-suspension cycle was repeated with decreasing volumes of SGWB (17.5 ml and then 5 ml) followed by an incubation of 20 min at 37°C after addition of lysozyme to a final concentration of 10 µg/ml. After a wash with 2 ml of SGWB, the cell pellet was re-suspended in 250 µl of SGWB, 5 aliquots of 50 µl were made and stored at -80°C.

| | | |
|---|---|---|
| **SGWB buffer** | Glycerol | 100 ml |
| | Sucrose | 171.15 g |
| | $dH_2O$ | ad. 1 l |
| | pH 7.0 with 100 mM NaOH (filter sterilized) | |

#### 2.2.1.4 Electroporation of *L. monocytogenes*

1 µg of precipitated plasmid DNA was mixed with 25 µl of electrocompetent *L. monocytogenes* and incubated on ice for 5 min; in the meanwhile, 1.5 mm electroporation cuvettes (Carl Roth GmbH + Co. KG) were also pre-cooled on ice. The electroporation mixture was gently placed between the two electrodes of the cuvette and pulsed (4000 Ω, 330 µF, 300 V (low V) with an electric field value of 12500 V/cm for a 0.15 cm cuvette). Following this, the electroporated cells were regenerated in 1 ml of sterile BHI broth by statically incubating it at 30°C for 1.5 h. This transformation sample was spun down, plated on selective BHI agar plates and incubated overnight at either 37°C or for up to three days at 30°C (depending on the vector used).

#### 2.2.1.5 Allelic replacement in *L. monocytogenes*

This method was employed to create clean gene deletion mutants of *L. monocytogenes* without the introduction of exogenous DNA fragments (antibiotic resistance markers) to disrupt gene function. This approach circumvents the undesirable polar effects on the expression of downstream genes that result from insertion of foreign DNA into a gene operon. The pMAD plasmid was utilized for this purpose as described by Arnaud *et al.* (Arnaud et al., 2004), where the upstream and downstream DNA fragments flanking the gene to be replaced were cloned in tandem into the plasmid backbone, being separated by a short DNA segment

comprising of the start codon, a restriction site and the stop codon of the gene to be deleted. Upon construction of this vector, it was electroporated into the *L. monocytogenes* strain of choice and plated on BHI agar plates containing X-Gal and erythromycin and incubated at 30°C for 2 days. Several blue colonies (clones carrying the plasmid as an extrachromosomal replicon) were randomly selected and streaked out upon the same, but fresh, plates and incubated for an additional 2 days at 42°C in order to facilitate chromosomal integration. Several colonies from these plates were inoculated into 3 ml of fresh BHI broth (without any antibiotics), which was initially incubated for 2 h at 30°C with shaking at 180 rpm and then was moved to 40°C for 6 h. The resultant culture was serially diluted and the $10^{-4}$ and $10^{-5}$ dilutions were plated on BHI agar plates containing only X-Gal. All white colonies were picked and streaked out in parallel on BHI X-Gal and BHI X-Gal erythromycin plates, to identify white clones that had undergone a double crossover event, and hence had lost the plasmid along with the antibiotic resistance marker in the process. PCR analysis was performed to corroborate the clean deletion of the gene of interest as well as the loss of the plasmid.

#### 2.2.1.6 *HimarI* mariner-based transposon mutagenesis

This approach was utilized in order to generate a library of transposon mutants by means of mutagenesis of the entire *L. monocytogenes* genome. This transposon mutant library would then be phenotypically screened for the disruption of specific bacterial functions, hence identifying the gene/s responsible for them. As described by Cao et al., (Cao et al., 2007), the *HimarI* mariner-based transposon delivery vector, pMC38, was electroporated into *L. monocytogenes* and selected on BHI agar plates containing erythromycin at 30°C. Five colonies were randomly chosen and grown overnight at 30°C in BHI broth supplemented with kanamycin and erythromycin with shaking at 180 rpm to allow for maintenance of the plasmid . These overnight cultures were diluted in a ratio of 1:200 in fresh BHI broth containing only erythromycin, followed by incubation at 30°C for 1 h with 180 rpm shaking (to allow the plasmid to replicate), after which the temperature was increased to 42°C for 6 h till an $OD_{600}$ value of 0.3 – 0.5 was achieved. At this point the transposition takes place, inserting the *ermC* cassette bearing transposon into the genome while the kanamycin cassette containing plasmid is lost. These cultures were serially diluted and plated on both BHI erythromycin as well as BHI kanamycin plates to determine the CFU/ml and rate of plasmid retention, and then mixed with 50% glycerol and frozen at -80°C.

### 2.2.2 Techniques for analysis and modification of DNA

DNA was resolved in $dH_2O$ and, unless otherwise stated, kept on ice. For the purpose of storage, these DNA containing aliquots (chromosomal DNA, oligonucleotides, PCR products, plasmids and DNA fragments) were always frozen and stored at -20°C and were defrosted on ice just prior to use. Sequencing of DNA based samples was done by the In-house sequencing facility at the Robert Koch Institute.

#### 2.2.2.1 Isolation of *L. monocytogenes* chromosomal DNA

A 3 ml overnight culture was established in BHI broth at 37°C with shaking at 250 rpm. 1 ml of this culture was centrifuged (15700 x g, 1 min) to harvest the cells and the resultant cell pellet was re-suspended with 400 µl of TES buffer to which lysozyme was added at a final concentration of 10 mg/ml. This mixture was incubated at 37°C with constant shaking for approx. 40 min – 1 h, followed by the addition of 40 µl of 20% SDS solution. Proteins were precipitated by adding 400 µl of phenol: chloroform: isoamyl alcohol (25:24:1) and shaking the mixture vigorously. Two distinct phases were obtained by centrifuging this mixture at 15700 x g for 4 min, after which the upper aqueous phase was carefully pipetted out into a separate 1.5 ml eppendorf tube containing 500 µl of chloroform. This suspension was thoroughly agitated and the aqueous phase was pipetted out into an eppendorf tube containing 1 ml of 100% ethanol after centrifugation. On gentle mixing, strands of precipitated DNA became apparent, which were then pelleted and washed with 70% ethanol. This DNA pellet was air-dried, re-suspended in 100 – 200 µl TE buffer and then utilized immediately or stored at -20°C.

| | | |
|---|---|---|
| **TES Buffer** | 1 M EDTA pH 7.5 | 1 ml |
| | 20% SDS | 5 ml |
| | 1 M Tris-HCl pH 7.5 | 10 ml |
| | $dH_2O$ | ad. 1 l |
| **TE Buffer (100 ml)** | 0.5 M EDTA pH 8.0 | 0.2 ml |
| | 1M Tris-HCl pH 8.0 | 1 ml |
| | $dH_2O$ | ad. 100 ml |

#### 2.2.2.2 Isolation of plasmid DNA

Extraction of plasmid DNA from *E. coli* TOP 10 strains was done utilizing the QIAprep spin miniprep kit (QIAGEN). *E. coli* TOP 10 harbouring the desired plasmid was firstly grown in 3 ml of LB broth containing the corresponding antibiotic over night at 37°C with aeration at 250 rpm. The cells were pelleted at 15700 x g for 1 min, after which the plasmid was extracted from them as per the manufacturer's instructions and resolved in 100 µl of $dH_2O$. The identity of the plasmid was always verified by means of a 1 h analytical restriction digest and verification of the insert´s sequence by DNA sequencing before being either used for further experiments or for storage at -20°C.

#### 2.2.2.3 Agarose gel electrophoresis and staining

Separation and visualization of DNA fragments, including plasmids and PCR products, were achieved using 1% agarose gels made with 1 x TAE buffer. Mixing the samples in a 5:1 ratio with 5 x loading buffer facilitated their loading and migration monitoring. The Mini-Sub®/wide Cell GT System (Bio-Rad Laboratories, Inc) with gel-casting trays and combs was used to pour and run these gels. Running conditions and time varied from 100 – 120 V and 30 – 45 min respectively, depending on the size of the gel, degree of separation needed and the final fate of the fragments (analytical or preparative). Visualization and image acquisition was accomplished using the Molecular Imager® Gel Doc™ XR documentation system running the Quantity One® 1-D analysis software ((Bio-Rad Laboratories, Inc).

#### 2.2.2.4 Polymerase chain reaction (PCR) techniques: standard, overlap extension, site-directed plasmid mutagenesis and inverse PCR

PCR reaction mixtures ranging from volumes 10 – 200 µl (depending on their purpose) were prepared in thin walled PCR µl reaction tubes. The oligonucleotide primers used for these reactions were custom designed and purchased from Eurofins MWG Operon. These reaction mixtures were always purified prior to subsequent use (except for recombinant plasmids created by overlap extension PCR) by means of the QIAquick PCR purification kit (QIAGEN) according to the manufacturer's instructions. After purification, these PCR products were either immediately utilized or were frozen and stored at -20°C.

### 2.2.2.4.1 Standard PCR

With respect to the quality and reliability of the DNA products needed, two different types of polymerases were utilized. For analytical PCRs to screen for positive clones of either *E. coli* harbouring the desired plasmids or *L. monocytogenes* mutants bearing the desired genotype, Taq DNA polymerase from Thermus aquaticus (New England Biolabs, Inc) was employed. However, due to its error-prone DNA synthesis and lack of proofreading ability (Tindall and Kunkel, 1988), Taq polymerase could not be used for DNA products that were to be used for cloning purposes. Hence to overcome the latter problem, Thermo Scientific® Phusion High-Fidelity DNA polymerase (New England Biolabs, Inc) was utilised for generating clonable DNA fragments. Standard protocols for PCRs using both enzymes are given in Table. 6, 7, 8 and 9.

**Table 6: PCR master mix for *Taq* DNA polymerase**

| Component | 100 µl | 50 µl | 30 µl |
|---|---|---|---|
| Template | 0.5 µl | 0.25 µl | 0.2 µl |
| Primer fw/rev | 0.5 µl/0.5 µl | 0.25 µl/0.25 µl | 0.2 µl/0.2 µl |
| 10 x Reaction buffer | 10 µl | 5 µl | 3 µl |
| 40 mM dNTPs | 1 µl | 0.5 µl | 0.3 µl |
| *Taq* Polymerase | 0.5 µl | 0.25 µl | 0.15 µl |
| $dH_2O$ | 77 µl | 43.5 µl | 26.15 µl |

**Table 7: PCR program for *Taq* DNA polymerase**

| Step | Temperature | Time | |
|---|---|---|---|
| Initial denaturation | 95°C | 5 min | |
| Denaturation | 95°C | 1 min | 30 x |
| Annealing | 52°C | 1 min | |
| Elongation | 72°C | 2 min/kb | |
| Hold | 16°C | ∞ | |

**Table 8: PCR master mix for Phusion DNA polymerase**

| Component | 100 µl | 50 µl | 30 µl |
|---|---|---|---|
| Template | 0.5 µl | 0.25 µl | 0.2 µl |
| Primer fw/rev | 0.5 µl/0.5 µl | 0.25 µl/0.25 µl | 0.2 µl |
| 5 x HF buffer | 20 µl | 10 µl | 6 µl |
| 40 mM dNTPs | 1 µl | 0.5 µl | 0.3 µl |
| Phusion Polymerase | 0.5 µl | 0.25 µl | 0.15 µl |
| $dH_2O$ | 67 µl | 38.5 µl | 23 µl |

**Table 9: PCR program for Phusion DNA polymerase**

| Step | Temperature | Time | |
|---|---|---|---|
| Initial denaturation | 95°C | 5 min | |
| Denaturation | 95°C | 30 sec | 30 x |
| Annealing | 48 - 60°C | 30 sec | |
| Elongation | 72°C | 30 sec/kb | |
| Hold | 16°C | ∞ | |

### 2.2.2.4.2 Overlap extension PCR

This highly reliable, efficient and restriction endonuclease-free cloning scheme was employed to clone a desired insert within a plasmid of choice. This required the simple and straightforward approach of designing chimeric primers bearing plasmid sequences at the 5' ends and the desired insert sequences at the 3' ends. PCR amplification was used to generate these chimeric inserts, which were subsequently utilized as mega-primers with the chosen plasmids as a circular template for a second PCR (Bryksin and Matsumura, 2010). Following 1 h restriction digestion with 1 µl of DpnI/100 µl of reaction mixture to destroy the original plasmid templates, 1, 2 and 5 µl of the resultant PCR products were transformed into 100 µl of competent *E. coli* TOP 10 cells to allow for establishment of the recombinant plasmids.

### 2.2.2.4.3 Site-directed plasmid mutagenesis

The site-directed mutagenesis PCR amplification process was used as described by Liu and Naismith (Liu and Naismith, 2008). This included the new scheme for primer design, which helped minimize dimerization of the primer pair allowing for their effective binding to the PCR products and utilization as the template. This method was used to incorporate specific point mutations into the insert sequence, already present in the plasmid backbone, modify insert sequences and also to remove *gfp*-tag sequences where required. PCR protocol and program for Phusion® DNA polymerase was used, however, an extension time of 1 min/kb was employed for all plasmids having a size greater than 4 kb.

### 2.2.2.4.4 Inverse PCR

This PCR technique, as described by Pozsgai and coworkers (Pozsgai et al., 2012), was employed to determine the site of integration of the *HimarI mariner* transposon in the desired

transposon mutant. 1 µg of chromosomal DNA isolated from this transposon mutant was subjected to TaqI digestion for 1 h, followed by a 20 min heat inactivation step. Ligation of 0.1 µg of the resultant digested DNA was carried out for 1 h at room temperature using T4 DNA ligase (New England Biolabs, Inc). A PCR was set up using primers SHW427/SHW428 and the ligation mixture as the template. This PCR product was purified and sent for sequencing to determine the identity of the Inverted Terminal Repeat (ITR) insertion sequence, followed by two bases, namely TA, and the chromosomal DNA sequence, specific to the site of insertion.

### 2.2.2.5 Restriction endonuclease digestion

All restriction endonuclease enzymes and their buffers were purchased from New England Biolabs, Inc and used as per their recommendations. Restriction digestion was used both for analytical as well as preparative purposes, with incubation varying from 1 h for the former to overnight for the latter. In situations requiring digestion of the template/insert with two different enzymes (double digestion), the combination of enzymes to be used was determined using the online tool Double Digest Finder (https://www.neb.com/tools-and-resources/interactive-tools/double-digest-finder) to ascertain the compatibility of the two enzymes in terms of the buffer and incubation temperature. As per the manufacturer's recommendation, 1 x BSA was also added to double digestion reaction mixture to reduce unspecific nucleotide cleavage. A general protocol describing the composition of standard restrictions digestions is given in Table. 10.

**Table 10: Restriction digests**

| Component | Analytical | Preparative |
|---|---|---|
| Template/ Insert | 5 µl | 40 µl |
| Restriction endocuclease | 0.5 µl | 2 µl |
| NEBuffer (10 x) | 1 µl | 5 µl |
| $dH_2O$ | 3.5 µl | 3 µl |

### 2.2.2.6 DNA ligation

T4 DNA ligase (New England Biolabs, Inc) was used to achieve ligation of DNA fragments with T4 DNA ligase reaction buffer, also being supplied by the manufacturer. The ligation reaction mixture included the template and insert added in a ratio of 1:3, with 2 µl each of the ligase and the 10 x buffer, and $dH_2O$ making up the final volume to 20 µl. To ensure efficient

ligation, the reaction mixture was placed in a lukewarm water-bath and incubated overnight at 4°C so that the reaction was exposed to a slowly decreasing temperature gradient.

#### 2.2.2.7 Other buffers used

| | | |
|---|---|---|
| **50 x TAE Buffer** | EDTA (0.5 M, pH 8.0) | 100 ml |
| | Glacial acetic acid | 57.1 ml |
| | Tris base | 242 g |
| | $dH_2O$ | ad. 1 l |
| **5 x DNA Loading Dye** | Glycerol | 3ml |
| | Bromophenol Blue | 0.025 g |
| | Xylene Cyanol FF | 0.025 g |
| | $dH_2O$ | ad. 10 ml |

### 2.2.3 Protein based experiments

When it came to working with proteins, aliquots of the protein samples in aqueous solution were stored at -20°C, defrosted prior to use, and were always kept on ice during the duration of being used for experiments to minimize degradation.

#### 2.2.3.1 Isolation of total cellular proteins from *L. monocytogenes*

Initially, 3ml overnight cultures were prepared for the required bacterial strains, which were then used to inoculate 50 ml of fresh BHI broth in 200 ml Erlenmeyer flasks (with/without additives) so as to generate cultures bearing an initial $OD_{600}$ value of 0.05. These cultures were cultivated at 37°C with aeration at 250 rpm till they achieved a final $OD_{600}$ value of approx. 1.0 – 1.5. To make the results more comparable, individual bacterial cultures were adjusted by diluting them accordingly with fresh BHI broth so that they possessed the same final $OD_{600}$ value for the same culture volume, e.g. all cultures would have an $OD_{600}$ value of 1.2 and a volume of 50 ml. The cultures were then spun down at 4629 x g for 5 min at 4°C in a pre-cooled centrifuge to harvest the cells. In case of filamentous mutants, due to a difficulty in forming compact pellets, a spin velocity of 12857 x g was employed instead. After a wash step with ZAP buffer, the cells were re-suspended in 1 ml of the same and transferred to 15 ml Falcon tubes. PMSF, which serves as a serine protease inhibitor (Turini et al., 1969), was

added to the tubes to a final concentration of 1 mM. The resuspensions were sonicated (HD 2070 MS 72, Bandelin Sonopuls) on an ice-water bath for 10 min using a power output of approx. 40 – 50% so as to disrupt the cells and facilitate release of cellular proteins. To remove cellular debris, the lysates were transferred to 1.5 ml eppendorf tubes and spun down in a pre-cooled table top centrifuge at 15700 x g for 2 min at 4°C. The supernatants were transferred to fresh eppendorf tubes and were spun down again. The cell pellets were discarded, and the supernatants containing the cellular proteins were either temporarily stored on ice prior to use or were stored for later use at -20°C.

| | | |
|---|---|---|
| **ZAP Buffer (1 l)** | 1 M Tris-HCl pH 7.5 | 100 ml |
| | 1M NaCl | 200 ml |
| | $dH_2O$ | ad. 1 l |

### 2.2.3.2 Isolation of extracellular proteins from *L. monocytogenes*

The bacterial strains were cultured and adjusted to possess the same culture volume bearing the same final $OD_{600}$ value, in the same manner as mentioned above, with the only difference being that the resultant supernatant from the first centrifugation step was also collected as it contained the secreted (extracellular) proteins. These extracellular proteins were precipitated by adding 100% (w/v) trichloroacetic acid to the supernatants to give a final concentration of 10% (w/v) followed by incubation at 4°C, overnight. These supernatants were then spun down at 4629 x g for 1 h at 4°C and the resultant precipitates were collected, dried, re-solubilized in 8 M urea and stored at -20°C (Halbedel et al., 2012).

### 2.2.3.3 Protein concentration determination (Bradford's method)

Bradford's reagent was prepared by mixing the Nanoquant solution (Bio-Rad Laboratories, Inc) with $dH_2O$ in a ratio of 1:5. 1 – 5 µl of the protein extracts were thoroughly mixed with 1 ml of this reagent and aliquoted into plastic cuvettes, were they were incubated for 5 min at room temperature. Absorption of these samples were measured at $\lambda$ = 595 nm in a photometer using the Bradford's reagent as the blank. Using these absorption values, the concentration of the protein extracts were calculated according to the following formula:

$$concentration\ (\mu g/\mu l) = \frac{Absoption\ at\ \lambda =\ 595\ nm}{0.0536 * volume\ of\ protein\ sample\ added\ in\ \mu l}$$

### 2.2.3.4 Polyacrylamide Gel Electrophoresis (SDS-PAGE) (Laemmli, 1970)

The gel cassette sandwich was assembled using the cover plate and the spacer plate, which were clamped together by means of the green casting frame. Once the two plates of the cassette sandwich were evenly aligned, the open bottom end was sealed using PARAFILM® M (Bemis Company, Inc., sold by Sigma-Aldrich Corporation), after which it was securely fastened into the casting stand. 1 ml $dH_2O$ was added to the assembly to check for any leaks.

The solution for the 12% polyacrylamide separation gel (running gel) was prepared as per the recipe mentioned below:

**Table 11: Composition of running gel**

| Component | 1 gel (5 ml) | 2 gels (10 ml) |
|---|---|---|
| Tris-HCl (1.5 M, pH 8.8) | 1.3 ml | 2.6 ml |
| 30% Acrylamide/Bisacrylamide | 2.0 ml | 4.0 ml |
| 20 % SDS | 25 µl | 50 µl |
| 10% APS | 50 µl | 100 µl |
| TEMED | 5 µl | 10 µl |
| $dH_2O$ | 1.6 ml | 3.25 ml |

The separation gel was poured in a manner that allowed for enough space between the bottoms of the combs placed in the stacking gel and the top of the former, to facilitate formation of compact bands of the loaded protein samples. 300 µl of 100% ethanol was poured on top of the separation gel to form a levelled straight edge as well as to get rid of any air bubbles between the two-gel interfaces. The gel was allowed to polymerize for approx. 30 min (the leftover separation gel solution was used as a polymerization control), and then the ethanol was removed using a tissue paper.

The solution for the stacking gel was prepared shortly after, utilizing the below mentioned recipe:

**Table 12: Composition of stacking gel**

| Component | 1 gel (5 ml) | 2 gels (10 ml) |
|---|---|---|
| Tris-HCl (0.5 M, pH 6.8) | 1.3 ml | 2.6 ml |
| 30% Acrylamide/Bisacrylamide | 0.65 ml | 1.3 ml |
| 20 % SDS | 25 µl | 50 µl |
| 10% APS | 50 µl | 100 µl |
| TEMED | 10 µl | 20 µl |
| $dH_2O$ | 3.05 ml | 6.1 ml |

The stacking gel was decanted onto the separation gel and the combs were inserted, avoiding air bubbles, followed by polymerization for approx. 20 min. This assembled gel cassette sandwich was then placed into the electrode assembly comprising of the sealing gasket, the upper electrode (cathode,) and the lower electrode (anode,). The electrode assembly and the gel cassette were fastened together (with the short plate side facing inwards) by means of the clamping frame to form the inner buffer chamber. This complete assembly was placed into the gel tank, which was then filled with 1 x SDS-PAGE Running Buffer.

The protein samples were denatured at 95°C for 5 min in 1 x Sample Loading Buffer; in the meanwhile, the combs were gently removed and the wells were rinsed to remove any residual polyacrylamide. The desired molecular weight marker [the pre-stained molecular weight marker (New England Biolabs, Inc) was used in case of subsequent western blotting] and the denatured protein samples were then loaded onto the gel and run at 150 V (constant) for approx. 75 – 90 min in 1 x SDS-PAGE Running Buffer, to separate the individual proteins. These gels were then either subjected to western blotting, or were coomassie or silver stained and analysed. The SDS-PAGE apparatus, including the plates for the gel cassettes and the combs were purchased from Bio-Rad Laboratories, Inc.

| | | |
|---|---|---|
| **10 x SDS-PAGE Running Buffer** | Tris base | 30 g |
| | SDS | 10 g |
| | Glycine | 144 g |
| | $dH_2O$ | ad. 1 l |
| **4 x SDS Loading Buffer** | 0.5 M Tris-HCl pH 6.8 | 4 ml |
| | Glycerol (100%) | 4 ml |
| | SDS | 0.8 g |
| | β-mercaptoethanol | 400 µl |
| | Bromophenol Blue | 0.01 g |
| | $dH_2O$ | ad. 10 ml |

**2.2.3.5 Coomassie staining**

The gels were gently removed from the cassette and placed in the fixing solution for 10 min, after which they were incubated overnight in the Coomassie staining solution. Destaining was

achieved using $dH_2O$ until an optimal contrast was obtained between the background and the protein bands. The stained gels were then documented by putting them into plastic wrapping film followed by scanning.

| | | |
|---|---|---|
| **Fixing Solution** | Methanol | 225 ml |
| | Acetic Acid | 50 ml |
| | $dH_2O$ | ad. 500 ml |
| **Coomassie Staining Solution** | 5 x Roti-Coomassie concentrate (Carl Roth GmbH + Co. KG) | 20 ml |
| | Methanol | 20 ml |
| | $dH_2O$ | 60 ml |

### 2.2.3.7 Western blotting

The Hoefer Semi-Dry Blotting device (Hoefer, Inc.) was utilized for carrying out western blotting. 4 pieces of Whatman Grade GB005 blotting paper (GE Healthcare Europe GmbH) and 1 piece of Immobilon®-$P^{SQ}$ PVDF (Polyvinylidene fluoride) transfer membrane (0.2 µm pore size, Merck Millipore GmbH), of the correct dimensions, were cut out for each gel and soaked in Transfer buffer and 100% methanol, respectively. Upon completion of SDS-PAGE, the blotting stack was assembled onto the blotting device by placing 2 pieces of Transfer buffer soaked Whatman paper on the bottom, followed by the equilibrated PVDF blotting membrane, the polyacrylamide gel and 2 more pieces of the buffer soaked Whatman paper on top, in that order. A roller was used to remove any air bubbles that may impede efficient blotting of the proteins. For optimal transfer of the protein bands from the gel onto the PVDF membrane, the apparatus was run at 100 mA (0.8 $mA/cm^2$) for 1.5 h. The PVDF membrane with the affixed proteins was then rinsed in Blotto solution overnight to prevent subsequent unspecific staining.

### 2.2.3.8 Antibody staining of blotted proteins

Depending on the protein and the specificity of its corresponding antibody, the primary antibody was diluted in Blotto solution (see Table. 13) and incubated with the blotted membrane for 1 – 3 h on a rotary shaker. Following 3 wash steps with Blotto solution lasting

for 10 min each, the membrane was incubated with the Blotto-diluted secondary antibody (α-mouse/α- rabbit-HRP = 1:10000, ) for an additional 1 – 3 h. The membrane was then washed twice with Blotto (10 min for each wash), once with 1 x PBS (10 min), and then moistened with a solution of SuperSignal™ ECL substrate: Peroxidase buffer (50:50, Thermo Fisher Scientific Inc.) in a petri dish. After removal of excess liquid with the aid of a paper towel, the membrane was packed in a plastic foil and documented utilizing the chemiluminescence imager (Chemi-Smart-3126 WL/26M, Vilber Lourmat) to detect for light signals generated as a result of the reaction between the horse-radish peroxidase (HRP) and the luminol-based substrate. Detection conditions included an open aperture, full resolution and exposure times of 30 sec – 15 min for the camera. An image was also taken for the membrane bearing the visible pre-stained marker under normal illumination, prior to chemiluminescence detection. Standard dilution factors for the antisera used in this study are given in Table. 12.

**Table 13: Primary antibodies used**

| Antibody | Dilution | Host organism |
|---|---|---|
| anti-DivIVA | 1:2500 | rabbit, polyclonal |
| anti-SecA2 | 1:3500 | rabbit, polyclonal |
| anti-p60 (MyBioSource) | 1:5000 | mouse, monoclonal |
| anti-His (Invitrogen) | 1:500 | mouse, monoclonal |
| anti-GFP (Invitrogen) | 1:5000 | mouse, monoclonal |

| | | |
|---|---|---|
| **Transfer Buffer** | Methanol (99.8%) | 75 ml |
| | 1 x SDS-PAGE Running Buffer | 425 ml |
| **Blotto Solution** | Skimmed-milk powder | 7.5 g |
| | Tween 20 | 300 µl |
| | 1 x PBS | ad. 300 ml |

### 2.3 *In vivo* protein crosslinking and co-purification of putative interaction partners

As a precautionary measure, handling of all solutions and bacterial cultures containing formaldehyde was done under the fume hood. The *L. monocytogenes* wild-type strain as well as the strains expressing the recombinant His-10 tagged bait proteins were cultured in 500 ml sterile BHI broth in 1 l Erlenmeyer flasks (37°C, 250 rpm shaking), starting with an $OD_{600}$ value of 0.05, till $OD_{600}$ = 1.0. 5 ml from each of these cultures was taken off, spun down, and the resultant pellets were stored at -20°C as pre-crosslinking samples. 37% formaldehyde

(pre-prepared solution, Sigma-Aldrich Corporation) was added to these cultures to a final concentration of 1% (v/v) and incubated at 37°C with shaking for another 20 min, for the purpose of covalently crosslinking proteins bearing close proximity to each other. These flasks were sealed right after the addition of formaldehyde using multiple layers of PARAFILM® M to prevent its evaporation inside the incubator. The crosslinking reaction was quenched by the addition of 6.25 ml of 1.5 M glycine, after which the flasks were re-sealed and incubated for 1 min at 37°C. These cultures were then centrifuged at 4629 x g for 5 min at 4°C to harvest the cell pellets which were stored at -20°C.

The cell pellets were de-frosted on ice and re-suspended in 2 ml UT buffer. Sonication was employed to disrupt these cell pellets on an ice-water bath for 1 h using a power output of 40%. These re-suspensions were centrifuged at 15700 x g for 5 min at room temperature to separate the cell debris, and the supernatants were transferred into 2 ml screw-cap vials and mixed with 150 µl of MagneHis solution (Promega Corporation) overnight. The magnetic beads in the vials were sedimented by a spin down at 5000 rpm for 1 min at RT (room temperature) and then the vials were placed onto a magnetic stand for 1 min and twirled around briefly allowing for the magnetic beads to move to the side of the tubes. The supernatants were taken off gently with the aid of a pipette and were replaced with 1.5 ml UT buffer, after which the magnetic beads were re-suspended. This wash step was repeated for a total of 5 times. After the final wash step, the vials were centrifuged at 15700 x g for 3 min followed by a 1 min placement on the magnetic stand as before and then the supernatants were replaced with 200 µl of Elution buffer. The samples were thoroughly mixed for 2 min at room temperature in this buffer, the vials were centrifuged as stated before, the resultant eluates were concentrated using Microcon®-30kDa Centrifugal Filter Unit with Ultracel-30 membrane (Merck Millipore GmbH) and stored at -20°C.

The eluates were analysed using SDS-PAGE followed by coomassie and silver staining, for which they were firstly aliquoted and mixed with a suitable volume of 4 x SDS Loading buffer followed by heating at 95°C for 1 h to achieve de-crosslinking. Western blots and zymograms were employed to check for the presence of a protein of interest and specific autolysins, respectively, which may have co-purified with the bait proteins. Controls used for the experiments included +/- heating at 95°C, +/- formaldehyde treatment (including a formaldehyde concentration gradient ranging from 0 – 1 % (v/v)) and control proteins as baits.

| | | |
|---|---|---|
| UT Buffer (500 ml) | HEPES | 11.94 g |
| | NaCl | 14.61 g |
| | Imidazole | 1.702 g |
| | Urea | 240.24 g |
| | Triton X-100 | 5 ml |
| | 1 M DTT | 500 µl (add just before use) |
| | 100 mM PMSF | 5 ml (add just before use) |
| | $dH_2O$ | ad. 500 ml |
| | pH 7.4 – 7.5 @ 25°C | |
| Elution Buffer (15 ml) | 1 M Tris-HCl pH 7.5 | 1.5 ml |
| | 1 M Imidazole pH 7.5 | 7.5 ml |
| | 20% SDS | 750 µl |
| | 1 M DTT | 150 µl (add just before use) |
| | $dH_2O$ | ad. 15 ml |
| | pH 7.4 – 7.5 @ 25°C | |

**2.4 Bacterial Adenylate Cyclase-based Two- Hybrid analysis (BACTH)**

This *in vivo* system was used to detect and characterize protein-protein interactions by exploiting the reconstitution of *Bordetella pertussis* adenylate cyclase activity, mediated by the aforementioned interactions, in *E. coli* (Karimova et al., 1998, Ladant and Ullmann, 1999). The open reading frame of each gene, coding for the respective protein to be tested, was initially cloned into each of the four BACTH plasmids so as to generate both N and C-terminal fusions of the T18 as well as the T25 fragment of the adenylate cyclase. To analyze putative protein-protein interactions, a matrix was established in a 96-well PCR plate, comprising of 1 µl of each of the two T25 fusion-fragment-coding plasmids of each protein on the Y-axis vs. 1 µl of each of the two T18 fusion-fragment-coding plasmids of the respective proteins on the X-axis, which allowed for testing of all permutations of protein interactions. Transformation, of each of the plasmid combinations, was done into 10 µl of chemically competent *E. coli* BTH101, in a manner similar to that already mentioned in section 2.2.2, followed by addition of 90 µl of sterile LB broth and regeneration for 2 h at 30°C. This matrix was then spotted onto BACTH plates (6 µl from each well) and incubated for 2 days at 30°C. The BACTH plates were prepared using pre-made 1% LB agar, which was

autoclaved, cooled to ~40°C and then supplemented with IPTG (0.1mM), X-Gal (50 µg/ml), kanamycin (25 µg/ml) and ampicillin (100 µg/ml), after which it was poured into 100 X 15 mm (petri dishes, Greiner Bio-One) plates. Positive interaction was characterised by a blue spot, while a white spot indicated no interaction. Empty pUT18 and pKT25 plasmids were also included in the matrix as negative controls.

## 2.5 Phenotypic characterization of *L. monocytogenes* mutants

### 2.5.1 Growth curves

Cultures for the desired *L. monocytogenes* strains were established in 20 ml of BHI broth in 50 ml Falcon tubes at 37°C with aeration at 250 rpm. Starting with an initial $OD_{600}$ of 0.05, the optical density at $\lambda = 600$ of the growing cultures was measured every hour for 8 h, directly followed by the next and final measurement at the 24 h time-point. These $OD_{600}$ values and their respective time-points were plotted on a graph (using Microsoft Excel) so as to generate the growth curves.

### 2.5.2 Swarming assay

The *L. monocytogenes* strains to be tested were stab inoculated onto soft LB agar plates (0.3% (w/v) agar) with the help of sterile, autoclaved toothpicks, making sure to allow for sufficient distance between individual inoculation points. After incubation for 1 day at 30°C, variable diameter halos were observed around the point of inoculation of the individual strains, indicating differences in swarming motility (Kearns and Losick, 2003).

### 2.5.3 Zymography

This method was utilized for autolysin secretion profiling which entailed the detection and analysis of autolysins in extracellular as well as cytosolic protein samples. A protocol similar to that described by Caroll et al. (Carroll et al., 2003) was used for this purpose. Extracellular and cytosolic protein fractions for each of the desired *L. monocytogenes* strains were separated on 12% polyacrylamide gels bearing 0.2% (w/v) *M. lysodeikticus* ATCC 4698 cells (autoclaved and lyophilized, Sigma-Aldrich Corporation). Renaturation of the separated proteins was achieved by gently shaking the gels for 24 h at room temperature, with multiple

changes of the Renaturation buffer (25 mM Tris-HCl pH7.5, 1% (v/v) Triton X-100). Bands of peptidoglycan hydrolysis were visualized as zones of increased transparency, which appeared black when imaged against a dark background.

The composition of the separating gel used in the zymogram is mentioned below:

**Table 14: Composition of running gel for zymography**

| Component | 1 gel (5 ml) |
|---|---|
| Tris-HCl (1.5 M, pH 8.8) | 1.3 ml |
| 2% (w/v) cells | 0.5 ml |
| 30% Acrylamide/Bisacrylamide | 2.0 ml |
| 20 % SDS | 25 µl |
| 10% APS | 50 µl |
| TEMED | 5 µl |
| $dH_2O$ | 1.1 ml |

### 2.5.4 Light and Fluorescence microscopy

Phase contrast microscopy was employed to document cells from bacterial cultures in their logarithmic growth phase ($OD_{600}$ = 0.4 – 0.8), so as to observe bacteria that were actively growing. Depending on the aspect of the morphology to be observed, samples were prepared with or without staining. Membrane and chromosome staining was achieved using 1 µl of nile red stain (100 µg/ml) and 10 µl of DAPI solution (100 µg/ml)/ 0.25 µl of Hoechst 33342 solution (1 mg/ml), respectively, in 100 µl of bacterial culture with a 20 min incubation, with shaking, at either 25 or 30°C (to observe certain GFP fusion proteins), or 37°C. 0.6 µl of these prepared samples were spotted onto glass slides coated with a thin film of 1.5% agarose. After briefly air-drying the samples, they were covered with thin glass coverslips and coated with immersion oil prior to viewing under the microscope. The Nikon Eclipse Ti microscope equipped with a 100 x phase contrast objective (Nikon Plan Apo, oil immersion) and a conjoint Nikon DS-MBWc CCD camera was used for image capture followed by processing using the accompanying NIS elements AR software package (version 3.22.11, build 728) or ImageJ.

For fluorescence microscopy imaging, the Nikon Instensilight C-HGFIE lamp was utilized for illuminating the samples. After subsequent passaging through different filters (TRITC filter for nile red staining, DAPI filter for DAPI staining, and FITC filter for GFP fusion proteins),

the images were captured and processed as stated above. Exposure times used varied from 1 – 6 sec depending on fluorescence intensity.

### 2.5.5 *In vitro* infection experiments

Eukaryotic cell culture techniques were employed to investigate bacterial invasion and intracellular growth kinetics of *L. monocytogenes* strains. Cells belonging to the non-phagocytic, human cervical cancer cell line, HeLa, were used as the eukaryotic host cells. A 24 well plate containing 1 ml of high-glucose DMEM medium [4.5 g/l glucose, 110 mg/l sodium pyruvate and 584 mg/l L-glutamine (GE Healthcare Life Sciences)] supplemented with 10% fetal calf serum) medium/well were seeded with $10^5$ HeLa cells in each well, and incubated for 1 day prior to the infection experiment in an incubator having a 5% $CO_2$ atmosphere at 37°C. Overnight pre-cultures were made for the *L. monocytogenes* strains in BHI medium at 37°C, which were then diluted to an $OD_{600}$ value of 0.2 in fresh BHI media followed by aliquoting and further dilution (1:100) in DMEM medium without fetal calf serum (FCS) to a final volume of 1 ml. The cultivated HeLa cells were washed thrice with 1 x PBS, after which the 1 ml aliquot of the listerial strains were applied to each well and centrifuged for 5 min at 800 rpm (Heraeus 8177 swing out rotor) to coat the HeLa cell layers with the bacterial cells. These bacterial cell-coated HeLa monolayers were incubated for 1 h at 37°C to facilitate infection. The excess bacterial cells that were unable to invade during the incubation were killed and removed from the surface of the HeLa cells by washing the monolayers thrice with 1 x PBS, incubating them with 2ml of FCS-free DMEM medium (containing 40µg/ml gentamicin) for 1 h at 37°C, followed by three more rounds of washing with 1 x PBS. Prior to lysing the infected HeLa cells for sampling, the monolayers were further incubated under the same conditions with 1 ml of FCS-free DMEM medium (containing 10µg/ml gentamicin). After removal of the medium from the monolayers, lysis of the infected HeLa cells was achieved using a short incubation step of 10 min with 1 ml of ice-cold PBS solution containing 0.1% (v/v) of Triton X-100, followed by thorough mixing (care was taken to avoid foam formation). The lysed suspensions were serially diluted in BHI medium followed by plating the appropriate dilutions on BHI agar plates with the help of the Eddy Jet (IUL Instruments) spiral plater. The recovered bacterial colonies were allowed to grow on the plates for roughly 18 h at 37°C, after which they were counted using the aCOLyte™ (Synbiosis) cell counter for determination of their CFU/ml values.

# 3. Results

## 3.1 DivIVA and its influence on autolysin secretion

Previous work on DivIVA showed that it influenced the secretion of two major virulence-associated autolysins, namely p60 (CwhA) and MurA (NamA), via the accessory secretion ATPase SecA2. The septal localization of these two autolysins was also shown to be DivIVA-dependent (Halbedel et al., 2012). This suggested that there might be either direct or indirect associations between these proteins, which were then tested using bacterial two hybrid and pull down experiments, respectively.

### 3.1.1 Protein-protein interactions of DivIVA with SecA2 and its substrates in bacterial two-hybrid experiments

Direct interactions between DivIVA, SecA2, p60 and MurA were tested by means of the bacterial two-hybrid approach, where the open reading frames of the corresponding genes were cloned into plasmids allowing for generation of N- and C-terminal fusions of the above proteins with T18 and T25 fragments of adenylate cyclase from *Bordetella pertussis*. Since multiple attempts to clone the *murA* gene into pUT18C resulted in failure, a decision was made to use only the T25 fusion variants of MurA for the analysis.

Strong self-interactions were observed for DivIVA, seen as blue coloured colonies on the selective LB plates (Fig. 6). This was in agreement with crystallographic data that demonstrated the ability of DivIVA to form dimers, tetramers and even higher order oligomers (van Baarle et al., 2013, Oliva et al., 2010).

Presence of a few blue colonies for self-interactions for SecA2 and p60 (encoded by *iap*) were also noticed in the same experiment (Fig. 6). This could probably be described as weak, self-interactions among individual protein molecules as a consequence of bearing close proximity to each other; hence, pointing towards the formation of dimers, which however was not tested further.

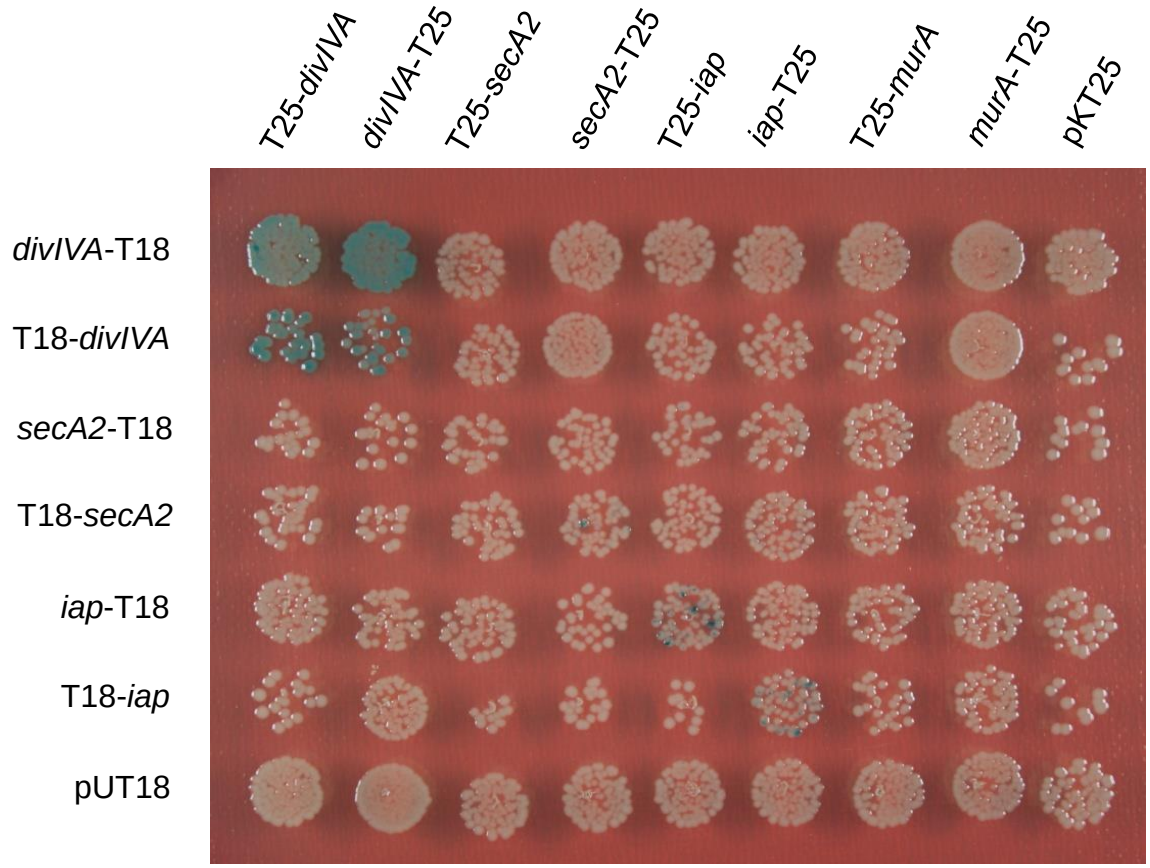


**Figure 6: Protein interactions between DivIVA and proteins from the SecA2 pathway observed with the bacterial two-hybrid assays.** The interaction matrix for the bacterial two-hybrid analysis consisted of the N- and C- terminal fusion constructs of *divIVA* (*lmo2020*), *secA2* (*lmo0583*), *iap* (*lmo0582*) and *murA* (*lmo2691*) with T-25 fragments, shown from left to right, and the T-18 fragments, shown from top to bottom (with the exception of *murA* constructs in this case), of *Bordetella pertussis* adenylate cyclase. Following co-transformation of these constructs into *E. coli* BTH101, 6 µl of each of the transformation mixtures were spotted onto LB plates containing X-Gal and selective for ampicillin and kanamycin resistance. These transformations were allowed to grow for 48 h at 30°C, after which they were photographed. Direct interactions between two protein partners were indicated by the blue coloured colonies. As a negative control, empty pKT25 and pUT18 plasmids were included in the matrix.

Surprisingly, no interactions were observed for the other pairings employed in the interaction matrix; However, this absence of evidence for direct protein interactions between DivIVA and SecA2, MurA or p60 does not provide evidence for the absence of any inter-protein interactions among these proteins. It could be possible that they were not detectable by this type of experiment. Alternatively, interactions between DivIVA, SecA2, p60 and MurA could be mediated via secondary protein-interaction partners.

### 3.1.2 Pull down experiments using His-tagged bait proteins

Since the bacterial two hybrid approach did not detect any direct protein-protein interactions, a pull down experiment was used to identify putative interaction partners of DivIVA. A $His_{10}$-tagged variant of DivIVA was employed, which was overexpressed from an ectopically placed chromosomal copy, as the primary bait protein. Similarly tagged variants of SecA2 and GpsB (paralogue of DivIVA) were utilized as co-purification controls. Proteins in the close

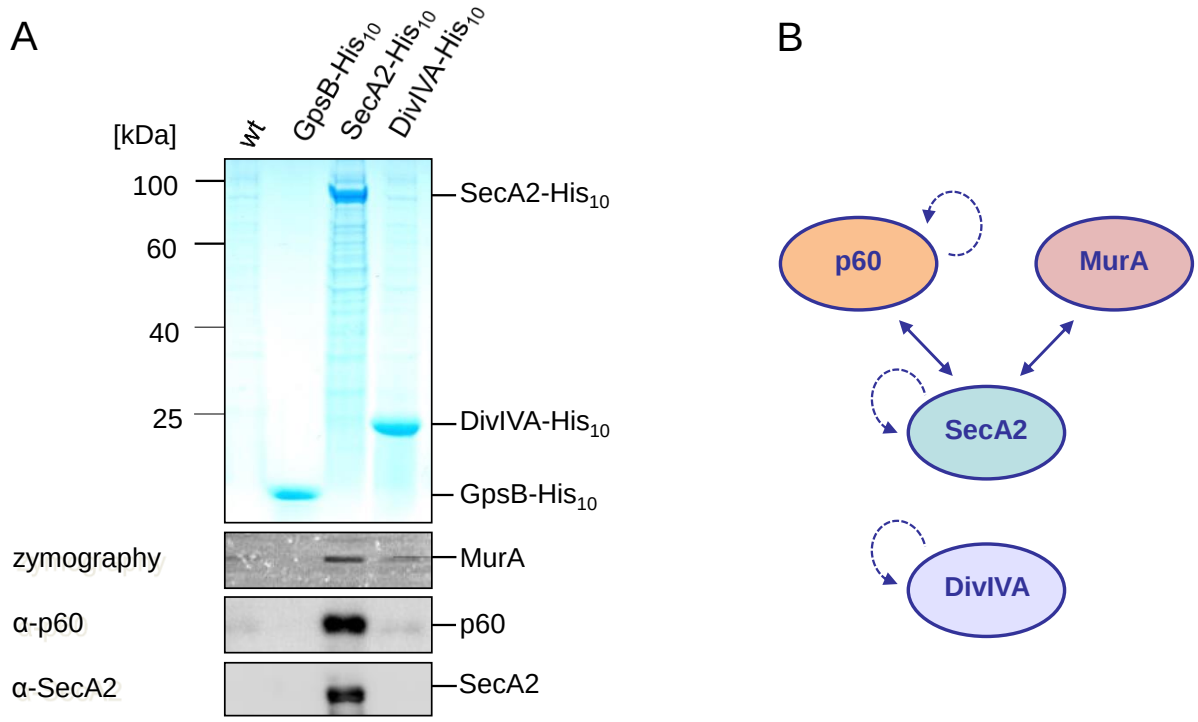


**Figure 7: Identification of the DivIVA target by pull-down.** (A) PAGE separation of pull down eluates on a 4-20% gradient polyacrylamide gel (Bio-Rad Laboratories, Inc) followed by overnight coomassie staining and water de-staining. Pull down of putative interaction partners with the $His_{10}$-tagged bait proteins was achieved without *in vivo* cross-linking with formaldehyde. Bright-blue bands signify enrichment of SecA2-$His_{10}$, DivIVA-$His_{10}$ and GpsB-$His_{10}$ bait proteins in the total cellular protein fractions of LMKK3 (*secA2-his*), LMKK4 (*divIVA-his*) and LMKK1 (*gpsB-his*), respectively. p60 and SecA2 co-purifications were visualized by western blotting followed by antibody staining with mouse anti-p60 (1:5000) and rabbit anti-SecA2 antibodies (1:3500) respectively, and their respective HRP-tagged secondary antibodies (1:10000). Zymography was employed for visualization of MurA, in non-denaturing co-purification experiments. (B) Schematic representation of interactions among SecA2, DivIVA, MurA and p60 as shown by pull down (solid double-sided arrows) and bacterial two-hybrid (curved, dashed arrows) experiments.

vicinity of the bait proteins that most probably would be the putative interaction partners, would co-purify with these bait proteins upon *in vitro* covalent crosslinking with

formaldehyde, followed by affinity purification with Ni-coated magnetic beads. However, due to difficulties faced in the downstream detection of the co-purified MurA protein as a result of such chemical cross-linking, two additional rounds of pull down were performed where the denaturing pull down incorporating formaldehyde crosslinking was abandoned in favour of non-denaturating (UT buffer was replaced with ZAP buffer) co-purification based on natural affinity of the target proteins for the bait proteins.

A coomassie-stained poly acrylamide gel, used to separate the co-purification eluates of the bait proteins, clearly showed the expression of the bait proteins and their purification (Fig. 7A). Upon zymography and immune staining analysis, a clear enrichment of p60 and MurA was observed with the SecA2-$His_{10}$ bait protein. This was in accordance with extracellular proteomic analysis, which showed that secretion of both, p60 and MurA, is SecA2-dependent (Lenz et al., 2003, Renier et al., 2013) and thus need to interact with SecA2. This however was the first instance that these proteins are shown to co-purify. In contrast, the enrichment levels of the aforementioned proteins in the eluate of the affinity-tagged DivIVA bait protein were indistinguishable from that seen in the un-tagged wild type control. This suggested that either DivIVA is not associated with these two autolysins to begin with or the amount of these autolysins which may be co-purifying with DivIVA is below the detection level for western blots and zymograms.

## 3.2 Domain-swap experiments to identify protein-protein interaction modules of *L. monocytogenes* DivIVA

Recently published data suggests that the lipid binding domain (LBD) of *B. subtilis* DivIVA is responsible for binding of the transmembrane protein, MinJ, which belongs to the Min system of division site selection. This model was concluded on the basis of domain swapping experiments, which included the expression of chimeric *Bs-57-Lm* DivIVA, consisting of the complete LBD of *B. subtilis* DivIVA (residues 1-57) fused to entire the C-terminal domain. This chimeric version of DivIVA was shown to cure the cell division defect of the *B. subtilis* Δ*divIVA* deletion mutant, due to a restoration of its interaction with MinJ, while still being unable to complement its sporulation defect due to its inability to bind to RacA (van Baarle et al., 2013).

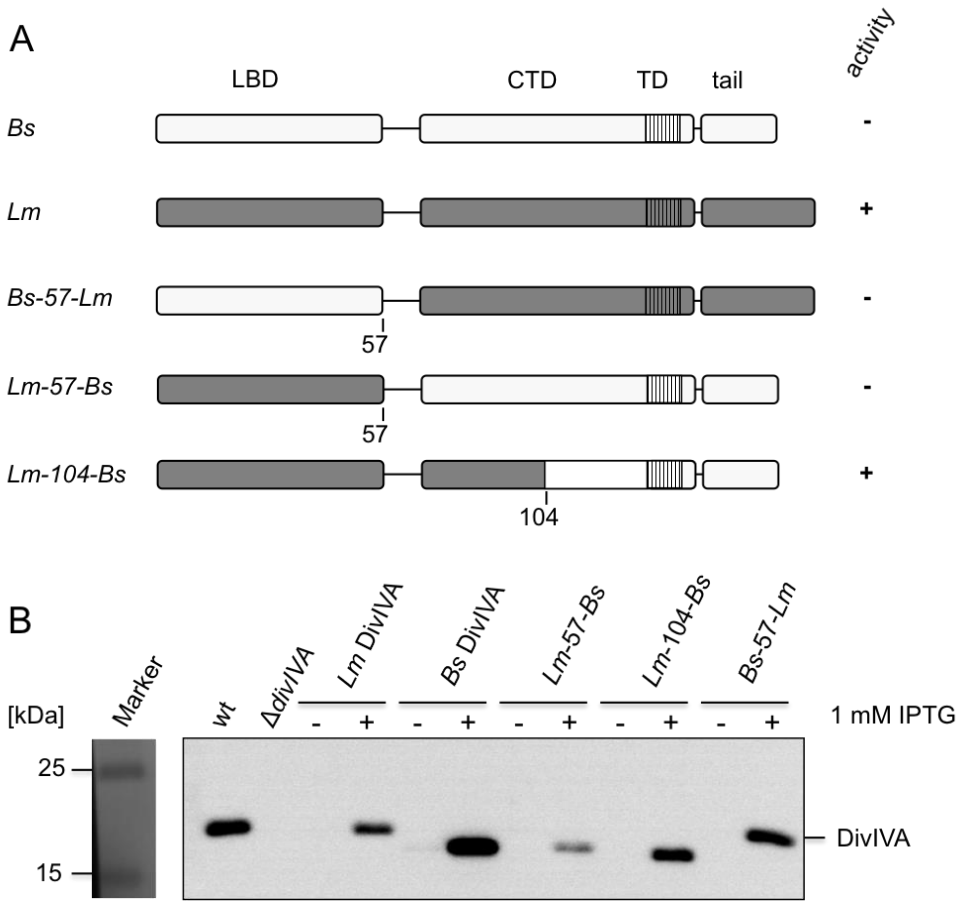


**Figure 8: Construction and expression of chimeric DivIVA proteins.** (A) Schematic representation of chimeric DivIVA proteins generated as fusion proteins bearing sections of *B. subtilis* (*Bs*, white construct*)* and *L. monocytogenes* (*Lm*, grey construct) DivIVA. Residues 1-57 represent the lipid binding domain of both *Lm* as well as *Bs* DivIVA proteins. Residue 104 signifies the start of a coiled-coil region for which both DivIVA proteins show a variability of three successive amino acid residues. The activity (+/-) symbol next to each DivIVA protein construct is an indication of its ability to restore wild-type cell separation and swarming motility when expressed in the *L. monocytogenes* Δ*divIVA* mutant. (B) Western blotting followed by visualization with a rabbit anti-DivIVA antibody (1:2500, specific for *Bs* DivIVA) staining. The strains bearing the constructs for the wild type as well as the chimeric DivIVA proteins in the Δ*divIVA* mutant i.e *Lm* DivIVA (LMS36), *Bs* DivIVA (LMKK8), *Lm*-57-*Bs* (LMKK12), *Lm*-104-*Bs* (LMKK13) and *Bs*-57-*Lm* (LMKK14) were grown in the presence (+) or absence (-) of 1 mM IPTG to check for expression of these chimeric proteins in the Δ*divIVA* background.

A domain-swapping approach similar to that mentioned above was used, where plasmids were generated and integrated at the $tRNA^{Arg}$ site of the *L. monocytogenes* chromosome, capable of expressing chimeric DivIVA proteins comprising of sections of *L. monocytogenes* (*Lm*) and *B. subtilis* (*Bs*) DivIVA. Expression of these constructs was under the control of an IPTG-inducible promoter. As a first test the ability of *Bs* DivIVA to complement the phenotype of the *L. monocytogenes* Δ*divIVA* mutant was tested. However, it was incapable of

restoring the wild-type phenotype (Fig. 9) despite being adequately expressed (Fig. 8B), indicating its biological inactivity in *L. monocytogenes*. In contrast, *Lm* DivIVA was able to complement the *ΔdivIVA* phenotype, confirming the validity of this approach (Fig. 9).

Three chimeric DivIVA versions were constructed: *Bs-57-Lm* (the entire LBD of *Lm* DivIVA was swapped with that of *Bs* DivIVA), *Lm-57-Bs* [the entire C-terminal domain (CTD), including the tetramerization domain (TD), and the C-terminal tail of *Lm* DivIVA was replaced with that of *Bs* DivIVA] and *Lm-104-Bs* (section of the *Lm* DivIVA CTD, starting from a short, non-conserved stretch of the coiled-coil domain to the C-terminal tail, was replaced with the corresponding *Bs* DivIVA region), as shown in Fig. 8A. All three chimeric DivIVA variants were sufficiently expressed upon induction with IPTG (Fig. 8B). Out of the three chimeras, only the strain expressing *Lm-104-Bs* could complement the Δ*divIVA* chaining defect; while *Lm-57-Bs* could not. This result was quite unexpected as in *B. subtilis* the analogous *Bs-57-Lm* DivIVA chimera was capable of curing the division defect seen in the corresponding Δ*divIVA* mutant (van Baarle et al., 2013).

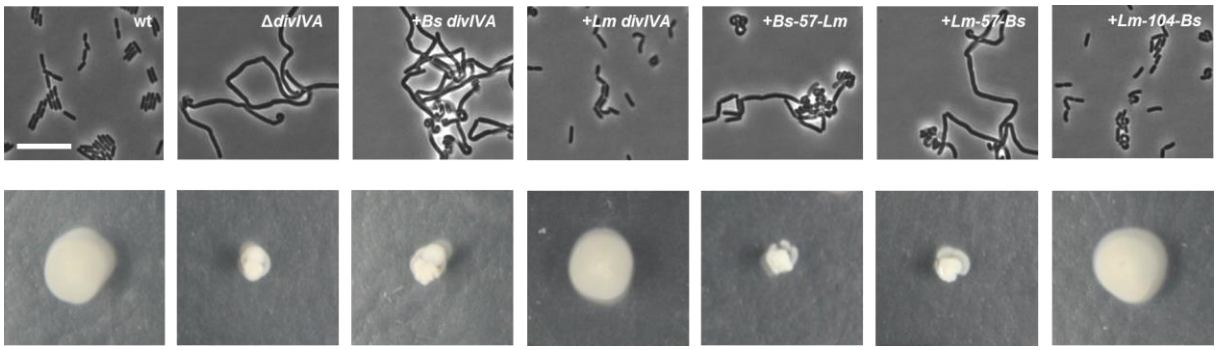


**Figure 9: Complementation experiments with chimeric DivIVA proteins.** Complementation of the wild-type cell division phenotype in the Δ*divIVA* deletion mutant background as displayed by the micrographs of *Lm* DivIVA (LMS36), *Bs* DivIVA (LMKK8), *Lm*-57-*Bs* DivIVA (LMKK12), *Lm*-104-*Bs* DivIVA (LMKK13) and *Bs*-57-*Lm* DivIVA (LMKK14) expressing strains in the top row, and the restoration of the wild-type swarming motility in the same set of strains in the bottom row. Chimeric DivIVA proteins comprising of full length DivIVA (from *Bs* or *Lm*), having certain sections interchanged with the corresponding sections from DivIVA of the other species (from *Lm* or *Bs*), were expressed from genetic constructs inserted at ectopic chromosomal loci in a Δ*divIVA* background (indicated by the "+" symbol) in the presence of 1 mM IPTG. Swarming motility experiments were carried out on 0.3% LB agar plates (containing 1 mM IPTG where necessary). Those were stab inoculated, allowed to grow for 24 h at 30°C, and then photographed. wt (EGD-e) and Δ*divIVA* (LMS2) strains were used as the positive and negative controls respectively. The scale bar is 5 µm.

This indicated that contrary to DivIVA in *B. subtilis* that requires only an intact LBD for wild type-like cell division, in *L. monocytogenes*, a small section of the CTD adjacent to the

flexible linker of DivIVA (residues 58-104), in addition to its LBD, is responsible for normal functioning of this protein. These finding were corroborated by swarming motility experiments performed with the same set of strains, which revealed that the *Lm-104-Bs* DivIVA expressing strain was able to swarm like the wild-type and the *Lm* DivIVA complementation strain (Fig. 9).

These results signify the importance of the role of the N-terminal LBD and a short adjacent region of the CTD of DivIVA in listerial autolysin secretion, and hint to the subcellular localization of its most relevant interaction partners. The LBD of DivIVA is known to be the domain responsible for binding it to the cytoplasmic membrane (Lenarcic et al., 2009, Letek et al., 2009, Oliva et al., 2010), hence any protein interacting with this domain would have to be either membrane bound or transmembrane in nature so as to bear a close enough proximity to it to facilitate such interactions. Consequently, it seems likely that transmembrane or membrane associated proteins establish the link between DivIVA and the SecA2-dependent protein secretion pathway.

### 3.3 Dependence of the Min division site selection system on DivIVA in *L. monocytogenes*

The Min system of division site selection has been extensively studied in *B. subtilis*, where DivIVA serves as its topological determinant, providing site specificity to the Min complex (Marston et al., 1998). As a result it allows for the spatial regulation of the cell division machinery, enabling cell division to occur in a symmetrical fashion (Bramkamp et al., 2008). Hence, when *divIVA* is deleted in *B. subtilis*, the cells form long filaments that are multinucleated, with the production of small, spherical, anucleated minicells at the cell-poles due to delocalized cell division (Edwards and Errington, 1997).

Previous work showed that the deletion of *divIVA* in *L. monocytogenes* resulted in the formation of long chains of cells that were unable to separate, post cell division (Halbedel et al., 2012); however, mini-cell formation was not observed in this Δ*divIVA* mutant. This led to the hypothesis that the Min system in *L. monocytogenes* may work in a DivIVA-independent manner.

### 3.3.1 Bioinformatic analysis of the *L. monocytogenes* division site selection system

Bioinformatic analysis involving sequence alignments of the MinCDJ proteins of *L. monocytogenes* and *B. subtilis* were performed. The *B. subtilis* MinJ protein sequence was subjected to similarity searches using the BLASTp tool, which helped to identify the gene *lmo2502* as the *L. monocytogenes minJ* homolog. Despite having just 30.52% identity along the entire length for the two proteins, the PDZ domain, of trypin-like proteases, at their C-terminal end seemed to be conserved (Fig. 10A). Homology coupled with the downstream location of the *minJ* gene with respect to the *ftsEX* operon in *L. monocytogenes* as well as *B.*

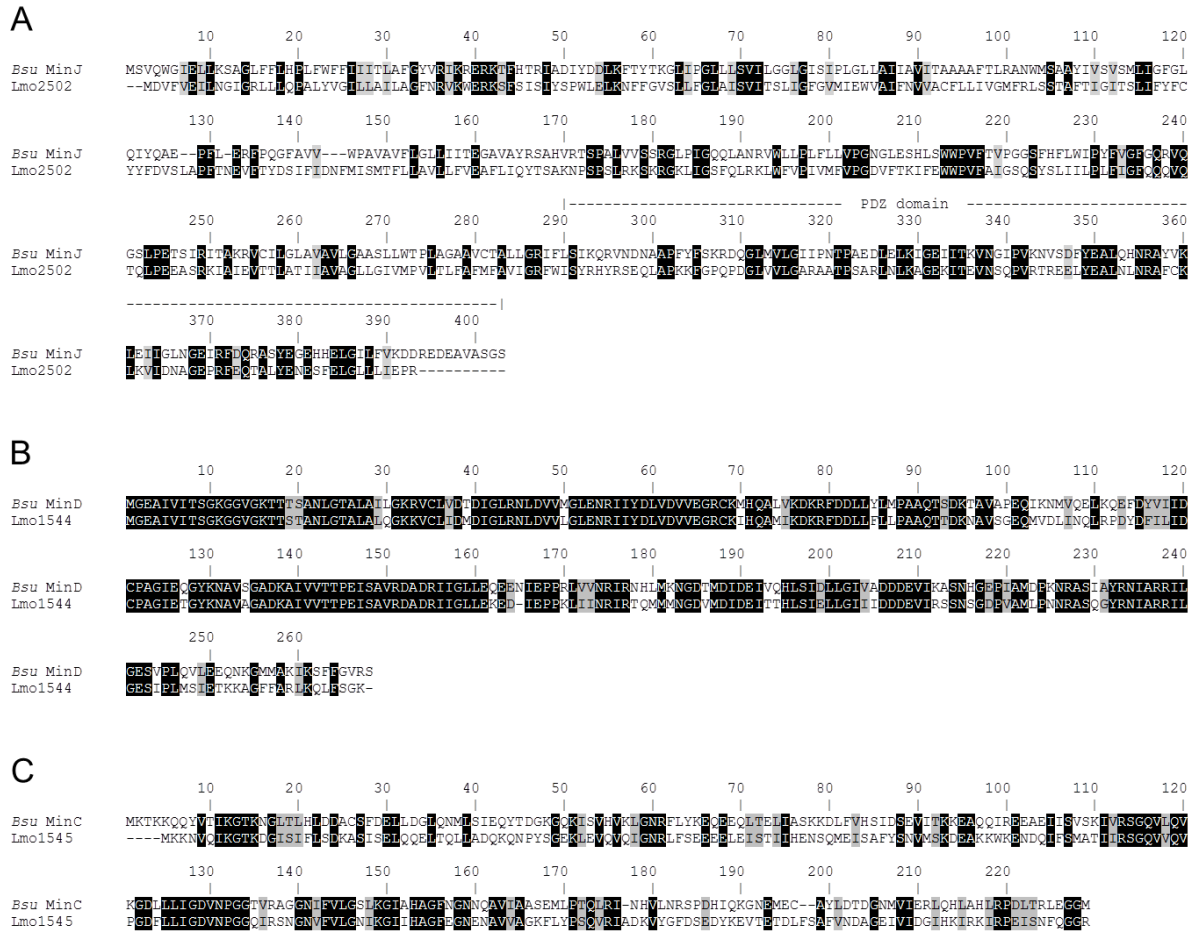


**Figure 10: Bioinformatic analysis of the Min system associated proteins of *L. monocytogenes*.** Sequence alignments between *Bacillus subtilis* and *L. monocytogenes* MinJ (A), MinD (B) and MinC (C). Black and grey highlighted areas (identical and similar amino acids, respectively) denote sequence conservation between *Bacillus subtilis* and *L. monocytogenes* for each of the three Min proteins. In panel A, the dashed line plotted over the alignment of the C- terminal region of both MinJ proteins represents the PDZ domain position.

*subtilis* suggests a possible similarity in function. The *lmo1545-1544* operon was found to encode the MinD and MinC homologs, respectively, in *L. monocytogenes* with the former bearing the highest degree of homology with that of *B. subtilis*, with 71.64% identity and 88% similarity (Fig. 10B). MinC, however, showed a greater diversity with only 37.12% identity (Fig. 10C). DivIVA, which is encoded by the gene *lmo2020*, is so far the only protein that has been studied among the above-mentioned proteins of the division site selection system in *L. monocytogenes*. The uncharacteristic phenotype displayed by the listerial Δ*divIVA* mutant demanded a closer look at the functioning of the Min system in this organism.

### 3.3.2 Protein-protein interactions among the components of the division site selection system

In order to test for direct protein-protein interactions among the Min proteins, C- and N-terminal fusions of the open reading frames of *lmo1545* (*minD*), *lmo1544* (*minC*) and *lmo2502* (*minJ*) with the T18 and T25 *B. pertussis* adenylate cyclase-encoding DNA fragments were generated in the four bacterial adenylate cyclase-based two-hybrid plasmids (BACTH). The inserts were cloned using primers that brought in XbaI and KpnI restriction sites at either end of their respective open reading frames, which were then digested using the relevant restriction endonuclease and ligated into similarly restriction cut plasmids. These BACTH plasmids were introduced into the interaction matrix and analysed as described in the materials and methods (Section 2.4).

Expression and functionality of the fusion proteins were indicated by the blue-coloration of the transformation mixtures upon plating them on selective LB plates bearing X-gal in self-pairings. Strong self-interactions (highlighted by the blue squares) were observed for all proteins; however, not in all permutations (Fig. 11A). These results were in accordance with crystallographic data showing the dimeric nature of MinC (Cordell et al., 2001). Our observation of self-interaction patterns of *L. monocytogenes* MinD was similar to that seen in bacterial two hybrid assays performed with MinD from *B. subtilis* (Bramkamp et al., 2008). However, pyrococcal and archeoglobal MinD homologs seemed to lack any such dimerization states upon crystallization (Cordell and Lowe, 2001, Sakai et al., 2001). MinJ from *L. monocytogenes* and *B. subtilis* also displayed similar self-interactions (Bramkamp et al., 2008), but this observation is still to be backed up by crystallographic analyses. With respect to inter-protein interactions among the components of the Min system, MinC showed direct

interactions with MinD, but not with either DivIVA or MinJ (Fig. 11A-B). As expected, MinD interacted with MinC and showed the strongest detectable interaction in the matrix with MinJ. The fact that MinD displayed interactions with DivIVA was surprising, the biological

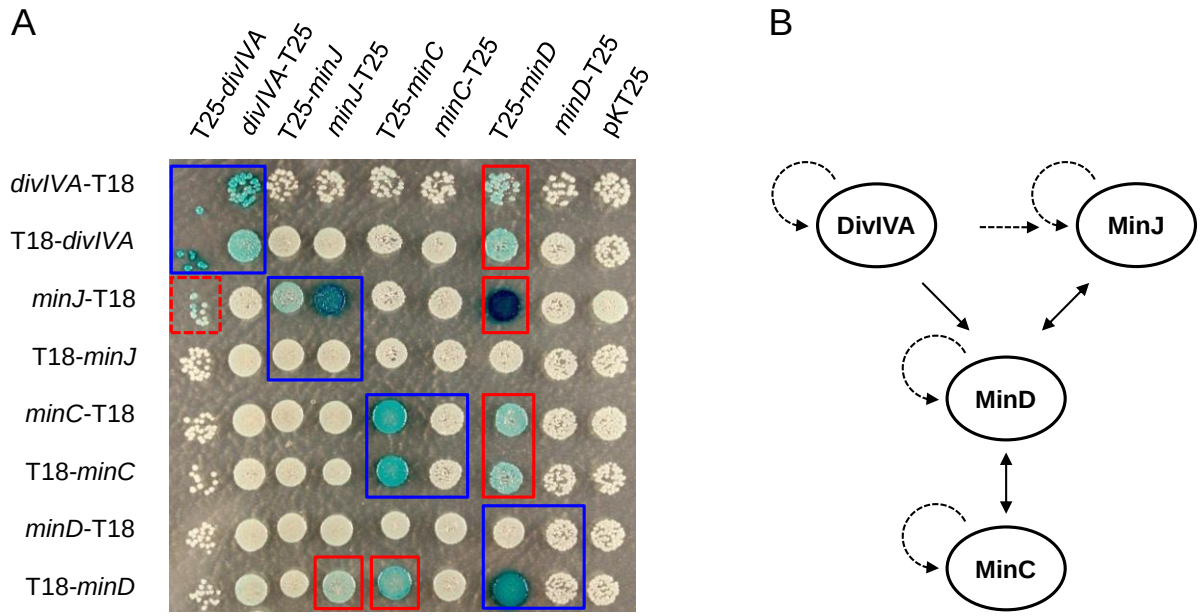


**Figure 11: Direct interactions between proteins belonging to the division site selection system of *L. monocytogenes*.** (A) Direct protein-protein interactions between *L. monocytogenes* DivIVA and Min system proteins, namely, MinJ, MinD and MinC, as detected by the bacterial two-hybrid experiment. Plasmids bearing the N- and C- terminal fusions of the adenylate cyclase T25 fragment (displayed row-wise) and T18 fragment (displayed column-wise) of *B. pertussis* with the *divIVA* (*lmo2020*), *minJ* (*lmo2502*), *minD* (*lmo1544*) and *minC* (*lmo1545*) genes, were co-transformed into the BTH101 strain of *E. coli* and spotted onto LB X-Gal Amp Kan plates as per the shown matrix. The blue coloured dots, which indicated direct protein interactions, were further categorized into self-interactions (blue boxes) and inter-protein interactions (red boxes). The inclusion of the empty pKT25 plasmid in the matrix served as the negative control. (B) A schematic representation of all direct interactions deduced from the bacterial two-hybrid analysis displayed in panel A. Solid arrows and dashed arrows implied inter-protein and self-interactions, respectively.

significance of which was highlighted by the presence of two positive hits out of the four permutations used for these two proteins. In *B. subtilis*, MinJ is known to be the protein that bridges DivIVA with MinD (Bramkamp et al., 2008, Patrick and Kearns, 2008), hence, this observation was completely unexpected. MinJ not only showed strong interactions with MinD, but also repeatedly displayed a less conspicuous interaction with DivIVA, characterised by a faint blue signal (red dashed box). Due to an apparent toxicity of the T25-DivIVA fusions employed in the analysis to the *E. coli* BTH101 strain, the interpretation of these pairings were hindered by the presence of only a few colonies. These results are in stark

contradiction to the concept of linear, hierarchical, protein-protein interactions among the components of the division site selection system of *B. subtilis* (DivIVA→MinJ→MinD→MinC). It seems not unlikely that in *L. monocytogenes*, there is a partial circumvention of the MinJ protein due to the MinD-DivIVA interaction.

### 3.3.3 Intracellular localization of fluorescent fusions of the Min system proteins

To better understand the effect of DivIVA on the distribution of the three Min proteins within the cells of *L. monocytogenes*, either N- or C-terminal fusions of these proteins with a GFP reporter were made and expressed in both the wild type as well as in the Δ*divIVA* deletion mutant. Fluorescence microscopy with the MinJ-GFP-expressing wild type strain (LMKK71, Fig. 12A) showed an enrichment of fluorescence at the septal loci accompanied with very slight, inconspicuous peripheral signals. Surprisingly, the fluorescence of MinJ-GFP along the septa of the cells remained unchanged even when expressed in the Δ*divIVA* mutant background (LMKK72, Fig. 12B). As MinJ is known to be a polytopic transmembrane protein, a minor circumferential fluorescence was expected. To put these observations into context, a quantitative method involving the measurement of fluorescence intensities along the longitudinal axis of post-divisional cells of the LMKK71 and LMKK72 strains across their septa was employed. Upon comparison of the intensity profiles of the aforementioned strains, a clear similarity in the slight septal enrichment of MinJ-GFP was noticed between the two strains (Fig. 12G), indicating that the septal localisation of MinJ is independent of DivIVA. Previous work by Bramkamp et al. showed that in *B. subtitlis*, there is a clear dependency of MinJ localization on DivIVA, which is in clear contrast to this observation in *L. monocytogenes*.

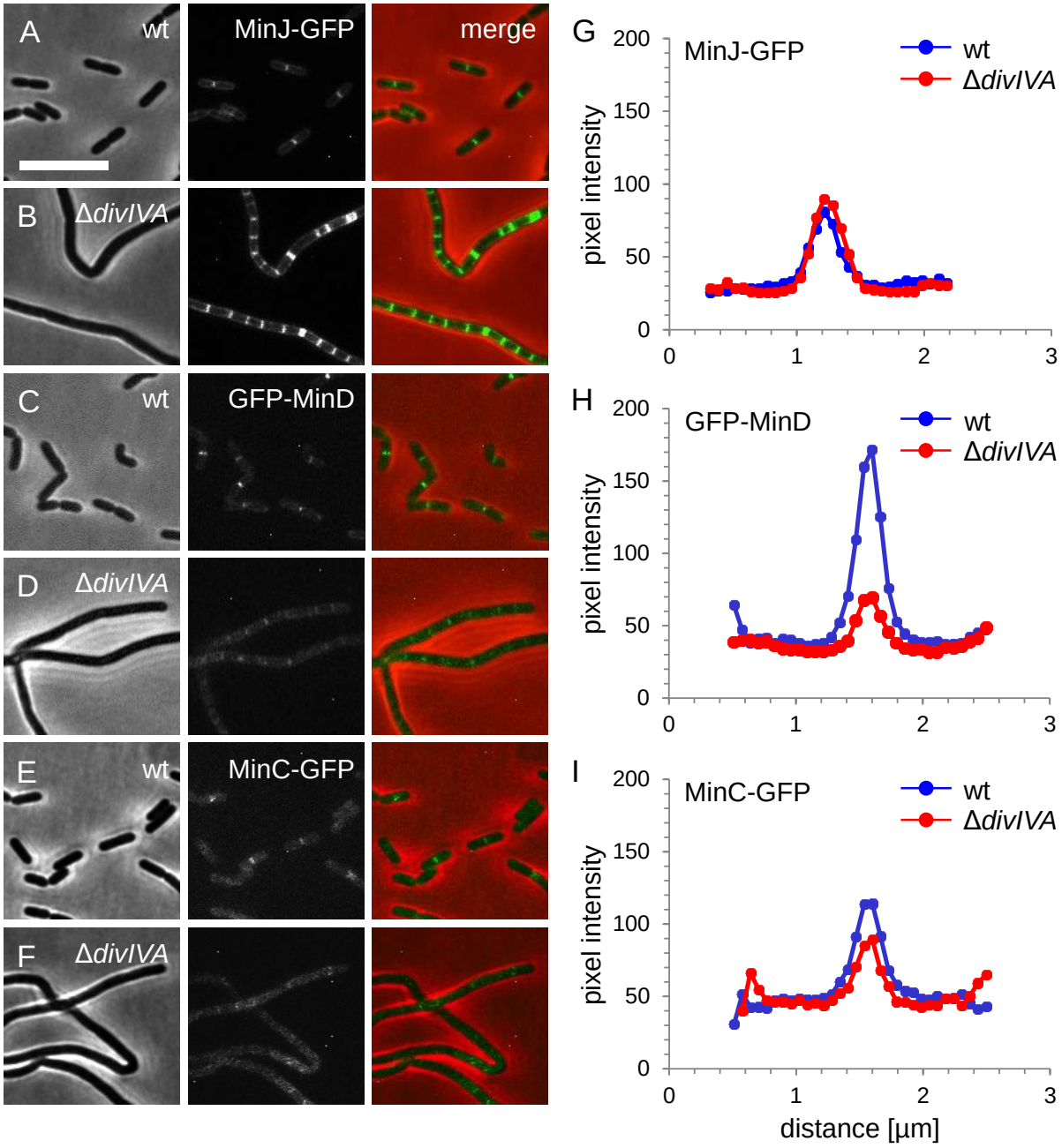


**Figure 12: Effects on subcellular localization of MinD, MinC and MinJ upon deletion of *divIVA*.** (A-F) Micrographs showing MinJ-GFP (A,B), GFP-MinD (C,D) and MinC-GFP (E,F) localization in *L. monocytogenes* wild-type (A,C,E) and Δ*divIVA* (B,D,F) backgrounds. Wild-type and Δ*divIVA* strains of *L. monocytogenes* expressing GFP fusions of MinD (wt-LMKK30; Δ*divIVA*-LMKK33), MinC (wt-LMKK29; Δ*divIVA*-LMKK32) and MinJ (wt-LMKK71; Δ*divIVA*-LMKK72), grown at 25°C or 30°C in BHI media (with or without 1 mM IPTG depending on the requirement), were subjected to fluorescence microscopy. Phase contrast and merged images, of the former with the GFP-fluorescence micrographs, were included for better comparison. The scale bar used is 5 µm. (G-I) Pixel intensity profiles of septally localized GFP signals for the images generated for the aforementioned strains. Visualization of the division septa required nile red staining. The intensities of the pixels corresponding to GFP signals were measured across the septa, along the longitudinal axis of 30 post-divisional cells that were randomly selected. The graphs shown represent the average intensity values.

The wild type strain expressing MinC-GFP (LMKK29) displayed a more intense septally localized fluorescence (Fig. 12E). However, upon deletion of *divIVA* in LMKK29 (LMKK32), the septal localization of the MinC-GFP fluorescence signal was noticeably reduced (Fig. 12F). These observations were confirmed by longitudinal axis fluorescence intensity profiles, which clearly showed a reduction in septal enrichment of MinC-GFP in LMKK32 as compared to that in LMKK29 (Fig. 12I).

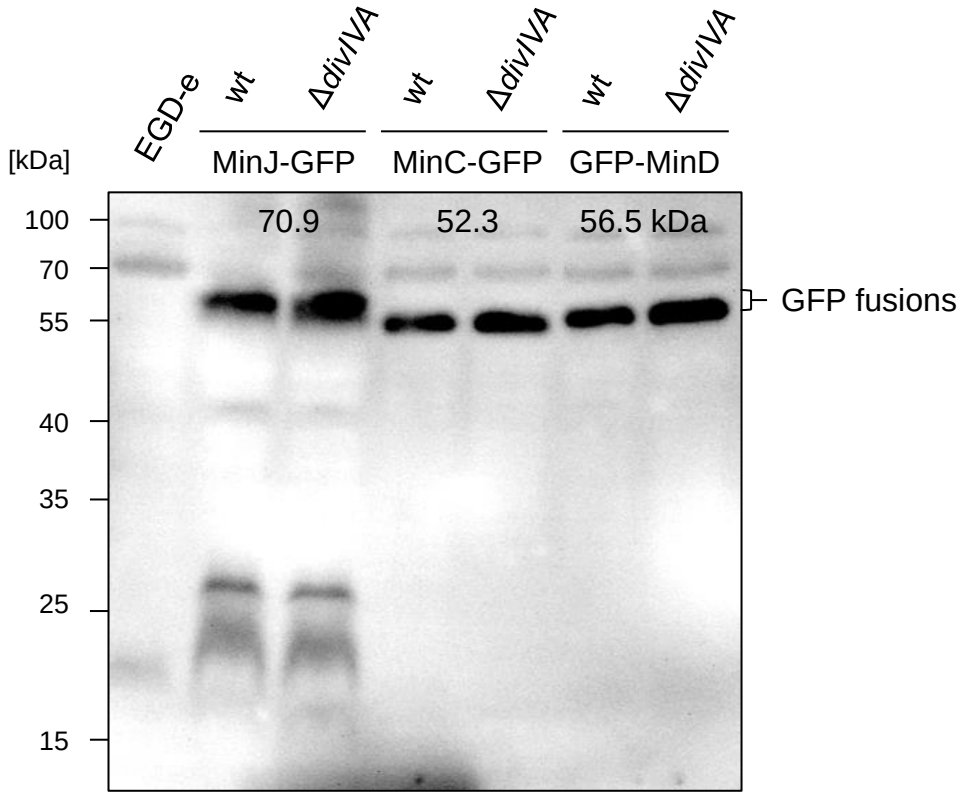


**Figure 13: Expression of GFP fusions of the Min proteins in the wild type and Δ*divIVA* mutant strains of *L. monocytogenes*.** Western blot displaying MinJ-GFP, MinC-GFP and GFP-MinD expression in wild type and Δ*divIVA* mutant strains. Strains LMKK71 (*minJ-gfp*), LMKK72 (Δ*divIVA minJ-gfp*), LMKK29 (*minC-gfp*), LMKK32 (Δ*divIVA minC-gfp*), LMKK30 (*gfp-minD*) and LMKK33 (Δ*divIVA minJ-gfp*) were cultured in BHI broth (1 mM IPTG was added to the MinC-GFP and GFP-MinD expressing strains) to exponential growth phase. Total cellular protein fractions (EGD-e, LMKK29, LMKK30, LMKK32, LMKK33) or extracts of membrane proteins (LMKK71, LMKK72) were separated using SDS-PAGE and stained using anti-GFP antiserum (1:5000 dilution) for GFP fusion protein visualization after Western blotting. The theoretical molecular weight corresponding to the GFP fusion proteins is indicated on the blot.

A similar septal enrichment pattern was observed for GFP-MinD upon expression in the wild type strain (LMKK30) (Fig. 12C), which was entirely lost upon deletion of *divIVA*

(LMKK33, Fig. 12D), and this was verified using confirmatory fluorescence intensity plots (Fig. 12H). MinC-GFP and GFP-MinD were expressed as full-length proteins in both the wild type as well as in the Δ*divIVA* mutant background, as indicated by western blots; however, MinJ-GFP displayed a somewhat lower molecular weight (64 kDa) than expected (71 kDa, Fig. 13). These results highlight the bi-functionality of DivIVA in *L. monocytogenes* in terms of its role played in the export of virulence-related autolysins via SecA2 (Halbedel et al., 2012), as well as its ability to recruit both MinC and MinD to the septum during cell division.

### 3.3.4 Phenotypic analysis of Δ*minCD* and Δ*minJ* mutants

Previously, attempts were made to insertionally disrupt all the three Min protein-expressing genes in *L. monocytogenes* EGD-e, namely *minJ*, *minD*, and *minC*, by the generation of pAUL-A constructs for the respective genes. It was observed that only the disruption of *minJ* was tolerated, while individual disruptions of *minC* and *minD* were not (Sven Halbedel, personal communication). This indicated an apparent lethality of the solitary disruption of either *minD* or *minC*, and the dispensability of *minJ*.

As an alternative strategy to obtain *L. monocytogenes* strains lacking *minCD*, the entire *minCD* operon was replaced with a single BamHI restriction site, flanked by a start and stop codon at either end (LMKK35). This was achieved using the pMAD derivative pSH378, which allowed for marker-free clean deletions (Arnaud et al., 2004). The same technique was also employed for generating a *minJ* clean deletion mutant (LMS120, Sven Halbedel). In order to study the effect of these deletions on cell division, microscopic analysis of logarithmically grown, membrane stained cells was performed for each strain. For the Δ*minCD* deletion mutant, a noticeable increase in cell length was observed (Fig. 14A). This effect was quantified by performing cell length measurements for approximately 300 cells for the Δ*minCD* mutant, and was compared to that of the Δ*minJ* and Δ*divIVA* mutants, as well as the EGD-e wild type strain. This quantification revealed an apparent elongation of cells upon *minCD* deletion, with an increase in average cell length from 1.2±0.3 µm as seen for the wild type, to 1.9±1.0 µm for the Δ*minCD* mutant. The Δ*divIVA* mutant also produced elongated cells, however, to a lesser extent (1.5±0.6 µm) as compared to that of the Δ*minCD* mutant, while the Δ*minJ* mutant (1.2±0.4 µm) was indistinguishable from the wild type. Plots of the cell length frequency distributions of each strain indicated that the apparent elongation of the

cells of the Δ*minCD* and Δ*divIVA* mutant strains was a heterogeneous phenomenon (Fig. 14B), since both strains produced both wild type-like as well as increased cell length sub-

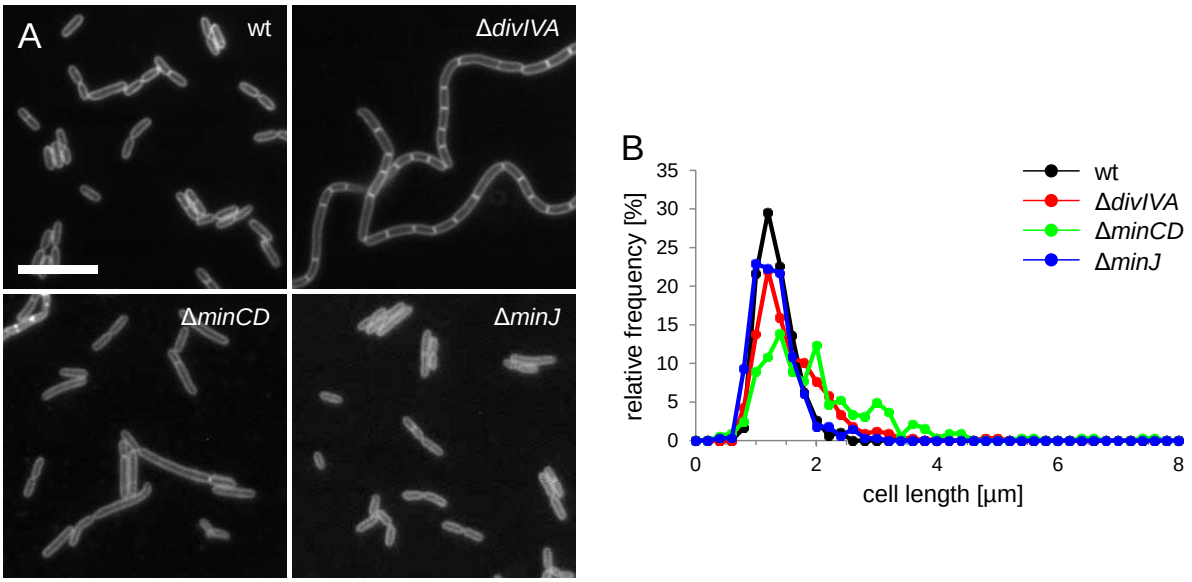


**Figure 14: Cell morphology of *L. monocytogenes min* mutants.** (A) Micrographs showing the cell morphological effects of *minCD* and *minJ* clean deletions in *L. monocytogenes*. Log-phase cells of listerial strains EGD-e (wt), LMKK35 (Δ*minCD*), LMS2 (Δ*divIVA*) and LMS120 (Δ*minJ*) were nile red stained and documented. The scale bar used is 5 µm. (B) Changes in cell length distribution profiles of *L. monocytogenes* cells upon deletion of *divIVA*, *minJ*, and *minCD*. The aforementioned strains were grown till $OD_{600}$ ~ 0.5 (mid-log phase) at 37°C in BHI broth prior to documentation, after which cell lengths were measured for a total of 301 cells of EGD-e (wt), 324 cells of LMKK35 (Δ*minCD*), 327 of LMS2 (Δ*divIVA*) and 332 cells of LMS120 (Δ*minJ*). The relative frequency of cells belonging to each predefined cell length class was determined and plotted.

populations. More importantly, it showed that the Δ*divIVA* mutant has a Δ*minCD*-like division phenotype that was hitherto unrecognized. The Δ*minCD* phenotype was cured by the introduction of an IPTG-controlled ectopic copy of the *minCD* operon (strain LMKK43) as was demonstrated by cell length measurements (Fig. 15B). This helped to rule out the possible contribution of any polar effects or uncharacterized suppressor mutations to the observed Δ*minCD* phenotype in strain LMKK35. The restoration of wild type cell length distribution in LMKK43 was IPTG dependent (Fig. 15A-B), and IPTG-dependent expression of MinD was confirmed by western blotting using a polyclonal antiserum generated against *B. subtilis* MinD that also recognized MinD from *L. monocytogenes* (Fig. 15C).

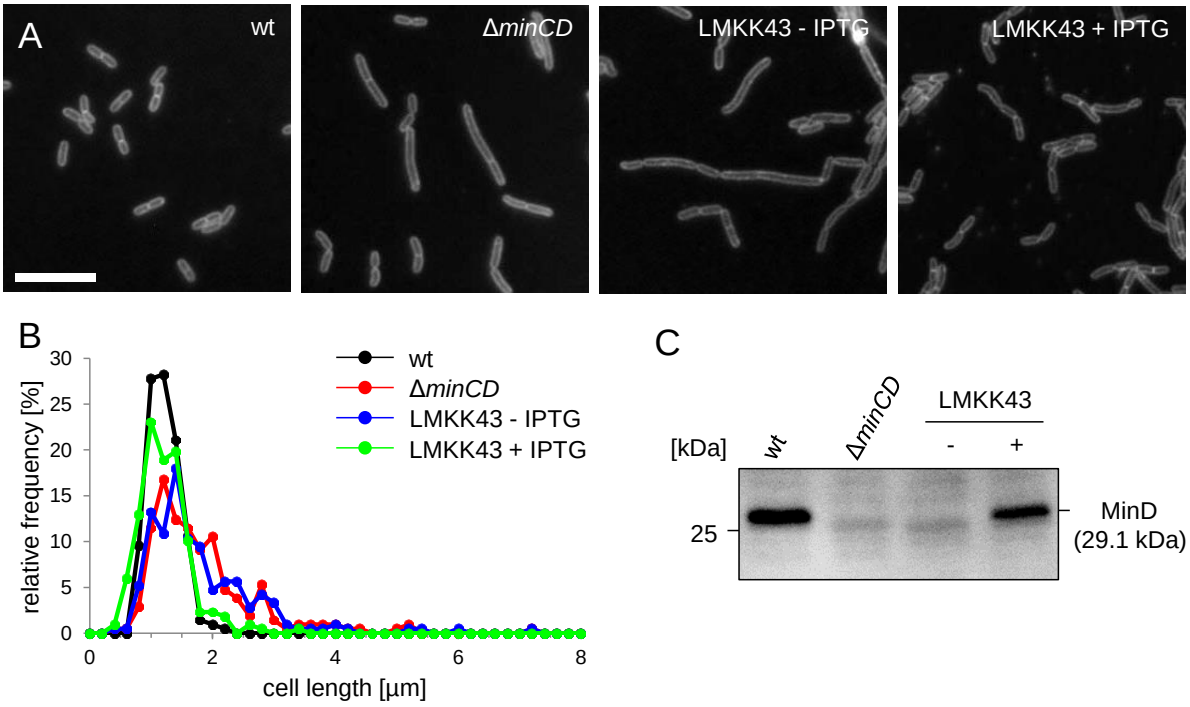


**Figure 15: Complementation of the *L. monocytogenes minCD* deletion mutant.** (A) Fluorescence micrographs displaying cell morphology of membrane stained (nile red) EGD-e (wt), LMKK35 (Δ*minCD*) and LMKK43 (IPTG inducible Δ*minCD*) cells. The scale bar used is 5 µm. The strains were grown at 37°C in BHI broth supplemented with 1 mM IPTG, where indicated, till they reached the mid-log phase, followed by sampling for microscopic analysis. (B) Cell length distribution profiles for the previously mentioned strains, cultivated and documented under identical conditions. Approximately 300 cells were measured per strain for their cell lengths. (C) MinD western blot for the same set of *L. monocytogenes* strains. Cells grown under the same conditions were harvested, cellular proteins were extracted, and MinD expression was visualized using an anti-MinD antiserum directed against *B. subtilis* MinD.

### 3.3.5 Distinction between Δ*divIVA* and Δ*secA2*mutant phenotypes of *L. monocytogenes*

Prior to the work described above, deletion mutants of *secA2* and *divIVA* were believed to be phenotypically identical, forming long chains of cells incapable of post-divisional separation due to defects in SecA2-dependent autolysin secretion at the site of septation (Halbedel et al., 2012). However, in the light of the new data obtained, it was tempting to speculate that the overwhelming formation of cell chains in the Δ*divIVA* mutant strain masked its characteristic *min* phenotype. To tackle this problem, a comparison was made between the Δ*divIVA* (LMS2) and Δ*secA2* (LMS81) strains on the basis of the relative frequency distributions of their cell lengths (Fig. 16A-B). The analysis revealed a stark similarity between the cell length distribution profiles of the wild type strain (EGD-e) and LMS81, whereas a greater degree of variability was seen for LMS2, which displayed a larger number of cells with elongated cell

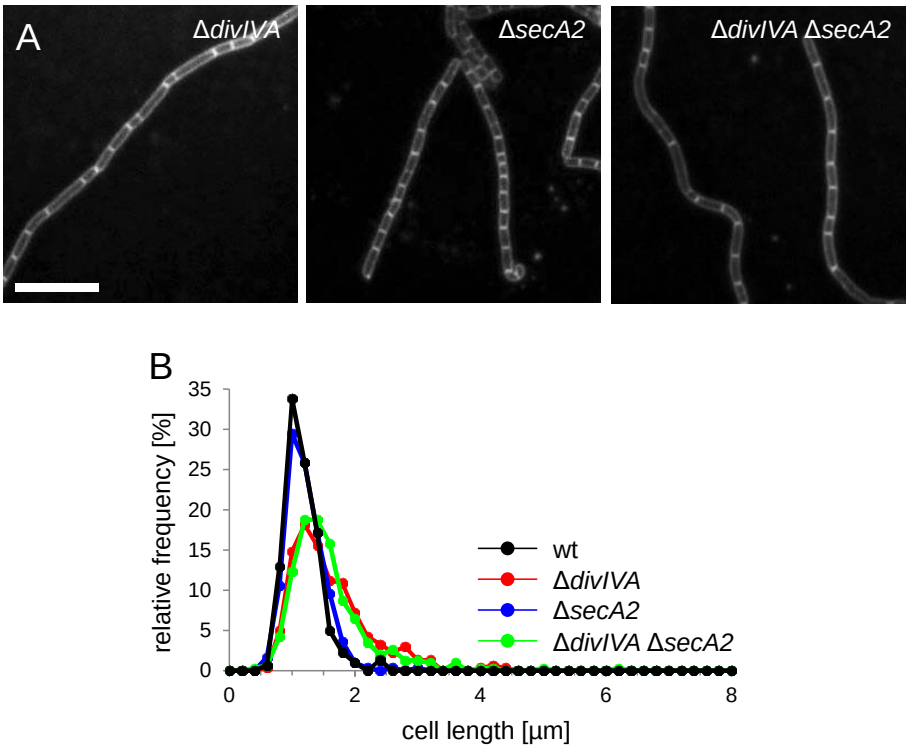


**Figure 16: Phenotypic distinction between Δ*divIVA* and Δ*secA2* strains of *L. monocytogenes*.** (A) Morphological comparisons between strains LMS2 (Δ*divIVA*), LMS81 (Δ*secA2*), and LMS127 (Δ*divIVA* Δ*secA2*) of *L. monocytogenes* . The scale bar used is 5 µm. Nile red staining was employed for mid-log phase cells of the respective strains, grown at 37°C in BHI broth, followed by fluorescent image capture. (B) Cell length distribution profiles of the above mentioned strains. In total, lengths of 303 cells of LMS2, 309 cells of LMS127 and 302 cells each of LMS81 and EGD-e (wt, control) were measured, processed and plotted.

lengths (Fig. 16B). This confirmed the assumption that the *L. monocytogenes* Δ*divIVA* mutant suffers from a cell division defect and showed that the Δ*divIVA* phenotype is a combinative effect on SecA2-dependent autolysin secretion as well as Min system-associated division site selection. To ascertain whether or not the secretion and division phenotypes of the *L. monocytogenes* Δ*divIVA* strain are coupled, a double mutant strain lacking both *divIVA* and *secA2* (LMS127) was created (Sven Halbedel). A cell length distribution plot generated for LMS127 bore a striking resemblance to that of the Δ*divIVA* strain (Fig. 16A-B), verifying the uncoupled and non-overlapping nature of the SecA2-dependent autolysin secretion and division site selection functions of *L. monocytogenes* DivIVA.

### 3.3.6 Verification of the linkage of DivIVA to the division site selection system using epistasis experiments

As a way of genetically confirming the association of DivIVA with the Min system of division site selection, double mutant strains of *L. monocytogenes* were generated involving the simultaneous knockout of *minCD* and *divIVA* (LMS125) and *minJ* and *divIVA* (LMS124). These strains, along with the relevant control strains (single mutants of *divIVA*, *minCD* and *minJ*), were cultured up to the mid-log phase and subjected to cell length measurement following a brief incubation (20 min) with nile red to stain their membranes. Cell length comparisons between the wild type strain EGD-e (1.2±0.3 µm for 303 cells measured) and the Δ*minJ* strain LMS120 (1.1±0.4 µm for 382 cells measured) showed close to no difference when it came to average cell lengths. However, the Δ*divIVA* strain LMS2 showed a slight degree of elongation (1.4±0.5 µm for 372 cells measured) as shown before. Surprisingly, a suppression of cell length elongation was observed upon combination of the *minJ* deletion with the Δ*divIVA* deletion (LMS124, 1.1±0.3 µm for 322 cells measured) as compared to the Δ*divIVA* single mutant (Fig. 17A). Cell length distribution plots highlighted this effect as a striking similarity was seen between the cell distribution profiles of the Δ*minJ* Δ*divIVA* double mutant and single mutant, Δ*minJ* (Fig. 17C). This dominance shown by the deletion of *minJ* over the *divIVA* knockout, in terms of regulation of cell length, reinforces the concept that both MinJ and DivIVA serve roles in the same pathway. They may however have counteracting effects on division site selection in *L. monocytogenes.* For the Δ*minCD* Δ*divIVA* double mutant strain (LMS125), an increase in average cell length was observed from 1.4±0.5 µm for that for the Δ*divIVA* single knockout mutant, as previously mentioned, to 1.8±1.0 µm for the 316 cells that were measured for the Δ*minCD* Δ*divIVA* double knockout (Fig. 17A). This was close, though similar, to that seen for the 380 cells measured for the Δ*minCD* single mutant strain, LMKK35 (1.9±1.2 µm). The cell length distribution plots for the aforementioned strains reiterated this fact (Fig. 17B), indicating non-additive effects of the *divIVA* and the *minCD* knockouts. The operation of MinCD at a position downstream of DivIVA was implied by the dominance that the Δ*minCD* deletion showed over the Δ*divIVA* mutation. A similar observation was made when a triple mutant, having both the *minCD* operon and the *minJ* gene deleted (LMKK54), was constructed, analyzed and compared to the respective single mutants. In this case, based on the cell length distribution profiles of the strains mentioned above (Fig. 17D), MinCD was confirmed to play a role downstream of MinJ.

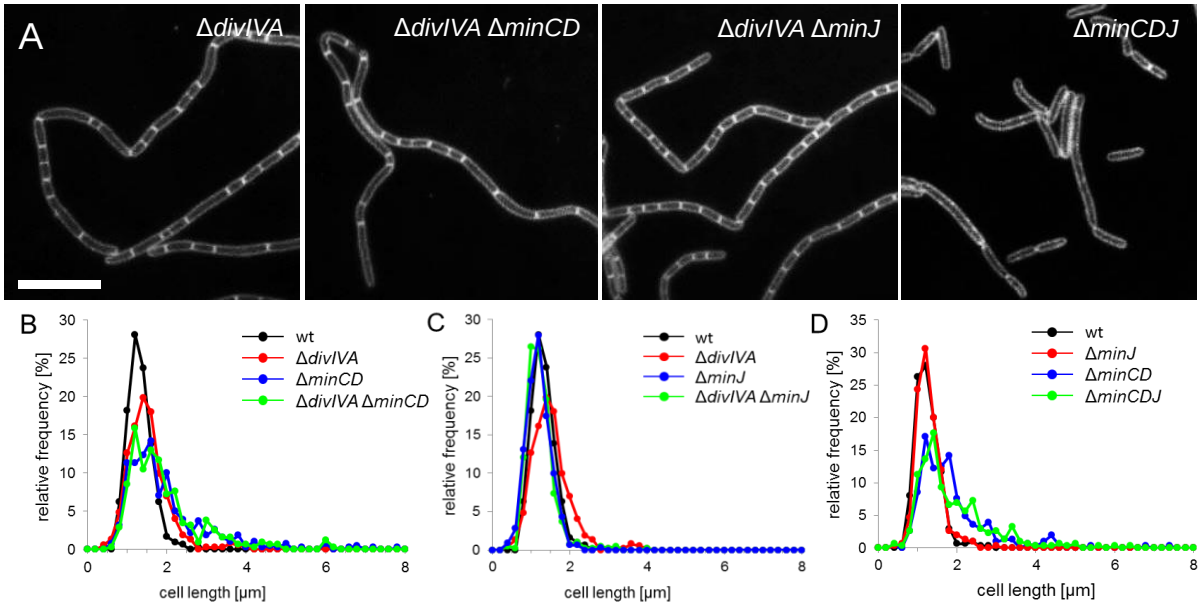


**Figure 17: Division phenotypes of *L. monocytogenes* Δ*divIVA* Δ*minCD*, Δ*divIVA* Δ*minJ* and Δ*minCDJ* mutants.** (A) Nile red stained cells of *L. monocytogenes* strains LMS2 (Δ*divIVA*), LMS125 (Δ*divIVA* Δ*minCD*), LMS124 (Δ*divIVA* Δ*minJ*) and LMKK54 (Δ*minCDJ*). The strains were subjected to growth at 37°C in BHI broth till they reached the mid-log phase, after which they were membrane stained and documented. The scale bar used is 5 µm. (B) The Δ*minCD* deletion phenotype was dominant over the Δ*divIVA* phenotype in the Δ*divIVA* Δ*minCD* double mutant. Cell length distribution profiles of EGD-e (wt), LMS2 (Δ*divIVA*), LMKK35 (Δ*minCD*) and LMS125 (Δ*divIVA* Δ*minCD*) were generated and analyzed. (C) Suppression of the *min* phenotype, as displayed by the Δ*divIVA* mutant, was achieved upon combining it with the Δ*minJ* deletion. Frequency plots for the cell length distributions of *L. monocytogenes* strains EGD-e (wt), LMS2 (Δ*divIVA*), LMS120 (Δ*minJ*) and LMS124 (Δ*divIVA* Δ*minJ*) denoted variations in cell lengths. (D) The Δ*minCDJ* triple mutant displayed a division phenotype similar to that of the Δ*minCD* mutant. EGD-e (wt), LMKK35 (Δ*minCD*), LMS120 (Δ*minJ*), and LMKK54 (Δ*minCDJ*) cell lengths were measured and the relative frequency of cells belonging to each cell length class was plotted.

### 3.3.7 Localization of the MinC and MinD proteins requires MinJ

A strong interaction was observed between MinJ and MinD in the bacterial two hybrid experiment, indicating that the localization of MinD might also be possibly influenced by MinJ. To test this, a Δ*minJ* mutant strain was generated that expressed GFP-MinD from an ectopic chromosomal copy (LMKK56). Upon growing this strain alongside the wild type control (LMKK30) to mid-log growth phase at 30°C in BHI broth, the septal localization of GFP-MinD in this strain was observed to be lost (Fig. 18B) as compared to the wild type control (Fig. 18A). Western blotting was performed, showing the expression of the full length GFP-MinD protein even in the Δ*minJ* mutant strain (LMKK56, Fig 18E); hence ruling out the possibility of proteolytic destabilization of GFP-MinD due to the absence of MinJ. For the strain expressing MinC-GFP in a Δ*minJ* mutant background (LMKK55), a similar lack of

localization of MinC-GFP fluorescence signals at the septal sites was observed (Fig. 18D) as compared to its corresponding wild type control strain (LMKK29, Fig. 18C). These results illustrate that in addition to DivIVA, MinJ is also essential for the appropriate subcellular localization of the MinCD complex and that both these proteins have a similar yet specific roles in the MinCD division site selection system.

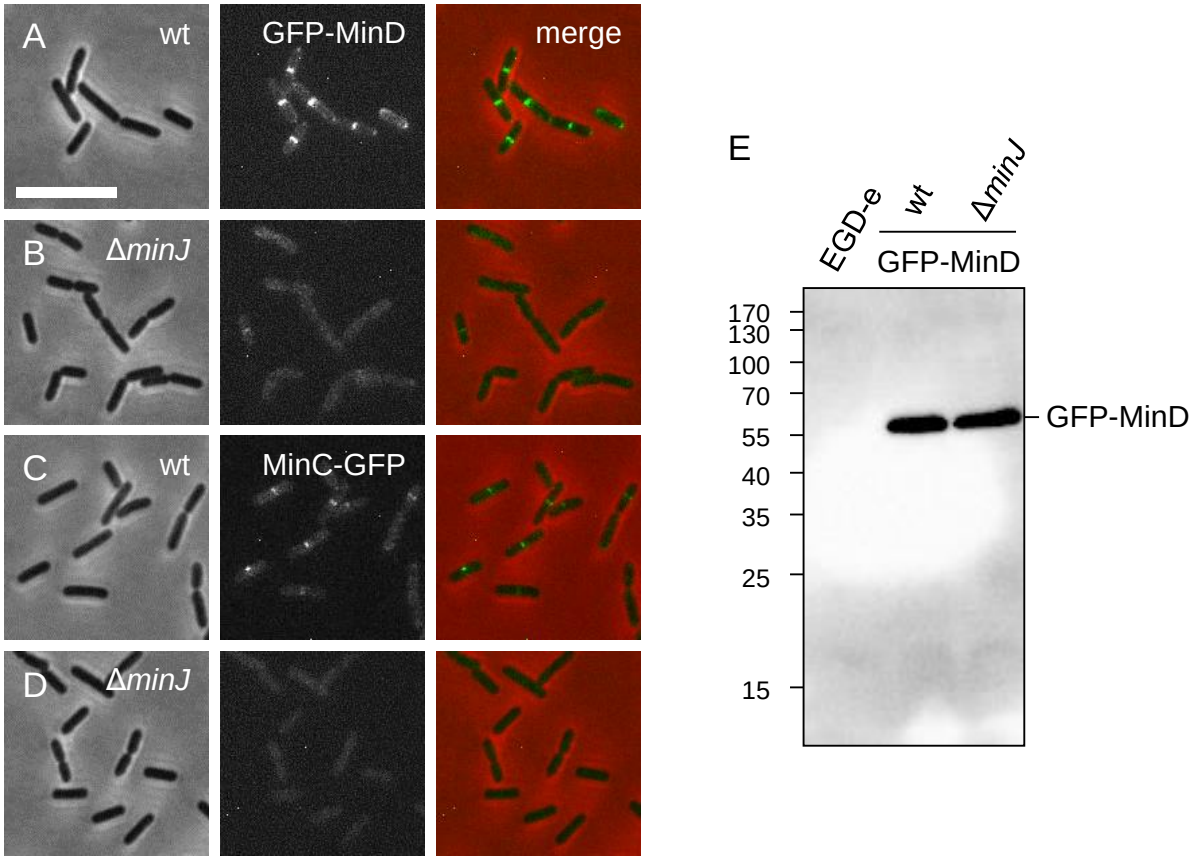


**Figure 18: Localization of MinCD proteins in the Δ*minJ* mutant.** Micrographs displaying GFP-MinD (A, B) and MinC-GFP (C, D) localization in wild type (A, C) or Δ*minJ* strains (B, D) of *L. monocytogenes*. Strains LMKK30 (*gfp-minD*) and LMKK56 (Δ*minJ gfp-minD*), as well as LMKK29 (*minC-gfp*) and LMKK55 (Δ*minJ minC-gfp*) were grown to the exponential growth phase in BHI broth supplemented with 1 mM IPTG at either 30°C or 25°C, respectively, and analyzed using both phase contrast (left column) and fluorescence microscopy (middle column). Merged images (right column) were included to facilitate better comparison. Scale bar is 5 µm. (E) Western blot showing expression of full-length GFP-MinD in the Δ*minJ* mutant background. Strains LMKK30 (*gfp-minD*) and LMKK56 (*ΔminJ gfp-minD*) were grown under identical conditions, followed by protein extraction, SDS PAGE separation and Western blotting using anti-GFP antibodies (1:3500 dilution, GE Healthcare). As a negative control, extracts from the wild type strain EGD-e of *L. monocytogenes* was used.

### 3.3.8 Effect of MinJ, MinCD and DivIVA on the localization of FtsZ

The Min system relies on its ability to spatially regulate the FtsZ ring, thereby influencing the process of division site selection. To better understand the influence of the MinCDJ and DivIVA proteins on cytokinetic ring formation in *L. monocytogenes*, intracellular localisation of FtsZ-GFP was analysed upon its constitutive expression in Δ*minJ*, Δ*minCD*, and Δ*divIVA* deletion mutants. FtsZ-GFP expression in the wild type strain (LMKK38) resulted in the display of bright fluorescent bands at the mid-cell loci (Fig. 19A), most of which did not

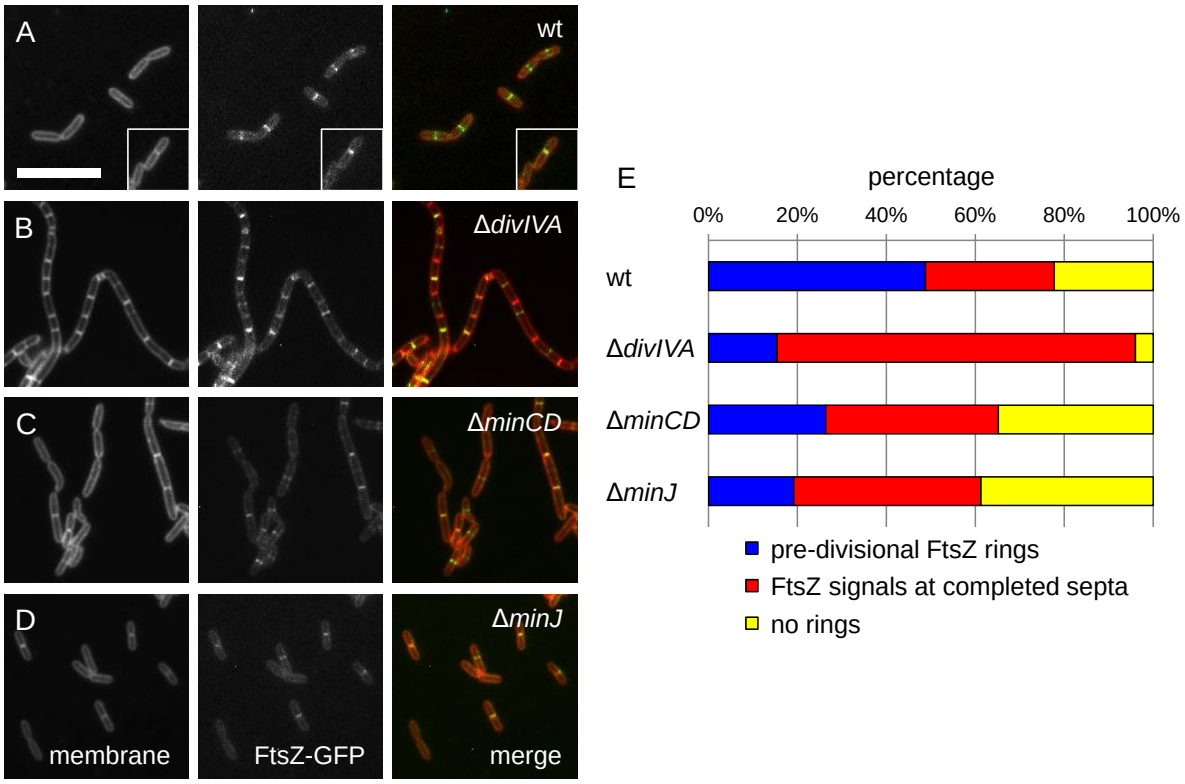


**Figure 19: Effects of Δ*divIVA*, Δ*minCD*, Δ*minJ* deletions on localization of FtsZ.** (A-D) Fluorescence micrographs displaying FtsZ-GFP localization patterns (centre panels) upon expression in *L. monocytogenes* strains LMKK38 (wt, A), LMKK39 (Δ*divIVA*, B), LMKK40 (Δ*minCD*, C), and LMKK41 (Δ*minJ*, D). The scale bar used is 5 µm. The strains were grown in BHI broth at 30°C in the presence of 1 mM IPTG till they reached the mid-logarithmic phase, followed by nile red staining and documentation using fluorescence microscopy. Membrane stained (left panel) and merged (right panel) images were comparatively used for mid-cell and cell boundary determination. (E) Bar chart indicating the percentage of cells bearing either pre-divisional FtsZ rings, FtsZ rings at the completed division septa or no rings whatsoever for the same set of strains described in panels A-D. Roughly 200 cells, per strain, were counted and characterized into the 3 categories.

initiate cell division, as shown by nile red based membrane staining. FtsZ-GFP which do not colocalize with membranous septa represent pre-divisional FtsZ rings (Fig. 19A). Also,

concentrated signals of FtsZ-GFP were shown to co-localize with the division septa, shortly after cell division, typical for constricted Z-rings in a fraction of cells (Fig. 19A insert). However, in a *divIVA* deletion strain (LMKK39, Δ*divIVA ftsZ-gfp*), less intense un-constricted FtsZ-ring-associated signals were observed at slightly off-centered loci. FtsZ-GFP signals, predominantly localizing to the membranes at closing division septa, were also observed (Fig. 19B). Similar observations were made for *minJ* (LMKK41, Δ*minJ ftsZ-gfp*) and *minCD* (LMKK40, Δ*minCD ftsZ-gfp*) deletion strains as well, with faint signals at either mid-cell or off-centered positions, as well as predominant, closed division septa-adjacent, membrane associated FtsZ-GFP fluorescence signals (Fig. 19C-D).

A quantitative comparison of the aforementioned strains was performed by grouping approximately 200 cells, per strain, into 3 classes on the basis of the stage of FtsZ-ring formation (Fig. 19E). The fraction of cells belonging to the class of pre-divisional FtsZ-ring bearing cells, was reduced to 16±3%, 24±2% and 18±3%, for the Δ*divIVA*, Δ*minCD* and Δ*minJ* mutant strains, respectively, as compared to that of the wild type strain (47±6%, n=3). For the proportion of cells having FtsZ-GFP signals at closed division septa, which the *divIVA* deletion mutant had an abundance of (80±4%), the *minCD* (33±6%) and *minJ* (30±10%) deletion strains showed only a modest increase in these subpopulations as compared to the value of 24±4% seen for the wild type strain. These data not only indicate a similarity in the impact on FtsZ-ring formation by DivIVA and the three Min proteins, but also highlight the possibility of a more significant contribution of DivIVA in FtsZ turnover upon achievement of constriction.

### 3.3.9 *L. monocytogenes* division site selection mutants and their minicelling phenotypes

The formation of minicells by Δ*minCD* and Δ*minJ* deletion mutants of *L. monocytogenes*, though at a lower frequency, was uncovered over the course of the previously mentioned investigations. The smaller size of *L. monocytogenes* cells coupled with the low frequency of minicelling as compared to that of either *E. coli* or *B. subtilis*, significantly hampered the conclusive identification of minicells in these *min* mutants. Hence, to improve the accuracy and reliability of minicell detection, GFP was expressed in the wild type, Δ*minJ*, Δ*minCD* as well as the Δ*divIVA* strain of *L. monocytogenes*. Strains LMS10 (*gfp*), LMKK36 (Δ*minCD gfp*), LMKK54 (Δ*divIVA gfp*) and LMKK37 (Δ*minJ gfp*) were cultured up to the mid-log phase and analyzed using microscopy following staining with DAPI and nile red. Minicells

were observed for both the Δ*minCD* and the Δ*minJ* strains, seen as spherical cells bearing membrane signals as well GFP fluorescence (Fig. 20A-B, white arrows); however, neither the wild type nor the Δ*divIVA* strain displayed this phenotype (data no shown). To our surprise, DAPI signals were found to be associated with these mincells, indicating that they might contain DNA. These DNA-associated DAPI signals however seemed to be circumferential and less intense as compared to the nucleoid-coupled DAPI signals of rod shaped cells (Fig. 20A-B). Subsequently, this peripheral DAPI fluorescence signal was believed to be either a bleed-through of the nile red membrane signal into the DAPI channel or an inherent problem with the DAPI staining itself. To ascertain as to which of the two previously mentioned problems it might be, simultaneous staining of the above strains with both DAPI and nile red was abandoned and was instead only DAPI stained. This uncovered an intrinsic flaw in the ability of the DAPI dye to effectively stain minicells, which resulted in a false membrane-bound DNA signal in the absence of both the nucleoid and the nile red membrane staining, probably due to unspecific membrane binding in the absence of DNA (data not shown). As a way to counteract this problem, staining with Hoechst 33342 was employed. This DNA staining method showed that the supposed minicells were in fact true minicells, characterized by a complete absence of any DNA signal upon deletion of the *min* genes (Fig. 20C-D, white arrows). Approximately 500 cells were counted for both the wild type and Δ*divIVA* deletion strains (LMS10 and LMKK54, respectively), to determine the minicelling frequency;

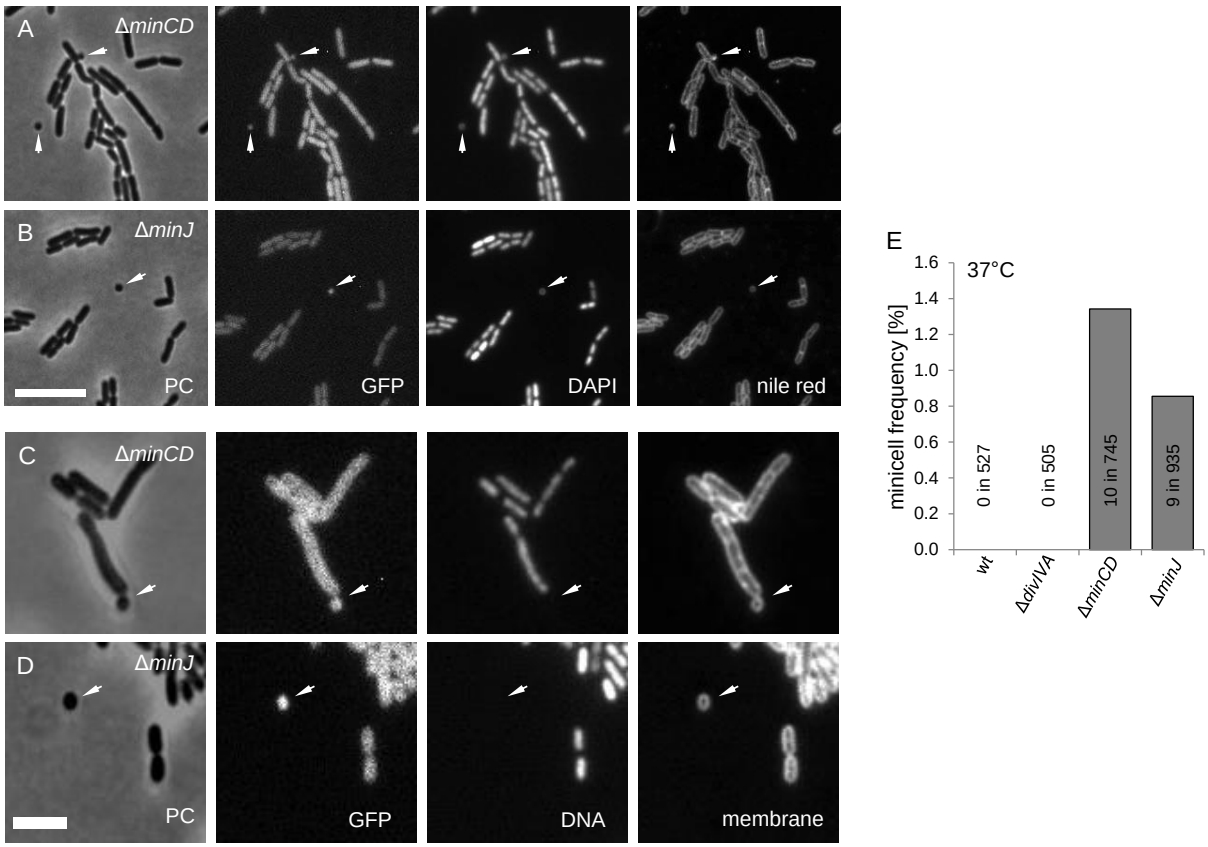


**Figure 20: Mini-cell formation associated with *L. monocytogenes* Δ*minJ and* Δ*minCD mutants*.** (A-B) Micrographs showing mini-cell formation in LMKK36 (panel A, Δ*minCD gfp*) and LMKK37 (panel B, Δ*minJ gfp*) strains of *L. monocytogenes*. The earlier mentioned strains were grown to mid-exponential growth phase in BHI broth at 37°C. Multi-channel microscopy was used to detect membrane (nile red stained), chromosomal (DAPI stained) and GFP signals. Phase contrast bright field images were also taken for the same sections and hence served as a reference. Mini-cells are marked with white arrows. The scale bar used is 5 µm. (C-D) Micrographs for the same set of strains under identical conditions; however, utilising Hoechst 33342 instead of DAPI for chromosomal staining. The scale bar used is 2 µm (E) Mini-celling frequency for the previously mentioned strains following identical growth and measurement criteria. LMS10 (wild type *gfp)* and LMS54 (Δ*divIVA gfp*) were included as control strains. Raw data indicating the number of minicells found in the total number of cells counted, for each strain, have been included in the plot.

however, under the conditions used, no minicells were found leading to a frequency of minicell formation of <0.2% (Fig. 20E) in wild type strain EGD-e. On the other hand, under the same conditions, the Δ*minCD* mutant strain (LMKK36) produced minicells with a frequency of 1.9%, while for the Δ*minJ* deletion strain (LMKK37) this frequency seemed to be slightly reduced bearing a value of only 0.9% (Fig. 20E).

Minicell formation seemed to be the only phenotypic characteristic that helped distinguish the Δ*minJ* mutant from the wild type strain in *L. monocytogenes*, and most interestingly, only this feature facilitated the documentation of the wild type phenotype-restoration in the Δ*minJ* deletion mutant. Strain LMKK44 was generated which was capable of expressing an IPTG-inducible ectopic copy of *minJ* in the Δ*minJ* strain. In fact, it was observed that under depletion conditions LMKK44 possessed a capability of producing minicells, which was lost

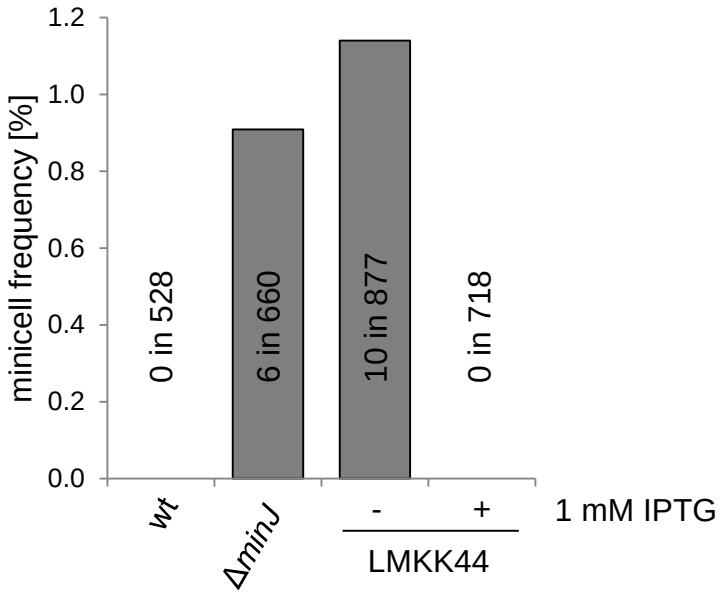


**Figure 21: Complementation of the Δ*minJ* mutant mini-celling phenotype.** Mini-celling frequency plots for the EGD-e (wt), LMS120 (Δ*minJ*) and LMKK44 (IPTG inducible Δ*minJ*) strains of *L. monocytogenes*. The aforementioned strains were cultivated in BHI liquid media containing IPTG (1 mM final concentration), where indicated, at 30°C. Following DAPI and nile red staining, the spherical, achromosomal mini-cells were enumerated. The raw data for the corresponding experiment has been shown.

upon induction of MinJ expression with 1mM IPTG (Fig. 21). This showed that the observed Δ*minJ* phenotype is caused by deletion of *minJ* and not by polar effects or unwanted second site mutations.

### 3.3.10 Increase in minicelling frequency in the Δ*minCD* mutant by expression of additional FtsZ copies

Previously performed FtsZ localization studies revealed an apparent increase in the minicell-forming frequency of the Δ*minCD* deletion mutant (strain LMKK40), as a result of the induction of FtsZ-GFP expression from an ectopically placed copy. This observation was interesting, as minicells of *L. monocytogenes*, like their parental rod shaped cells, might possibly harbor the capability of invading eukaryotic host cells, e.g. macrophages. Such invasive competence of these minicells could potentially be exploited for targeted pharmaceutical interventions in the fields of gene and cancer therapy; hence, this incremental effect on minicell frequency was further investigated. When strain LMKK40 (Δ*minCD*

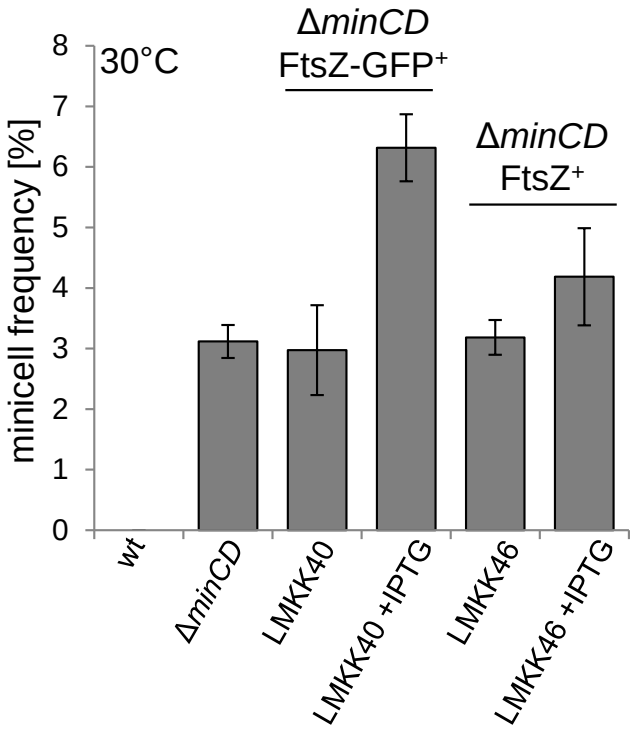


**Figure 22: Increased minicell formation in the Δ*minCD* mutant upon overexpression of FtsZ variants.** Enhancement in the mini-celling frequency of the Δ*minCD* mutant as a result of overexpression of wild-type and GFP fusion variants of *L. monocytogenes* FtsZ. EGD-e (wt), LMKK35 (Δ*minCD*), LMKK46 (Δ*minCD ftsZ*$^+$) and LMKK40 (Δ*minCD ftsZ-gfp*$^+$) were grown to $OD_{600}$=0.5, corresponding to the logarithmic growth phase, at 30°C in BHI broth (containing 1 mM IPTG when indicated). The ratio of mini-cells for these strains was ascertained from the DAPI and nile red stained micrographs. Three independent experiments were conducted for the purpose of calculating standard deviations and average values.

*attB::Phelp-lacO-ftsZ-gfp*) was grown under uninduced conditions at 30°C, it produced minicells at a frequency of approximately 3%, which was similar as compared to that seen for the Δ*minCD* mutant strain (LMKK35) under the same settings. Upon cultivation of LMKK40 in the presence of 1 mM IPTG, FtsZ-GFP expression was induced leading to an increase in the mini-celling frequency to 6.3±0.6% (Fig. 22). Due to worries over the functionality of the GFP fusion of FtsZ, which was not verified via complementation studies, a Δ*minCD* strain expressing an untagged version of FtsZ (LMKK46) was similarly constructed and analyzed. A similar increase in minicell formation (4.2±0.8%) was observed for LMKK46 (Δ*minCD attB::Phelp-lacO-ftsz*), however, to a lesser extent as compared to LMKK40, examined within the same parameters (Fig. 22). A putative restriction in the accessibility of FtsZ-regulating proteins, such as FtsA (Din et al., 1998), EzrA (Singh et al., 2007) or SepF (Krol et al., 2012), to the C-terminus of FtsZ due to its fusion to GFP, might explain the higher rate of FtsZ ring constrictions at the cell poles in the FtsZ-GFP expressing strain.

### 3.4 Identification of the domains of DivIVA associated with the division-site selection and autolysin secretion functions in *L. monocytogenes*

As described previously, DivIVA in *L. monocytogenes* serves a dual function. Firstly, it is involved in the correct placement of the divisome at the mid cell region during cell division via its association with the Min system, and secondly it facilitates the secretion of cell-separation associated autolysins, namely p60 and MurA, after the completion of cell division via the accessory ATPase SecA2. It is still unclear which domain(s) of DivIVA are responsible for these two functions, and whether they can be separated. Domain-swap experiments were performed with DivIVA, involving chimeras where sections of *L. monocytogenes* DivIVA were swapped with its homologous counterparts from *B. subtilis* (see chapters 3.2). However, these analyses were performed prior to the knowledge of the dual function of DivIVA.

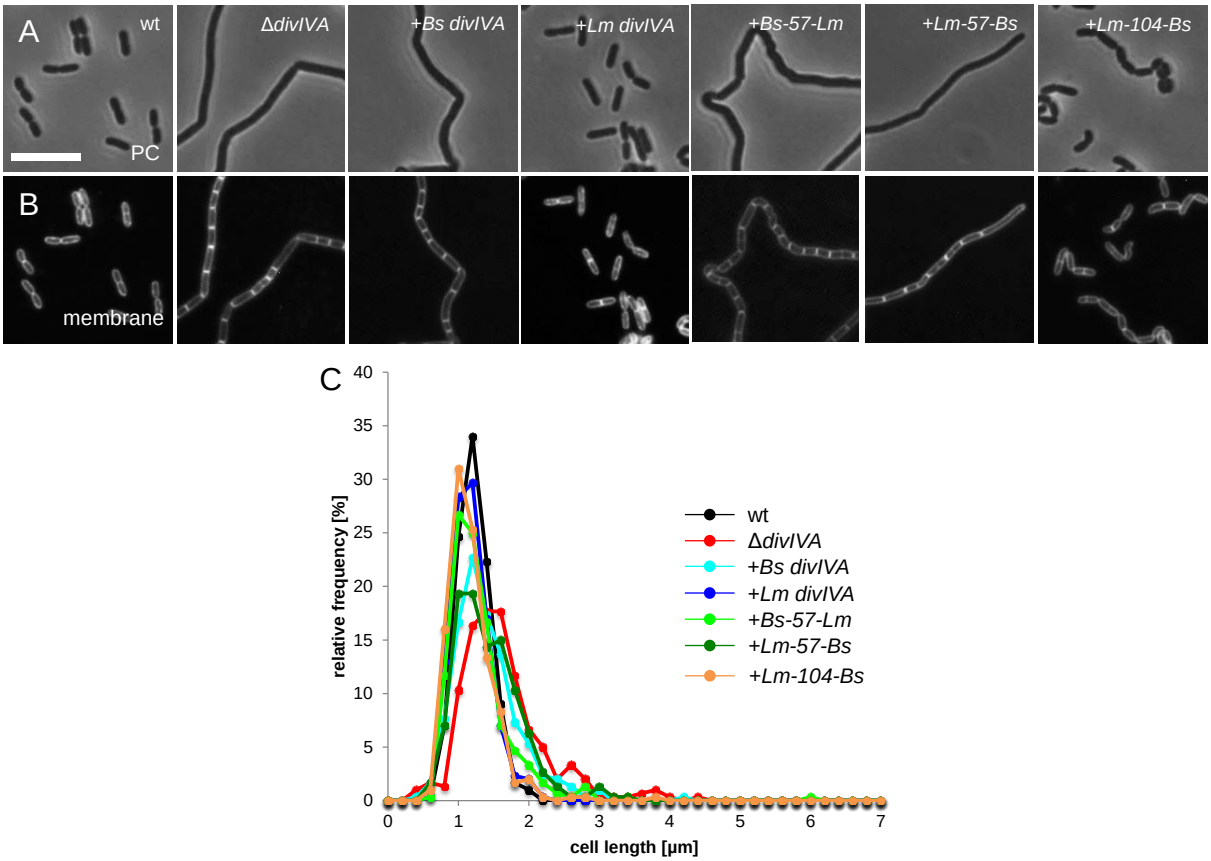


**Figure 23: DivIVA domains responsible for cell division and cell separation.** (A-B) Phase contrast and fluorescence micrographs exhibiting cell morphology of nile red stained (membrane) EGD-e (wt), LMS2 (Δ*divIVA*), LMKK8 (Δ*divIVA +Bs divIVA*), LMS30 (Δ*divIVA +Lm divIVA*), LMKK14 (Δ*divIVA +Bs-57-Lm*), LMKK12 (Δ*divIVA +Lm-57-Bs*) and LMKK13 (Δ*divIVA +Lm-104-Bs*) cells. The scale bar used is 5 µm. The strains were cultured at 37°C in BHI broth supplemented with 1 mM IPTG, where indicated, till they reached the mid-logarithmic phase, followed by sampling and microscopic analysis. (C) Cell length distribution plots for the aforementioned strains, which were cultivated and documented under the same conditions. Roughly 300 cellswere measured per strain.

Hence, cell lengths of logarithmically growing cells of the EGD-e (wt), LMS2 (Δ*divIVA*), LMKK8 (Δ*divIVA +Bs divIVA*), LMS30 (Δ*divIVA +Lm divIVA*), LMKK14 (Δ*divIVA +Bs-57-Lm*), LMKK12 (Δ*divIVA +Lm-57-Bs*) and LMKK13 (Δ*divIVA +Lm-104-Bs*) strains (Fig. 23A-B) were measured. On plotting the cell length distribution profiles of the aforementioned strains (Fig. 23C), it became evident that the *Lm-104-Bs* chimera of DivIVA was able to complement both the division as well as the cell separation/autolysin secretion phenotypes of the Δ*divIVA* mutant. However that was not the case with the strains expressing either the *Lm-57-Bs* chimera or *Bs divIVA*, where both the cell division and cell separation defects were apparent. Interestingly, the strain expressing the *Bs-57-Lm* chimera of DivIVA displayed wild type cell lengths, but still had the cell chaining aberration, which was a clear indication of the

restoration of only the cell division defect of the Δ*divIVA* mutant but not of the cell separation phenotype. This highlights the importance of the C-terminal coiled-coil domain with respect to its role in division site selection; however, it seems that just its starting section (amino acid residue position 71-104) is required to mediate this function. It also indicates that the N-terminal lipid binding domain along with the adjacent regions stretching up to amino acid residue position 104 facilitate the SecA2-dependent autolysin secretion. Since the LBD of DivIVA proteins can interact with transmembrane proteins, while the CTD interacts with cytosolic binding partners (van Baarle et al., 2013), this points towards a possible interaction with a transmembrane component of the SecA2-dependent protein secretion system. Nevertheless, further experimentation is required, starting with the construction of more domain-swap chimeras bearing stepwise exchanges within the above mentioned domain sections, to narrow down the interaction surfaces involved in either of the two functions of DivIVA.

## 3.5 Experiments aiming at the identification of other putative interaction partners of *L. monocytogenes* DivIVA

A fresh perspective was needed to tackle the problem of identifying more potential DivIVA interaction partners. Rather than focusing on specific, known interaction partners of DivIVA, derived from literature screenings for homologues found in other closely related firmicutes such as *B. subtilis*, a broader approach was required.

### 3.5.1 Transposon mutagenesis-based genome wide screening method

As an alternative strategy to identify supposed interaction partners of DivIVA, a genome wide transposon mutagenesis scheme was employed. This technique would allow for the creation of a collection of *L. monocytogenes* mutants, each bearing a disruption of a single gene in the genome, due to random insertion of the transposon, covering the entire genome. The logic behind the use of this approach dictated that the disruption of any gene, coding for a specific protein belonging to a proposed pathway, would interrupt the entire cascade. Such an interruption, if leading to a phenotypic dissimilarity to the wild type, could be exploited to uncover the genes involved in that pathway.

It is known that a Δ*divIVA* deletion mutant of *L. monocytogenes* forms elongated chains of cells due to a defect in secretion of autolysins (Halbedel et al., 2012), which translates to cell colonies having a rough surface morphology (Machata et al., 2005, Halbedel et al., 2012); and this phenotypic variation would be used for screening for mutants of DivIVA interaction partners. Such transposon-insertion mutants, like the Δ*divIVA* mutant, would also sediment in liquid cultures despite agitation. Firstly, transposon mutagenesis was carried out using the protocol described in section 2.2.1.6. After the final 40°C step of the transposition protocol,

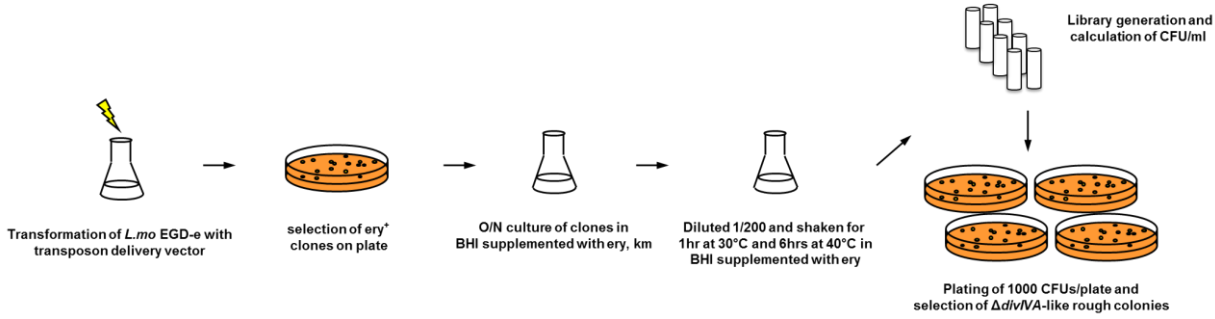


**Figure 24: Transposon mutagenesis and screening.** Schematic representation of the transposon mutant library construction and screening. The transposon delivery vector, pMC38, was used for electroporation into EGD-e (wt) and random insertion of the *HimarI* mariner transposon into its genome. The subsequent steps involved are shown in the figure and described in the text.

enrichment of the resultant cultures was done which entailed the re-suspension of the sedimented cell fractions in 1 ml of BHI broth, followed by addition of equal volumes of glycerol and freezing at -80°C. These glycerol stock cultures, following cfu/ml value determination (0.9 - 1.82 x $10^9$), were used as the transposon mutant libraries for screening (Fig. 24). The number of colonies to be plated out ($n$), to cover all transposon insertion events in the genes of interest (size $g$) in the genome (size $l$), with minimum probability of $P$, was calculated using the formula below:

$$n = \log(1 - P) / \log(1 - (g/l))$$

Hence, it was determined that approximately 13200 colonies from the transposon-insertion mutant libraries would have to be plated and screened to find a transposon mutant, having an insertion in a gene coding for a DivIVA interaction partner, with a probability of 99% (average $g$ = 1.032 kb, $l$ = 2.944 mb). A total of 30 plates were streaked out with 1000 colonies per selective BHI plate containing erythromycin (5 µg/ml), and screened for Δ*divIVA*-like rough colony morphology (Fig. 24). This led to the identification of 36 rough colony isolates.

During the screening process, all the rough colonies that were picked were patched out on 2 sets of selective plates of BHI, the first set containing only erythromycin, while the other bore both erythromycin and kanamycin (10µg/ml). This was done to exclude any *L. monocytogenes* clones, which still possessed the transposon delivery vector backbone. PCR verification for the *divIVA* and *secA2* loci of the isolates was performed to rule out clones with transposon insertions in either of these two genes; as such mutants would also display rough colony morphology. Out of the 36 rough isolates that were identified, 19 of them had a transposon insertion event at the chromosomal *secA2* loci; however, none of them had an insertion in the *divIVA* gene. 16 of the 17 remaining isolates, which did not have an insertion in either of the two aforementioned genes, still possessed the vector backbone integrated in their genome despite being screened on BHI plates containing kanamycin (10 µg/ml) (data not shown). This screening procedure led to the identification of a single, potential DivIVA interaction partner mutant which was designated LMKK18, which did not have Tn insertions in *secA2* or *divIVA*. During the screening process, one isolate, which had a colony morphology that was smoother than that of the wild type, was also identified. This so-called "super-smooth" variant did not match the screening criteria (data not shown); nonetheless, it had a unique phenotype and hence was isolated so as to be characterized in the future.

### 3.5.2 Phenotypic characterization of rough transposon insertion isolate, LMKK18

Macroscopic analysis of the LMKK18 transposon insertion mutant at 10 x magnification revealed Δ*divIVA*-like rough colony morphology (Fig. 25A). This mutant also displayed the classical cell-chaining phenotype, similar to a Δ*divIVA* mutant strain LMS2 (Fig. 25B). Swarming motility assays performed over 24 h indicated a defect in swarming capabilities, which was comparable to that observed for the Δ*divIVA* deletion strain (Fig. 25C). The p60 autolysin secretion profile of strain LMKK18 in comparison to the wild type strain (EGD-e)

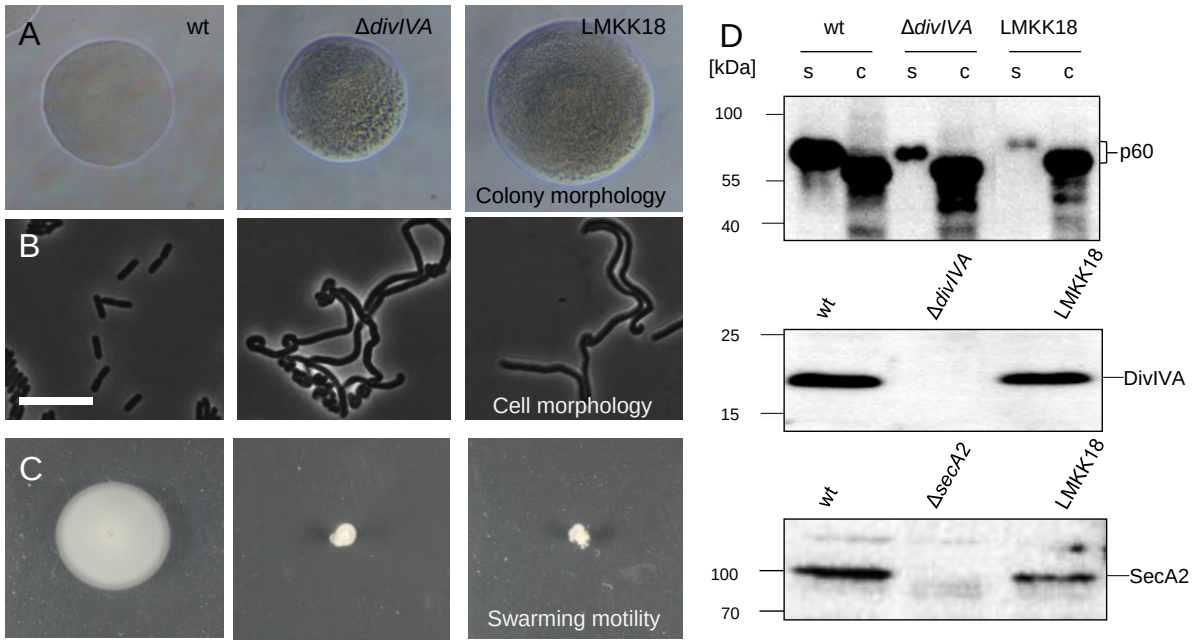


**Figure 25: Phenotypic characterization of the rough transposon insertion mutant LMKK18 of *L. monocytogenes*.** (A) Colony morphology for EGD-e (wt), LMS2 (Δ*divIVA*) and LMKK18 (transposon insertion mutant) visualized at 10 x magnification under a phase-contrast microscope (ph3 phase ring). (B) Cell morphology for the same set of strains. The scale bar used is 5 µm. (C) Swarming motility for the aforementioned strains. Swarming halos were documented after 24h of growth at 30°C on LB plates containing 0.3% agar. (D) Western blots for the previously mentioned strains under identical conditions. Cellular and extracellular protein extracts were checked for expression of p60 (top blot, extracellular fractions of the respective strains, "s", included, α-p60 – 1:5000), DivIVA (middle blot, α-DivIVA – 1:2500) and SecA2 (bottom blot, α-SecA2 – 1:3500). LMS81 (Δ*secA2*) was used as a control for the SecA2 western blot.

as well as LMS2 (Δ*divIVA*) was tested by Western blotting in both extracellular and cytosolic fractions of cell cultures. This showed that LMKK18 synthesizes p60 but does not secrete it. However, a slightly stronger deficiency in terms of p60 secretion was noticed for the LMKK18 strain, where a less intense band, as compared to that of the LMS2 strain, was perceived in the supernatant fraction of the cell cultures (Fig. 25D, topmost western blot). Expression levels of both DivIVA and SecA2 in LMKK18 were verified to be equivalent to that seen for the wild type, via western blotting and staining with the corresponding antibodies (Fig. 25D), middle and bottommost western blots, respectively). This shows that strain LMKK18 has a *divIVA*-like phenotype which is not the result of transposon insertions in *secA2* or *divIVA*.

### 3.5.3 Transposon insertion site determination in transposon mutant of *L. monocytogenes* and its bioinformatics-based analysis

To determine the site of transposon insertion in the genome of the LMKK18 strain of *L. monocytogenes*, inverse PCR was utilized as described in section 2.2.2.4.4 (Pozsgai et al., 2012). To reconfirm the sequencing results, in addition to TaqI (recognizing the sequence "TCGA", followed by a staggered cut at T) seven other restriction enzymes (BamHI, KpnI, NcoI, SalI, XbaI, EcoRI and SpeII, 6 base pair recognition sites), were used to randomly cleave the chromosome. Once ligation was achieved to circularize the chromosomal fragments, the same inverse PCR protocol, using primers SHW427/428, was employed to amplify the desired product. Sequencing results obtained with inverse PCR products, irrespective of the restriction endonuclease used, repeatedly indicated that the insertion of the transposon took place in the *lmo0720* gene at codon position 29, causing its disruption (Fig. 26).

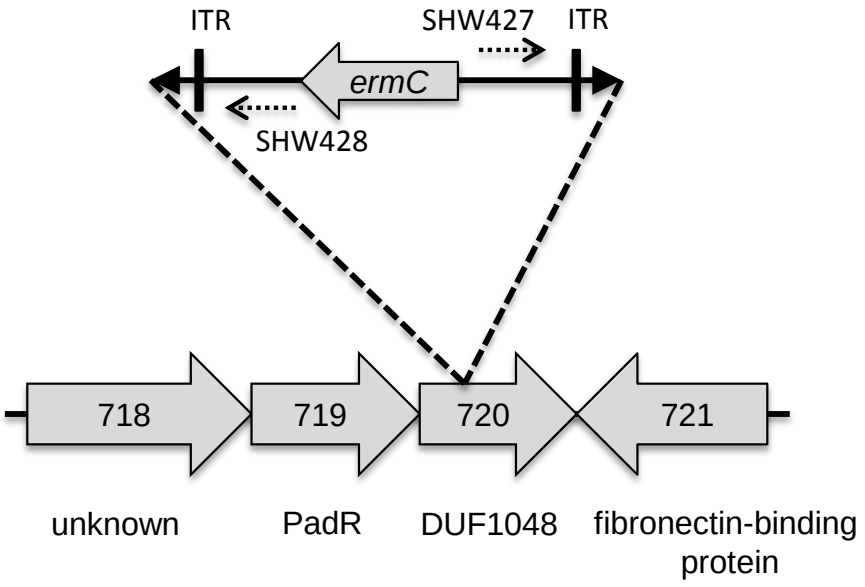


**Figure 26: Determination of the transposon insertion site in *L. monocytogenes* transposon mutant.** Schematic representation of the site of insertion of the transposon in the genome of EGD-e (wt). Inverse PCR was performed with the primer pair SHW427/428 and site of insertion was determined to be in the gene *lmo0720*. The *ermC* cassette of the transposon allowed for erythromycin based selection of the mutants. *lmo0720* was found to have the DUF1048 domain who's function is not yet known.

Bioinformatics indicated that *lmo0720* is a so far uncharacterized gene, with homologs in other bacterial species belonging to the class Bacilli. A conserved domain comparison indicated that its protein product possesses a domain belonging to the DUF1048 superfamily, the function of which, however, is still not known. Gene *lmo0720* was found to be part of an operon having one more gene, residing upstream to it, namely, *lmo0719*. Blastp analysis revealed that the protein Lmo0719 is a predicted transcriptional regulator belonging to the PadR-like family of transcriptional repressors. The *lmo0719-0720* operon is flanked by the upstream gene *lmo0718*, coding for a protein of unknown function, and the downstream gene *lmo0721*, which transcribes and translates for a protein binding to fibronectin (Fig. 26).

In order to rule out that the rough phenotype of LMKK18 results from point mutations in *secA2* or *divIVA*, gene sequences for *divIVA* and *secA2* from LMKK18 (transposon insertion mutant) were sequenced This revealed the presence of a single point mutation in the *secA2* gene, causing a G484E substitution in the expressed SecA2 protein, whereas *divIVA* had its wild type sequence unaltered.

### 3.5.4 Genetic and structural relevance of the *secA2G484E* mutation

Sequence alignments of *L. monocytogenes* EGD-e SecA2 with the SecA proteins from *B. subtilis*, *E. coli* and *L. monocytogenes*, display a high degree of sequence conservation (Fig. 27A). The substitution mutation in the *secA2* gene, causing a change in the protein sequence at the residue position 484 from glycine to glutamic acid, was shown to reside in the intramolecular regulator of ATPase IRA2 domain of the protein (Fig. 27A). It is known that IRA1 and IRA2 collectively function as a molecular switch, coupling translocation of proteins to hydrolysis of ATP (Karamanou et al., 1999) and that IRA2 itself binds to the ATPase catalytic machinery, the nucleotide binding domain NBD1, ensuring optimal nucleotide turnover (hydrolysis of ATP and release of ADP) (Sianidis et al., 2001). Taking into account the sequence homology between SecA and SecA2, it seemed likely that the domain architecture of the two would be considerably similar. Hence, the position of the G484 mutation was modelled onto the SecA crystal structure of *B. subtilis* (Osborne et al., 2004). It corresponds to the conserved GRGTD motif in *B. subtilis* SecA. As can be seen in (Fig. 27B), the G484E mutation in the IRA2 domain lies in close proximity to important nucleotide binding residues of the neighbouring NBD domain, possibly affecting either ATP binding itself, or its turnover.

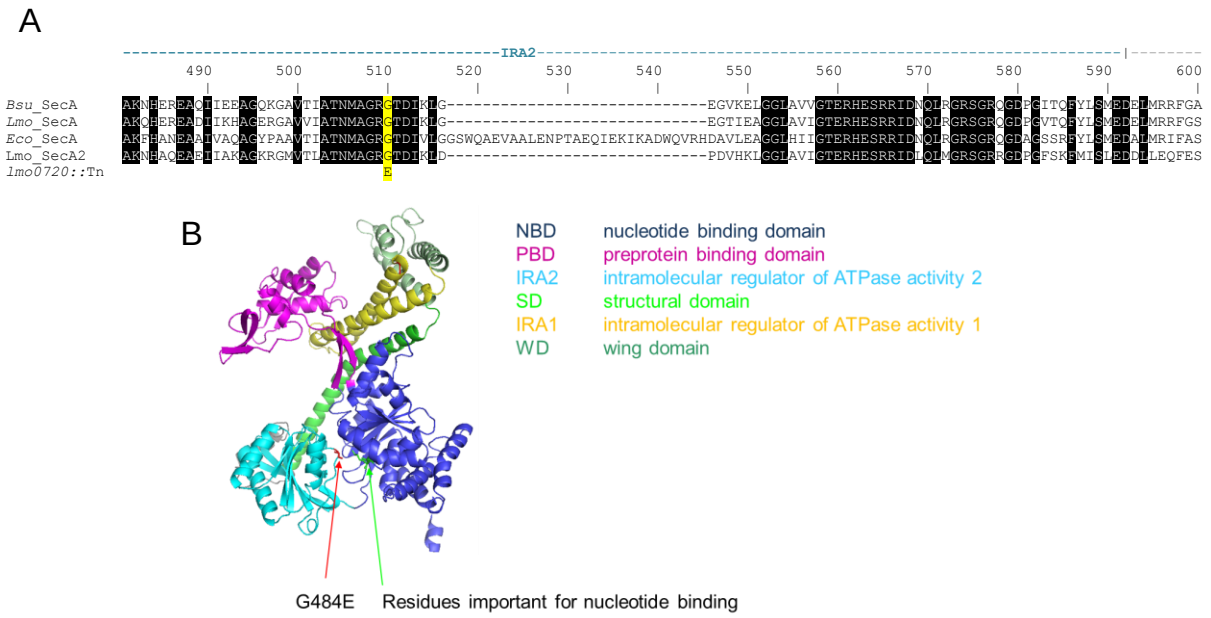


**Figure 27: Putting the *secA2G484E* mutation into genetic and structural contexts.** (A) Sequence alignment of SecA proteins of *B. subtilis*, *L. monocytogenes*, and *E. coli* with SecA2 of *L. monocytogenes* EGD-e (wt) and LMKK18 (*lmo0720::Tn secA2G484E*) strains. Black highlighted regions indicate sequence conservation (identical amino acids). The yellow shaded region within the IRA2 domain of SecA2 shows the point mutation that results in a change of the glycine residue to glutamic acid (G→E). (B) Location of the G484E mutation in the crystal structure of SecA from *B. subtilis* (Osborne et al., 2004). The G484E mutation bears close proximity to the nucleotide binding residues of the NBD domain. The coloring scheme of the domains is given on the right side of the structure.

### 3.5.5 Phenotypic consequences of the *secA2G484E* mutation

To better understand the effect of the *G484E* substitution mutation in the *secA2* gene, a construct was generated, putting the mutated *secA2G484E* version under the control of constitutive promoter. As a control, a similar construct was generated, however, bearing the wild type *secA2* gene to rule out any effects caused solely due to overexpression. A dominant negative effect was observed for the strain overexpressing SecA2G484E from an ectopic locus in its chromosome (LMKK25), resulting in a partial chaining phenotype, while the strain overexpressing the unaltered SecA2 (LMKK24) was indistinguishable from the wild type control strain (data not shown). Deletion of *secA2* from LMKK24 (resulting in strain LMKK27) had no effect on either cell or colony morphology, due to successful complementation of the Δ*secA2* deletion by the ectopic SecA2 expression, whereas in strain LMKK28 (Δ*secA2+secA2G484E*) a complete manifestation of the chaining phenotype similar to that seen for the Δ*secA2* mutant (strain LMS81) was observed (Fig. 28A).

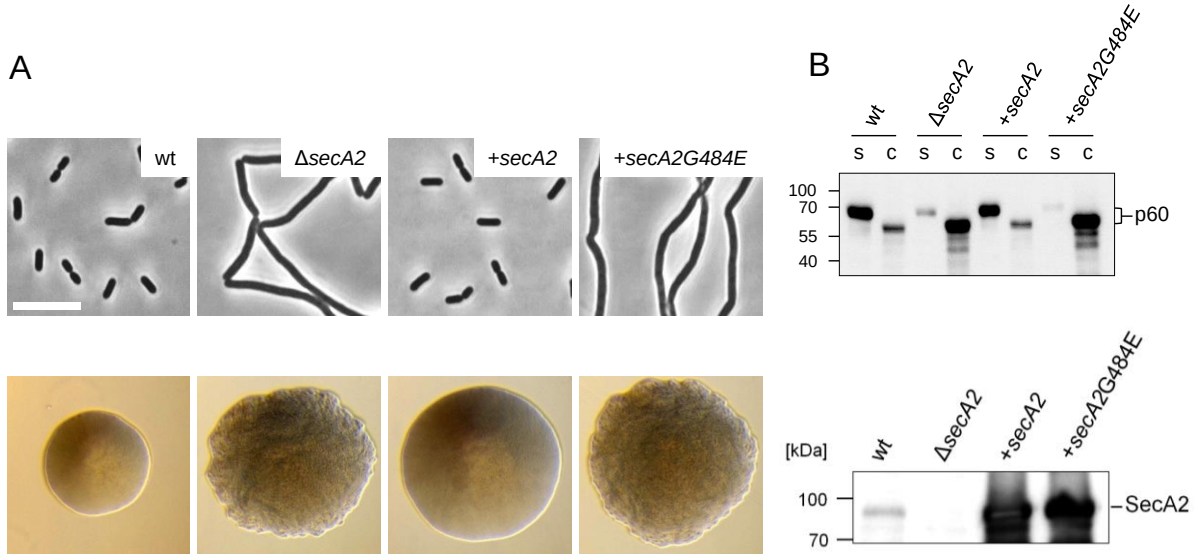


**Figure 28: Effects of the *secA2G484E* mutation.** (A) Cell (top row) and colony (bottom row) morphology of *L. monocytogenes* EGD-e (wt), LMS81 (Δ*secA2*), LMKK27 (Δ*secA2* with constitutive expression of ectopic *secA2*) and LMKK28 (Δ*secA2* with constitutive expression of ectopic *secA2G484E*). The scale bar used is 5 µm. Phase-contrast images of the colonies were documented directly from the plate using 10 x magnification and the phase ring (ph3). (B) p60 and SecA2 western blots for the same set of strains. The p60 western blots, which also included the supernatant (extracellular protein fraction, "s") along with the cellular (cytoplasmic protein fraction, "c") protein fractions of the associated strains, were antibody stained with mouse anti-p60 bearing a dilution of 1:5000. Immune staining for the SecA2 western blots, containing only the cytoplasmic protein fractions of the previously mentioned strains, was performed with a rabbit anti-SecA2 (1:3500) antiserum.

Secretion profiles of these strains were examined using western blots for p60 with monoclonal, anti-p60 antibodies, which confirmed a Δ*secA2*-like secretion defect for LMKK28 (Δ*secA2+secA2G484E*), however, wild-type-like extracellular and cytosolic p60 banding patterns were observed for LMKK27 (Δ*secA2+secA2*). Full-length expression of SecA2 as well as its G484E variant was verified by Western blotting and staining with a polyclonal anti-SecA2 antibody, ruling out the possibility that SecA2G484E would not be expressed or proteolytically unstable (Fig. 28B). This result raises the question as to what extent the *lmo720::Tn* insertion or the *secA2G484E* mutation contributes to the rough phenotype of the LMKK18 isolate.

### 3.5.6 Complementation of the transposon insertion mutant

In order to separate the effects of the *lmo0720::Tn* insertion and the *secA2G484E* mutation in strain LMKK18, a constitutively expressed ectopic copy of *secA2-gfp* was brought into the

LMKK18 isolate. As a control, the same was done for the Δ*secA2* mutant strain. The resultant strains, namely LMKK20 (*lmo0720::Tn secA2G484E attB::*$P_{help}$*-secA2-gfp neo*) and LMKK21 (Δ*secA2 attB::*$P_{help}$*-secA2-gfp neo*), were analysed for their cell morphology as well as their colony appearance . During the course of these experiments, it became apparent that despite initial success with the complementation of the chaining phenotype and the resultant

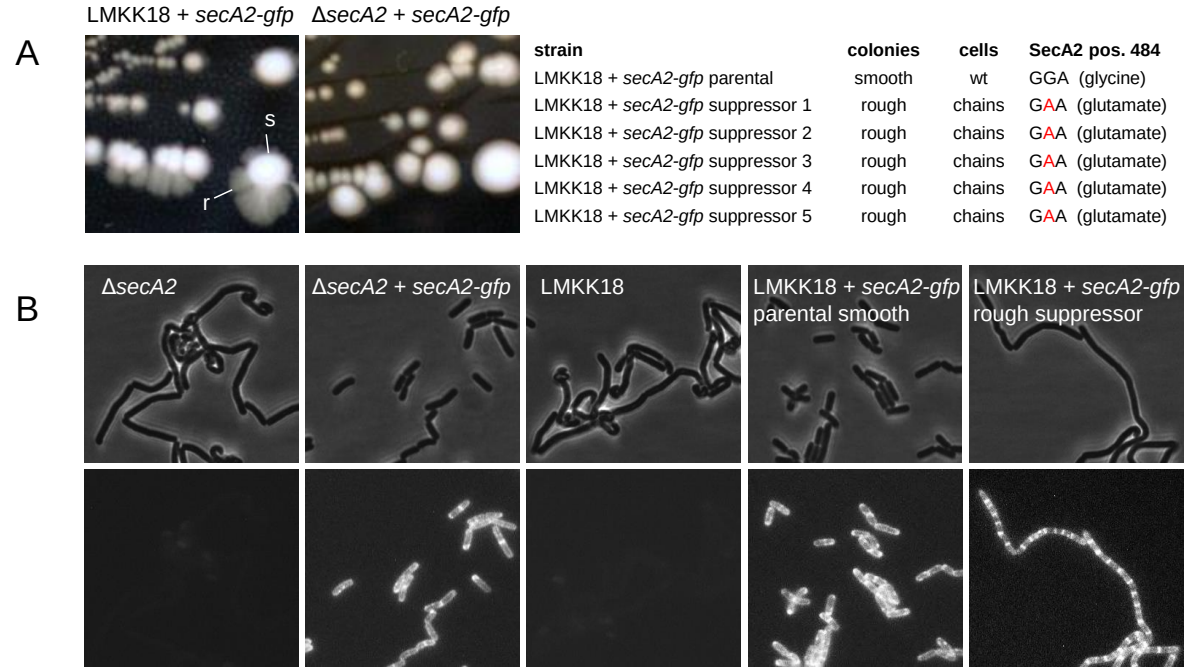


| strain | colonies | cells | SecA2 pos. 484 |
|---|---|---|---|
| LMKK18 + *secA2-gfp* parental | smooth | wt | GGA (glycine) |
| LMKK18 + *secA2-gfp* suppressor 1 | rough | chains | GAA (glutamate) |
| LMKK18 + *secA2-gfp* suppressor 2 | rough | chains | GAA (glutamate) |
| LMKK18 + *secA2-gfp* suppressor 3 | rough | chains | GAA (glutamate) |
| LMKK18 + *secA2-gfp* suppressor 4 | rough | chains | GAA (glutamate) |
| LMKK18 + *secA2-gfp* suppressor 5 | rough | chains | GAA (glutamate) |

**Figure 29: Reacquisition of the G484E mutation despite successful complementation of the *lmo0720::Tn* mutant with *secA2-gfp*.** (A) Images of LMKK20 (LMKK18 < *lmo0720::Tn*> complemented with ectopically expressed *secA2-gfp*) and LMKK21 (Δ*secA2* complemented with ectopically expressed *secA2-gfp*) after 48 h of growth on BHI agar plates at room temperature.

rough colony morphology of the transposon insertion mutant, colonies of the complemented strain LMKK20 spontaneously developed rough outgrowths along the periphery of the otherwise smooth colonies (Fig. 29A). Such suppressor mutants appeared at a very high frequency, within 48 hours of growth of LMKK20 on non-selective BHI plates and they were not observed with strain LMKK21 (Δ*secA2* + *secA2-gfp*). 5 of these suppressors were randomly chosen from different areas of the plate, to make sure that they belonged to different clonal populations, after which their *secA2-gfp* chromosomal loci were amplified and sequenced. Surprisingly, all the 5 suppressor mutants bore the same G484E substitution mutation in the ectopically introduced *secA2-gfp* (Fig. 29A). During cell morphological

analysis of these suppressors, no alterations were observed either in the localization patterns of SecA2G484E-GFP or in the intensity of the fusion proteins themselves, further pointing towards an aberration in the activity of SecA2G484E rather than in its stability (Fig. 29B). The fact that a recurrence of only this very specific mutation rather than random alterations along the entire length of the SecA2-GFP fusion were observed, hinted to a possible specific effect of the insertion of the transposon in the gene *lmo0720* on the dysregulation of SecA2.

### 3.5.7 Deletion of the genes of the *lmo0719-720* operon and their morphological effects

To better comprehend the effects of the transposon-associated insertional disruption, *L. monocytogenes* strains were created bearing clean deletions of either the *lmo0719* gene (LMKK42) or *lmo0720* (LMKK26) or the entire operon itself (LMKK31). Glycerol stocks of the respective strains were streaked out to single colonies on BHI agar plates and kept at room temperature for 72 h. The wild type *L. monocytogenes* strain, EGD-e, and transposon insertion mutant strain, LMKK18, were used as controls. Single colonies of the single mutant strains (LMKK42 and LMKK26), observed under a microscope at 4 x magnification also seemed to show no apparent morphological variations as compared to *L. monocytogenes* EGD-e. However, the double mutant strain LMKK31 (Δ*lmo0719-720*) displayed the appearance of spontaneous, rough outgrowths, seen as heterogeneous rough patches (r) along the circumference of the normally smooth colonies (s) (Fig. 30A, right column). Unfortunately, such occurrences were observed at a very low frequency and lacked reproducibility in successive attempts. Due the fact that such smooth-rough transitions, both stable and unstable upon passaging, are also known to arise spontaneously in wild type *L. monocytogenes* (Lenz and Portnoy, 2002), with the unstable variants being able to revert back from the rough to the smooth colony phenotype (Zachar and Savage, 1979), we had to rule out similar observations made with LMKK31 as unspecific and unstable aberrations. This demonstrated that the deletion of *lmo0719* or *lmo0720* does not stimulate the transition from the smooth to the rough phenotype. For determination of cell morphology, overnight cultures of the same set of strains were used to seed fresh cultures that were grown to the mid-logarithmic growth phase, stained with nile red membrane stain, and analysed for their cell lengths.

Cell morphologies of the gene deletion strains for the *lmo0719-720* operon were indifferent from that of the wild type (Fig. 30A, left column) and these cells did not reveal chain

formation. Upon plotting the cell length distributions of the above-mentioned strains, it became apparent that the cell lengths of LMKK18 were comparable to that observed for the wild type (Fig. 30B). These data coupled with the previously described chaining morphology of LMKK18, confirmed beyond all reasonable doubt that its phenotype was a consequence of the *secA2G484E* mutation and did not include any effect on cell division, thereby resulting in long, Δ*secA2*-like cell chains comprising of cells having wild type cell lengths.

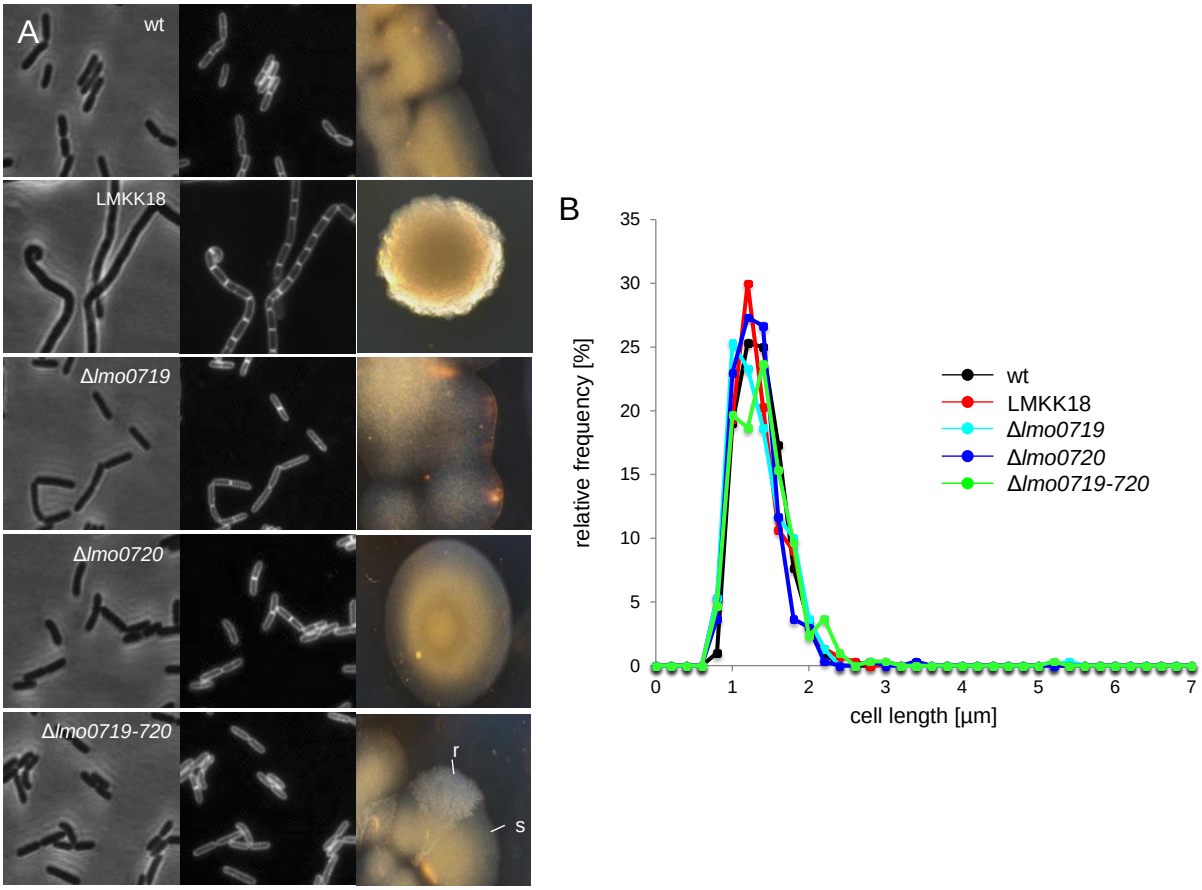


**Figure 30: Deletion of the *lmo0719-720* operon and its effects on cell and colony morphology.** (A) Cell (left and middle column) and colony (right column) morphology of EGD-e (wt), LMKK18, LMKK42 (Δ*lmo0719*), LMKK26 (Δ*lmo0720*) and LMKK31 (Δ*lmo0719-720*). Cells for each of the above strains were cultured up to the mid-log phase in BHI medium at 37°C, after which they were nile red stained and subjected to microscopy. BHI agar plates were streaked out with the respective strains taken from glycerol stocks and allowed to grow at room temperature for 72 h followed by phase contrast imaging at 4 x magnification. (B) Cell-length distribution profiles of the aforementioned strains under identical conditions. 300 cells were measured per strain.

The cell length distribution profiles of the single and double *lmo0719-720* operon gene deletion mutants were in congruence with both the cell and colony morphological data, which

showed a lack of any discernable difference when compared with the wild type phenotype (Fig. 30B). Taken together, lack of *lmo0720*, *lmo0719* or of both genes simultaneously does not cause a Δ*divIVA*- or Δ*secA2*-like chaining phenotype nor does it stimulate smooth-rough transition of *L. monocytogenes*.

### 3.5.8 Growth and autolysin secretion characteristics of the *lmo0719-720* operon mutants of *L. monocytogenes*

As the morphological studies of the mutant strains in the *lmo0719-0720* operon did not indicate the existence of Δ*divIVA*- or Δ*secA2*-like chaining phenotypes, further phenotypic characterization of these strains was required to better ascertain the putative effects, if any, of the transposon insertion in this gene locus.

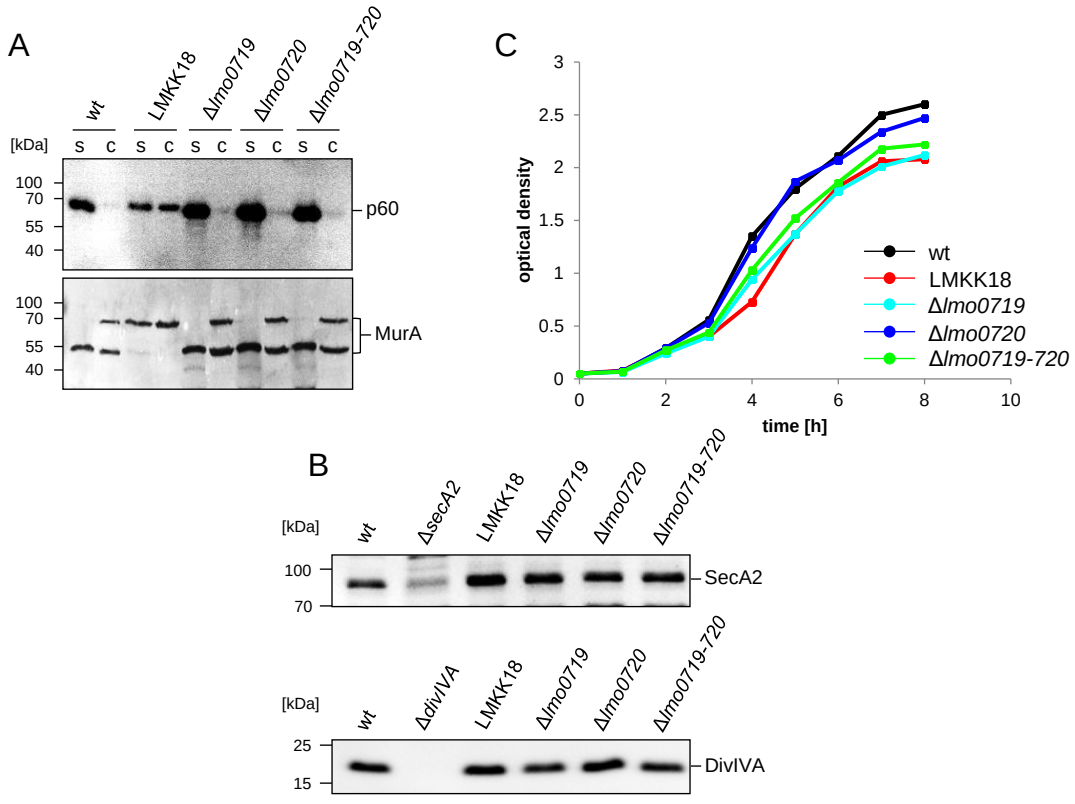


**Figure 31: Growth and secretion profiles of the *lmo0719-720* operon mutants of *L. monocytogenes*.** (A) Western blot for p60 and zymography for MurA detection in supernatant (s) and cytosolic (c) fractions of EGD-e (wt), LMKK18, LMKK42 (Δ*lmo0719*), LMKK26 (Δ*lmo0720*) and LMKK31 (Δ*lmo0719-720*). Cultures for the strains were grown in BHI broth at 37°C till $OD_{600nm}$ = 1.0. A monoclonal mouse anti-p60 (1:5000) antiserum was used for p60 detection. (B) Anti-SecA2 and anti-DivIVA western blots for the same set of strains. *L. monocytogenes* strains LMS81 (Δ*secA2*) and LMS2 (Δ*divIVA*) were used as controls. Polyclonal rabbit anti-SecA2 (1:3500) and anti-DivIVA (1:5000) antibodies were used for the detection of the respective proteins. (C) Growth curves for the *lmo0719-lmo0720* mutant strains. Optical density ($OD_{600nm}$) was measured every hour for 8 h starting from $OD_{600nm}$= 0.05 along growth in BHI broth at 37°C.

*L. monocytogenes* strains EGD-e (wt), LMKK18 (*lmo0720::Tn secA2G484E*), LMKK42 (Δ*lmo0719*), LMKK26 (Δ*lmo0720*) and LMKK31 (Δ*lmo0719-720*) were cultured up to an $OD_{600nm}$ value of 1.0, after which proteins from their supernatant (s) as well as their cytosolic fractions (c) were harvested. For the detection of p60 in both the protein fractions of the bacterial cultures, western blotting was performed followed by staining with mouse monoclonal anti-p60 antibodies (1:5000 dilution). Zymographic analyses for MurA secretion were also carried out for the same set of protein samples. These data collectively showed wild type-like autolysin processing and secretion patterns for the *lmo0719-720* operon mutants, while reiterating the obvious p60 and MurA secretion defects seen for LMKK18 (Fig. 31A). Western blotting for SecA2 and DivIVA expression was also performed. However, these too showed no changes in the expression of these proteins in the *lmo0719-720* operon mutants as compared to that in the wild type (Fig. 31B). This allows the conclusion that Lmo0719 and Lmo0720 do not influence expression of DivIVA, SecA2, p60 and MurA or the activity of the SecA2 secretion pathway.

Growth characteristics of the *lmo0719-720* operon mutants were also investigated by means of growth curves (Fig. 31C). At first glance, these data revealed an apparent growth defect displayed by the LMKK18 strain in comparison to the wild type. The curve of the Δ*lmo0719* mutant (LMKK42) was remarkably similar to that of LMKK18, while that of the *lmo0720* deletion mutant (LMKK26) was rather closer to the wild type. The *lmo0719-720* operon deletion mutant (LMKK31) had an intermediate growth profile that lay between that of LMKK42 and LMKK26, hinting to the possibility that the protein products of these two genes may serve opposing roles in a yet uncharacterized regulatory pathway.

### 3.5.9 Swarming motility of the *L. monocytogenes lmo0719-720* operon deletion mutants

The LMKK18 strain has hitherto been described to display a Δ*divIVA*-like swarming motility deficiency in 24h swarming assays, which is why the *lmo0719-720* operon mutants were also subjected to the same analysis. Like done before, the strains EGD-e (wt), LMKK18 (*lmo0720::Tn secA2G484E*), LMKK42 (Δ*lmo0719*), LMKK26 (Δ*lmo0720*) and LMKK31 (Δ*lmo0719-720*) were subjected to the standard 24h swarming assays. At this time point, a clear defect in swarming behavior was seen only for LMKK18, while the *lmo0719-720* operon mutants seemed to exhibit wild type circular halo formation as a result of unimpeded motility (Fig. 32A). When these plates were left on the bench at ambient room temperature

for 6 days, the colonies swarmed outwards in a synchronized fashion, forming rings of alternating translucent and opaque sections (Fig. 32B). It is known that this behaviour of *L. monocytogenes* is driven by a blue-light receptor, coded for by *lmo0799*, which induces the $\sigma^B$ stress sigma factor thereby affecting global gene expression in response to light-dependent oxidative stress (Tiensuu et al., 2013). It was observed that the Δ*lmo0719* mutant (LMKK42) was unable to form such

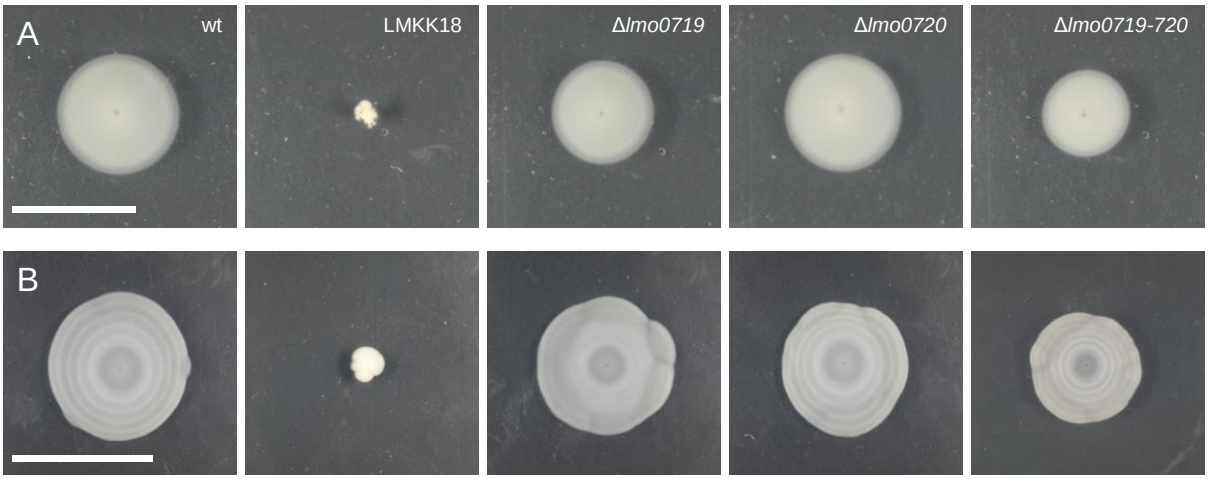


**Figure 32: Swarming defect of the *L. monocytogenes* Δ*lmo0719* mutant.** (A-B) Swarming motility assay for EGD-e (wt), LMKK18 (*lmo0720::Tn secA2G484E*), LMKK42 (Δ*lmo0719*), LMKK26 (Δ*lmo0720*) and LMKK31 (Δ*lmo0719-720*). (A) Soft LB agar plates [0.3% (w/v)], stab inoculated with the above strains from glycerol stocks, were incubated at 30°C for 24 h and then documented. (B) The same plates inoculated with the same strains, photographed after 6 days of growth at room temperature. Scale in A indicates 1.095 cm, while that in B indicates 3.987 cm.

alternating rings, while *lmo0720* mutant (LMKK26) was able to. Most surprisingly, the *lmo0719-720* double deletion mutant (LMKK31) seemed to retain this behaviour despite the absence of *lmo0719*, further fuelling the notion that Lmo0719 and Lmo0720 are functionally contradictory.

Wild type strains overexpressing either *lmo0719* (LMKK34) or *lmo0720* (LMKK19) from an ectopic site, via IPTG induction, were generated to assess their effects on swarming motility. However, neither of these two strains displayed any deviations from the wild type (EGD-e) (data not shown). As the Δ*lmo0719* mutant showed the more obvious defect in alternating ring formation, an attempt was made to complement this strain by bringing in an ectopic copy

of the *lmo0719* gene, placed under the control of an IPTG-inducible promoter (LMKK62), nevertheless, this strategy failed to counteract the swarming aberration (data not shown).

### 3.5.10 Proteomic analysis of the transposon insertion isolate and the *lmo0719-720* operon mutants

Throughout the course of the investigations, it was believed that the G484E mutation in the *secA2* gene, which was observed in the LMKK18 strain, was due to a deregulatory effect brought on by the transposon insertion in the *lmo0720* gene belonging to the *lmo0719-720* operon. This point of view was further strengthened by the emergence of rough colony revertants within the successfully complemented LMKK18 strain (LMKK20), due to the recurrence of the same mutation at the newly introduced, ectopic *secA2-gfp* loci. As the *lmo0719* gene has been predicted to encode a protein that belongs to the PadR family of transcriptional regulators (Huillet et al., 2006), it is assumed that its disruption would probably lead to either induction or repression of specific genes. Therefore proteomic analysis involving 1D SDS-PAGE coupled with MALDI-TOF Mass spectrometry was opted for so as to detect proteins which are induced or repressed due to the absence or disruption of the *lmo0719-720* operon.

For this purpose, strains LMKK18 (*lmo0720::Tn secA2G484E*), LMKK42 (Δ*lmo0719*), LMKK26 (Δ*lmo0720*) and LMKK31 (Δ*lmo0719-720*) were grown in BHI medium at 37°C till $OD_{600nm}$ = 1.0, after which their total cellular proteins were extracted. The *L. monocytogenes* wild type strain EGD-e, LMS81 (Δ*secA2*), LMKK20 (*lmo0720::Tn secA2G484E + secA2-gfp*) and LMKK20R (*lmo0720::Tn secA2G484E + secA2-gfp G484E*) were used as controls for this experiment. The 1D SDS-PAGE analysis revealed 7 unique protein bands that were brighter in comparison to their counterparts in the other gel lanes, indicating protein enrichment due to possible upregulation of these proteins (Fig. 33). These bands were cut out from the gel, numbered and sent for protein identification utilising MALDI-TOF mass spectrometry (Dr. Dirk Albrecht, Institut f. Mikrobiologie, Universität Greifswald). Protein band "1" could not be identified as the analysis did not return any significant hits; however the rest of the protein bands were successfully recognised (Fig. 33). The expression of superoxide dismutase was enhanced in the strain LMKK20, while the Δ*lmo0719* mutant was upregulated for a predicted alcohol dehydrogenase (now known to be the *Listeria* adhesion protein), an ABC transporter

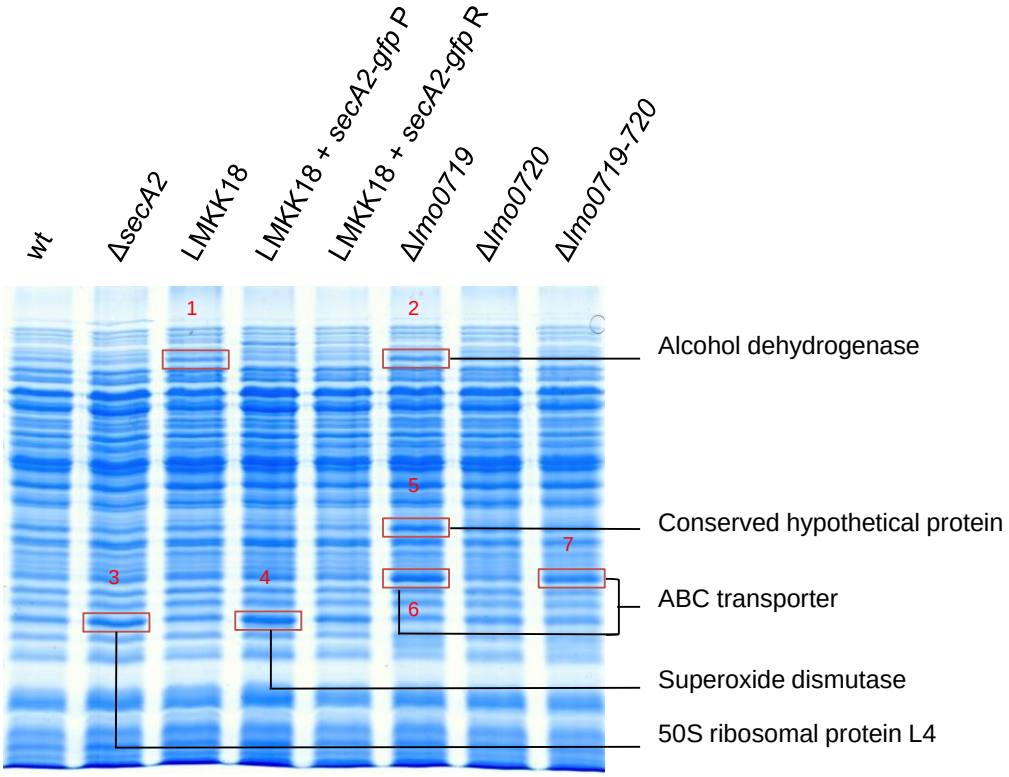


| Sample No. | Putative gene | Description | Mol wt | pI |
|---|---|---|---|---|
| 1 | N/A | N/A | N/A | N/A |
| 2 | *lmo1634* | similar to Alcohol-acetaldehyde dehydrogenase | 94681.6 | 6.9287 |
| 3 | *lmo2631/ rplD* | ribosomal protein L4 | 22603.2 | 10.7674 |
| 4 | *lmo1439/ sod* | superoxide dismutase | 22631.1 | 5.1023 |
| 5 | *lmo2637* | conserved lipoprotein | 32741.5 | 6.5759 |
| 6 | *lmo0979* | similar to daunorubicin resistance ATP-binding proteins | 27661.7 | 5.088 |
| 7 | *lmo0979* | similar to daunorubicin resistance ATP-binding proteins | 27661.7 | 5.088 |

**Figure 33: Identification of upregulated proteins of the transposon-insertion mutant and deletion mutants of the *lmo0719-720* operon.** 1D SDS-PAGE of the total cellular protein fractions of *L. monocytogenes strains* EGD-e (wt), LMS81 (Δ*secA2*), LMKK18 (*lmo0720::Tn secA2G484E*), LMKK20 (*lmo0720::Tn secA2G484E + secA2-gfp*), LMKK20R (*lmo0720::Tn secA2G484E + secA2-gfp G484E*), LMKK42 (Δ*lmo0719*), LMKK26 (Δ*lmo0720*) and LMKK31 (Δ*lmo0719*). The aforementioned strains were cultured to $OD_{600nm}$ = 1.0 in BHI broth at 37°C. The designation "P" and "R" signify strains LMKK20 and LMKK20R, respectively. The experiment was performed in duplicates using the same strains and culturing conditions, after which 12% polyacrylamide gels were used for the gel electrophoresis followed by coomassie staining. Bands of upregulated proteins were cut out, numbered (red boxes) and identified using MALDI-TOF mass spectrometry. A summary of the proteins identified by the mass spectrometric analysis, along with the corresponding genes, their description as well as their molecular weight and isoelectric point has been provided in the table.

as well as an unknown conserved protein. When compared to the Δ*lmo0719* mutant, the Δ*lmo0719-720* double mutant displayed an upregulation only for the same ABC transporter,

whereas the Δ*lmo0720* single mutant showed no distinction from the wild type. The fact that Lmo0719 can have an impact on the expression of other genes is in line with its annotation as a PadR-like transcriptional regulator. The significance of these results is yet to be deciphered; nonetheless it provides an interesting lead, which can be exploited in the future to better understand the correlation between the *lmo0719-720* operon and its effect on the SecA2-dependent secretion of proteins.

### 3.5.11 Reestablishment of the transposon insertion event in *L. monocytogenes* and its phenotypic consequences

Inverse PCRs, which were used to determine the site of transposon insertion in the genome of the LMKK18 strain, had previously confirmed that the transposon had inserted in such a manner that the embedded erythromycin resistance cassette was transcribed in the direction opposite to that of the genes lying upstream to the insertion site (Fig. 26). Based on the results of the gene deletion studies carried out for the *lmo0719-720* operon, it was hypothesized that the orientation of the erythromycin cassette, within the genomically inserted transposon, was responsible for polar effects on the transcription of upstream genes which do not arise in the clean deletion mutants. To test this, we recreated the transposon insertion event in the wild type background by allelic exchange using the pMAD vector system as described by Arnaud et al. The whole *lmo0720* gene, with the integrated transposon, as well as the DNA sections flanking the gene were PCR amplified from the LMKK18 strain (*lmo0720::Tn secA2G484E*) and cloned into a pMAD vector using an appropriate restriction endonuclease pair. This pMAD vector (pKK64) was then used to replace the chromosomal *lmo0720* gene loci of the wild type *L. monocytogenes* EGD-e strain with the *lmo0720::Tn* gene fragment from LMKK18. The resultant reconstituted transposon insertion mutant LMKK64 was put through a series of tests to check for changes in its swarming motility, colony morphology and SecA2-dependent autolysin secretion. The swarming halo produced by the LMKK64 strain (*lmo0720::Tn*) was similar to that of the wild type and bore no resemblance whatsoever to the swarming-impaired LMKK18 strain or the Δ*secA2* mutant (LMS81) (Fig. 34A). Upon incubating the plates at room temperature on the bench, LMKK64 was able to form alternating rings of opaque and translucent regions, just like the wild type strain (Fig. 34B).

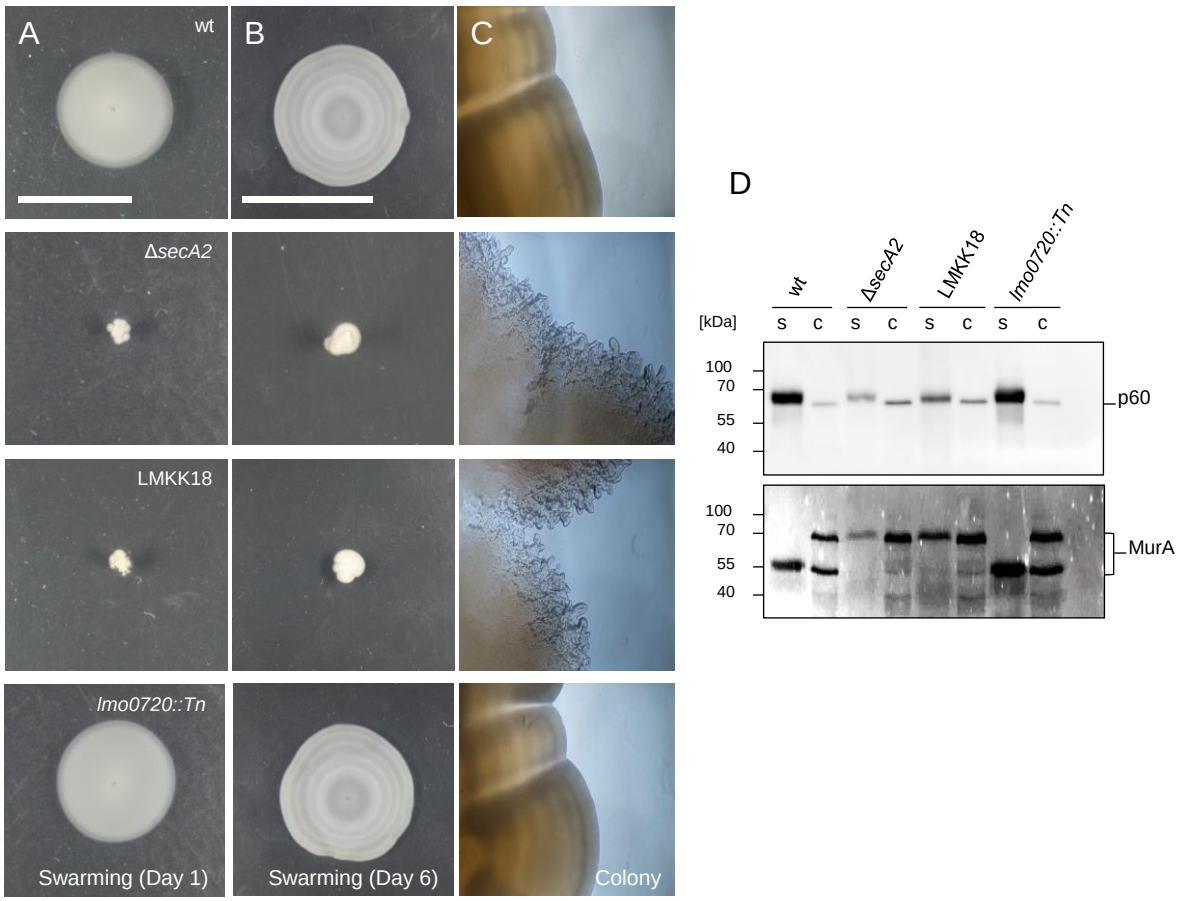


**Figure 34: Virulence-associated characteristics of the reconstituted transposon-insertion mutant.** (A-B) Swarming assay for *L. monocytogenes* strains EGD-e (wt), LMKK18 (*lmo0720::Tn secA2G484E*), LMS81 (Δ*secA2*) and LMKK64 (*lmo0720::Tn*). (A) Soft LB agar plates [0.3% (w/v)], stab inoculated with the above strains from glycerol stocks, were incubated at 30°C for 24 h and then documented. (B) The same plates inoculated with the same strains, photographed after 6 days of growth at room temperature. Scale in A indicates 1.095 cm, while that in B indicates 3.987 cm. (C) Colony morphology phase contrast images of the same set of strains taken at 4 x magnification. Colonies were streaked out from glycerol stocks, incubated at room temperature for 72 h on BHI plates, and directly documented from the plate. (D) Western blotting for p60 and zymography for MurA detection from supernatant (s) and cytosolic (c) fractions of bacterial cultures grown to $OD_{600nm}$ = 1.0 in BHI broth at 37°C. 1:5000 dilution of mouse monoclonal anti-p60 antisera was used for detection of the p60 western.

When streaked out to single colonies and allowed to grow at room temperature for 72 h on BHI agar plates, the *lmo0720::Tn* mutant produced smooth colonies throughout without the emergence of a single rough colony suppressor (Fig. 34C). Western blotting revealed that it also displayed wild type p60 and MurA secretion patterns when the supernatant and cytosolic fractions, extracted from its bacterial cultures, were analysed (Fig. 34D). This shows that the sole presence of a LMKK18-like transposon insertion in *lmo0720* alone does not cause any effects on motility, autolysin secretion or smooth-rough transition. Genome sequencing was performed (Dr. Jennifer Bender, FG-13, Robert Koch Institute, Wernigerode) to ascertain the

presence of any secondary mutations elsewhere in the chromosome of the LMKK18 strain; however this led to the recognition of the *G484E* mutation in the chromosomal *secA2* loci to be the sole secondary mutation in this strain.

### 3.5.12 Virulence of *lmo0719-720* operon mutants in an HeLa cell infection assay

The *L. monocytogenes* wild type strain (EGD-e), the *lmo0720::Tn* transposon insertion mutant (LMKK64), mutants lacking Δ*lmo0719* (LMKK42), or Δ*lmo0720* (LMKK26) as well as the Δ*lmo0719-720* double mutant (LMKK31), were used to infect HeLa cells to check for

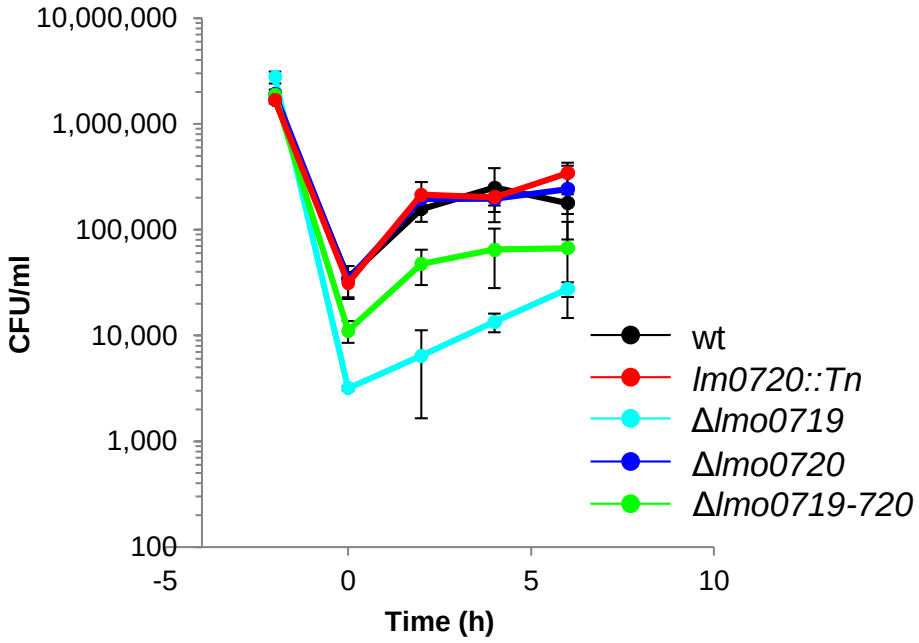


**Figure 35: Determination of the *in vitro* infection characteristics of the lmo0719-720 operon mutants using cell culture assays.** Intracellular growth kinetics of the strains EGD-e (wt), LMKK64 (*lmo0720::Tn*), LMKK42 (Δ*lmo0719*), LMKK26 (Δ*lmo0720*) and LMK31 (Δ*lmo0719-720*) in HeLa cells (moi = 10). The bacterial inoculum was added to the HeLa cells at the time point -2 h, followed by infection for 1 h and killing of extracellular bacteria with gentamycin, with 1 h of incubation. CFU/ml was determined for the intracellular bacterial strains following sampling at 2 h intervals, starting immediately post infection up to 6 h. The experiment was performed in triplicate to calculate the standard deviations.

their capacity to infect and replicate intracellularly within eukaryotic host cells (Fig. 35). CFU/ml values measured at time point zero (immediately after infection) helped to ascertain the bacterial invasion potential of the aforementioned strains. The Δ*lmo0719* single mutant

and the Δ*lmo0719-720* double mutant displayed CFU/ml values (at 0 h) that were ~ 10 fold and 3 fold lesser than that of the wild type, respectively. This indicated that the Δ*lmo0719* mutant had a clear defect in terms of bacterial invasion, while the invasion deficiency of the Δ*lmo0719-720* double mutant was rather intermediate (Fig. 35). CFU/ml values (at 0 h) of the reconstituted transposon mutant (LMKK64) and the Δ*lmo0720* single mutant were however similar to that of the wild type, thereby suggesting native invasion potential of these strains (Fig. 35). All the mutant strains used in this experiment showed intracellular growth curves that were either wild type-like or parallel to that of the wild type strain (Fig. 35), therefore ruling out any notion of defective intracellular growth kinetics.

# 4. Discussion

## 4.1 Influence of DivIVA on secretion of autolysins

DivIVA was previously found to play a role in the secretion of the two major autolysins, p60 and MurA, so as to facilitate the separation of the daughter cells after completion of cell division in *L. monocytogenes* (Halbedel et al., 2012). The secretion of both these proteins is dependent on the accessory ATPase SecA2, which is known to be responsible for the displacement of a certain set of proteins from the cytoplasm to the extracellular space (Halbedel et al., 2012, Lenz et al., 2003, Lenz and Portnoy, 2002, Machata et al., 2005). A variety of observations made by Halbedel et al. hinted to the possible influence of DivIVA on the SecA2-dependent secretion of these autolysins (Halbedel et al., 2012). Firstly, a GFP-fusion protein of SecA2 was shown to display the same septal localization pattern as that of DivIVA; however its septal recruitment was DivIVA-independent. Secondly, the phenotype of the Δ*divIVA* mutant starkly resembled that of the Δ*secA2* mutant in terms of its chaining morphology, its secretome including the processing and secretion of both p60 and MurA, and its attenuated virulence. Thirdly, both the Δ*divIVA* and the Δ*secA2* mutants of *L. monocytogenes* were shown to be a combination of the less virulent and less chaining single mutants of the *iap* (p60) and *murA* genes. Based on these observations it was concluded that both SecA2 and DivIVA belong to the same biochemical pathway responsible for the eventual outward translocation of p60 and MurA (Halbedel et al., 2012).

### 4.1.1 Modes of DivIVA activity

It was therefore hypothesized that DivIVA influences the secretion of these autolysins based on two putative models (Fig. 36): 1. As per the first model, DivIVA modulates the activity of SecA2 by establishing interactions with it, thereby enabling SecA2 to take up the pre-protein versions of both p60 and MurA at the site of cell division, processing it and exporting it to the extracellular space in the vicinity of the constricting septum (Fig. 36A). The likelihood of the model is supported by the subcellular septal enrichment of both DivIVA and SecA2 during division site constriction (Halbedel et al., 2012). 2. DivIVA behaves only as a scaffolding protein according to the second model and

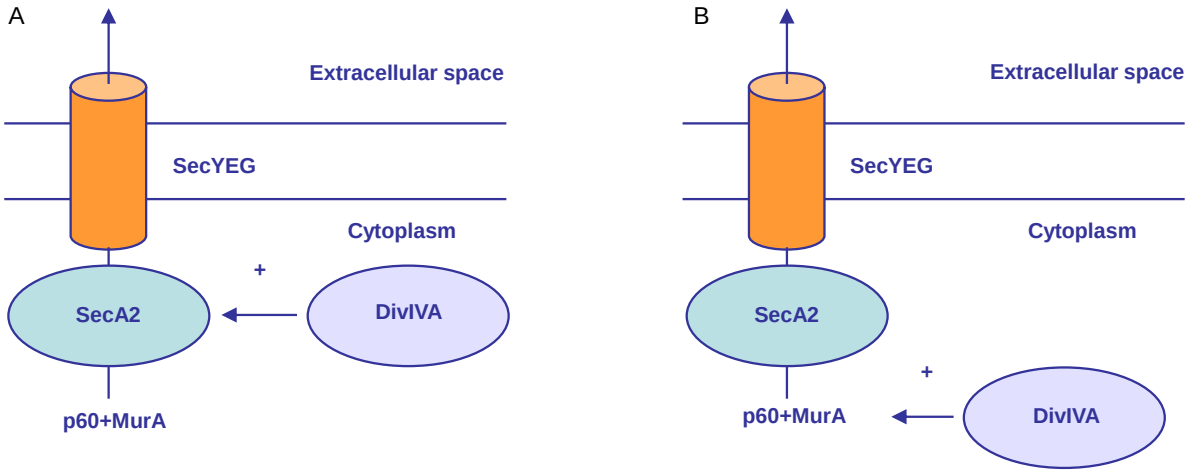


**Figure 36: Effect of DivIVA on autolysin secretion.** Illustrations showing the two putative models of DivIVA activity related to secretion of SecA2-dependent autolysins. (A) This model pertains to the direct influence of DivIVA on the modulation of SecA2 activity, enabling it to take up the pre-protein versions of p60 and MurA and secrete them. (B) DivIVA serves as a scaffold by recruiting the pre-protein forms of p60 and MurA to the division site, where they then interact with SecA2 and are secreted.

serves to recruit the unprocessed pre-p60 and pre-MurA proteins to the site of septal constriction, where they interact with SecA2, which then cleaves off their signal peptides and translocates them to the outside of the cell (Fig. 36B). The DivIVA-dependent septal localization of GFP fusions of both p60 and MurA strongly argue in favour of this model (Halbedel et al., 2012). Both these models would take into account the activity of DivIVA in precisely localizing these autolysins so as to restrict their secretion only to the constricting division site, where they would degrade freshly synthesized peptidoglycan to allow for separation of the daughter cells (Halbedel et al., 2012).

### 4.1.2 Absence of detectable inter-protein interactions between DivIVA, SecA2 and p60

To test the two models proposed above, direct interactions of DivIVA, SecA2, p60 and MurA were tested using the bacterial two-hybrid assay. The absence of blue colonies in all the inter-protein combinations suggested an inability to detect any direct interactions between these proteins. These observations were completely contradictory to the hypothesized modes of DivIVA activity, however the results did not conclusively rule out the presence of direct interactions between these proteins. Even though the bacterial two-hybrid assay is more practical as compared to the widely used yeast two-hybrid system, it does have certain drawbacks such as a tendency to display false positive interactions due to an inherent ability

of some proteins to interact with any non-related protein (termed as "sticky proteins") (Battesti and Bouveret, 2012). False negatives are also a potential problem either due to possible misfolding and instability of the fusion proteins or simply due to hindrances in protein interactions by the fused T18 and T25 domains (Battesti and Bouveret, 2012). Also, this assay is primarily used to detect only direct interactions and does not take into account the presence of intermediate protein interaction partners, which might serve to bridge the tested protein set.

In addition, self-interactions were also observed for DivIVA, SecA2 and p60. Strong direct interactions observed in all 4 combinations used for DivIVA reinforces the fact that DivIVA also forms dimeric complexes in *L. monocytogenes*, similar to that observed in *B. subtilis* (van Baarle et al., 2013). Considering the high degree of sequence homology between *B. subtilis* and *L. monocytogenes* DivIVA (59% identity, 78% similarity), similar dimerization is expected of the listerial DivIVA and it would be safe to assume that it could also possibly form higher order oligomers like its *B. subtilis* counterpart (van Baarle et al., 2013). Only a few blue colonies that were seen for self-interaction pairings of SecA2 and p60 as compared to that for DivIVA, could be described as weak self-interaction; however as the bacterial two-hybrid assay is a qualitative rather than a quantitative experiment, it is not a true indication of the strength of the interaction. Putative self-interaction of MurA could not be tested as only the T25-fragment fusion constructs could be generated for MurA, possibly due to a lethal effect of the *murA* gene being present as a high copy number plasmid construct on the *E. coli* TOP10 host.

### 4.1.3 p60 and MurA bind to SecA2 but not to DivIVA

The pull down strategy was employed to check for the putative participation of intermediate interaction partners in mediating interactions of DivIVA with SecA2 and/or p60 and MurA. 1D SDS PAGE analysis of the pull down eluates has shown that p60 does in fact co-purify with SecA2. This was visualized as a clear enrichment of bands of p60 (detected using monoclonal anti-p60 antibodies) in the pull down complexes of the SecA2-His10 bait protein (Fig. 7A). MurA was however not detectable when using the in vivo cross-linking strategy, probably due to a loss of native conformation of the protein despite heat-induced de-crosslinking. To rectify the MurA detection issue, additional rounds of non-denaturing, native pull downs were performed under identical conditions. This modified strategy enabled the

zymogram-based visualization of MurA, which is also enriched in the SecA2-His10 bait protein eluates (Fig. 7A). This also confirms the observations made in exoproteomic studies where levels of p60 (CwhA) in the extracellular milieu of a *L. monocytogenes* Δ*secA2* mutant were dramatically reduced as compared to its wild-type strain (Renier et al., 2013). Zymograms used in other studies also indicate a similar absence of p60 and MurA secretion in Δ*secA2* mutants (Lenz et al., 2003).

Identical levels of enrichment of the two autolysins in both denaturing and native pull downs with the DivIVA-His10 bait and the wild type control strain, as well as the absence of co-purification of DivIVA with the SecA2-His 10 bait and vice versa, strongly point to the inability of DivIVA to bind to either SecA2 or its autolysin substrates (p60 and MurA). Unfortunately due to the inherent bacteriolytic activities of p60 (Wuenscher et al., 1993) and MurA (Carroll et al., 2003), affinity-tagged overexpression constructs of their genes could not be utilized to perform reciprocal co-purification studies as a method to verify the absence of DivIVA-p60 or DivIVA-MurA interactions. It is difficult to say whether the unexpected lack of detectable interactions is in fact a result of absence of interactions, interference in the establishment of interactions or just a problem with their detectability. The placement of the His10 tag itself at the C-terminal end of the bait proteins may affect its binding to putative interaction partners. As mentioned earlier, the C-terminal domain of DivIVA has been shown to be responsible for its interaction with various interaction partners (van Baarle et al., 2013) and the presence of a His tag may hinder the presentation of the C-terminal residues required for interaction. The mechanics of the cross-linking process itself may also result in a loss of interaction. The formation of amino derivatives of the interacting proteins during crosslinking by formaldehyde (Sutherland et al., 2008) may affect binding characteristics of the protein. In addition, intramolecular covalent crosslinking may affect protein folding and hence the exposure of protein surface residues necessary for inter-protein interactions (Suckau et al., 1992). This drawback was circumvented using the native pull down strategy; however the increased background interference due to the non-specific interactions limited this strategy only to the detection of MurA. The levels of the interacting proteins that are being pulled down may also be below the lower detection limit of western blots and zymograms. Pull down strategies using alternative affinity tags may provide the answer to getting higher co-purification efficiencies with lower non-specific background interference so as to detect any faint signals of putative interaction partners, if any. Strep tagging on the other hand has been shown to provide very good signal-to-noise ratios when used to purify protein complexes that

were *in vivo* cross-linked using formaldehyde in *B. subtilis* (Herzberg et al., 2007), and would therefore be a viable strategy to detect any faint protein-protein interactions that were undetectable using the His10 tagging strategy in *L. monocytogenes*. Possibly, a different organism could also be used as the host for the heterologous expression and *in vivo* cross-linking of the hypothesized interaction partners of *L. monocytogenes* DivIVA. *B. subtilis* being a very well characterized organism and a close relative of *L. monocytogenes*, would ideally suit this purpose as pull down strategies are well optimized in this organism. The only drawback being that this strategy would limit the study to the identification of interactions between only those hypothesized protein that have been cloned into the non-native host and hence would not allow for the identification of novel interaction partners.

### 4.2 Role of DivIVA in division-site selection during cell division in *L. monocytogenes*

Division-site selection involves the placement of the cell division machinery precisely at the mid-cell. As mentioned earlier, this mid-cell localization of the divisiome is facilitated by the NOC and Min systems, which work in a concerted manner to ensure that none of the genetic material is lost during its transfer from the parent cell to the daughter cells. In *B. subtilis*, DivIVA is known to restrict the activity of the Min system to the division septum-adjacent areas (van Baarle and Bramkamp, 2010), and in its absence, cells undergo filamentation and delocalized cell division leading to the formation of minicells (Edwards and Errington, 1997, Marston et al., 1998, Cha and Stewart, 1997). In *L. monocytogenes* however, the phenotypic consequence of the deletion of *divIVA* is quite different. Initially the *L. monocytogenes* Δ*divIVA* mutant was thought to display the same filamentation phenotype as seen in *B. subtilis*, but these filaments were later shown to be chains of cells that undergo cell division but are unable to separate from each other (Halbedel et al., 2012). The functioning of the Min system in a DivIVA-independent manner in *L. monocytogenes* was further argued by the lack of observable minicelling in the Δ*divIVA* mutant.

#### 4.2.1 DivIVA belongs to the same division-site selection pathway as the Min system

Nothing much was hitherto known about the Min system in *L. monocytogenes* except for the fact that it contains homologs for all the three Min system protein, namely MinC, MinD and MinJ. Other than MinD, neither of the remaining two Min proteins bears a high degree of homology with its *B. subtilis* counterparts. Therefore a possibility of slight differences in the

functioning of the Min system in *L. monocytogenes* was expected, including a putative DivIVA-independent behavior. The construction of deletion mutants of the *L. monocytogenes min* genes and their phenotypic comparison with corresponding gene deletion mutants of *B. subtilis,* was the most logical way to uncover functional differences between the homologous Min proteins. The cell elongation phenotype of the Δ*minCD* operon deletion mutant of *L. monocytogenes* was similar to that observed for the equivalent gene deletion mutants of *B. subtilis* (Levin et al., 1998). As the MinCD complex is a negative regulator of FtsZ ring assembly (deBoer et al., 1992), there is inefficient FtsZ turnover and consequent depletion of its cytoplasmic pool in the *B. subtilis* Δ*minCD* mutant (Rodrigues and Harry, 2012). Therefore, this FtsZ depletion leads to a defect in the timing of cell division (Gregory et al., 2008), thereby resulting in polar (preexisting division sites) rather than midcell placement of the FtsZ ring (Levin et al., 1998) and cell elongation. Therefore, the similarity in phenotypes of these analogous Δ*minCD* mutants of *B. subtilis* and *L. monocytogenes* indicates a functional conservation of MinC and MinD. The similarity of the cell length distribution profiles of the Δ*minCD* and Δ*divIVA* hinted to a possible association of the Min system with DivIVA. Unexpectedly, the elongated subpopulations of cells of the *L. monocytogenes* Δ*minCD* mutant were longer and more frequently occurring than that of the Δ*divIVA* mutant rather than bearing an identical degree of elongation (Fig. 14B). This could be explained by the fact that in a Δ*divIVA* mutant, MinCD is still present but in a possibly unregulated state and hence could either marginally inhibit maturation of additional Z-rings adjacent to the preexisting division site (new cell poles) or partially disassemble the preexisting division machinery (Bramkamp et al., 2008, van Baarle and Bramkamp, 2010), therefore allowing some FtsZ monomers to assemble into Z-rings at the mid-cell region of the daughter cells, although not with the same degree of efficiency. While in the Δ*minCD* mutant, the inhibitor MinC is itself absent hence leading to either a maturation of new FtsZ-rings adjacent to the old division locus rather than at mid-cell or to a failure to degrade the old division apparatus that would then continue to re-constrict at the newly formed poles, ultimately forming disproportionate cells. In both the Δ*divIVA* and Δ*minCD* mutants, one would expect decreased FtsZ turnover as most of FtsZ monomers would still be associated with the preexisting division complex or would be recruited to septation site-adjacent regions, therefore leaving insufficient amounts of FtsZ monomers to polymerize at the mid-cell. This theory of cytoplasmic FtsZ pool-depletion was confirmed by the intracellular localization patterns of FtsZ-GFP in the Δ*divIVA* and Δ*minCD* mutants of *L. monocytogenes*, which showed that there was a clear decrease in the number of cells bearing pre-divisional Z-rings at their mid-

cell region for both these mutant strains as compared to those of the wild type strain (Fig. 19E)

On the other hand, the phenotypic consequence of the deletion of the *L. monocytogenes minJ* gene was completely contrary to what is known for the corresponding *B. subtilis* variant. While deletion of *minJ* leads to extensive filamentation of the cells of *B. subtilis* (Bramkamp et al., 2008, Patrick and Kearns, 2008), deletion of *minJ* in *L. monocytogenes* seemed to have no conspicuous effect on its cell morphology, which was like that of the wild type (Fig. 14A-B). Cell lengths measurements of the *L. monocytogenes* Δ*minJ* mutant cells confirmed this curious observation as no cell elongation was observed whatsoever, despite a Δ*divIVA*-like reduction in the number of cells bearing mid-cell Z-rings (Fig. 19E). If the function of MinJ was to serve as a bridging protein between DivIVA and the MinCD complex like that seen in *B. subtilis* (Bramkamp et al., 2008), the deletion of *minJ* in *L. monocytogenes* would probably result in Δ*divIVA*-like cell elongation as MinCD would still be present but would function in a deregulated manner (due to its delocalization); however, cell lengths of the Δ*minJ* mutant were rather shown to be wild type-like. Therefore, compared to its behavior in *B. subtilis*, no definitive mode of function could be postulated for MinJ in *L. monocytogenes* based on these observations alone.

Combinatorial double and triple mutants generated for *divIVA, minCD and minJ* helped to better understand whether the putative homolog of *B. subtilis* MinJ is in fact involved in the Min system of *L. monocytogenes* to begin with. The indication that the identified MinJ homolog of *L. monocytogenes* belongs to the same pathway as the MinCD complex came from the observation that the Δ*minCDJ* triple mutant had the same cell length distribution profile as the Δ*minCD* mutant. If MinJ were to belong to some other pathway, either an additive effect (longer cell lengths than that of the Δ*minCD* mutant) or a complementary effect (reduced cell lengths compared to that of the Δ*minCD* mutant) would be observed for the Δ*minCDJ* triple mutant. Rather it became clear that MinCD, being the actual inhibitor of FtsZ, lies downstream of MinJ in the same pathway as the deletion of *minCD* had a cell elongation effect that was dominant over that of the *minJ* deletion. Identical cell length distribution profiles of the Δ*minCD* and the Δ*minCD* Δ*divIVA* triple mutant added further strength to the notion that DivIVA too belongs to the same pathway, with MinCD lying downstream to it due the observed dominant effect of the Δ*minCD* phenotype over that of the Δ*divIVA* mutant. As an extrapolation of the previous two deductions, it can be said that

DivIVA and MinJ also belong to the same pathway; however, if the apparent curing of the cell length elongation defect of the Δ*divIVA* mutant by the deletion of *minJ* in the Δ*divIVA* Δ*minJ* double mutant is also taken into consideration, it points to opposing roles played by DivIVA and MinJ in the same pathway rather than the notion that they belong to two different pathways.

### 4.2.2 DivIVA has a dual function in *L. monocytogenes*

Both the *divIVA* and *secA2* deletion mutants in *L. monocytogenes* were thought to be phenotypically indistinguishable due to their identical cell chaining and autolysin secretion defects as well as their attenuated virulence in terms of invasion of eukaryotic host cells and cell-to-cell spreading (Halbedel et al., 2012). On the basis of this argument and the lack of observable minicell formation, DivIVA was thought to play no role in division site selection in *L. monocytogenes* unlike that seen in *B. subilis.* However, the epistasis studies that were done as part of this thesis have shown that this argument is no longer valid, with DivIVA showing a clear association with the Min system. If the phenotypes of Δ*divIVA* and Δ*secA2* mutants in *L. monocytogenes* were to be truly identical, one would expect the Δ*secA2* mutant to also have elongated cell lengths similar to that of the Δ*divIVA* mutant in addition to the cell chaining defect. This was however not the case as the cell length frequency distribution profile of the Δ*secA2* mutant was identical to that of the wild type rather than to that of the Δ*divIVA* mutant (Fig. 16B), indicating that the Δ*secA2* mutant only has an autolysin secretion defect similar to that of the Δ*divIVA* mutant (seen as cell chaining) but not a cell division defect (seen as cell length elongation). The dominant effect of the Δ*divIVA* mutant over the Δ*secA2* mutant became apparent during cell length measurements, which showed that the Δ*divIVA* Δ*secA2* double mutant had the same cell length frequency distribution profile as that of the Δ*divIVA* mutant rather than that of the Δ*secA2* mutant (Fig. 16B). This dominant effect of the Δ*divIVA* mutant signified that the cell length elongation defect of the Δ*divIVA* mutant is not dependent on the presence of SecA2.

### 4.2.3 The dependencies of the Min proteins in *L. monocytogenes* are non-linear

Previous studies have shown that in *B. subtilis*, DivIVA and the proteins of the Min system follow a linear hierarchy of interdependencies for their recruitment to the division site-adjacent regions of the cells starting with DivIVA and followed by MinJ, MinD & MinC, in

the described order (Bramkamp et al., 2008, Marston et al., 1998, Patrick and Kearns, 2008). These observation were corroborated by bacterial two-hybrid tests which showed that adjacent proteins in the hierarchy interacted with each other while the non-adjacent proteins did not (Bramkamp et al., 2008, Patrick and Kearns, 2008). However, when bacterial two-hybrid analyses were performed to check for direct interactions between the DivIVA and Min proteins of *L. monocytogenes*, DivIVA seemed to show direct interactions with MinD in addition to its interaction with MinJ. Considering the high degree of conservation of DivIVA and MinD among *B. subtilis* and *L. monocytogenes*, this interaction between listerial DivIVA and MinD seemed quite unusual as in *B. subtilis*, such an interaction has never been documented (Bramkamp et al., 2008, Patrick and Kearns, 2008). This observation suggests that in *L. monocytogenes*, DivIVA has acquired the ability to interact with an additional protein within the Min system, the implications of which are still not understood. The intracellular localization patterns of GFP fused listerial Min proteins, in the presence and absence of DivIVA in *L. monocytogenes*, helped shed some light on this unfamiliar mode of association of the Min system with DivIVA. The reduction in septal enrichment of GFP-MinD upon deletion of *divIVA* was expected as DivIVA is known to facilitate the accumulation of MinD at negatively curved membrane regions in *B. subtilis* (such as at newly formed poles), and therefore the absence of DivIVA results in a loss of this enrichment (Marston et al., 1998). A similar decrease in septal MinC-GFP signals, as that seen for GFP-MinD, in a Δ*divIVA* background is probably due to a MinD-dependent localization of MinC, like that observed in *B. subtilis* (Marston and Errington, 1999). Hence delocalization of MinD in a Δ*divIVA* mutant results in the consequential delocalization of MinC. The fact that the septal localization pattern of MinJ-GFP remained unperturbed, despite the deletion of *divIVA*, indicates that localization of MinJ to the regions adjacent to the division septa is DivIVA-independent in *L. monocytogenes*. This was in contrast to that observed in *B. subtilis*, where the septal and polar localization of MinJ-GFP was abolished in a Δ*divIVA* mutant (Bramkamp et al., 2008). Another interesting observation was the complete loss of septal localization of MinC-GFP and GFP-MinD upon deletion of *minJ*. This observation however is in accordance with GFP-MinD localization patterns in a *B. subtilis* Δ*minJ* mutant, where the GFP-MinD goes from being polarly localized in the wild type, to becoming completely diffused in the cytoplasm upon deletion of *minJ* (Bramkamp et al., 2008). Considering the presence of six transmembrane spans at the N-terminal region of MinJ, as seen in *B. subtilis* (Patrick and Kearns, 2008), it is possible that MinJ serves the purpose of a membrane anchor for the MinCD complex. Therefore it seems that the function of DivIVA in *Listeria* is to either

localize the MinCD complex at the division septum or to retain MinCD that has already localized to the septum by MinJ, or both. However in either of these mentioned scenarios, DivIVA does not seem to have an influence on MinJ localization.

Based on the subcellular localization patterns of the Min proteins and their dependence on DivIVA/MinJ, as well as their inter-protein interactions among themselves and with DivIVA, a bifurcated rather than a linear sequence of interdependencies for Min system protein recruitment in *L.* monocytogenes has been hypothesized. As per this model, MinJ serves to anchor the MinCD complex to the cell membrane via an interaction with MinD, while DivIVA facilitates localization and retention of the membrane-bound MinCD complex at the division septum via its interaction to both MinD and MinJ. MinJ-based membrane anchoring of MinCD could be explained by the observation that MinD possesses only an amphipathic helix at its C-terminal end that enables a superficial protein-lipid interaction for reversible, ATP-dependent membrane association (Szeto et al., 2002). This feature of MinD is useful in *E. coli,* where rapid, bipolar membrane trafficking of the MinCD complex by MinE (Hu and Lutkenhaus, 2001), is required for efficient division-site placement (Raskin and de Boer, 1999). However in *B. subtilis* that has MinJ and DivIVA rather than MinE, MinCD shows dynamic movement but from the new pole (division septum of the parent cell) to the septum (mid-cell region of the daughter cell), in a putatively passive instead of an active manner, with septal localization that is stable rather than transient (Gregory et al., 2008). Also, the rate at which MinC (and therefore MinD) is redistributed laterally in *B. subtilis* is slower than the diffusion rates of cytoplasmic and membrane proteins of similar sizes (Gregory et al., 2008), which could be explained by either more interactions of MinCD with surrounding proteins or a stable interaction with the membrane (increased hydrodynamic resistance via interactions would result in slower diffusion rates). This stable interaction of MinD with the membrane could be possibly mediated via the integral membrane protein, MinJ. *L. monocytogenes* cells are smaller in size (0.9 - 1.5 µm) as compared to *B. subtilis* cells (3 - 5 µm) and therefore have a relatively lower cell volume, with smaller distances between the cell poles and the septum. As MinCD in both these organisms would be expected to have similar diffusion rates due to their similar molecular weights and sequence conservation (Nenninger et al., 2010), one could expect a variability in the redistribution rates of MinCD between these organisms, with listerial MinCD putatively having a reduced rate of redistribution due to lesser flexibility in its lateral motion along the membrane. This reduction in the redistribution rate of listerial MinCD would possibly ensure precise temporal control of its arrival at the division septum in

these shorter cells. The presence of the additional interaction of MinD with DivIVA at the septum-adjacent regions, in addition to the MinD-MinJ interaction, could putatively provide the restriction needed to the lateral motion of MinCD by increasing MinCD retention times at the pre-existing septum.

An interesting insight discussed by Imrich Barak states that during the shift from vegetative growth to sporulation, *B. subtilis* DivIVA is believed to switch its function from regulating cell division to facilitating chromosome segregation from the parent cell to the forespore compartment by exchanging MinJ of the Min system for the centromere-binding RacA protein (Barak, 2013, Ben-Yehuda et al., 2003). This argument is no longer valid, as DivIVA is also found on both sides of the asymmetric septum in sporulating cells (Eswaramoorthy et al., 2014), which still show expression of the DivIVA protein (Thomaides et al., 2001). Therefore, there would be no need for DivIVA to switch from MinJ to RacA as there would still be sufficient amounts of DivIVA present within the prespore compartment to anchor RacA, without the need to dissociate from the Min system.

### 4.2.4 Minicell behavior of *min* mutants and strategies to increase minicell formation frequencies of *L. monocytogenes*

Previous studies always described a lack of minicell formation and absence of an obvious division phenotype in the *L. monocytogenes* Δ*divIVA* mutant, which led to the hypothesis of a DivIVA-independent function of the Min system (Halbedel et al., 2012, Kaval and Halbedel, 2012). In this thesis, the same absence of minicelling behavior was observed for the Δ*divIVA* deletion mutant (Fig. 20E), however, as previously elaborated, DivIVA is in fact associated with the Min system for determination of the site of septation. GFP-expressing *min* mutants showed that deletion of *minCD* or *minJ* caused formation of minicells (Fig. 20C-D), albeit with a lesser frequency of occurrence (1.9% and 0.9 %, respectively) (Fig. 20E) than observed for the corresponding *B. subtilis* (~20%) (Perry and Edwards, 2004) and *E. coli* (~30%) (Shih et al., 2002) mutants. The smaller cell size of *L. monocytogenes* could be a possible reason for this reduced minicell formation frequency as there would be lesser nucleoid-free cytoplasmic space available in the vicinity of the pre-existing division septum for the formation of additional FtsZ-rings. Considering the fact that the *L. monocytogenes min* mutants do display minicell formation, one would expect the same for the Δ*divIVA* mutant. The lack of any observable minicells could possibly be explained by the masking effect of cell chaining.

Minicells that would putatively form at the new poles of the Δ*divIVA* mutant cells would stay attached to the adjacent cells rather than dislodging. The criteria used in this as well as previous studies for classifying any cellular entity as a minicell required them to be spherical and achromosomal, but if a minicell were to be flanked by two normal sized or even elongated cells, the shape of this minicell would be distorted by the cross-walls of the neighboring cells leading to mischaracterization. The presence of small cellular compartments (resembling the size of an average listerial minicell) that were enclosed between the polar cross-walls of the elongated neighboring cells was observed; however, due to the presence of bright DNA stained cells flanking such small compartments, it was difficult to determine whether or not DNA truly was absent in these comportments. Hence, confirmation of minicell formation, if any, in the Δ*divIVA* mutant was problematic.

Minicells of intracellular pathogenic bacteria are interesting as they are expected to have the same surface chemistry and architecture of their parent cells, and are completely achromosomal due to aberrant cell division at chromosome free spaces at the new cell poles of the progenitor cells. Minicell producing strains and methodologies for the purification of their resultant minicells have been described and patented for *S. typhimurium*, *E. coli* and *S. flexneri* as well as *L. monocytogenes*, however it is claimed that they yield only $10^8$ - $10^9$ purified listerial minicells from a 10L culture (Brahmbhatt and Macdiarmid, 2003). One advantage of minicells derived from gram-positive bacteria over those derived from gram-negative bacteria is that they have a more rigid cell wall structure, which makes such minicells less prone to collapsing (Brahmbhatt and Macdiarmid, 2003). This rigidity of the gram-positive-derived minicells would probably also increase their purification yields, as fewer minicells would be lost during downstream processing due to mechanical stress. As per scanning electron microscopy analysis, the surface ultrastructure of the listerial minicells is claimed to be identical to its parental strains (Brahmbhatt and Macdiarmid, 2003). Hence it is likely that these minicells also possess a similar distribution of surface-bound proteins as that of the progenitor strains, which could possibly enable these minicells to invade eukaryotic cells in a manner similar to the parental listerial strains. Studies have been performed for minicells derived from *S. typhimurium*, which show that these minicells are engulfed by mouse macrophages into phagosomes, followed by subsequent lysis of the internalized minicells due to a possible fusion of the phagosome and the lysosome (Brahmbhatt and Macdiarmid, 2003). However nothing much is known about the ability of such *Listeria*-derived minicells to infect either phagocytic or non-phagocytic eukaryotic cells. Though,

studies have been performed with *L. monocytogenes* Internalin A (InlA)-coated beads which show that they are able to trigger E-cadherin receptor-mediated phagocytosis by epithelial cells, leading to internalization of these beads into phagosomes followed by phagosomal acidification and phagosome-lysosomal fusion (Blanchette et al., 2009). Considering that InlA is accumulated at the bacterial poles in *L. monocytogenes* (Lebrun et al., 1996), listerial minicells would be expected to bear this surface bound InlA protein. Therefore, it is plausible that these minicells would be internalized by epithelial cells in a similar fashion and degraded in the phagolysosomes. The likelihood of these minicells escaping from the phagosomes into the host cytoplasm, or also spreading to neighboring cells, would be low as expression and secretion of the phagosome-disrupting protein listeriolysin O (LLO) (Portnoy et al., 1988) would be absent in these achromosomal minicells. Therefore the listerial minicells could be used as delivery vectors for therapeutic compounds that need hydrolytic processing to activate them, prior to their release into the host cytoplasm. Such minicells could be beneficial when only a localized, dose-dependent therapeutic effect is desired as such minicells, as explained above, would also be unable to spread to neighbouring cells. However, if drug delivery to other cellular compartments of the host cells were to be required, specific genes for the required infection stages of *L. monocytogenes* could be cloned into appropriate expression systems and transformed into the listerial minicells, so as to achieve a more targeted, therapeutic outcome.

This PhD thesis was also aimed at genetically modifying minicell-forming *min* mutants so as to increase their minicell formation frequencies. The increase in minicell-formation frequencies of the Δ*minCD* mutant strain upon overexpression of FtsZ could be explained by an overall increase in the cytoplasmic pool of FtsZ, which would probably result in formation of more FtsZ-rings in the vicinity of the pre-existing division complex at the old division sites. However, the overexpression of the GFP variant of FtsZ in the Δ*minCD* mutant strains seemed to further increase minicell formation, possibly due to the fact that the C-terminal end of FtsZ is known to be the binding region for some of its interaction partners such as FtsA, as well as some proteins involved in FtsZ regulation, namely SepF and EzrA (Din et al., 1998, Krol et al., 2012, Singh et al., 2007). Therefore, a putative loss of FtsZ's capability of binding to such proteins via its C-terminal region, due to the fused GFP protein at the FtsZ C-terminus, could further increase its dysregulation and consequently result in greater minicell-formation. Considering the untapped potential that listerial minicells might possess in the field of novel therapeutic interventions, the above genetic modifications and other similar

strategies for increasing minicell-formation could make the production and use of *L. monocytogenes*-derived minicells, as drug delivery vectors, a more economically viable option.

### 4.3 The division and secretion function of *L. monocytogenes* DivIVA can be separated

During the course of this PhD thesis, *L. monocytogenes* DivIVA was revealed of having a dual function, with it playing a role in both the control of SecA2-dependent secretion of autolysins for separation of cells post-cell division as well as in the selection of the site of division via the Min system. Domain-swap analysis was performed as mentioned previously (Chapter 3.2, schematic illustration of the DivIVA chimeras) to ascertain whether *Lm* DivIVA, with its two domain architecture (Oliva et al., 2010), utilizes its N-terminal LBD and C-terminal coiled-coil domain as two separate interaction modules to facilitate interactions with transmembrane/membrane bound proteins and cytosolic protein, respectively, like that done by *B. subtilis* DivIVA (van Baarle et al., 2013).

All the *Lm-Bs* chimeric DivIVA-expressing strains were found to display the Δ*divIVA*/Δ*secA2*-like chaining cell morphology accompanied by a defect in cell swarming (Fig. 9), with the exception of one strain. This one strain, which expressed the chimeric *Lm-104-Bs* DivIVA displayed a complementation of the wild type phenotype including both its cell morphology and swarming motility, while the strain expressing *Lm-57-Bs* showed the Δ*divIVA* phenotype (Fig. 9). Hence it's plausible that not only the N-terminal lipid-binding domain, but also the flexible linker and a short stretch of the C-terminal domain are required for full functionality of DivIVA. It also led to the assumption that the interaction partner responsible for its association with the SecA2-dependent protein secretion pathway possibly binds to the DivIVA region spanning from amino acid residues 1-104.

As a continuation of phenotypic characterization of these chimeric DivIVA-expressing strains, the comparative cell length measurement and frequency distribution strategy was employed as a way to reveal possible defects in cell division in the target strains based on subtle variations in cell lengths when compared to the wild type control. Out of all the chimeras, the *Lm-104-Bs* DivIVA-expressing strain showed restoration of both wild type cell division (cell length frequency distribution profiles which were similar to the wild type strain) as well as autolysin secretion (non-chaining morphology of the wild type), while the *Bs-57-*

*Lm* DivIVA-expressing mutant displayed only the curing of the cell division defect (wild type-like frequency distribution profiles) but not the autolysin secretion defect (Δ*divIVA*-like cell chaining morphology) (Fig. 23 A-C). These results reiterated the importance of the *Lm* DivIVA N-terminal domain (residues 1-57) coupled with the linker (residues 58-70) and the short section of the CTD (residues 71-104) for mediating SecA2-dependent autolysin secretion. It also indicates that only the linker and the residues 71-104 of DivIVA are required to carry out its interaction with the Min system, most probably with MinD. However, it is still not known whether these two interaction surfaces (1. Interaction surface for proteins involved in autolysin secretion. 2. Interaction surface for association of DivIVA with the Min system) are overlapping or not and whether they can be separated. Therefore it would be interesting to check whether a chimeric DivIVA-variant could be made that would potentially cure only the autolysin secretion defect but not the cell division defect, in which case the listerial cells expressing such constructs would display Δ*minCD*-like cell morphology. Such a chimeric construct would help determine whether the autolysin secretion and division-site selection-associated functions of DivIVA are possibly separable.

### 4.4 The G484 residue in the IRA2 domain of SecA2 is important for facilitating autolysin secretion in *L. monocytogenes*

While trying to identify new *secA2*/*divIVA*-related genes by transposon mutagenesis, a strain (LMKK18) was isolated that did not have a transposon insertion in the either the *divIVA* or *secA2* chromosomal loci or in their immediate flanking regions. This mutant rather bore the insertion of the transposon in the *lmo0719* gene belonging to the *lmo0719-720* operon. Preliminary phenotypic characterization of this transposon mutant revealed a Δ*divIVA*-like cell and colony morphology as well as a similar defect in swarming motility (Fig. 25A, B, C). It even displayed a similar p60 secretion profile as compared to the Δ*divIVA* mutant, while still expressing full-length proteins for DivIVA and SecA2 as seen in western blots (Fig. 25D). However, sequencing to reconfirm the absence of transposon insertions in *divIVA* and *secA2* led to the identification of a point mutation in *secA2* that resulted in a G484E amino acid substitution in the expressed SecA2 protein. The phenotypic consequence of this mutation was checked by expressing the mutant *secA2G484E* as well as a wild type *secA2* allele (control) in a Δ*secA2* deletion background. While the native SecA2 was able to complement the Δ*secA2* phenotype, SecA2G484E was unable to do so (Fig. 28A-B). The full-length expression of both the native and mutant proteins was verified using western blots.

Hence it was concluded that the Δ*divIVA*/Δ*secA2*-like phenotype of the transposon insertion mutant (LMKK18) was a result of the G484E substitution mutation.

*L. monocytogenes* SecA2 shares a high degree of homology with SecA proteins of *E. coli* (39% identity), *L. monocytogenes* (45% identity) and *B. subtilis* (46% identity) (Fig. 27A), while also possessing similar domains and an overall similarity in domain architecture with SecA proteins of these organisms (Bensing et al., 2014). Therefore this mutation was mapped to a highly conserved stretch of residues in the IRA2 (intramolecular regulator of ATPase) domain of SecA (Fig. 27A). IRA2 is part of a two domain complex which also includes IRA1, which work together to couple the translocation of proteins to ATP hydrolysis (Karamanou et al., 1999). IRA2 therefore regulates the ATPase activity of SecA by binding to the ATPase motor, NBD1, making sure that there is optimal binding of ATP and efficient release of the hydrolyzed ADP (Sianidis et al., 2001). The crystal structure of *B. subtilis* SecA (Osborne et al., 2004) shows that the G484 residue lies in close proximity to the ATP binding site (GEGKT, residue position 98-102) of the NBD1 domain; therefore, it is logical to assume that the substitution of the uncharged glycine residue (G) with a negatively charged glutamic acid residue (E) at position 484 of SecA2 would lead to an electrostatic repulsive effect on the negatively charged phosphate groups of ATP, thereby affecting its ability to bind at NBD1 (complete loss/reduced affinity of ATP binding at NBD). The larger size of glutamic acid as compared to glycine might also introduce steric hindrances and hence effectively reduce the size of the binding pocket for ATP binding. Such a mutation would consequently lead to either a disruption or a reduction of ATPase activity of SecA2. ATPase assays confirmed this hypothesis where a loss of basal ATPase activity was observed for purified SecA2G484E due to this mutation (Sven Halbedel, personal communication).

Attempts were made to cure the *secA2G484E* mutation of the transposon insertion mutant by expressing an ectopic copy of *secA2-gfp*. However, despite initial success in restoring the wild-type phenotype, appearance of rough colony suppressor mutants at a high frequency was noticed within a period of 48 h (Fig. 29A). When 5 of these suppressor mutants were randomly chosen and sequenced for their ectopic *secA2-gfp* loci, all of them were shown to exhibit the same *G484E* substitution mutation (Fig. 29A). The control Δ*secA2* strain that also expressed an ectopic *secA2-gfp* copy displayed a similar emergence of suppressor mutants; however, these suppressors formed at a lower frequency and bore random mutations in their *secA2-gfp loci*. The reemergence of this specific *G484E* mutation in the transposon mutant

(LMKK18) was believed to be a consequence of the gene disruption caused by the transposon insertion.

### 4.5 Identification of novel transcriptional regulators encoded by *lmo0719* and *lmo0720*

The insertion of the transposon was found to be in the *lmo0720* gene (Fig. 26); however the only thing known about this gene so far is that it contains a domain, which is part of the DUF1048 superfamily, and as the name suggests, has a so far unknown function. The gene, however, belongs to a two-gene operon also containing *lmo0719*, which is predicted to encode a novel transcriptional regulator belonging to the family of PadR-like transcriptional repressors. The name of this family of transcription factors is based on the phenolic acid decarboxylation repressor, which is responsible for the repression of genes of Gram-positive bacteria such as *Lactobacillus plantarum* and *B. subtilis* that are linked to the phenolic acid stress response (Gury et al., 2004, Tran et al., 2008). Only a minority of the members of the PadR-like protein family have been studied, including the archetypal PadR protein (Gury et al., 2004). The PadR-like proteins have been shown to function either as transcriptional activators as in the case of AphA, which in *Vibrio cholerae* has been shown to stimulate the expression of virulence genes (Kovacikova et al., 2003), or as transcriptional repressors like that seen for LadR and LmrR that repress expression of genes coding for the multi-drug resistance pumps MdrL and LmrCD in *L. monocytogenes* and *Lactococcus lactis*, respectively (Huillet et al., 2006, Agustiandari et al., 2008). Phylogenetic analyses further segregate these PadR-like proteins into two distinct subfamilies: 1. Subfamily I, which contains proteins having longer sequences of approx. 176 amino acids (e.g LadR of *L. monocytogenes*). 2. Subfamily II, containing the more distant (in terms of phylogeny) proteins bearing shorter sequences of about 110 amino acids. The same analysis also shows that Lmo0719 of *L. monocytogenes* belongs to this second subfamily (Huillet et al., 2006).

Single mutants for *lmo0719* and *lmo0720* genes as well as the entire operon deletion mutant (Δ*lmo0719-720*) were prepared to assess the impact of the transposon insertion in this genomic locus, which was believed to trigger the appearance of the *G484E* suppressor mutation, probably due to a deregulation of SecA2 activity; however that was observed not to be the case. Colony morphologies of these mutants did not show any sign of a spontaneous shift from the smooth to the rough phenotype (Fig. 30A, right column), neither did the cells of these mutants display any cell chaining (Fig. 30A, left and middle column). No difference

was observed in the p60 and MurA secretion profiles of these mutants as compared to the wild type strain (Fig. 31A) and the same was true for the expression of SecA2 and DivIVA (Fig. 31B). Hence, it seems that the individual or collective lack of the two aforementioned genes neither causes the Δ*secA2*-like chaining phenotype nor the transition from the smooth to the rough colony morphology. The insertion of the transposon itself at the *lmo0720* chromosomal loci of the transposon mutant was also taken into account. Due to the reverse orientation of the erythromycin resistance cassette present in the transposon (Fig. 26), polar effects were expected on the transcription of the genes lying upstream to the point of transposon insertion, which is why a strain was constructed that had the chromosomal loci of the wild type *lmo0720* gene replaced with the *lmo0720::Tn* loci of the transposon mutant. Nonetheless, phenotypic characterization of this mutant as well revealed no such morphological or secretion defects (Fig. 34A-D). The appearance of this specific *G484E* mutation therefore could not be explained.

Despite the fact that there were no obvious morphological changes upon deletion of *lmo0719-720* operon genes, certain physiological aberrations were noticed. Growth curves for the *lmo0719-720* operon mutants showed a similarity between the growth kinetics of the LMKK18 transposon insertion mutant and the Δ*lmo0719* single mutant, with both of them bearing an apparent growth defect as compared to the wild type strain. On the other hand the growth curve of the Δ*lmo0720* single mutant was more like that of the wild type, while the *lmo0719-720* double deletion mutant bore an intermediate growth defect with its growth curve lying between that of the Δ*lmo0719* and Δ*lmo0720* single mutants (Fig. 31C). This was the first clue hinting to potential opposing roles of the encoded products of these two genes in a so far unknown regulatory pathway.

Swarming motility assays at first did not show any variations in the swarming behavior of the single as well as double mutants of the *lmo0719-720* operon genes, with these mutants displaying wild type-like halo formation. On the other hand, the LMKK18 strain demonstrated the characteristic Δ*secA2*-like motility defect after 24 h itself (Fig. 32A). However, when these swarming plates were incubated for 6 days at ambient room temperature, it was noticed that the Δ*lmo0719* single mutant had lost its ability to produce concentric rings of alternating opaque and translucent sections and rather seemed to form only a continuous halo (Fig. 32B). The light and dark cycle-induced concentric halo formation has been described for *L. monocytogenes*, with the opaque sections signifying bacterial

subpopulations with an increased ability to counter light-induced oxidative stress during periods of light, and the translucent sections representing subpopulations with reduced oxidative stress-survivability as a consequence of the dark periods. This phenomenon is thought to be regulated by the $\sigma^B$ stress sigma factor, whose induction is dependent on the blue-light receptor Lmo0799 (Tiensuu et al., 2013). In addition, $\sigma^B$ is also known to regulate genes responsible for the survival of *L. monocytogenes* under other environmental stress conditions such as low pH and carbon starvation (Ferreira et al., 2003, Kazmierczak et al., 2003). In the presence of light, the Lmo0799 protein is believed to prevent energy resources from being utilized for motility, and instead is thought to redirect such energy for the production of extracellular polymeric substances (EPS) so as to protect the colonies from light induced oxidative stress (Tiensuu et al., 2013). Hence in the absence of *lmo0799,* such energy redirection is probably lost and might lead to uninterrupted motility and reduced survivability to oxidative stress due to loss of induction of the $\sigma^B$ –associated pathway (Tiensuu et al., 2013). As there are also other gene products which respond to increase in levels of reactive oxygen species (ROS) via the $\sigma^B$-dependent pathway (Tiensuu et al., 2013), it is plausible that Lmo719 also mediates such a $\sigma^B$-dependent energy resources re-channelling from motility to either EPS production or some other form of ROS protection. Such a role of Lmo0719 is not unlikely considering the similarity in swarming defect of the Δ*lmo0719* and Δ*lmo0799* mutants.

### 4.5.1 Lmo719 as a putative repressor of a multidrug resistance ABC transporter

Preliminary proteomic analysis to check for the proteins which were induced or repressed upon deletion of the Lmo0719 transcriptional regulator-encoding gene showed an increase in the expression of an ABC transporter (Lmo0979), alcohol dehydrogenase (Lmo1634) as well as a conserved predicted protein (Lmo2637), The Lmo0979 protein, which is hypothesized to be a daunorubicin/daunomycin resistance ATP-binding protein, seems to bear resemblance (52% identity, 69% similarity, identified by blastp analysis) to the LmrC subunit of the heterodimeric ATP-binding cassette transporter LmrCD of *Lactococcus lactis* (formerly known as YdaG). LmrCD, which confers multidrug resistance against daunomycin, ethidium bromide and Hoechst 33342, is regulated by the PadR-like transcriptional repressor, LmrR (Agustiandari et al., 2008). Like *lmrCD*, *lmo0979* belongs to a two-gene operon that also contains the gene *lmo0980*, which supposedly codes for an ABC transporter transmembrane component and most probably is associated with Lmo0979 to form a drug efflux pump (Fig.

37). Therefore it is plausible that putative PadR-like repressor Lmo0719, like LmrR, may function as a transcriptional repressor of the putative multidrug transporter coded for by the *lmo0979-980* operon (Fig. 37).

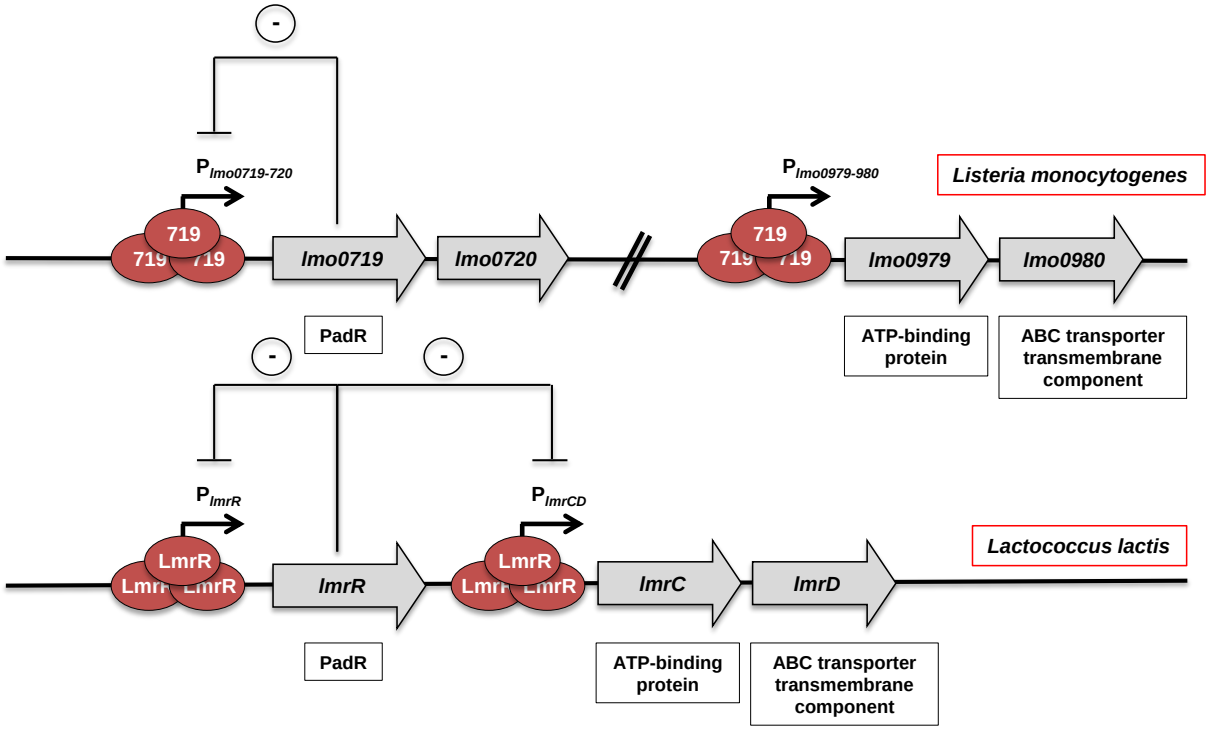


**Figure 37: Similarity between *lmo0719* and *LmrR*.** Illustration showing the hypothesized model of transcriptional repression mediated via the PadR-like repressor Lmo719 in *L. monocytogenes* as compared to that by LmrR in *L. lactis* [the LmrR model is an adaptation of the figure from Agustiandari et al. (2011)]. The primary difference between the two models is that in *L. monocytogenes*, Lmo0719 regulates expression of an operon that is a long way downstream from the *lmo0719* gene, while in *L. lactis*, the repressor LmrR regulates the operon lying immediately downstream to the *lmrR* gene. The target operon in both cases bear a similar architecture, with *lmo0979/lmrC* and *lmo0980/lmrD* coding for the ATP-binding protein and ABC transporter transmembrane component, respectively. Protein Lmo0719 has been abbreviated as 719. Repression of transcription is indicated by the (-) symbol.

### 4.5.2 A possible effect of *lmo0719* deletion on stress response pathways

Lmo1634 on the other hand has been previously identified as the Lap protein (*Listeria* adhesion protein), which is responsible for bacterial adhesion to the host cells as well as mediation of transepithelial translocation of the adhered *L. monocytogenes* cells (Burkholder and Bhunia, 2010, Burkholder et al., 2009, Jagadeesan et al., 2010). The function of the hypothesized lipoprotein Lmo2637 is so far unknown; however, a proteomic study by Port and Freitag has indicated an increased secretion for this protein in a *L. monocytogenes* mutant

strain bearing high PrfA activity (Port and Freitag, 2007). PrfA is a transcriptional regulator that is known to positively regulate various factors involved in every vital step in the pathogenesis of *L. monocytogenes* (Vazquez-Boland et al., 2001). Interestingly, the PrfA regulon expression is bimodally regulated by the $\sigma^B$ stress sigma factor, where increase in stress conditions (increased PrfA induction of its genes) results in downregulation of PrfA by $\sigma^B$ (Ollinger et al., 2009) (Fig. 38). Independent transcriptomic studies have shown that both these Lmo1634 and Lmo2637 proteins are also regulated by regulatory pathways under the control of the HrcA [heat regulation at CIRCE (inverted-repeat chaperone expression)] and CtsR (class three stress gene repressor) repressor proteins (Hu et al., 2007a, Hu et al., 2007b) (Fig. 3). While $\sigma^B$ positively regulates class II stress response genes (Kazmierczak et al., 2003, Kazmierczak et al., 2006, McGann et al., 2007, Nadon et al., 2002), the HrcA and CtsR repressor proteins are known to repress the class I and III stress response genes, respectively (Chatterjee et al., 2006, Joerger et al., 2006, Hu et al., 2007a). A transcriptomic study by Hu et, al. has described an interlink between the $\sigma^B$, HrcA and CtsR-dependent regulatory pathways, with $\sigma^B$ having a direct inductive effect on expression of the HrcA repressor; also in the same study, both Lmo1634 and Lmo2637 have been shown to be downregulated by HrcA and upregulated by CtsR (Hu et al., 2007a) (Fig. 38). Therefore an increase in Lmo1634 and Lm02637 protein accumulation, as viewed in the 1D-SDS PAGE analysis, suggests a probable reduction in the HrcA repressor protein expression and induction of the PrfA regulon due to possibly reduced $\sigma^B$ levels. The Δ*lmo0799*-like swarming defect observed for the Δ*lmo0719* mutant would similarly also fit the notion of reduced $\sigma^B$ levels due to the loss of induction of the $\sigma^B$-dependent pathway. The slight growth defect and decreased bacterial invasion observed for Δ*lmo0719* mutant could possibly be due the collective accumulation of potentially cytotoxic PrfA, HrcA and Lmo0719 regulon gene products due a loss of $\sigma^B$ and Lmo0719-dependent regulation.

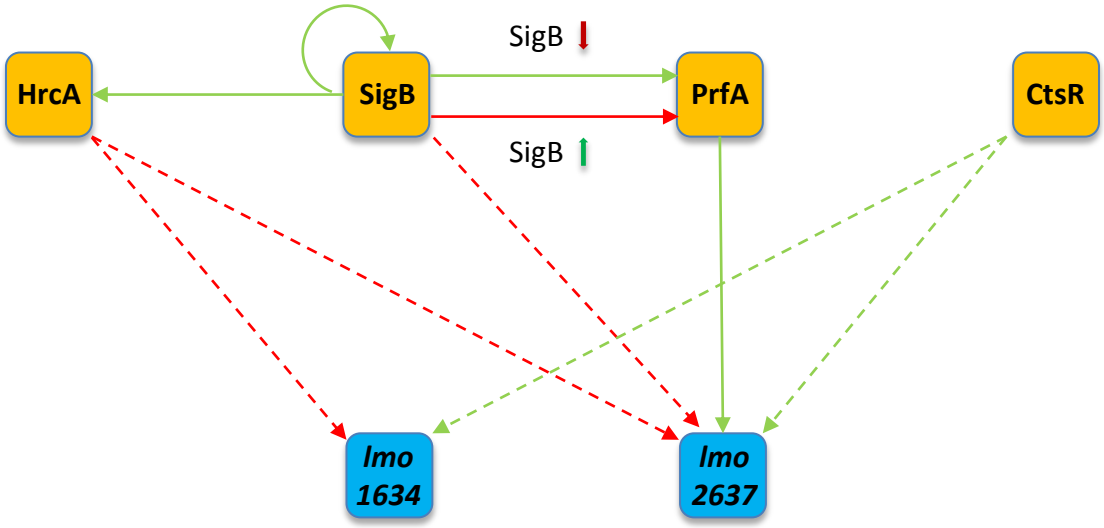


**Figure 38: Co-regulatory effects on the expression of *lmo1634* and *lmo2637*.** Illustration showing the interconnectivity between the major stress response and virulence regulatory pathways and their influence on the expression of *lmo1634* (Lap) and *lmo2637* [adaptation of figure from Hu et al. (2007a)] . Class I, II and III stress response genes are controlled by regulatory pathways mediated by the regulatory proteins HrcA, SigB ($\sigma^B$) and CtsR, respectively, while PrfA controls the expression of a variety of virulence-associated genes belonging to the PrfA regulon. The regulatory effects of these pathways can be either direct (solid arrow) or indirect (dashed arrow) causing either upregulation (green arrow) or downregulation (red arrow) of the target genes. The curved arrow indicates self regulation.

### 4.5.3 Lmo0720 as a putative inhibitor of $\sigma^B$ stress sigma factor

A putative role for the *lmo0720* gene product could be hypothesized based on the model for the functioning of the earlier mentioned LmrR-dependent LmrCD multidrug resistance transporter proposed by Agustiandari et, al. (Agustiandari et al., 2011). According to the this model, LmrR tightly regulates *lmrCD* expression by not only binding to the promoter region of *lmrCD* but by also binding to the promoter ahead of the *lmrR* gene itself, thereby exerting a strong auto-repressive control over expression (Agustiandari et al., 2011). As *lmrR* is directly upstream of *lmrCD* (Agustiandari et al., 2011), a putative deletion of the *lmrR* gene would result in upregulation of *lmrCD* expression. If regulation of the *lmo0719-720* operon were to be compared to this LmrR-dependent LmrCD model, a deletion of the *lmo0719* gene would putatively lead to the upregulation of *lmo0720* (Fig. 39). Considering the swarming resuscitation and partial complementation of the growth and bacterial invasion of the Δ*lmo0719* mutant upon simultaneous deletion of *lmo0720*, Lm0720 could possibly serve as a putative inhibitor of $\sigma^B$. As $\sigma^B$ is known to carry out autoinduction (Raengpradub et al., 2008), a putative inhibition of the $\sigma^B$ pathway by Lmo0720 would prevent its autoinduction

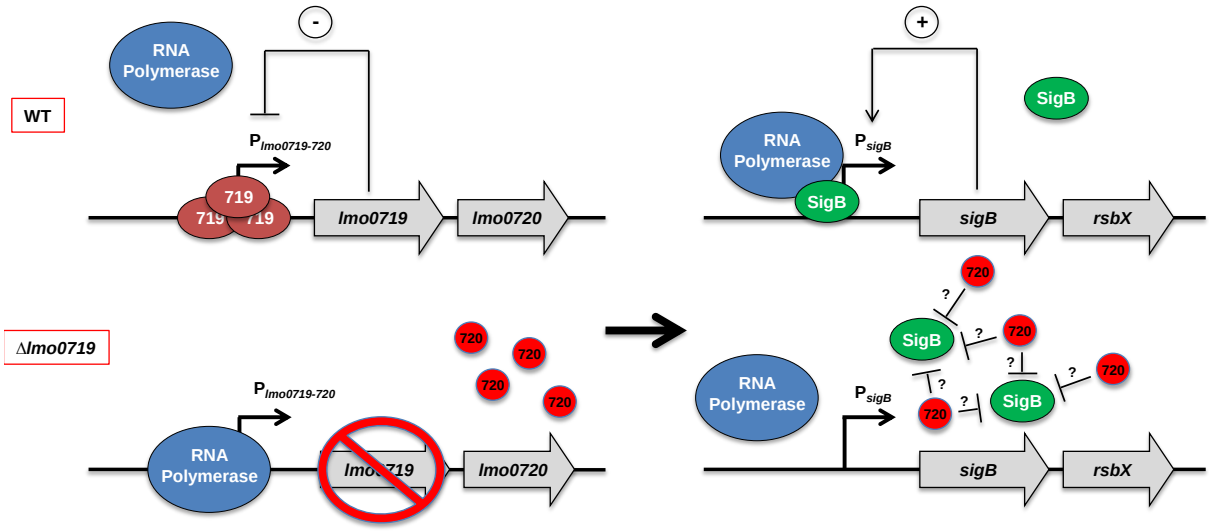


**Figure 39: Influence of the *lmo0719-720* operon on the σ$^{B}$-dependent regulator pathway in *L. monocytogenes*.** Illustration showing the hypothesized model of regulation of the σ$^{B}$-dependent stress response pathway in the wild type *L. monocytogenes* strain, and the consequential deregulation of this pathway in the Δ*lmo0719* mutant. According to this model, σ$^{B}$ is inhibited by the putative σ$^{B}$-inhibitor, Lmo0720, whose expression is upregulated in the absence of *lmo0719* in the Δ*lmo0719* mutant. This therefore leads to a repression of the σ$^{B}$-dependent pathway, which results in an increase in levels of the Lap (Lmo1634) and Lmo2637 proteins (observed in the 1D-SDS PAGE analysis) as well as disruption of swarming motility (loss of halo formation in the swarming assay) in the Δ*lmo0719* mutant as compared to that in the wild type. Whether Lmo720 interacts with SigB to confer inhibition is unknown. Protein Lmo0719 and Lmo0720 have been abbreviated as 719 and 720, respectively. Induction or repression of transcription is indicated by the (+) or (-) symbols, respectively.

and therefore disrupt the σ$^{B}$ response (Fig. 39). Therefore, the wild type-like phenotypic characteristics of the Δ*lmo0720* mutant could be explained by an unperturbed σ$^{B}$-dependent regulatory pathway, where all the stress responses of *L. monocytogenes* are operational. The partial phenotype of the Δ*lmo0719-720* mutant could be explained by the resuscitation of the σ$^{B}$-dependent pathway in the absence of Lmo0720, which would restore Lmo0799-dependent oxidative stress response (halo formation) and reduce the stress burden imposed by the deregulated HrcA and PrfA regulon expression. However, the putative stress due to overexpression of the *lmo0979-980* would still be possibly present in the Δ*lmo0719-720* mutant. This putative role of Lmo0720 as an anti-sigma factor would have to be tested using a series of transcriptomic analyses using the wild type and the *lmo0719-720* operon deletion mutants.

### 4.6 Significance of the *G484E* mutation in the *secA2* gene

Genome sequencing that was carried out to ascertain the presence of single nucleotide polymorphisms (SNPs) elsewhere in the chromosome of the LMKK18 strain also revealed no such mutations (data not shown). Therefore the appearance of the *secA2G484E* mutation in LMKK18 rather seems to be a spontaneous occurrence, which possibly influences the consequential acquirement of the same *G484E* mutation in the ectopically introduced *secA2-gfp* that was used to cure the chaining defect of this strain. The hint to such an influence of the *secA2G484E* allele was observed when it was ectopically overexpressed in the wild type strain, where this mutant allele displayed a dominant negative effect over the wild type *secA2* in the form of partial chaining (data not shown). One possible explanation for the dominant negative effect observed for *secA2G484E* could be the formation of dimers. As weak self-interactions were observed for SecA2 in the bacterial two-hybrid analysis performed earlier, it is plausible that SecA2G484E forms heterodimers with wild type SecA2, thereby rendering the native SecA2 incapable of binding its substrates. Similarly, heterodimerization could also be expected upon overexpression of SecA2-GFP in the LMKK18 mutant. If the putative SecA2-GFP-SecA2G484E heterodimer were to be toxic for the cells, one would expect appearance of random mutations in either *secA2G484E* or *secA2-gfp* as a means of inactivating and thereby counteracting deleterious effects of such heterodimers; however recurrence of the specific *G484E* mutation in *secA2-gfp* rather than its random mutational inactivation seems to confer some form of advantage to the cells expressing the mutant *secA2G484E-gfp* variant. It is likely that SecA2 variants possessing the G484E mutation are enzymatically diminished instead of being inactive, which could be less metabolically demanding than expressing an inactive form of the protein. Work done by Monk et.al, suggests that the rough colony morphology of *L. monocytogenes*, due to deregulation of the SecA2 secretion pathway, does have its merits when it comes to host colonization (Monk et al., 2004). The argument posed was that due to reduced secretion of the highly immunogenic p60 protein as a result of SecA2 disruption/deregulation (therefore reduced immunogenicity), *L. monocytogenes* rough colony variants are able to evade the host immune response and colonize organs such as the gall bladder (Monk et al., 2004). Nonetheless, more work is required to ascertain the true biological significance of *G484E* mutation in *secA2*.

## References

ABACHIN, E., POYART, C., PELLEGRINI, E., MILOHANIC, E., FIEDLER, F., BERCHE, P. & TRIEU-CUOT, P. 2002. Formation of D-alanyl-lipoteichoic acid is required for adhesion and virulence of Listeria monocytogenes. *Mol Microbiol,* 43**,** 1-14.

ADAMS, D. W. & ERRINGTON, J. 2009. Bacterial cell division: assembly, maintenance and disassembly of the Z ring. *Nat Rev Microbiol,* 7**,** 642-53.

AGUSTIANDARI, H., LUBELSKI, J., VAN DEN BERG VAN SAPAROEA, H. B., KUIPERS, O. P. & DRIESSEN, A. J. 2008. LmrR is a transcriptional repressor of expression of the multidrug ABC transporter LmrCD in Lactococcus lactis. *J Bacteriol,* 190**,** 759-63.

AGUSTIANDARI, H., PEETERS, E., DE WIT, J. G., CHARLIER, D. & DRIESSEN, A. J. 2011. LmrR-mediated gene regulation of multidrug resistance in Lactococcus lactis. *Microbiology,* 157**,** 1519-30.

ALVAREZ-DOMINGUEZ, C., MADRAZO-TOCA, F., FERNANDEZ-PRIETO, L., VANDEKERCKHOVE, J., PAREJA, E., TOBES, R., GOMEZ-LOPEZ, M. T., DEL CERRO-VADILLO, E., FRESNO, M., LEYVA-COBIAN, F. & CARRASCO-MARIN, E. 2008. Characterization of a Listeria monocytogenes protein interfering with Rab5a. *Traffic,* 9**,** 325-37.

ALVAREZ-DOMINGUEZ, C., VAZQUEZ-BOLAND, J. A., CARRASCO-MARIN, E., LOPEZ-MATO, P. & LEYVA-COBIAN, F. 1997. Host cell heparan sulfate proteoglycans mediate attachment and entry of Listeria monocytogenes, and the listerial surface protein ActA is involved in heparan sulfate receptor recognition. *Infect Immun,* 65**,** 78-88.

ARCHAMBAUD, C., NAHORI, M.-A., PIZARRO-CERDA, J., COSSART, P. & DUSSURGET, O. 2006. Control of Listeria Superoxide Dismutase by Phosphorylation. *Journal of Biological Chemistry,* 281**,** 31812-31822.

ARNAUD, M., CHASTANET, A. & DEBARBOUILLE, M. 2004. New vector for efficient allelic replacement in naturally nontransformable, low-GC-content, gram-positive bacteria. *Appl Environ Microbiol,* 70**,** 6887-91.

BARAK, I. 2013. Open questions about the function and evolution of bacterial Min systems. *Front Microbiol,* 4**,** 378.

BATTESTI, A. & BOUVERET, E. 2012. The bacterial two-hybrid system based on adenylate cyclase reconstitution in Escherichia coli. *Methods,* 58**,** 325-34.

BEAN, G. J., FLICKINGER, S. T., WESTLER, W. M., MCCULLY, M. E., SEPT, D., WEIBEL, D. B. & AMANN, K. J. 2009. A22 disrupts the bacterial actin cytoskeleton by directly binding and inducing a low-affinity state in MreB. *Biochemistry,* 48**,** 4852-7.

BEN-YEHUDA, S., RUDNER, D. Z. & LOSICK, R. 2003. RacA, a bacterial protein that anchors chromosomes to the cell poles. *Science,* 299**,** 532-6.

BENSING, B. A., SEEPERSAUD, R., YEN, Y. T. & SULLAM, P. M. 2014. Selective transport by SecA2: an expanding family of customized motor proteins. *Biochim Biophys Acta,* 1843**,** 1674-86.

BERNHARDT, T. G. & DE BOER, P. A. J. 2005. SimA, a nucleoid-associated, FtsZ binding protein required for blocking septal ring assembly over chromosomes in E coli. *Molecular Cell,* 18**,** 555-564.

BI, E. F. & LUTKENHAUS, J. 1991. FtsZ ring structure associated with division in Escherichia coli. *Nature,* 354**,** 161-4.

BLANCHETTE, C. D., WOO, Y. H., THOMAS, C., SHEN, N., SULCHEK, T. A. & HIDDESSEN, A. L. 2009. Decoupling internalization, acidification and phagosomal-endosomal/lysosomal fusion during phagocytosis of InlA coated beads in epithelial cells. *PLoS One,* 4**,** e6056.

BLASIOS, V., BISSON-FILHO, A. W., CASTELLEN, P., NOGUEIRA, M. L., BETTINI, J., PORTUGAL, R. V., ZERI, A. C. & GUEIROS-FILHO, F. J. 2013. Genetic and biochemical characterization of the MinC-FtsZ interaction in Bacillus subtilis. *PLoS One,* 8**,** e60690.

BONAZZI, M., VEIGA, E., PIZARRO-CERDA, J. & COSSART, P. 2008. Successive post-translational modifications of E-cadherin are required for InlA-mediated internalization of Listeria monocytogenes. *Cell Microbiol,* 10**,** 2208-22.

BRAHMBHATT, H. & MACDIARMID, J. 2003. Intact minicells as vectors for dna transfer and gene therapy in vitro and in vivo. Google Patents.

BRAMHILL, D. 1997. Bacterial cell division. *Annual Review of Cell and Developmental Biology,* 13**,** 395-424.

BRAMKAMP, M., EMMINS, R., WESTON, L., DONOVAN, C., DANIEL, R. A. & ERRINGTON, J. 2008. A novel component of the division-site selection system of Bacillus subtilis and a new mode of action for the division inhibitor MinCD. *Mol Microbiol,* 70**,** 1556-69.

BRAMKAMP, M. & VAN BAARLE, S. 2009. Division site selection in rod-shaped bacteria. *Curr Opin Microbiol,* 12**,** 683-8.

BRILEY, K., JR., PREPIAK, P., DIAS, M. J., HAHN, J. & DUBNAU, D. 2011. Maf acts downstream of ComGA to arrest cell division in competent cells of B. subtilis. *Mol Microbiol,* 81**,** 23-39.

BRÖTZ-OESTERHELT, H., BEYER, D., KROLL, H.-P., ENDERMANN, R., LADEL, C., SCHROEDER, W., HINZEN, B., RADDATZ, S., PAULSEN, H., HENNINGER, K., BANDOW, J. E., SAHL, H.-G. & LABISCHINSKI, H. 2005. Dysregulation of bacterial proteolytic machinery by a new class of antibiotics. *Nat Med,* 11**,** 1082-1087.

BRYKSIN, A. V. & MATSUMURA, I. 2010. Overlap extension PCR cloning: a simple and reliable way to create recombinant plasmids. *Biotechniques,* 48**,** 463-5.

BUBERT, A., KUHN, M., GOEBEL, W. & KOHLER, S. 1992. Structural and functional properties of the p60 proteins from different Listeria species. *J Bacteriol,* 174**,** 8166-71.

BUDDELMEIJER, N. & BECKWITH, J. 2002. Assembly of cell division proteins at the E. coli cell center. *Current Opinion in Microbiology,* 5**,** 553-557.

BUDDELMEIJER, N., JUDSON, N., BOYD, D., MEKALANOS, J. J. & BECKWITH, J. 2002. YgbQ, a cell division protein in Escherichia coli and Vibrio cholerae, localizes in codependent fashion with FtsL to the division site. *Proceedings of the National Academy of Sciences of the United States of America,* 99**,** 6316-6321.

BURKHOLDER, K. M. & BHUNIA, A. K. 2010. Listeria monocytogenes uses Listeria adhesion protein (LAP) to promote bacterial transepithelial translocation and induces expression of LAP receptor Hsp60. *Infect Immun,* 78**,** 5062-73.

BURKHOLDER, K. M., KIM, K. P., MISHRA, K. K., MEDINA, S., HAHM, B. K., KIM, H. & BHUNIA, A. K. 2009. Expression of LAP, a SecA2-dependent secretory protein, is induced under anaerobic environment. *Microbes Infect,* 11**,** 859-67.

CABANES, D., DEHOUX, P., DUSSURGET, O., FRANGEUL, L. & COSSART, P. 2002. Surface proteins and the pathogenic potential of Listeria monocytogenes. *Trends Microbiol,* 10**,** 238-45.

CAMBERG, J. L., VIOLA, M. G., REA, L., HOSKINS, J. R. & WICKNER, S. 2014. Location of dual sites in E. coli FtsZ important for degradation by ClpXP; one at the C-terminus and one in the disordered linker. *PLoS One,* 9**,** e94964.

CAMEJO, A., CARVALHO, F., REIS, O., LEITAO, E., SOUSA, S. & CABANES, D. 2011. The arsenal of virulence factors deployed by Listeria monocytogenes to promote its cell infection cycle. *Virulence,* 2**,** 379-94.

CAO, M., BITAR, A. P. & MARQUIS, H. 2007. A mariner-based transposition system for Listeria monocytogenes. *Appl Environ Microbiol,* 73**,** 2758-61.

CARBALLIDO-LOPEZ, R. & FORMSTONE, A. 2007. Shape determination in Bacillus subtilis. *Current Opinion in Microbiology,* 10**,** 611-616.

CARROLL, S. A., HAIN, T., TECHNOW, U., DARJI, A., PASHALIDIS, P., JOSEPH, S. W. & CHAKRABORTY, T. 2003. Identification and characterization of a peptidoglycan hydrolase, MurA, of Listeria monocytogenes, a muramidase needed for cell separation. *J Bacteriol,* 185**,** 6801-8.

CHA, J. H. & STEWART, G. C. 1997. The divIVA minicell locus of Bacillus subtilis. *J Bacteriol,* 179**,** 1671-83.

CHAKRABORTY, T., LEIMEISTER-WACHTER, M., DOMANN, E., HARTL, M., GOEBEL, W., NICHTERLEIN, T. & NOTERMANS, S. 1992. Coordinate regulation of virulence genes in Listeria monocytogenes requires the product of the prfA gene. *J Bacteriol,* 174**,** 568-74.

CHATTERJEE, S. S., HOSSAIN, H., OTTEN, S., KUENNE, C., KUCHMINA, K., MACHATA, S., DOMANN, E., CHAKRABORTY, T. & HAIN, T. 2006. Intracellular gene expression profile of Listeria monocytogenes. *Infect Immun,* 74**,** 1323-38.

CHICO-CALERO, I., SUAREZ, M., GONZALEZ-ZORN, B., SCORTTI, M., SLAGHUIS, J., GOEBEL, W. & VAZQUEZ-BOLAND, J. A. 2002. Hpt, a bacterial homolog of the microsomal glucose- 6-phosphate translocase, mediates rapid intracellular proliferation in Listeria. *Proc Natl Acad Sci U S A,* 99**,** 431-6.

CLAESSEN, D., EMMINS, R., HAMOEN, L. W., DANIEL, R. A., ERRINGTON, J. & EDWARDS, D. H. 2008. Control of the cell elongation–division cycle by shuttling of PBP1 protein in Bacillus subtilis. *Molecular Microbiology,* 68**,** 1029-1046.

COLLINS, M. D., WALLBANKS, S., LANE, D. J., SHAH, J., NIETUPSKI, R., SMIDA, J., DORSCH, M. & STACKEBRANDT, E. 1991. Phylogenetic analysis of the genus Listeria based on reverse transcriptase sequencing of 16S rRNA. *Int J Syst Bacteriol,* 41**,** 240-6.

CORDELL, S. C., ANDERSON, R. E. & LOWE, J. 2001. Crystal structure of the bacterial cell division inhibitor MinC. *EMBO J,* 20**,** 2454-61.

CORDELL, S. C. & LOWE, J. 2001. Crystal structure of the bacterial cell division regulator MinD. *FEBS Lett,* 492**,** 160-5.

COSSART, P., PIZARRO-CERDA, J. & LECUIT, M. 2003. Invasion of mammalian cells by Listeria monocytogenes: functional mimicry to subvert cellular functions. *Trends Cell Biol,* 13**,** 23-31.

DAJKOVIC, A., LAN, G., SUN, S. X., WIRTZ, D. & LUTKENHAUS, J. 2008. MinC spatially controls bacterial cytokinesis by antagonizing the scaffolding function of FtsZ. *Curr Biol,* 18**,** 235-44.

DANIEL, R. A., HARRY, E. J. & ERRINGTON, J. 2000. Role of penicillin-binding protein PBP 2B in assembly and functioning of the division machinery of Bacillus subtilis. *Mol Microbiol,* 35**,** 299-311.

DANIEL, R. A., NOIROT-GROS, M. F., NOIROT, P. & ERRINGTON, J. 2006. Multiple interactions between the transmembrane division proteins of Bacillus subtilis and the role of FtsL instability in divisome assembly. *Journal of Bacteriology,* 188**,** 7396-7404.

DAVEY, P. G. 2000. Antimicrobial chemotherapy. *In:* LEDINGHAM, J. G. G. & WARRELL, D. A. (eds.) *Concise Oxford textbook of medicine.* Oxford: Oxford : Oxford University Press, 2000.

DEBOER, P. A. J., CROSSLEY, R. E. & ROTHFIELD, L. I. 1992. ROLES OF MINC AND MIND IN THE SITE-SPECIFIC SEPTATION BLOCK MEDIATED BY THE MINCDE SYSTEM OF ESCHERICHIA-COLI. *Journal of Bacteriology,* 174**,** 63-70.

DEN BLAAUWEN, T., DE PEDRO, M. A., NGUYEN-DISTECHE, M. & AYALA, J. A. 2008. Morphogenesis of rod-shaped sacculi. *Fems Microbiology Reviews,* 32**,** 321-344.

DIAZ, E., FERRANDEZ, A., PRIETO, M. A. & GARCIA, J. L. 2001. Biodegradation of aromatic compounds by Escherichia coli. *Microbiol Mol Biol Rev,* 65**,** 523-69.

DIN, N., QUARDOKUS, E. M., SACKETT, M. J. & BRUN, Y. V. 1998. Dominant C-terminal deletions of FtsZ that affect its ability to localize in Caulobacter and its interaction with FtsA. *Mol Microbiol,* 27**,** 1051-63.

DOMANN, E., WEHLAND, J., ROHDE, M., PISTOR, S., HARTL, M., GOEBEL, W., LEIMEISTER-WACHTER, M., WUENSCHER, M. & CHAKRABORTY, T. 1992. A novel bacterial virulence gene in Listeria monocytogenes required for host cell microfilament interaction with homology to the proline-rich region of vinculin. *Embo j,* 11**,** 1981-90.

DONOVAN, C., SIEGER, B., KRAMER, R. & BRAMKAMP, M. 2012. A synthetic Escherichia coli system identifies a conserved origin tethering factor in Actinobacteria. *Mol Microbiol,* 84**,** 105-16.

DOS SANTOS, V. T., BISSON-FILHO, A. W. & GUEIROS-FILHO, F. J. 2012. DivIVA-mediated polar localization of ComN, a posttranscriptional regulator of Bacillus subtilis. *J Bacteriol,* 194**,** 3661-9.

DRAMSI, S., BISWAS, I., MAGUIN, E., BRAUN, L., MASTROENI, P. & COSSART, P. 1995. Entry of Listeria monocytogenes into hepatocytes requires expression of inIB, a surface protein of the internalin multigene family. *Mol Microbiol,* 16**,** 251-61.

DRAMSI, S., BOURDICHON, F., CABANES, D., LECUIT, M., FSIHI, H. & COSSART, P. 2004. FbpA, a novel multifunctional Listeria monocytogenes virulence factor. *Mol Microbiol,* 53**,** 639-49.

DREVETS, D. A. & BRONZE, M. S. 2008. Listeria monocytogenes: epidemiology, human disease, and mechanisms of brain invasion. *FEMS Immunol Med Microbiol,* 53**,** 151-65.

DUMAN, R., ISHIKAWA, S., CELIK, I., STRAHL, H., OGASAWARA, N., TROC, P., LOWE, J. & HAMOEN, L. W. 2013. Structural and genetic analyses reveal the protein SepF as a new membrane anchor for the Z ring. *Proc Natl Acad Sci U S A,* 110**,** E4601-10.

EDWARDS, D. H. & ERRINGTON, J. 1997. The Bacillus subtilis DivIVA protein targets to the division septum and controls the site specificity of cell division. *Mol Microbiol,* 24**,** 905-15.

ERICKSON, H. P., TAYLOR, D. W., TAYLOR, K. A. & BRAMHILL, D. 1996. Bacterial cell division protein FtsZ assembles into protofilament sheets and minirings, structural homologs of tubulin polymers. *Proc Natl Acad Sci U S A,* 93**,** 519-23.

ERRINGTON, J., DANIEL, R. A. & SCHEFFERS, D. J. 2003. Cytokinesis in bacteria. *Microbiology and Molecular Biology Reviews,* 67**,** 52-+.

ESWARAMOORTHY, P., WINTER, P. W., WAWRZUSIN, P., YORK, A. G., SHROFF, H. & RAMAMURTHI, K. S. 2014. Asymmetric division and differential gene expression during a bacterial developmental program requires DivIVA. *PLoS Genet,* 10**,** e1004526.

FADDA, D., PISCHEDDA, C., CALDARA, F., WHALEN, M. B., ANDERLUZZI, D., DOMENICI, E. & MASSIDDA, O. 2003. Characterization of divIVA and other genes located in the chromosomal region downstream of the dcw cluster in Streptococcus pneumoniae. *J Bacteriol,* 185**,** 6209-14.

FADDA, D., SANTONA, A., D'ULISSE, V., GHELARDINI, P., ENNAS, M. G., WHALEN, M. B. & MASSIDDA, O. 2007. Streptococcus pneumoniae DivIVA: localization and interactions in a MinCD-free context. *J Bacteriol,* 189**,** 1288-98.

FERREIRA, A., SUE, D., O'BYRNE, C. P. & BOOR, K. J. 2003. Role of Listeria monocytogenes sigma(B) in survival of lethal acidic conditions and in the acquired acid tolerance response. *Appl Environ Microbiol,* 69**,** 2692-8.

FINBERG, R. W., MOELLERING, R. C., TALLY, F. P., CRAIG, W. A., PANKEY, G. A., DELLINGER, E. P., WEST, M. A., JOSHI, M., LINDEN, P. K., ROLSTON, K. V., ROTSCHAFER, J. C. & RYBAK, M. J. 2004. The importance of bactericidal drugs: Future directions in infectious disease. *Clinical Infectious Diseases,* 39**,** 1314-1320.

FINLAY, B. B. & FALKOW, S. 1989. Common themes in microbial pathogenicity. *Microbiol Rev,* 53**,** 210-30.

FLÄRDH, K. 2003. Essential role of DivIVA in polar growth and morphogenesis in Streptomyces coelicolor A3(2). *Mol Microbiol,* 49**,** 1523-36.

FLEURIE, A., MANUSE, S., ZHAO, C., CAMPO, N., CLUZEL, C., LAVERGNE, J. P., FRETON, C., COMBET, C., GUIRAL, S., SOUFI, B., MACEK, B., KURU, E., VANNIEUWENHZE, M. S., BRUN, Y. V., DI GUILMI, A. M., CLAVERYS, J. P., GALINIER, A. & GRANGEASSE, C. 2014. Interplay of the serine/threonine-kinase StkP and the paralogs DivIVA and GpsB in pneumococcal cell elongation and division. *PLoS Genet,* 10**,** e1004275.

FREITAG, N. E. 2006. From hot dogs to host cells: how the bacterial pathogen Listeria monocytogenes regulates virulence gene expression. *Future microbiology,* 1**,** 89-101.

FREITAG, N. E., PORT, G. C. & MINER, M. D. 2009. Listeria monocytogenes - from saprophyte to intracellular pathogen. *Nat Rev Microbiol,* 7**,** 623-8.

GAILLARD, J. L., BERCHE, P., FREHEL, C., GOUIN, E. & COSSART, P. 1991. Entry of L. monocytogenes into cells is mediated by internalin, a repeat protein reminiscent of surface antigens from gram-positive cocci. *Cell,* 65**,** 1127-41.

GEDDE, M. M., HIGGINS, D. E., TILNEY, L. G. & PORTNOY, D. A. 2000. Role of listeriolysin O in cell-to-cell spread of Listeria monocytogenes. *Infect Immun,* 68**,** 999-1003.

GEOFFROY, C., RAVENEAU, J., BERETTI, J. L., LECROISEY, A., VAZQUEZ-BOLAND, J. A., ALOUF, J. E. & BERCHE, P. 1991. Purification and characterization of an extracellular 29-kilodalton phospholipase C from Listeria monocytogenes. *Infect Immun,* 59**,** 2382-8.

GERDES, K., MOLLER-JENSEN, J. & BUGGE JENSEN, R. 2000. Plasmid and chromosome partitioning: surprises from phylogeny. *Mol Microbiol,* 37**,** 455-66.

GILBERT, R. J. 2010. Cholesterol-dependent cytolysins. *Adv Exp Med Biol,* 677**,** 56-66.

GLASER, P., FRANGEUL, L., BUCHRIESER, C., RUSNIOK, C., AMEND, A., BAQUERO, F., BERCHE, P., BLOECKER, H., BRANDT, P., CHAKRABORTY, T., CHARBIT, A., CHETOUANI, F., COUVE, E., DE DARUVAR, A., DEHOUX, P., DOMANN, E., DOMINGUEZ-BERNAL, G., DUCHAUD, E., DURANT, L., DUSSURGET, O., ENTIAN, K. D., FSIHI, H., GARCIA-DEL PORTILLO, F.,

GARRIDO, P., GAUTIER, L., GOEBEL, W., GOMEZ-LOPEZ, N., HAIN, T., HAUF, J., JACKSON, D., JONES, L. M., KAERST, U., KREFT, J., KUHN, M., KUNST, F., KURAPKAT, G., MADUENO, E., MAITOURNAM, A., VICENTE, J. M., NG, E., NEDJARI, H., NORDSIEK, G., NOVELLA, S., DE PABLOS, B., PEREZ-DIAZ, J. C., PURCELL, R., REMMEL, B., ROSE, M., SCHLUETER, T., SIMOES, N., TIERREZ, A., VAZQUEZ-BOLAND, J. A., VOSS, H., WEHLAND, J. & COSSART, P. 2001. Comparative genomics of Listeria species. *Science,* 294**,** 849-52.

GOFFIN, C. & GHUYSEN, J. M. 1998. Multimodular penicillin binding proteins: An enigmatic family of orthologs and paralogs. *Microbiology and Molecular Biology Reviews,* 62**,** 1079-+.

GREGORY, J. A., BECKER, E. C. & POGLIANO, K. 2008. Bacillus subtilis MinC destabilizes FtsZ-rings at new cell poles and contributes to the timing of cell division. *Genes Dev,* 22**,** 3475-88.

GROISMAN, E. A. & OCHMAN, H. 1996. Pathogenicity islands: bacterial evolution in quantum leaps. *Cell,* 87**,** 791-4.

GUEIROS-FILHO, F. J. & LOSICK, R. 2002. A widely conserved bacterial cell division protein that promotes assembly of the tubulin-like protein FtsZ. *Genes Dev,* 16**,** 2544-56.

GURY, J., BARTHELMEBS, L., TRAN, N. P., DIVIES, C. & CAVIN, J. F. 2004. Cloning, deletion, and characterization of PadR, the transcriptional repressor of the phenolic acid decarboxylase-encoding padA gene of Lactobacillus plantarum. *Appl Environ Microbiol,* 70**,** 2146-53.

HAEUSSER, D. P., HOASHI, M., WEAVER, A., BROWN, N., PAN, J., SAWITZKE, J. A., THOMASON, L. C., COURT, D. L. & MARGOLIN, W. 2014. The Kil peptide of bacteriophage lambda blocks Escherichia coli cytokinesis via ZipA-dependent inhibition of FtsZ assembly. *PLoS Genet,* 10**,** e1004217.

HALBEDEL, S., HAHN, B., DANIEL, R. A. & FLIEGER, A. 2012. DivIVA affects secretion of virulence-related autolysins in Listeria monocytogenes. *Mol Microbiol,* 83**,** 821-39.

HANDLER, A. A., LIM, J. E. & LOSICK, R. 2008. Peptide inhibitor of cytokinesis during sporulation in Bacillus subtilis. *Mol Microbiol,* 68**,** 588-99.

HARRY, E., MONAHAN, L. & THOMPSON, L. 2006. Bacterial cell division: the mechanism and its precison. *Int Rev Cytol,* 253**,** 27-94.

HELLOIN, E., JANSCH, L. & PHAN-THANH, L. 2003. Carbon starvation survival of Listeria monocytogenes in planktonic state and in biofilm: a proteomic study. *Proteomics,* 3**,** 2052-64.

HERZBERG, C., WEIDINGER, L. A., DORRBECKER, B., HUBNER, S., STULKE, J. & COMMICHAU, F. M. 2007. SPINE: a method for the rapid detection and analysis of protein-protein interactions in vivo. *Proteomics,* 7**,** 4032-5.

HU, Y., OLIVER, H. F., RAENGPRADUB, S., PALMER, M. E., ORSI, R. H., WIEDMANN, M. & BOOR, K. J. 2007a. Transcriptomic and phenotypic analyses suggest a network between the transcriptional regulators HrcA and sigmaB in Listeria monocytogenes. *Appl Environ Microbiol,* 73**,** 7981-91.

HU, Y., RAENGPRADUB, S., SCHWAB, U., LOSS, C., ORSI, R. H., WIEDMANN, M. & BOOR, K. J. 2007b. Phenotypic and transcriptomic analyses demonstrate interactions between the transcriptional regulators CtsR and Sigma B in Listeria monocytogenes. *Appl Environ Microbiol,* 73**,** 7967-80.

HU, Z. & LUTKENHAUS, J. 2001. Topological regulation of cell division in E. coli. spatiotemporal oscillation of MinD requires stimulation of its ATPase by MinE and phospholipid. *Mol Cell,* 7**,** 1337-43.

HUILLET, E., VELGE, P., VALLAEYS, T. & PARDON, P. 2006. LadR, a new PadR-related transcriptional regulator from Listeria monocytogenes, negatively regulates the expression of the multidrug efflux pump MdrL. *FEMS Microbiol Lett,* 254**,** 87-94.

JAGADEESAN, B., KOO, O. K., KIM, K. P., BURKHOLDER, K. M., MISHRA, K. K., AROONNUAL, A. & BHUNIA, A. K. 2010. LAP, an alcohol acetaldehyde dehydrogenase enzyme in Listeria, promotes bacterial adhesion to enterocyte-like Caco-2 cells only in pathogenic species. *Microbiology,* 156**,** 2782-95.

JEMTH, P. & GIANNI, S. 2007. PDZ domains: Folding and binding. *Biochemistry,* 46**,** 8701-8708.

JENSEN, S. O., THOMPSON, L. S. & HARRY, E. J. 2005. Cell division in Bacillus subtilis: FtsZ and FtsA association is Z-ring independent, and FtsA is required for efficient midcell Z-Ring assembly. *J Bacteriol,* 187**,** 6536-44.

JOERGER, R. D., CHEN, H. & KNIEL, K. E. 2006. Characterization of a spontaneous, pressure-tolerant Listeria monocytogenes Scott A ctsR deletion mutant. *Foodborne Pathog Dis,* 3**,** 196-202.

JONQUIERES, R., BIERNE, H., FIEDLER, F., GOUNON, P. & COSSART, P. 1999. Interaction between the protein InlB of Listeria monocytogenes and lipoteichoic acid: a novel mechanism of protein association at the surface of gram-positive bacteria. *Mol Microbiol,* 34**,** 902-14.

KANG, C. M., NYAYAPATHY, S., LEE, J. Y., SUH, J. W. & HUSSON, R. N. 2008. Wag31, a homologue of the cell division protein DivIVA, regulates growth, morphology and polar cell wall synthesis in mycobacteria. *Microbiology,* 154**,** 725-35.

KARAMANOU, S., VRONTOU, E., SIANIDIS, G., BAUD, C., ROOS, T., KUHN, A., POLITOU, A. S. & ECONOMOU, A. 1999. A molecular switch in SecA protein couples ATP hydrolysis to protein translocation. *Mol Microbiol,* 34**,** 1133-45.

KARIMOVA, G., PIDOUX, J., ULLMANN, A. & LADANT, D. 1998. A bacterial two-hybrid system based on a reconstituted signal transduction pathway. *Proc Natl Acad Sci U S A,* 95**,** 5752-6.

KAVAL, K. G. & HALBEDEL, S. 2012. Architecturally the same, but playing a different game: the diverse species-specific roles of DivIVA proteins. *Virulence,* 3**,** 406-7.

KAZMIERCZAK, M. J., MITHOE, S. C., BOOR, K. J. & WIEDMANN, M. 2003. Listeria monocytogenes sigma B regulates stress response and virulence functions. *J Bacteriol,* 185**,** 5722-34.

KAZMIERCZAK, M. J., WIEDMANN, M. & BOOR, K. J. 2006. Contributions of Listeria monocytogenes sigmaB and PrfA to expression of virulence and stress response genes during extra- and intracellular growth. *Microbiology,* 152**,** 1827-38.

KEARNS, D. B. & LOSICK, R. 2003. Swarming motility in undomesticated Bacillus subtilis. *Mol Microbiol,* 49**,** 581-90.

KIRCHNER, M. & HIGGINS, D. E. 2008. Inhibition of ROCK activity allows InlF-mediated invasion and increased virulence of Listeria monocytogenes. *Mol Microbiol,* 68**,** 749-67.

KOCKS, C., GOUIN, E., TABOURET, M., BERCHE, P., OHAYON, H. & COSSART, P. 1992. L. monocytogenes-induced actin assembly requires the actA gene product, a surface protein. *Cell,* 68**,** 521-31.

KOCKS, C., MARCHAND, J. B., GOUIN, E., D'HAUTEVILLE, H., SANSONETTI, P. J., CARLIER, M. F. & COSSART, P. 1995. The unrelated surface proteins ActA of Listeria monocytogenes and IcsA of Shigella flexneri are sufficient to confer actin-based motility on Listeria innocua and Escherichia coli respectively. *Mol Microbiol,* 18**,** 413-23.

KOHLER, S., BUBERT, A., VOGEL, M. & GOEBEL, W. 1991. Expression of the iap gene coding for protein p60 of Listeria monocytogenes is controlled on the posttranscriptional level. *J Bacteriol,* 173**,** 4668-74.

KOLB-MAURER, A., GENTSCHEV, I., FRIES, H. W., FIEDLER, F., BROCKER, E. B., KAMPGEN, E. & GOEBEL, W. 2000. Listeria monocytogenes-infected human dendritic cells: uptake and host cell response. *Infect Immun,* 68**,** 3680-8.

KOVACIKOVA, G., LIN, W. & SKORUPSKI, K. 2003. The virulence activator AphA links quorum sensing to pathogenesis and physiology in Vibrio cholerae by repressing the

expression of a penicillin amidase gene on the small chromosome. *J Bacteriol,* 185**,** 4825-36.

KROL, E., VAN KESSEL, S. P., VAN BEZOUWEN, L. S., KUMAR, N., BOEKEMA, E. J. & SCHEFFERS, D. J. 2012. Bacillus subtilis SepF binds to the C-terminus of FtsZ. *PLoS One,* 7**,** e43293.

KUHN, M. & GOEBEL, W. 1989. Identification of an extracellular protein of Listeria monocytogenes possibly involved in intracellular uptake by mammalian cells. *Infect Immun,* 57**,** 55-61.

LADANT, D. & ULLMANN, A. 1999. Bordatella pertussis adenylate cyclase: a toxin with multiple talents. *Trends Microbiol,* 7**,** 172-6.

LAEMMLI, U. K. 1970. Cleavage of structural proteins during the assembly of the head of bacteriophage T4. *Nature,* 227**,** 680-5.

LEAVER, M., DOMÍNGUEZ-CUEVAS, P., COXHEAD, J. M., DANIEL, R. A. & ERRINGTON, J. 2009. Life without a wall or division machine in Bacillus subtilis. *Nature,* 457**,** 849-853.

LEBRUN, M., MENGAUD, J., OHAYON, H., NATO, F. & COSSART, P. 1996. Internalin must be on the bacterial surface to mediate entry of Listeria monocytogenes into epithelial cells. *Mol Microbiol,* 21**,** 579-92.

LECUIT, M. 2007. Human listeriosis and animal models. *Microbes Infect,* 9**,** 1216-25.

LENARCIC, R., HALBEDEL, S., VISSER, L., SHAW, M., WU, L. J., ERRINGTON, J., MARENDUZZO, D. & HAMOEN, L. W. 2009. Localisation of DivIVA by targeting to negatively curved membranes. *EMBO J,* 28**,** 2272-82.

LENZ, L. L., MOHAMMADI, S., GEISSLER, A. & PORTNOY, D. A. 2003. SecA2-dependent secretion of autolytic enzymes promotes Listeria monocytogenes pathogenesis. *Proc Natl Acad Sci U S A,* 100**,** 12432-7.

LENZ, L. L. & PORTNOY, D. A. 2002. Identification of a second Listeria secA gene associated with protein secretion and the rough phenotype. *Mol Microbiol,* 45**,** 1043-56.

LETEK, M., FIUZA, M., ORDÓÑEZ, E., VILLADANGOS, A. F., FLÄRDH, K., MATEOS, L. M. & GIL, J. A. 2009. DivIVA uses an N-terminal conserved region and two coiled-coil domains to localize and sustain the polar growth in Corynebacterium glutamicum. *FEMS Microbiology Letters,* 297**,** 110-116.

LETEK, M., ORDONEZ, E., VAQUERA, J., MARGOLIN, W., FLARDH, K., MATEOS, L. M. & GIL, J. A. 2008. DivIVA is required for polar growth in the MreB-lacking rod-shaped actinomycete Corynebacterium glutamicum. *J Bacteriol,* 190**,** 3283-92.

LEVIN, P. A., SHIM, J. J. & GROSSMAN, A. D. 1998. Effect of minCD on FtsZ ring position and polar septation in Bacillus subtilis. *J Bacteriol,* 180**,** 6048-51.

LIU, H. & NAISMITH, J. H. 2008. An efficient one-step site-directed deletion, insertion, single and multiple-site plasmid mutagenesis protocol. *BMC Biotechnol,* 8**,** 91.

LLUCH-SENAR, M., QUEROL, E. & PINOL, J. 2010. Cell division in a minimal bacterium in the absence of ftsZ. *Mol Microbiol,* 78**,** 278-89.

LOOSE, M. & MITCHISON, T. J. 2014. The bacterial cell division proteins FtsA and FtsZ self-organize into dynamic cytoskeletal patterns. *Nat Cell Biol,* 16**,** 38-46.

LUTKENHAUS, J. 1993. FTSZ RING IN BACTERIAL CYTOKINESIS. *Molecular Microbiology,* 9**,** 403-409.

MACHATA, S., HAIN, T., ROHDE, M. & CHAKRABORTY, T. 2005. Simultaneous deficiency of both MurA and p60 proteins generates a rough phenotype in Listeria monocytogenes. *J Bacteriol,* 187**,** 8385-94.

MACHEBOEUF, P., CONTRERAS-MARTEL, C., JOB, V., DIDEBERG, O. & DESSEN, A. 2006. Penicillin binding proteins: key players in bacterial cell cycle and drug resistance processes. *Fems Microbiology Reviews,* 30**,** 673-691.

MADIGAN, M. T., MARTINKO, J. M., BROCK, T. D. & PARKER. J. 2000. Cell Division and Sexual Reproduction. *In:* MADIGAN, M. T. (ed.) *Brock biology of microorganisms.* 9, illustrated ed. New Jersey: Prentice Hall, 2000.

MARGOLIN, W. 2000. Themes and variations in prokaryotic cell division. *Fems Microbiology Reviews,* 24**,** 531-548.

MARGOLIN, W. 2005. FtsZ and the division of prokaryotic cells and organelles. *Nat Rev Mol Cell Biol,* 6**,** 862-71.

MARINO, M., BANERJEE, M., JONQUIERES, R., COSSART, P. & GHOSH, P. 2002. GW domains of the Listeria monocytogenes invasion protein InlB are SH3-like and mediate binding to host ligands. *Embo j,* 21**,** 5623-34.

MARINO, M., BRAUN, L., COSSART, P. & GHOSH, P. 1999. Structure of the lnlB leucine-rich repeats, a domain that triggers host cell invasion by the bacterial pathogen L. monocytogenes. *Mol Cell,* 4**,** 1063-72.

MARSTON, A. L. & ERRINGTON, J. 1999. Selection of the midcell division site in Bacillus subtilis through MinD-dependent polar localization and activation of MinC. *Mol Microbiol,* 33**,** 84-96.

MARSTON, A. L., THOMAIDES, H. B., EDWARDS, D. H., SHARPE, M. E. & ERRINGTON, J. 1998. Polar localization of the MinD protein of Bacillus subtilis and its role in selection of the mid-cell division site. *Genes Dev,* 12**,** 3419-30.

MCGANN, P., WIEDMANN, M. & BOOR, K. J. 2007. The alternative sigma factor sigma B and the virulence gene regulator PrfA both regulate transcription of Listeria monocytogenes internalins. *Appl Environ Microbiol,* 73**,** 2919-30.

MCLAUGHLAN, A. M. & FOSTER, S. J. 1998. Molecular characterization of an autolytic amidase of Listeria monocytogenes EGD. *Microbiology,* 144 ( Pt 5)**,** 1359-67.

MENGAUD, J., OHAYON, H., GOUNON, P., MEGE, R. M. & COSSART, P. 1996. E-cadherin is the receptor for internalin, a surface protein required for entry of L. monocytogenes into epithelial cells. *Cell,* 84**,** 923-32.

MENICHE, X., OTTEN, R., SIEGRIST, M. S., BAER, C. E., MURPHY, K. C., BERTOZZI, C. R. & SASSETTI, C. M. 2014. Subpolar addition of new cell wall is directed by DivIVA in mycobacteria. *Proc Natl Acad Sci U S A,* 111**,** E3243-51.

MIGOCKI, M. D., FREEMAN, M. K., WAKE, R. G. & HARRY, E. J. 2002. The Min system is not required for precise placement of the midcell Z ring in Bacillus subtilis. *EMBO Rep,* 3**,** 1163-7.

MILOHANIC, E., JONQUIERES, R., COSSART, P., BERCHE, P. & GAILLARD, J. L. 2001. The autolysin Ami contributes to the adhesion of Listeria monocytogenes to eukaryotic cells via its cell wall anchor. *Mol Microbiol,* 39**,** 1212-24.

MILOHANIC, E., JONQUIERES, R., GLASER, P., DEHOUX, P., JACQUET, C., BERCHE, P., COSSART, P. & GAILLARD, J. L. 2004. Sequence and binding activity of the autolysin-adhesin Ami from epidemic Listeria monocytogenes 4b. *Infect Immun,* 72**,** 4401-9.

MOHAMMADI, T., VAN DAM, V., SIJBRANDI, R., VERNET, T., ZAPUN, A., BOUHSS, A., DIEPEVEEN-DE BRUIN, M., NGUYEN-DISTECHE, M., DE KRUIJFF, B. & BREUKINK, E. 2011. Identification of FtsW as a transporter of lipid-linked cell wall precursors across the membrane. *Embo j,* 30**,** 1425-32.

MONAHAN, L. G., LIEW, A. T., BOTTOMLEY, A. L. & HARRY, E. J. 2014. Division site positioning in bacteria: one size does not fit all. *Front Microbiol,* 5**,** 19.

MONK, I. R., COOK, G. M., MONK, B. C. & BREMER, P. J. 2004. Morphotypic conversion in Listeria monocytogenes biofilm formation: biological significance of rough colony isolates. *Appl Environ Microbiol,* 70**,** 6686-94.

MONK, I. R., GAHAN, C. G. & HILL, C. 2008. Tools for functional postgenomic analysis of listeria monocytogenes. *Appl Environ Microbiol,* 74**,** 3921-34.

MUKHERJEE, A. & LUTKENHAUS, J. 1998. Purification, assembly, and localization of FtsZ. *Methods Enzymol,* 298**,** 296-305.

MURRAY, T., POPHAM, D. L. & SETLOW, P. 1998. Bacillus subtilis cells lacking penicillin-binding protein 1 require increased levels of divalent cations for growth. *J Bacteriol,* 180**,** 4555-63.

NADON, C. A., BOWEN, B. M., WIEDMANN, M. & BOOR, K. J. 2002. Sigma B contributes to PrfA-mediated virulence in Listeria monocytogenes. *Infect Immun,* 70**,** 3948-52.

NENNINGER, A., MASTROIANNI, G. & MULLINEAUX, C. W. 2010. Size dependence of protein diffusion in the cytoplasm of Escherichia coli. *J Bacteriol,* 192**,** 4535-40.

NOIRCLERC-SAVOYE, M., LE GOUELLEC, A., MORLOT, C., DIDEBERG, O., VERNET, T. & ZAPUN, A. 2005. In vitro reconstitution of a trimeric complex of DivIB, DivIC and FtsL, and their transient co-localization at the division site in Streptococcus pneumoniae. *Molecular Microbiology,* 55**,** 413-424.

OLIVA, M. A., HALBEDEL, S., FREUND, S. M., DUTOW, P., LEONARD, T. A., VEPRINTSEV, D. B., HAMOEN, L. W. & LOWE, J. 2010. Features critical for membrane binding revealed by DivIVA crystal structure. *EMBO J,* 29**,** 1988-2001.

OLLINGER, J., BOWEN, B., WIEDMANN, M., BOOR, K. J. & BERGHOLZ, T. M. 2009. Listeria monocytogenes sigmaB modulates PrfA-mediated virulence factor expression. *Infect Immun,* 77**,** 2113-24.

OSBORNE, A. R., CLEMONS, W. M., JR. & RAPOPORT, T. A. 2004. A large conformational change of the translocation ATPase SecA. *Proc Natl Acad Sci U S A,* 101**,** 10937-42.

PANDIRIPALLY, V. K., WESTBROOK, D. G., SUNKI, G. R. & BHUNIA, A. K. 1999. Surface protein p104 is involved in adhesion of Listeria monocytogenes to human intestinal cell line, Caco-2. *J Med Microbiol,* 48**,** 117-24.

PARADIS-BLEAU, C., SANSCHAGRIN, F. & LEVESQUE, R. C. 2005. Peptide inhibitors of the essential cell division protein FtsA. *Protein Engineering Design & Selection,* 18**,** 85-91.

PATRICK, J. E. & KEARNS, D. B. 2008. MinJ (YvjD) is a topological determinant of cell division in Bacillus subtilis. *Mol Microbiol,* 70**,** 1166-79.

PEDERSEN, L. B., ANGERT, E. R. & SETLOW, P. 1999. Septal localization of penicillin-binding protein 1 in Bacillus subtilis. *J Bacteriol,* 181**,** 3201-11.

PERRY, S. E. & EDWARDS, D. H. 2004. Identification of a polar targeting determinant for Bacillus subtilis DivIVA. *Mol Microbiol,* 54**,** 1237-49.

PILGRIM, S., KOLB-MAURER, A., GENTSCHEV, I., GOEBEL, W. & KUHN, M. 2003. Deletion of the gene encoding p60 in Listeria monocytogenes leads to abnormal cell division and loss of actin-based motility. *Infect Immun,* 71**,** 3473-84.

PINHO, M. G., DE LENCASTRE, H. & TOMASZ, A. 2001. An acquired and a native penicillin-binding protein cooperate in building the cell wall of drug-resistant staphylococci. *Proceedings of the National Academy of Sciences of the United States of America,* 98**,** 10886-10891.

PORT, G. C. & FREITAG, N. E. 2007. Identification of novel Listeria monocytogenes secreted virulence factors following mutational activation of the central virulence regulator, PrfA. *Infect Immun,* 75**,** 5886-97.

PORTNOY, D. A., JACKS, P. S. & HINRICHS, D. J. 1988. Role of hemolysin for the intracellular growth of Listeria monocytogenes. *J Exp Med,* 167**,** 1459-71.

POZSGAI, E. R., BLAIR, K. M. & KEARNS, D. B. 2012. Modified mariner transposons for random inducible-expression insertions and transcriptional reporter fusion insertions in Bacillus subtilis. *Appl Environ Microbiol,* 78**,** 778-85.

RAENGPRADUB, S., WIEDMANN, M. & BOOR, K. J. 2008. Comparative analysis of the sigma B-dependent stress responses in Listeria monocytogenes and Listeria innocua strains exposed to selected stress conditions. *Appl Environ Microbiol,* 74**,** 158-71.

RAMIREZ-ARCOS, S., LIAO, M., MARTHALER, S., RIGDEN, M. & DILLON, J. A. 2005. Enterococcus faecalis divIVA: an essential gene involved in cell division, cell growth and chromosome segregation. *Microbiology,* 151**,** 1381-93.

RASKIN, D. M. & DE BOER, P. A. 1999. MinDE-dependent pole-to-pole oscillation of division inhibitor MinC in Escherichia coli. *J Bacteriol,* 181**,** 6419-24.

REIS, O., SOUSA, S., CAMEJO, A., VILLIERS, V., GOUIN, E., COSSART, P. & CABANES, D. 2010. LapB, a novel Listeria monocytogenes LPXTG surface adhesin, required for entry into eukaryotic cells and virulence. *J Infect Dis,* 202**,** 551-62.

RENIER, S., CHAMBON, C., VIALA, D., CHAGNOT, C., HEBRAUD, M. & DESVAUX, M. 2013. Exoproteomic analysis of the SecA2-dependent secretion in Listeria monocytogenes EGD-e. *J Proteomics,* 80c**,** 183-195.

RODRIGUES, C. D. & HARRY, E. J. 2012. The Min system and nucleoid occlusion are not required for identifying the division site in Bacillus subtilis but ensure its efficient utilization. *PLoS Genet,* 8**,** e1002561.

SABET, C., TOLEDO-ARANA, A., PERSONNIC, N., LECUIT, M., DUBRAC, S., POUPEL, O., GOUIN, E., NAHORI, M. A., COSSART, P. & BIERNE, H. 2008. The Listeria monocytogenes virulence factor InlJ is specifically expressed in vivo and behaves as an adhesin. *Infect Immun,* 76**,** 1368-78.

SAKAI, N., YAO, M., ITOU, H., WATANABE, N., YUMOTO, F., TANOKURA, M. & TANAKA, I. 2001. The three-dimensional structure of septum site-determining protein MinD from Pyrococcus horikoshii OT3 in complex with Mg-ADP. *Structure,* 9**,** 817-26.

SALLEN, B., RAJOHARISON, A., DESVARENNE, S., QUINN, F. & MABILAT, C. 1996. Comparative analysis of 16S and 23S rRNA sequences of Listeria species. *Int J Syst Bacteriol,* 46**,** 669-74.

SAMBROOK, J., FRITSCH, E.F., AND MANIATIS, T. 1989. *Molecular Cloning: A Laboratory Manual,* Cold Spring Harbor, NY, Cold Spring Harbor Laboratory Press.

SASS, P., JOSTEN, M., FAMULLA, K., SCHIFFER, G., SAHL, H. G., HAMOEN, L. & BROTZ-OESTERHELT, H. 2011. Antibiotic acyldepsipeptides activate ClpP peptidase to degrade the cell division protein FtsZ. *Proc Natl Acad Sci U S A,* 108**,** 17474-9.

SAUVAGE, E., KERFF, F., FONZE, E., HERMAN, R., SCHOOT, B., MARQUETTE, J. P., TABURET, Y., PREVOST, D., DUMAS, J., LEONARD, G., STEFANIC, P., COYETTE, J. & CHARLIER, P. 2002. The 2.4-A crystal structure of the penicillin-resistant penicillin-binding protein PBP5fm from Enterococcus faecium in complex with benzylpenicillin. *Cell Mol Life Sci,* 59**,** 1223-32.

SCHEFFERS, D. J. & ERRINGTON, J. 2004. PBP1 is a component of the Bacillus subtilis cell division machinery. *Journal of Bacteriology,* 186**,** 5153-5156.

SCHEFFERS, D. J., JONES, L. J. & ERRINGTON, J. 2004. Several distinct localization patterns for penicillin-binding proteins in Bacillus subtilis. *Mol Microbiol,* 51**,** 749-64.

SCHUBERT, W. D., GOBEL, G., DIEPHOLZ, M., DARJI, A., KLOER, D., HAIN, T., CHAKRABORTY, T., WEHLAND, J., DOMANN, E. & HEINZ, D. W. 2001. Internalins from the human pathogen Listeria monocytogenes combine three distinct folds into a contiguous internalin domain. *J Mol Biol,* 312**,** 783-94.

SHIH, Y. L., FU, X., KING, G. F., LE, T. & ROTHFIELD, L. 2002. Division site placement in E.coli: mutations that prevent formation of the MinE ring lead to loss of the normal midcell arrest of growth of polar MinD membrane domains. *Embo j,* 21**,** 3347-57.

SIANIDIS, G., KARAMANOU, S., VRONTOU, E., BOULIAS, K., REPANAS, K., KYRPIDES, N., POLITOU, A. S. & ECONOMOU, A. 2001. Cross-talk between catalytic and regulatory elements in a DEAD motor domain is essential for SecA function. *EMBO J,* 20**,** 961-70.

SIEVERS, J. & ERRINGTON, J. 2000. The Bacillus subtilis cell division protein FtsL localizes to sites of septation and interacts with DivlC. *Molecular Microbiology,* 36**,** 846-855.

SINGH, J. K., MAKDE, R. D., KUMAR, V. & PANDA, D. 2007. A membrane protein, EzrA, regulates assembly dynamics of FtsZ by interacting with the C-terminal tail of FtsZ. *Biochemistry,* 46**,** 11013-22.

SINGH, J. K., MAKDE, R. D., KUMAR, V. & PANDA, D. 2008. SepF increases the assembly and bundling of FtsZ polymers and stabilizes FtsZ protofilaments by binding along its length. *J Biol Chem,* 283**,** 31116-24.

SMALL, E., MARRINGTON, R., RODGER, A., SCOTT, D. J., SLOAN, K., ROPER, D., DAFFORN, T. R. & ADDINALL, S. G. 2007. FtsZ polymer-bundling by the Escherichia coli ZapA orthologue, YgfE, involves a conformational change in bound GTP. *J Mol Biol,* 369**,** 210-21.

SMUTNY, M. & YAP, A. S. 2010. Neighborly relations: cadherins and mechanotransduction. *J Cell Biol,* 189**,** 1075-7.

SOUSA, S., CABANES, D., BOUGNERES, L., LECUIT, M., SANSONETTI, P., TRAN-VAN-NHIEU, G. & COSSART, P. 2007. Src, cortactin and Arp2/3 complex are required for E-cadherin-mediated internalization of Listeria into cells. *Cell Microbiol,* 9**,** 2629-43.

STOKES, N. R., SIEVERS, J., BARKER, S., BENNETT, J. M., BROWN, D. R., COLLINS, I., ERRINGTON, V. M., FOULGER, D., HALL, M., HALSEY, R., JOHNSON, H., ROSE, V., THOMAIDES, H. B., HAYDON, D. J., CZAPLEWSKI, L. G. & ERRINGTON, J. 2005. Novel inhibitors of bacterial cytokinesis identified by a cell-based antibiotic screening assay. *Journal of Biological Chemistry,* 280**,** 39709-39715.

SUAREZ, M., GONZALEZ-ZORN, B., VEGA, Y., CHICO-CALERO, I. & VAZQUEZ-BOLAND, J. A. 2001. A role for ActA in epithelial cell invasion by Listeria monocytogenes. *Cell Microbiol,* 3**,** 853-64.

SUCKAU, D., MAK, M. & PRZYBYLSKI, M. 1992. Protein surface topology-probing by selective chemical modification and mass spectrometric peptide mapping. *Proc Natl Acad Sci U S A,* 89**,** 5630-4.

SUN, N., CHAN, F. Y., LU, Y. J., NEVES, M. A., LUI, H. K., WANG, Y., CHOW, K. Y., CHAN, K. F., YAN, S. C., LEUNG, Y. C., ABAGYAN, R., CHAN, T. H. & WONG, K. Y. 2014. Rational design of berberine-based FtsZ inhibitors with broad-spectrum antibacterial activity. *PLoS One,* 9**,** e97514.

SUTHERLAND, B. W., TOEWS, J. & KAST, J. 2008. Utility of formaldehyde cross-linking and mass spectrometry in the study of protein-protein interactions. *J Mass Spectrom,* 43**,** 699-715.

SZETO, T. H., ROWLAND, S. L., ROTHFIELD, L. I. & KING, G. F. 2002. Membrane localization of MinD is mediated by a C-terminal motif that is conserved across eubacteria, archaea, and chloroplasts. *Proc Natl Acad Sci U S A,* 99**,** 15693-8.

THANBICHLER, M. & SHAPIRO, L. 2006. MipZ, a spatial regulator coordinating chromosome segregation with cell division in Caulobacter. *Cell,* 126**,** 147-62.

THOMAIDES, H. B., FREEMAN, M., EL KAROUI, M. & ERRINGTON, J. 2001. Division site selection protein DivIVA of Bacillus subtilis has a second distinct function in chromosome segregation during sporulation. *Genes Dev,* 15**,** 1662-73.

TIENSUU, T., ANDERSSON, C., RYDEN, P. & JOHANSSON, J. 2013. Cycles of light and dark co-ordinate reversible colony differentiation in Listeria monocytogenes. *Mol Microbiol,* 87**,** 909-24.

TILNEY, L. G. & PORTNOY, D. A. 1989. Actin filaments and the growth, movement, and spread of the intracellular bacterial parasite, Listeria monocytogenes. *J Cell Biol,* 109**,** 1597-608.

TINDALL, K. R. & KUNKEL, T. A. 1988. Fidelity of DNA synthesis by the Thermus aquaticus DNA polymerase. *Biochemistry,* 27**,** 6008-13.

TRAAG, B. A. & VAN WEZEL, G. P. 2008. The SsgA-like proteins in actinomycetes: small proteins up to a big task. *Antonie Van Leeuwenhoek,* 94**,** 85-97.

TRAN, N. P., GURY, J., DARTOIS, V., NGUYEN, T. K., SERAUT, H., BARTHELMEBS, L., GERVAIS, P. & CAVIN, J. F. 2008. Phenolic acid-mediated regulation of the padC gene, encoding the phenolic acid decarboxylase of Bacillus subtilis. *J Bacteriol,* 190**,** 3213-24.

TREMOULET, F., DUCHE, O., NAMANE, A., MARTINIE, B. & LABADIE, J. C. 2002. Comparison of protein patterns of Listeria monocytogenes grown in biofilm or in planktonic mode by proteomic analysis. *FEMS Microbiol Lett,* 210**,** 25-31.

TURINI, P., KUROOKA, S., STEER, M., CORBASCIO, A. N. & SINGER, T. P. 1969. The action of phenylmethylsulfonyl fluoride on human acetylcholinesterase, chymotyrpsin and trypsin. *J Pharmacol Exp Ther,* 167**,** 98-104.

TURNER, R. D., RATCLIFFE, E. C., WHEELER, R., GOLESTANIAN, R., HOBBS, J. K. & FOSTER, S. J. 2010. Peptidoglycan architecture can specify division planes in Staphylococcus aureus. *Nat Commun,* 1**,** 26.

TZAGOLOFF, H. & NOVICK, R. 1977. GEOMETRY OF CELL-DIVISION IN STAPHYLOCOCCUS-AUREUS. *Journal of Bacteriology,* 129**,** 343-350.

VAN BAARLE, S. & BRAMKAMP, M. 2010. The MinCDJ system in Bacillus subtilis prevents minicell formation by promoting divisome disassembly. *PLoS One,* 5**,** e9850.

VAN BAARLE, S., CELIK, I. N., KAVAL, K. G., BRAMKAMP, M., HAMOEN, L. W. & HALBEDEL, S. 2013. Protein-protein interaction domains of Bacillus subtilis DivIVA. *J Bacteriol,* 195**,** 1012-21.

VAN DER VEEN, S. & ABEE, T. 2011. Contribution of Listeria monocytogenes RecA to acid and bile survival and invasion of human intestinal Caco-2 cells. *Int J Med Microbiol,* 301**,** 334-40.

VAZQUEZ-BOLAND, J. A., KUHN, M., BERCHE, P., CHAKRABORTY, T., DOMINGUEZ-BERNAL, G., GOEBEL, W., GONZALEZ-ZORN, B., WEHLAND, J. & KREFT, J. 2001. Listeria pathogenesis and molecular virulence determinants. *Clin Microbiol Rev,* 14**,** 584-640.

VEIGA, E. & COSSART, P. 2005. Listeria hijacks the clathrin-dependent endocytic machinery to invade mammalian cells. *Nat Cell Biol,* 7**,** 894-900.

VON KOCKRITZ-BLICKWEDE, M., ROHDE, M., OEHMCKE, S., MILLER, L. S., CHEUNG, A. L., HERWALD, H., FOSTER, S. & MEDINA, E. 2008. Immunological mechanisms underlying the genetic predisposition to severe Staphylococcus aureus infection in the mouse model. *Am J Pathol,* 173**,** 1657-68.

WANG, J., GALGOCI, A., KODALI, S., HERATH, K. B., JAYASURIYA, H., DORSO, K., VICENTE, F., GONZALEZ, A., CULLY, D., BRAMHILL, D. & SINGH, S. 2003. Discovery of a small molecule that inhibits cell division by blocking FtsZ, a novel therapeutic target of antibiotics. *Journal of Biological Chemistry,* 278**,** 44424-44428.

WAXMAN, D. J. & STROMINGER, J. L. 1983. PENICILLIN-BINDING PROTEINS AND THE MECHANISM OF ACTION OF BETA-LACTAM ANTIBIOTICS. *Annual Review of Biochemistry,* 52**,** 825-869.

WEART, R. B., NAKANO, S., LANE, B. E., ZUBER, P. & LEVIN, P. A. 2005. The ClpX chaperone modulates assembly of the tubulin-like protein FtsZ. *Mol Microbiol,* 57**,** 238-49.

WERBER, D., HILLE, K., FRANK, C., DEHNERT, M., ALTMANN, D., MULLER-NORDHORN, J., KOCH, J. & STARK, K. 2013. Years of potential life lost for six major enteric pathogens, Germany, 2004-2008. *Epidemiol Infect,* 141**,** 961-8.

WILLEMSE, J., BORST, J. W., DE WAAL, E., BISSELING, T. & VAN WEZEL, G. P. 2011. Positive control of cell division: FtsZ is recruited by SsgB during sporulation of Streptomyces. *Genes Dev,* 25**,** 89-99.

WU, L. J. & ERRINGTON, J. 2003. RacA and the Soj-Spo0J system combine to effect polar chromosome segregation in sporulating Bacillus subtilis. *Mol Microbiol,* 49**,** 1463-75.

WU, L. J. & ERRINGTON, J. 2004. Coordination of cell division and chromosome segregation by a nucleoid occlusion protein in Bacillus subtillis. *Cell,* 117**,** 915-925.

WU, L. J. & ERRINGTON, J. 2012. Nucleoid occlusion and bacterial cell division. *Nat Rev Microbiol,* 10**,** 8-12.

WU, L. J., ISHIKAWA, S., KAWAI, Y., OSHIMA, T., OGASAWARA, N. & ERRINGTON, J. 2009. Noc protein binds to specific DNA sequences to coordinate cell division with chromosome segregation. *Embo j,* 28**,** 1940-52.

WU, S. W., DE LANCASTRE, H. & TOMASZ, A. 2001. Recruitment of the mecA gene homologue of Staphylococcus sciuri into a resistance determinant and expression of the resistant phenotype in Staphylococcus aureus. *Journal of Bacteriology,* 183**,** 2417-2424.

WUENSCHER, M. D., KOHLER, S., BUBERT, A., GERIKE, U. & GOEBEL, W. 1993. The iap gene of Listeria monocytogenes is essential for cell viability, and its gene product, p60, has bacteriolytic activity. *J Bacteriol,* 175**,** 3491-501.

XU, H., CHATER, K. F., DENG, Z. & TAO, M. 2008. A cellulose synthase-like protein involved in hyphal tip growth and morphological differentiation in streptomyces. *J Bacteriol,* 190**,** 4971-8.

ZACHAR, Z. & SAVAGE, D. C. 1979. Microbial interference and colonization of the murine gastrointestinal tract by Listeria monocytogenes. *Infect Immun,* 23**,** 168-74.

ZORZI, W., ZHOU, X. Y., DARDENNE, O., LAMOTTE, J., RAZE, D., PIERRE, J., GUTMANN, L. & COYETTE, J. 1996. Structure of the low-affinity penicillin-binding protein 5 PBP5fm in wild-type and highly penicillin-resistant strains of Enterococcus faecium. *J Bacteriol,* 178**,** 4948-57.

## Acknowledgements

First of all I would like to thank my parents Gautam and Vidya, to whom I dedicate this research, for their encouragement and for providing me the means and motivation to follow my interest in the field of biological sciences.

No words could describe my gratitude to my project supervisor, mentor and friend, Dr. Sven Halbedel, for trusting me and taking me under his wing as his first doctoral student, for providing me with the opportunity to work on this project in his laboratory, for his focused guidance, undying patience, unstinted support and untiring assistance throughout my thesis work. I am grateful to Prof. Dr. Antje Flieger for agreeing to take over my academic supervision, for her scientific inputs and for taking time to read and assess my doctoral thesis. I am also grateful to Prof. Dr. André Fleißner and Prof. Dr. Susanne Engelmann for their willingness to participate as members of my doctoral thesis committee and for going out of their way to peruse and evaluate my thesis.

I am grateful to the Siemens/DAAD Post Graduate Program for funding my doctoral research at the esteemed Robert Koch Institute, therefore granting me the platform and the resources to expand my professional horizons. I am thankful to the Fakultät für Lebenswissenschaften at TU Braunschweig as well for allowing me to participate in their doctoral program.

I would also like to thank Dr. Dirk Albrecht at the Institut f. Mikrobiologie, Universität Greifswald for his assistance with the MALDI-TOF mass spectrometric analysis of our protein samples, as well as Dr. Jennifer Bender at FG-13, RKI Wernigerode for helping us out with the genomic sequencing of our transposon mutant strain.

Last but not the least I would like to make some “schnell” shoutouts to my dearest lab mates:

Frau Birgitt Hahn: Your expertise in performing eukaryotic cell cultures for our group, for which I am most grateful of course, can only be trumped by your “young-at-heart” and caring nature. I will miss all the home-grown fruits and scrumptious cakes which you so lovingly provided us with.

Jeanine: Our lab-mutti! Without you our lab would be in a state of complete chaos. I will miss those “I got some exciting results” dances in the middle of the lab that you so often performed as well as the cherry-filled cakes you so often baked. Yum yum.

Chrissi: Your energetic personality is what keeps us pepped up through all those dull and dark days. Your inner child is a constant reminder for us to live it up.

Steffi/s and PietschMi and the rest of the guys sitting in the offices under the roof, including Chrissi and Jeanine: You guys have helped me settle down comfortably in this small, little town and made it my home-away-from-home, for which I cannot thank you enough.

# Curriculum Vitae

## ***Personal Details***

| | |
|---|---|
| Name: | Karan Gautam Kaval |
| Date of Birth: | 2nd August 1987 |
| Nationality: | Indian |
| Address: | Schreiberstrasse 19, 38855 Wernigerode |

## ***University Education and Scientific activities***

**2011-2014** Dissertation at the Division for Enteropathogenic Bacteria and Legionella, Robert Koch Institute, Wernigerode under the supervision of Dr. Sven Halbedel. Research Project: "Identification of functional binding partners of *Listeria monocytogenes* DivIVA". Project was funded by the Siemens/DAAD Post Graduate Program.

**2010-2011** Research Technician in the Department of Infection and Immunity, University of Sheffield, U.K, under the supervision of Dr. Mark Thomas. Involved in projects dealing with the elucidation of function of different components of the Type 6 Secretion System of Gram Negative bacteria, *Burkholderia cenocepacia.*

**2009-2010** MSc Molecular Medicine at the University of Sheffield, U.K
Research project: "Bacterial Cell Division - investigating the roles played by FtsQ, FtsL and FtsB in cell division of *Escherichia coli*" at the Krebs Institute, MBB, University of Sheffield, under the supervision of Prof. Simon Foster. Grade: Distinction (1:1)

**2005-2009** B.Tech Biotechnology at VIT University, Vellore, India
Final semester research project: "Chemical characterization, antioxidant and antimicrobial studies of carotenoid pigments from *Vitis vinifera*" at the School of Bio Sciences and Technology, VIT university, under the supervision of Dr. R. Siva. Grade: 8.45/10

***Publications***

**Kaval, K. G., Rismondo, J. & Halbedel, S.** (2014). A function of DivIVA in *Listeria monocytogenes* division site selection. *Mol Microbiol,* 94**,** 637-54.

**van Baarle, S., Celik, I. N., Kaval, K. G., Bramkamp, M., Hamoen, L. W. & Halbedel, S.** (2013). Protein-protein interaction domains of *Bacillus subtilis* DivIVA. *J Bacteriol,* 195**,** 1012-21.

**Kaval, K. G. & Halbedel, S.** (2012). Architecturally the same, but playing a different game: the diverse species-specific roles of DivIVA proteins. *Virulence,* 3**,** 406-7.